12-2012

Fate and Reactivity of Natural and Manufactured Nanoparticles in Soil/Water Environments

Allison Vandevoort
Clemson University, arickvvoort@gmail.com

FATE AND REACTIVITY OF NATURAL AND MANUFACTURED NANOPARTICLES IN SOIL/WATER ENVIRONMENTS

A Dissertation
Presented to
the Graduate School of
Clemson University

In Partial Fulfillment
of the Requirements for the Degree
Doctor of Philosophy
Plant and Environmental Sciences

---

by
Allison René Rick VandeVoort
December 2012

Accepted by:
Dr. Yuji Arai, Committee Chair
Dr. John Andrae
Dr. Cindy Lee
Dr. Horace Skipper

ABSTRACT

Nanoparticles (NPs), < 100 nm in diameter, make up the smallest component of solid material. This small size often causes increased reactivity in soil/water environments, which is true for both natural NPs, such as very fine clay particles, and for manufactured nanoparticles, such as silver nanoparticles (AgNPs). As the importance of these particles is more widely recognized, and as manufactured nanoparticles, especially AgNPs, are increasing in production, it is essential to consider their effect on terrestrial and aquatic environments. The studies presented in this dissertation show that both the physicochemical characteristics of the NPs (e.g., particle size, surface coating, elemental composition), as well as soil-water interfacial chemistry (e.g., ionic strength, ligand concentration, pH), are instrumental in predicting environmental fate and reactivity.

Ligand type and concentration were especially important in NP reactivity and bioavailability. Using the hard/soft acid/base concept, the effect of phosphate ligand (hard base) on Fe/Al (hard acid) oxyhydroxide natural NPs was investigated in Chapters 2 and 3. Adding phosphate to soil NPs and reference nano-minerals (Fe-(oxyhydr)oxides and kaolinite) caused coagulation or dispersion, changing the particle size of the NPs, as well as affecting the amount of phosphate in its bioavailable (i.e., dissolved) form. A review of the literature in Chapters 1 and 3 revealed that changes in the soil conditions, and therefore, soil colloids/NPs (e.g., increasing organic matter via amendments), also has a direct impact on the soil NP-facilitated phosphate transport processes.

Silver, a soft acid, reacts readily with thiol functional groups, soft bases, in humic substances prevalent in soil environments. The effect of soil constituents on AgNP reactivity and phase transformation was investigated in Chapters 4 and 5. The presence of solid surfaces facilitated sorption and phase transformation in all AgNPs studied over the course of 30 days, especially when compared to the same AgNPs aged in aqueous environments in the absence of soil. When the bioavailability of Ag (as ionic and NPs), a known antimicrobial agent, was assessed via denitrification experiments in Chapter 5, the AgNPs exhibited much less toxicity than expected, perhaps due to their strong sorption onto soil particles, as observed in the adsorption isotherm experiments conducted in Chapter 4.

A more in-depth study of Ag(I) and AgNPs, and their interactions with cysteine, an amino acid with a thiol functional group, at the goethite-water interface in Chapter 6 revealed that, while cysteine enhanced the sorption of Ag(I) on goethite surfaces by forming inner-sphere ternary surface complexes, AgNP sorption to goethite was largely unaffected by cysteine. The behavior suggests hydrophobic interactions of AgNPs on goethite surfaces, revealing the effects of a soft ligand on Ag are via species specific (Ag(I) or AgNPs) mineral interactions, and are important in predicting AgNP fate in soil systems.

This dissertation provides a novel viewpoint of natural and manufactured NP interactions in soil environments. These interactions are dictated by both particle-specific

characteristics and environmental conditions. When environmental conditions, especially the presence of reactive ligands (based on the hard/soft acid/base theory), are altered by anthropogenic or indigenous means, the reactivity of certain NPs changes dramatically, impacting the bioavailability of contaminants such as phosphate, Ag(I), or AgNPs.

DEDICATION

To my parents, who, as my first teachers, instilled in me a love of learning and endless curiosity; and who have always given me unconditional love and support.

And to Rob, for following me to South Carolina and giving me love and patience when I needed it most.

ACKNOWLEDGEMENTS

The work presented in this dissertation would not have been possible without the help and guidance of many people. First and foremost, I would like to thank my advisor, Dr. Yuji Arai, for his continuous support and guidance through my doctoral studies. I also thank my committee members Dr. John Andrae, Dr. Cindy Lee, and Dr. Horace Skipper.

The experiments carried out in this project were successful due, in large part, to the assistance of the following people: Dr. Brian Powell, for the use of zeta-potential, dynamic light scattering, and ICP-MS instruments, and for guidance taking measurements; Dr. Simon Scott, for assistance with and use of the ultra-high-speed centrifuge; Dr. Tanju Karanfil, and Onur Apul for BET surface area measurements; the entire staff of the Clemson Electron Microscope Facility, especially Dr. JoAn Hudson, Dr. Taghi Darroudi, and Dr. Haijun Qian; Aaron Edgington and Kim Newton for assistance with particle size measurements on equipment maintained by the Clemson University Environmental Toxicology Program; and Kathy Moore at Clemson Agricultural Services, for ICP-AES measurements. Special thanks also go out to the faculty and staff of the National Synchrotron Light Source at Brookhaven National Laboratory and the Stanford Synchrotron Radiation Lightsource, at which synchrotron-based measurements were conducted; in particular Dr. Antonio Lanzirotti and Dr. Ryan Tappero. In addition, I would like to thank my lab mates and other friends in the graduate school at Clemson University, for their encouragement and support.

I wish to thank my family, especially my parents Douglas and Kyle Rick, for their unending support of my goals and education. I would not be the person I am today without their love, and the many opportunities they were able to provide for me. Finally, thank you to my husband, Robert VandeVoort, for his encouragement, assistance, patience, and love.

This work was funded by the Clemson University Public Service in Agriculture Fellowship and the 2011 Agriculture and Food Research Initiative Competitive Grants Program, Nanotechnology for Agriculture and Food systems (#2011-03580).

TABLE OF CONTENTS

Page

TITLE PAGE i

ABSTRACT ii

DEDICATION v

ACKNOWLEDGEMENTS vi

LIST OF TABLES xi

LIST OF FIGURES xii

CHAPTER

1. INTRODUCTION AND LITERATURE REVIEW 1

    1.1. Nanoparticles 1
    1.2. Phosphorus in Soil/Water Environments 2
    1.3. Silver in Soil/Water Environments 33
    1.4. References 60

2. ROLE OF NATURAL NANOPARTICLES IN PHOSPHORUS TRANSPORT PROCESSES IN ULTISOLS 85

    2.1. Abstract 85
    2.2. Introduction 86
    2.3. Materials and Methods 89
    2.4. Results and Discussion 96
    2.5. References 109

Table of Contents (Continued)

Page

3. REACTION CONDITIONS CONTROL SOIL COLLOID FACILITATED PHOSPHORUS RELEASE IN AGRICULTURAL ULTISOLS 127

3.1. Abstract 127
3.2. Introduction 128
3.3. Materials and Methods 132
3.4. Results and Discussion 135
3.5. References 148

4. PARTICLE SPECIFIC CHEMICAL FATE OF NANOSILVER IN REDUCING SOILS 167

4.1. Abstract 167
4.2. Introduction 167
4.3. Materials and Methods 170
4.4. Results and Discussion 176
4.5. References 187

5. SPATIAL DISTRIBUTION OF SILVER NANOPARTICLES IN REDUCING SOIL ENVIRONMMENTS AND THEIR EFFECT ON DENITRIFYING BACTERIA 203

5.1. Abstract 203
5.2. Introduction 204
5.3. Materials and Methods 207
5.4. Results 213
5.5. Discussion 218
5.6. References 228

Table of Contents (Continued)

Page

6. CYSTEINE AFFECTED AQUEOUS-SILVER(I) AND -SILVER NANOPARTICLE SORPTION AT THE GOETHITE-WATER INTERFACE 243
6.1. Abstract 243
6.2. Introduction 244
6.3. Materials and Methods 246
6.4. Results and Discussion 250
6.5. References 262

7. CONCLUSIONS AND SIGNIFICANT FINDINGS 278

LIST OF TABLES

Table		Page
1.1.	Common phosphate minerals	78
1.2.	Point of zero charge of common soil minerals	79
1.3.	Shared charge of several anions	80
1.4.	Hard and soft acids and bases	81
1.5.	Common silver minerals	82
2.1.	Physicochemical properties of SC surface soils	115
2.2.	Metal(loid) microwave digestion of SC surface soils	116
2.3.	Inorganic P fractionation of SC surface soils	117
2.4.	Least-squares analysis of Fe K-edge bulk XAS of SC surface soils	118
3.1.	Summary of selected colloidal P literature	153-156
4.1.	Characteristics of manufactured silver nanoparticles	191
4.2.	Physicochemical properties of Toccoa surface soil	192
4.3.	Linear combination fit of Ag K-edge μ-XANES of AgNP dissolution samples	193
4.4.	Linear combination fit of Ag K-edge bulk XAS of AgNPs aged in soil	194
4.5.	Principle component analysis of Ag K-edge bulk XAS of AgNPs aged in soil	195
5.1.	Toccoa soil native bacteria denitrification kinetics in the presence of Ag(I) and AgNPs	233
6.1.	Chemical components of the Ag(I)-cysteine system	267
6.2.	Chemical components of the AgNP-cysteine system	268

LIST OF FIGURES

Figure		Page
1.1.	Energy profiles for soil complexes	83
1.2.	Concentration of common ligands in natural waters	84
2.1.	SEM, EDS, and TEM images of soil nanoparticles	119
2.2.	Fe K-edge EXAFS spectra of soil nanoparticles	120
2.3.	Batch desorption of SC surface soils	121-123
2.4.	Batch replenishment desorption of SC surface soils	124
2.5.	pH titration curves of SC soil nanoparticles	125
2.6.	P retention on SC soil nanoparticle suspensions as function of pH	126
3.1.	Flow chart of particle separation techniques	157
3.2.	TEM and EDS of soil nanoparticles identifying amorphous Al-Si material	158
3.3.	TEM and EDS of soil nanoparticles identifying nano-hematite	159
3.4.	TEM and EDS of soil nanoparticles identifying kaolinite	160
3.5.	pH dependent release of soil colloids as function of *I*	161
3.6.	Average particle diameter of goethite, hematite, and kaolinite at varying *I* by DLS	162
3.7.	pH dependent release of soil colloids as function of P concentration	163
3.8.	Zeta potential of goethite, muscovite, kaolinite, and hematite as function of P concentration	164
3.9.	Particle size (DLS) of goethite, hematite, and kaolinite as function of P concentration	165
3.10.	P release from Cecil soil as function of P concentration	166

List of Figures (Continued)

Figure Page

4.1. Batch dissolution of AgNPs 196

4.2. Ag K-edge μ-XANES of AgNP dissolution samples 197

4.3. Linear combination fit spectra of Ag K-edge μ-XANES of AgNP dissolution samples 198

4.4. Adsorption isotherm for Ag(I) and AgNPs on Toccoa soil 199

4.5. Ag K-edge bulk XAS of AgNPs aged in Toccoa soil 200

4.6. Linear combination fit spectra of Ag K-edge bulk XAS of AgNPs aged in soil 201

4.7. Principal component analysis of Ag K-edge bulk XAS of AgNPs aged in soil 202

5.1. Toccoa soil native bacteria denitrification kinetics in the presence of Ag(I) and AgNPs 234-235

5.2. Histogram of denitrification activity 236

5.3. AgNP particle diameter determined by DLS 237

5.4. Ag K-edge μ-XRF maps of Toccoa soil thin section containing AgNPs from denitrification study 238

5.5. Ag K-edge μ-XANES of selected spots from μ-XRF maps 239

5.6. SEM and EDS images of Toccoa soil thin section containing AgNPs from denitrification study 240-242

6.1. Silver(I) and AgNP sorption onto goethite in the presence of cysteine 269

6.2. Ball and stick figures of potential molecular configurations of various Ag(I), AgNP, cysteine, and/or goethite complexes 270-273

6.3. Molar ratio of Ag(I)-cysteine complex to available Ag(I) in complexation experiments 274

List of Figures (Continued)

Figure Page

6.4. Silver(I) sorption onto goethite as a function of *I*.....275

6.5. Zeta potential measurements of goethite suspensions with and without Ag(I) as a function of background electrolyte 276

6.6. Sorption of cysteine on goethite as a function of silver species 277

CHAPTER ONE

INTRODUCTION AND LITERATURE REVIEW

1.1 Nanoparticles

Nanotechnology is emerging as one of the primary technological advances of our day. The use of manufactured nanoparticles in industrial, medical, and consumer products has grown exponentially within the past decade, according to the database maintained by the Project on Emerging Nanotechnologies at the Woodrow Wilson International Center for Scholars (PEN, 2010). In addition, advances in laboratory and analytical technologies have allowed researchers to investigate the role of natural nanoparticles (e.g., soil nanoparticles) in environmental processes.

Soil nanoparticles, and colloidal-sized soil particles, are often overlooked in traditional adsorption/desorption experiments. These particles are small enough to be carried through soil/water environments with pore water, yet contain solid-phase constituents. In this way, it is possible for nano-sized soil particles to constitute a mobile solid phase within these environments (de Jonge et al., 2004). This is an important realm to investigate, as solid phase contaminants are often thought of as immobile. In particular, the role of nanoparticles may become important in the transport of phosphorus through agricultural soils (Kretzschmar et al., 1999).

Of all the nanoparticle-based technologies, nanosilver, in particular, has gained commercial popularity through its use as an antimicrobial agent. The toxicity of nanosilver to bacteria, algae, and small aquatic invertebrates in pure culture systems has

been well documented in the scientific literature (Bielmyer et al., 2002; Morones et al., 2005; Navarro et al., 2008; Sondi and Salopek-Sondi, 2004). Its reliable antimicrobial activity is the reason that it has been adopted in such a wide variety of uses.

As nanosilver and other nano-technologies become more popular and more prevalent in consumer goods, it is important for consumers to understand human health risks, as well as ecosystem and environmental risks. It is essential to study the effects of nanosilver in natural scenarios to determine the total consequences of its use. The greatest risk of nanosilver contamination in soil environments is decreased or suppressed biogeochemical cycling by beneficial bacteria. Of special interest is the nitrogen cycle, due to its undeniable importance for humans and agriculture. Human agricultural activities depend on many parts of the N cycle in order to maintain efficiency and supply food for the global population.

1.2 Phosphorus in Soil/Water Environments

1.2.1 Phosphorus Chemistry

Phosphorus (P) a non-metal from Group VA on the periodic table; it has an atomic number of 15 and an atomic weight of 30.97 g/mol. Other Group VA members include nitrogen (N), arsenic (As), antimony (Sb), and bismuth (Bi). Although P and N are the only members of Group VA that are essential to life, the chemistry of P more closely resembles As than N (Corbridge, 2000). The electron configuration of P is [Ne] $3s^2$ $3p^3$. Phosphorus most often occurs in nature as the orthophosphate anion (commonly called phosphate), a molecule composed of a single P atom in its stable +5 valence state

covalently bonded to four oxygen (O) atoms in a tetrahedral formation. Free P is not found in nature (Corbridge, 2000).

Phosphorus tends to be less bioavailable in water than its fellow plant nutrient, N, leading to a longer residence time in natural environments (McGechan and Lewis, 2002). Within soils, P occurs in both organic forms and inorganic forms. Typically, the organic fraction of P comprises between 20 and 80 percent of the total P present in the soil (Dalal, 1977). Both orthophosphate and organic phosphate are known to be strongly retained in inorganic and organic components of soils (Celi et al., 2003). The majority of organic P in the soil occurs as phytic acid, a very stable P complex originating from plant material (Arai and Sparks, 2007). Inositol P also comprises an important portion of soil organic P, and can comprise up to half of soil organic P (Dalal, 1977). Inositol hexaphosphate is a form of organic phosphate composed of six orthophosphate molecules bound to a six-carbon ring structure. Organic P occurs as both the relatively stable humic acids, and also as the more easily degradable fulvic acids, phospholipids, nucleic acids, and similar materials (Sharpley and Rekolainen, 1997). Dissolved organic P is typically sourced by organic matter (OM), and occurs in runoff waters (Heathwaite, 1997). Organic P is formed when inorganic P is immobilized by organisms that utilize inorganic P and convert it into a part of their biomass (Dalal, 1977). Phosphorus mineralization occurs when P within organic residues is converted to soluble P. Phosphatase enzymes from bacteria are required to catalyze phosphate release (Mullen, 2005). Phosphorus mineralization is affected by soil pH, calcium concentration, and bicarbonate

concentration. As pH increases from approximately 3 to 8, the mineralization rate increases by 10 times (Harrison, 1982).

In its inorganic form, phosphate is soluble in water as the species, PO_4^{3-}. This molecule is most thermodynamically favored in typical soil or water environments as the following species: $H_2PO_4^-$ (pK_a = 2.1) and HPO_4^{2-} (pK_a = 7.2). In strongly basic conditions, phosphate will be available as PO_4^{3-} (pK_a = 12.3). Overall, the solubility of these various metal-phosphate complexes is controlled by the pH of the soil solution, as well as the P concentration, ionic strength, temperature, pressure and the concentrations of multivalent cations.

1.2.2 Historical and Current Uses of Phosphorus

Phosphorus was first discovered and isolated as a pure element in 1669 by Hennig Brandt in his attempts at alchemy by distilling urine, due to the calcium and magnesium phosphates found in urine (Toy, 1987). In its pure form, P is transparent white and waxy-crystalline, and will glow in the dark; it will spontaneously combust at 30º C (Toy, 1987).

Phosphorus is most widely known as a primary ingredient in commercial plant fertilizers due to its role as a limiting nutrient in plant growth (Sharpley et al., 2001). The earliest P-based fertilizers were created from animal bones, which contain carbonated hydroxylapatite ($Ca_5(PO_4)_3(OH)$). These bone fertilizers quickly became insufficient, and the mining of phosphate rocks has become the main source of P-based fertilizers in the modern era (Toy, 1987). Apatite is a main source of phosphate as a nutrient for plants where it is a major mineral, and can be used as a fertilizer in soils with pH < 6.2

(Addiscott and Thomas, 2000). The first known apatite sources in the United States (US) were discovered in 1837 in South Carolina; this later became the first mined phosphate in the US in 1867 (Cathcart, 1980). Fertilizer is the predominant use of mined P, making up around 90% of the industrial consumption (FIPR, 2004). Early fertilizers made directly of rock phosphate caused diminished plant growth after several years of application due to the cadmium and uranium deposits also common in the rock (Filippelli, 2002). Modern fertilizers may be either synthetic, manufactured using either di-ammonium or mono-ammonium phosphate (Addiscott and Thomas, 2000); or they may be animal-based. Animal-based fertilizers are produced from the waste products, such as manure or poultry litter, of livestock animals. Ammonium phosphate fertilizers are the most prevalent type of synthetic fertilizer in the US (Corbridge, 2000). Another synthetic modern fertilizer, called superphosphate ($3Ca(H_2PO_4)_2$), is manufactured by the reaction occurring between sulfuric acid and phosphate rock, which results in mono-calcium phosphate fertilizer (Corbridge, 2000).

There are a variety of other industrial uses for this element. Besides fertilizers, P is also used as a food additive, especially as phosphoric acid, a common source of the tart flavor of colas and other carbonated beverages (Ellinger, 1972). Phosphorus, in various molecular configurations, is also found as an agent in cheese emulsifying, in meat curing, and as a polishing agent in toothpastes. Since P is readily combustible in the atmosphere, it has also been used in warfare as the fillings of shells and grenades, as well as in the manufacturing of matches (Toy, 1987). In 2011, the US produced 28.4×10^6 tons of phosphate rock for commercial and industrial uses (USGS, 2012).

1.2.3 Concentration in Uncontaminated Soils and Waters

Phosphorus is present in both particulate and dissolved forms in freshwater and marine systems. The particulate fraction is typically retained in its mineral lattice and does not participate in the biogeochemical P cycle (Filippelli, 2002). In sediments resulting from previous marine activity, the amount of organic P decreases with soil depth. At the surface, the concentration of P is 4-6 μmol/g to as little as 1-2 μmol/g (Filippelli, 2002). Phosphorus concentrations in soils vary with soil type. In general, the typical concentration of P in soil is in the range of 0.02-0.50 % by weight (Corbridge, 2000). In contrast, phosphate rock, or apatite, can have from 10.5-15.0 percent (by weight) P (Corbridge, 2000). However, depositing more than 75-150 mg/kg on farmland, depending on soil type and soil pH, will result in over-fertilization and runoff of P into the water system (Sharpley, 1995).

The concentration of the phosphate ion in surface freshwaters is near zero, since it will be taken up almost immediately by phytoplankton and other aquatic photosynthetic organisms (Filippelli, 2002). Phosphate concentrations as low as 0.04 mg/L cause eutrophication in freshwater (Sims et al., 1996). In the ocean, inorganic P is measurable, but still present in very small amounts. On average, there is 0.07 mg P per L of ocean water occurring naturally (Redfield, 1958). In general, P is not found in the atmosphere since it has no gaseous phase (Corbridge, 2000).

1.2.4 The Phosphorus Cycle

Phosphorus is very common in the environment, as it is required by every organism for life. Organisms are made up of approximately 2 percent by dry weight of P (Snoeyink and Jenkins, 1980). It is often the limiting nutrient in aquatic systems for photosynthetic species (Snoeyink and Jenkins, 1980). For this reason, a great deal of the P in the environment is bound in biomass as organic P compounds. In organisms, it is used as a building block of the sugar-phosphate structure of DNA and RNA, as an energy storage device in the form of adenosine triphosphate, and as a strengthening agent in structural elements such as bones (FIPR, 2004). Additionally, it is required in the process of C uptake by plants in terrestrial ecosystems (Filippelli, 2002). Plants obtain P as inorganic phosphate primarily from the decomposition of OM within soils, as well as through weathering of phosphate minerals. Animals obtain phosphate through the digestion of plant material. The non-cellular parts of human bones are composed of approximately 60 percent tricalcium phosphate, while human teeth contain approximately 70 percent tricalcium phosphate in the form of hydroxylapatite (Toy, 1987).

There are also cases of phosphate over-exposure, not only in ecosystems as eutrophication, but also in organisms. In humans, very little P is needed to meet the requirements for life. Over-exposure to pure P will result in a condition called P necrosis of the jaw, or “phossy jaw,” a common ailment among employees of match factories in the late 1800s (Marx, 2008). Today, patients taking bisphosphonates for osteoporosis may exhibit similar symptoms (Marx, 2008). The lethal dose of pure P to humans is just 0.1 g (Toy, 1987).

The chemical weathering of P minerals, such as apatite, is the primary natural release mechanism of bio-available P into soils as the species HPO_4^{2-}. In contrast, when minerals are physically weathered, P remains attached to the mineral structure (as $Ca_5(PO_4)_3OH$) and cannot be used by organisms (Filippelli, 2002). Only a very small fraction of the total soil P is plant-available as free, dissolved orthophosphate – typically less than 0.01% (Brady and Weil, 2008). Many plant roots contain mycorrhizal fungi that live in symbiosis with the root cells, and help the plant uptake vital nutrients, especially P. These fungi are able to reach P that may be out of the reach of plant roots, and can also exude phosphatase, an enzyme used to speed the process of chemical weathering of apatite – increasing its bioavailability (Dodd et al., 1987).

The primary anthropogenic source of P to natural environments is from agricultural areas, when large amounts of P-based fertilizer are applied to crop lands. Application of these fertilizers, either synthetic or animal-based, in excess of plant requirements, causes leaching of phosphate and other nutrients into the watershed (Sharpley et al., 2001). In this way, they will become watershed contaminants in the form of non-point pollution.

The massive addition of traditionally limiting nutrients to water systems such as lakes, streams, and even the ocean from commercial agriculture, has caused large algal blooms, known as eutrophication (Torbert and Potter, 2004). Just as it is the limiting nutrient for plant growth, P is also the limiting nutrient for algal growth in lakes and streams (Addiscott and Thomas, 2000). Eutrophication is classified by a large algal bloom, and also the resulting growth and eventual death and decay of algae organisms,

which creates an oxygen deficiency in the water system, due to the great oxygen demand required for both algal metabolism, and the decomposition of dead algae (Daniel et al., 1998). Eutrophication-caused oxygen deficiencies can cause summer fish kills. The emergence of *Pfiesteria piscicida*, a toxic dinoflagellate, in the Gulf of Mexico, Chesapeake Bay, and Neuse River of North Carolina, is of particular concern as it leads to declining ecosystem health in the way of fish kills, and also has caused ill health effects in humans (Burkholder and Glasgow, 1997; Torbert and Potter, 2004). In addition, blooms of *Cyanobacteria* further these problems while also decreasing the quality of drinking water and forming the carcinogenic compound trihalomethane during water treatment through chlorination (Kotak et al., 1993).

In addition to agricultural runoff, P can also be removed from soil systems as biomass – especially in crop harvest. It is estimated that this practice removes 5 to 50 kg per ha per year (Brady and Weil, 2008). The process of harvesting crops accounts for more P removal per ha annually than erosion loss of P-bound soil particles and dissolved P in runoff combined, which constitute 0.1 to 10 kg per ha and 0.01 to 3 kg per ha annually, respectively (Brady and Weil, 2008).

Microbes and other soil organisms can uptake inorganic phosphate and incorporate it into their biomass – this process is termed immobilization (Mullen, 2005). To make organic phosphate, often in the form of phospholipids, nucleic acids, and other essential compounds for life, to be available for plants and microbial use it must be mineralized and transformed back into inorganic phosphate. Microbes possess both intra- and extracellular phosphatase enzymes, which perform mineralization and release

inorganic phosphate, which is also available for plant uptake (Dalal, 1977). Both mineralization and immobilization can occur simultaneously in soil systems (Dalal, 1977).

Geochemical Occurrence

Most of the phosphate is present as apatite in low-temperature geochemical environment (Hughes and Rakovan, 2002). It contains phosphate oxyanions linked together by calcium cations to form a hexagonal framework (Filippelli, 2002). The apatitic phosphate minerals are commonly known as phosphate rock. A list of common phosphate minerals can be found in Table 1.1 (Corbridge, 2000).

Sediment that contains weathered phosphate rock is termed phosphorite, which can be incorporated into sandstone, limestone, and other sedimentary rocks (Cathcart, 1980). Most phosphorite sediments originate from marine environments, which are almost exclusively carbonate-fluorapatite due to the deposition of carbonate-rich marine biomass such as diatoms and bivalves (Altschuler, 1973).

Naturally occurring sources of P can cause the release of phosphate into fresh waters due to the local abundance in the subsurface sediments (Chitrakar et al., 2006). Some P mineral compounds exhibit increased solubility under anaerobic or acidic conditions. An example is strengite ($FePO_4 \cdot 2H_2O$), which shows optimum dissolution under low pH and reducing conditions (Patrick et al., 1973).

Phosphorus minerals, such as apatite, are prevalent in geologic areas that were once ocean basins, which is due to the high concentration of P in the shells and bones of marine organisms that were deposited in these areas when they were covered by water

(Toy, 1987). In regions with calcareous sediments, phosphate may be attracted to calcite surfaces, causing the precipitation of monocalcium phosphate. The precipitation of phosphate lessens the chances of it leaching into water systems (Addiscott and Thomas, 2000). Apatite may also occur as igneous phosphate rock, though this is rarer than its common occurrence in sedimentary rock (Corbridge, 2000). Of the igneous apatites, fluorapatite is the most abundant (Filippelli, 2002). In the US, Florida has the greatest amount of P minerals, though they are also present in South Carolina, Tennessee, and several western states (Cathcart, 1980; Toy, 1987). World-wide, the largest and most note-worthy sources of P come from deposits in Morocco, the US, Russia, Kazakhstan, and China (Corbridge, 2000).

The soils of South Carolina are typically Ultisols, with some bands of Inceptisols and Entisols. Typically, these soil orders are characterized by having acidic soils comprised predominately of the phyllosilicate mineral kaolinite, as well as the aluminum oxide gibbsite. These are commonly typical of tropical climates, but due to the high level of weathering in the upstate of South Carolina, they are also prevalent in this area (Norfleet et al., 1993). In acidic soils, such as those in South Carolina, phosphate is typically found in the iron- or aluminum-bound inorganic form such as strengite and variscite (Brady and Weil, 2008).

1.2.5 Sorption

Anion Sorption

Sorption of ions in the soil occurs when ionic particles adhere to soil surfaces. Anions, such as several species of phosphate, are particularly attracted to silicate and oxide minerals, specifically the protonated surface hydroxide groups (McBride, 1994). Anion adsorption is often associated with the pH of the soil solution, termed the "adsorption envelope" (Hingston et al., 1967). The adsorption envelope changes with the pKa of the conjugate acid of the anion being sorbed (Hingston et al., 1972). A polyprotic acid, such as phosphate, will have several adsorption peaks through pH levels, at each pKa value (Hingston et al., 1972). Soil particle surfaces develop electrostatic charges through either: 1) isomorphic substitution with ions of differing valence, or 2) the reaction of surface functional groups through ions in solution (Sposito, 2008).

There are three mechanisms of ion adsorption onto soil particles: (1) non-specific, or outer-sphere, adsorption; (2) specific, or inner-sphere, adsorption; and (3) diffuse-ion swarm, where no surface complexes form, though fully dissociated ions hover near the charged surface in response to electrostatic interactions (Sposito, 2008). Depending on the mechanism of sorption, the formation of these complexes is varyingly reversible. The process of sorbed anion removal is known as desorption, and is an important process in determining anion availability for plants, as well as in determining the probability that the anion will leach out from the soil system. Figure 1.1 displays an easily reversible complex (a) and a more stable, less reversible complex (b).

It is important to note, in Figure 1.1, the vastly different energy of the reaction (ΔH) between a reversible and irreversible soil complex, which indicates the amount of energy that must be overcome for the surface complex to break apart, allowing desorption to occur. Outer-sphere, or non-specific adsorption, complexes allow anions to more easily desorb, thus reversing the adsorption reaction. Inner-sphere, or specific adsorption, complexes, on the other hand, are very difficult to break apart.

Cations (e.g., Al, Fe) on soil mineral surfaces generally act as Lewis acid sites when a positively charged water molecule is attached, creating a very reactive surface functional group that is easily exchangeable for anion bonding (Sposito, 2008). When a surface functional group combines with an ion from soil solution, inner-sphere and outer-sphere surface complexes are formed (Sposito, 2008). Adsorption mechanisms and processes of these surface species are summarized below.

Specific adsorption, termed ligand exchange, occurs when an anion displaces water molecules and/or hydroxyl ions on the surface of a soil mineral particle for adsorption (Hingston et al., 1972). Due to the lack of a water molecule between the anion and the Lewis acid site on the surface of the soil particle (Goldberg and Sposito, 1985), it is called an inner-sphere surface species. Inner-sphere complexation occurs through covalent bonding because of the dependency on particular electron configuration in the surface functional group and ion in solution (Sposito, 2008). For this reason, inner-sphere complexes are not readily exchangeable.

Soil surface charge has some effect in inner-sphere adsorption reactions. The point of zero charge (PZC) of a soil or mineral is defined as the pH at which half of the

edge sites and functional groups on the soil particles are protonated and half are de-protonated (Sparks, 2003). Anions that are the conjugate base of a strong acid (e.g., H_2SO_4) will experience full dissociation (SO_4^{2-}). When the proton dissociates from this acid, it has the power to remove surface hydroxyl groups or water molecules, revealing surfaces sites for additional adsorption reactions to occur (Hingston et al., 1972). This results in a decrease in the positive charge on the soil surfaces. Anions that are the conjugate base of weak acids (e.g., phosphate, H_3PO_4) will experience incomplete dissociation (e.g., HPO_4^{2-}). These anions may adsorb onto soil surfaces when the pH is less than the PZC of the mineral (Hingston et al., 1972). These ions can even complete adsorption onto surfaces sites when they have no net charge through hydrolysis (Goldberg and Sposito, 1985). This type of specific adsorption will result in a negatively charged soil surface.

Altered soil surface charge density via ligand exchange reaction can be monitored using zeta potential or electrophoretic mobility (EM) values. Typically, ligand exchange reactions are particularly favored in low pH conditions, below the PZC, due to the availability of surface hydroxide groups to accept protons and disperse (McBride, 1994). A ligand exchange reaction involves: a release of hydroxyl ions into solution, a preference for particular solution anions, an irreversible or very slow desorption, and a net change in surface charge making it more negative (McBride, 1994).

Non-specific adsorption of anions occurs only when the pH of the soil solution is below the PZC of the soil. At this point, soil surfaces are positively charged due to an excess of adsorbed hydrogen ions. The law of solution neutrality results in spectator

anions from soil solution balancing their positive charge. Anions are electrostatically attracted to the positively-charged soil particles when the pH of the soil solution is below the PZC of the soil, resulting in the formation of outer-sphere surface species. Outer-sphere surface species have more than one water molecule between anions and mineral surfaces. When the pH of the soil solution is equal to the PZC of the soil, non-specific adsorption becomes negligible due a zero net charge, which does not attract cations or anions to the soil. Soil minerals will have sorption interactions with hydrogen or hydroxide ions depending on the pH of the soil solution, and the behavior of the surfaces as acid or base (Hingston et al., 1972).

While various spectroscopic methods (e.g., attenuated total reflectance (ATR) Fourier transform infrared spectroscopy (FTIR), and X-ray absorption spectroscopy (XAS)) have been used to understand the adsorption mechanism of anions on soil mineral surfaces, there are several indirect methods that can be effectively used in understanding the surface coordination environment of adsorbed species. Two macroscopic methods (ionic strength effects on anion adsorption and zeta potential) and the data interpretation are summarized below.

The background electrolyte (e.g., NaCl, $NaNO_3$) concentration, or ionic strength, is a measure of the amount of charged particles present in a solution, which can affect anion sorption in several ways. High ionic strength can cause competition for available soil surface sites. Since outer-sphere adsorption (non-specific) relies on electrostatic interactions to operate, it is sensitive to this competition, and will therefore occur less often in soil solutions of high ionic strength (Hayes et al., 1988). The strong adsorption of

phosphate, through inner-sphere interactions, is not at all sensitive to changes in ionic strength (Hayes et al., 1988). Due to the differences in sensitivity of inner-sphere and outer-sphere complexes to high ionic strength, ionic strength variations can be used to determine the amount of inner- vs. outer-sphere complexes formed by specific anions (Hayes et al., 1988). Ryden and co-workers (1977) reported that a phosphate adsorption isotherm on New Zealand loamy soils was not significantly affected by ionic strength ([NaCl] =0.001 – 1M). More recently, Arai and Sparks (2001) showed no ionic strength dependent phosphate adsorption on amorphous iron oxyhydroxide at pH 4 – 7.5. Similarly, phosphate adsorption on birnessite at pH 2 – 8.5 was not affected by changes in salinity (Yao and Millero, 1996a). Based on the theory above, the results might indicate the formation of inner-sphere surface species on the adsorbents.

While the variable ionic strength method is commonly used in distinguishing the adsorption mechanism of oxyanions in soil minerals, the data should be also carefully interpreted based on 1) ionic strength effects on the diffused double layer thickness and 2) pH effect on ionic strength. Increasing the ionic strength of the soils solution reduces the thickness of the diffused double layer, providing easier access for ions to approach the mineral-water interface. Ionic strength induced phosphate adsorption in soils was previously reported (Bar-Yosef et al., 1988). Ionic strength is subject to change with increasing pH. Since alkaline systems (pH > 7) generally contain high bicarbonate concentrations (> millimolar), it is difficult to maintain constant ionic strength. For this reason, ionic strength studies are best performed under mildly acidic to acidic conditions or in the absence of CO_2.

While the PZC defines the point of zero net charge on overall soil surfaces, the isoelectric point (IEP) is used to define the point of zero net charge on a particular molecule or particle. Electrophoretic mobility measurements are a useful microscopic approach for not only determining the IEP of pure components but also for obtaining information that can be used to indirectly distinguish bulk surface complexes at colloidal/water interfaces. Non-specific ion adsorption of indifferent electrolyte at the outside of the shear plane (i.e., formation of outer-sphere complexes via van der Waals forces) generally do not affect the IEP but it could cause shifts in the value of EM if present at high concentration (Hunter, 1981). The shear plane is at the outer edge of the inner part of the double layer and near the outer Helmholtz plane or the Stern layer, depending on the models to describe the interface (Hunter, 1981). Inner-sphere complexes, however, cause shifts in both EM and IEP due to specific ion adsorption inside the shear plane (Hunter, 1981). In other words, oxyanion inner-sphere adsorption does increase the net negative charge on the surface. With this knowledge, one can indirectly distinguish the predominant surface complexes on pure colloidal materials using EM measurements.

There are some EM data suggesting predominantly inner-sphere phosphate complexes on metal oxides. Electrophoretic mobility measurements of phosphate adsorbed on ferrihydrite, goethite and boehmite (γ-AlOOH) have shown that inner-sphere complexes form due to charge reversal and a lower IEP with increasing P loading level (Anderson and Malotky, 1979; Arai and Sparks, 2001; Bleam et al., 1991; Hansmann and Anderson, 1985; Tejedor-Tejedor and Anderson, 1990).

Phosphate Sorption on Mineral Surfaces

Phosphate sorption in soils and sediments is often associated with the PZC of adsorbents, which determines whether or not reactive sites will be (de-)protonated at given soil pH values. In general, a low soil pH favors phosphate sorption, as this will likely result in a high degree of protonation at the reactive sites (e.g., edge sites of phyllosilicate minerals). Protonated sites are favorable for phosphate sorption due to the charge attraction between the positively charged mineral surfaces and phosphate anions. Adsorption of phosphate by minerals typically decreases as pH increases as the mineral surfaces develop more de-protonated reactive sites. The phosphate sorption on negatively charged mineral surfaces can be described using the hard and soft acids and bases principle (HSAB principle). Metal ions in most soil minerals (e.g., phyllosilicates, goethite, and gibbsite) belong to one of Lewis acid groups, hard acids. The hard acids like Fe^{3+} and Al^{3+} do not have easily excited outer core electrons (non-polarizable), and are often associated with hard bases (e.g., OH^-, PO_4^{3-}) via ionic bonds. The strong phosphate affinity on metal oxyhydroxides at pH_{water} > PZC is apparent in the binding of a phosphate anion with a metal-OH group on the soil surface through ligand exchange (McBride, 1994). In this reaction, a metal is a Lewis acid that allows for the isomorphic substitution of a phosphate ion for the surface hydroxyl group, thereby forming a very stable surface complex (Sposito, 2008).

Metal oxyhydroxide complexes play an important role in the fate of phosphate in soils thereby controlling their concentrations in the surrounding waters (Chitrakar et al., 2006). Numerous investigations indicated biphasic adsorption (i.e., fast uptake followed

by a slow uptake) and specific adsorption (i.e., inner-sphere surface complexation) processes on variable charge mineral surfaces via ligand exchange mechanisms (Addiscott and Thomas, 2000). Results of macroscopic and spectroscopic investigations are summarized below.

Many studies showed the biphasic adsorption of phosphate in contact with soils and soil mineral surfaces (e.g., aluminum oxyhydroxide, allophane, ferrihydrite, and kaolinite) over different time scales (hours to months) (Afif et al., 1995; Barrow, 1974; Barrow, 1985; Beek and van Riemsdijk, 1982; Black, 1943; Coleman, 1944; Edzwald et al., 1976; Hingston et al., 1974; Kafkafi et al., 1967; Madrid and Posner, 1979; McGechan and Lewis, 2002; Parfitt, 1979; Parfitt, 1989; Ryden et al., 1977; van Riemsdijk et al., 1977; Willett et al., 1988). In general, the initial fast adsorption is followed by a continuous slow adsorption with increasing time at both high and low pH values. Arai and Sparks (2007) reported biphasic phosphate adsorption on ferrihydrite surfaces. The initial phosphate uptake increased with decreasing pH from 9.5 to 4. Fast uptake was followed by a slow reaction with increasing time. Whereas 98.2 % adsorption (2.70 $\mu mol/m^2$) at pH 4 was achieved after 24 hr, slow adsorption continued at pH > 4 after 24 hr. Only 58 % (1.59 $\mu mol\ m^{-2}$) of total P uptake was achieved at pH 9.5 after 24 hr and the slow phosphate uptake continued after 24 hr.

Ligand exchange reactions occur at all phosphate concentration levels, though the reaction sites change. When phosphate concentration is low, Lewis acid sites are used (forming monodentate complexes); as concentration increases, phosphate becomes able to displace hydroxyl groups from the surface (forming bidentate complexes); and at very

high concentrations, the hydroxyl bridges between two mineral atoms may be broken to form adsorption sites, forming binuclear complexes (Goldberg and Sposito, 1985).

In an early benchmark FTIR study by Parfitt et al. (1975), they showed one phosphate ion has the capability of replacing two surface water molecules or hydroxide ions in a ligand exchange reaction, resulting in a binuclear complex. This has been shown to occur on hematite, goethite, and lepidocrocite, among others (Atkinson et al., 1974; Parfitt et al., 1975). These complexes are stable enough to occur in the presence or absence of water molecules (Parfitt and Atkinson, 1976). Similar complexes may also form with SO_4^{2-} and SeO_3^{2-} (Parfitt and Russell, 1977). Martin and Smart in 1987 demonstrated the use of X-ray photoelectron spectroscopy for analyzing phosphate and other anion adsorption onto goethite. Through this technique, they observed the preference of phosphate to adsorb to soil minerals as an inner-sphere bidentate complex (Martin and Smart, 1987). However, Martin et al. (1988) later suggested that phosphate may form crystalline precipitates on the surface of goethite resulting from its partial dissolution, instead of adsorbing.

To better understand the phosphate coordination environment on metal oxyhydroxide surfaces, more advanced FTIR measurements were employed by several researchers. Using the diffuse reflectance FTIR spectroscopy and ATR-FTIR, inner-sphere bidentate bridging surface species are suggested in hematite and ferrihydrite (Arai and Sparks, 2001; Persson et al., 1996). All of these studies show that phosphate adsorption onto iron oxide minerals is largely controlled by pH, and that phosphate may form bridging ligands, especially at low pH levels.

The degree of ligand exchange reactions is variable in different soil minerals. The phosphate retention is influenced by 1) the availability of surface sites as a function of surface area and 2) surface charge density associated with pH and PZC of minerals. Amorphous minerals (e.g., allophane, ferrihydrite) generally have much higher surface area than crystalline metal oxides (e.g., hematite and γ-Al_2O_3) and phyllosilicates (e.g., kaolinite and montmorillonite). In addition, the surface charge density of minerals that is controlled by PZC and soil pH could influence the phosphate retention. In general, minerals that have low PZC values (e.g., MnO_2 ~2, and phyllosilicates ~3-5) have much lower affinity for phosphate anions than high PZC minerals like gibbsite (PZC ~9). Table 1.2 outlines the PZC and specific surface areas of several common minerals (Goldberg and Glaubig, 1987; Gustafsson, 2001; Hussain et al., 1996; Kämpf et al., 2000; Sparks, 2003; Stumm and Morgan, 1996).

While hematite sorbs more phosphate than kaolinite, it cannot sorb as much as goethite, and less still than ferrihydrite (Parfitt, 1989). Lepidocrocite (γ-FeOOH), goethite and hematite (α-Fe_2O_3) readily retain phosphate, though hematite has a lower adsorption capacity than either lepidocrocite or goethite (Madrid and De Arambarri, 1985). Aluminum oxides, such as pseudo-boehmite and gibbsite (γ-$Al(OH)_3$), also have greater phosphate sorption potential than kaolinite, due to their increased surface area (Muljadi et al., 1966). Allophane ($Al_2O_3 \cdot (SiO_2)_{1.3\text{-}2} \cdot (H_2O)_{2.5\text{-}3}$) can sorb more phosphate than ferrihydrite, goethite, or hematite (Parfitt, 1989). Gibbsite strongly sorbs phosphate anions, though not as strongly as hydrous ferric oxides (Bache, 1964). In general, allophane has one of the highest phosphate adsorption capacities, probably due to its very

high surface area (Parfitt, 1989). The effect of surface area on phosphate sorption is also documented among synthetic goethite that has different crystallinity and surface areas. Phosphate adsorption to goethite increased with greater surface area – this was especially true for the slow desorption reactions, in which the attachment of phosphate is limited by the diffusion of it in its anionic form to open edge sites on the goethite mineral face, which does not hold for very crystalline goethite (Torrent et al., 1992). The heavily crystalline forms do not allow for any diffusion of phosphate anions, resulting in a complete absence of a desorption slow reaction (Parfitt, 1989).

The high PZC of aluminum oxyhydroxides (e.g., boehmite ~8.2) (Stumm and Morgan, 1996) electrostatically attract phosphate anions to their surfaces since they are highly protonated at neutral or slightly acidic pH values. Aluminum oxides, such as boehmite (γ-AlOOH) form inner-sphere adsorption complexes with phosphate anions, which bind directly to aluminum atoms in the mineral structure (Bleam et al., 1991; Van Emmerik et al., 2007). Adsorption of phosphate onto phyllosilicate clay minerals tends to be less pronounced than its adsorption onto Al/Fe oxyhydroxides (Arai and Sparks, 2007), which is due to a lower PZC for clay minerals in general, causing a decrease in the amount of electrostatic attraction between the phosphate anion and the surfaces of the clay minerals. For the phyllosilicate mineral like kaolinite, phosphate adsorption increases slightly as pH increases from 3 up to 5, where it peaks, but then decreases again with increased pH beyond 5 (Chen et al., 1973). Black (1943) showed that kaolinite clays showed the most P fixation at pH 4.8. The low affinity of phosphate in phyllosilicates (e.g., kaolinite and montmorillonite) can be enhanced when iron oxyhydroxides are added

to increase the total surface area (Sei et al., 2002). Manganese dioxide (δ-MnO_2) that has PZC ~2.8 can also retain phosphate via both inner- and outer-sphere surface complexes; sorption of negatively-charged phosphate can occur due to surface exchange reactions with metal ions from solution, which neutralizes the negatively-charged surface at pH 4 – 8 (Yao and Millero, 1996b). Higher pH values would result in decreasing outer-sphere surface complexes since the negatively charged surface charge density is high.

Phosphorus Sorption in Soils

The phosphate sorption capacity of soils generally relies on three factors: the amount of aluminum oxyhydroxides, the amount of iron oxyhydroxides, and, to a lesser degree, the amount of OM present in the soil (Maguire et al., 2001). This is because the overall PZC of a soil will typically be reflective of inorganic and organic components of soils (Sparks, 2003). The acidic red clayey soils (i.e., Ultisols), which are predominant in South Carolina (e.g., Kamprath, 1999), as well as other regions worldwide such as those of Ireland are especially good examples of soils that have a sorption capacity dictated by their degree of organic components. In soils with high levels of OM (e.g., Histosols), such as those enhanced by peat, phosphate adsorption increases (Bloom, 1981). Clay content may also increase P sorption capacity in certain soils (Mozaffari and Sims, 1994). Phosphate sorption processes in various soils are summarized below.

In highly weathered, generally nutrient-poor soils, such as Oxisols and Ultisols, P sorption is typically dominated by iron oxide content and/or anthropogenic OM inputs. Oxisols are very highly weathered, and are commonly found in tropical regions. P is commonly sorbed by iron oxides in Oxisols, such as goethite and gibbsite (Fontes and

Weed, 1996). As agricultural soils are fertilized, P is added every year often in excess of plant nutrient requirements. Excess P in the soil is known to build up over time, causing extremely high levels of tightly bound, plant-unavailable P for years after fertilization. A commonly available animal-based fertilizer, such as poultry litter, has been shown to have these results in Delaware Ultisols (Mozaffari and Sims, 1994). Mozaffari and Sims (1994) found that their focus soils could continue to adsorb additional P even at a very high P saturation level. Once a soil can no longer adsorb any additional P, it has reached its sorption capacity. Phosphate bound to oxalate-extractable, amorphous iron and aluminum oxides, will exhibit a slow but constant phosphate desorption rate (Arai et al., 2005).

Histosols are OM rich soils found in warm sub-tropical regions such as the Florida Everglades. They are characterized by having high amounts of slowly decomposing plant material. In these highly organic soils, P sorption increases with Fe and Al content (Larsen et al., 1959). P sorption in Histosols is more strongly correlated with free carbonate concentration than OM concentration, as well as total ash, calcium concentration, and pH (Porter and Sanchez, 1992). Similarly, Spodosols also show a correlation between high Al content and high P sorption (Nair et al., 1998).

Mollisols are high in OM and carbonates. They are typical of the Great Plains region of the US. In these soils, the degree of availability of P is usually controlled by the proportion of organic P in the soils (Zamuner et al., 2008). Vertisols are clay-rich soils prevalent in south Texas and Australia. These soils often have low P availability (López-

Piñeiro and Navarro, 1997). In these soils, calcium carbonate typically controls P sorption (López-Piñeiro and Navarro, 1997).

As reviewed in the previous sections, iron oxyhydroxides strongly sorb phosphate anions. Therefore, soils that are high in oxidized iron have a great phosphate retention capacity. Ultisols, such as those found in South Carolina, are known for their high iron oxyhydroxide content, and therefore, also their phosphate adsorption capacity (Taylor and Schwertmann, 1974). If these iron oxides are removed from the soil via chemical extraction, a drastic decrease in phosphate adsorption capacity will result (Borggaard, 1983). Soils in South Carolina generally have high P concentrations, ranging from 113 to 1418 mg/kg total, highest in the lower Coastal Plain and lowest in the Blue Ridge Mountain regions (Franklin et al., 2006).

Illite has a greater phosphate adsorption capacity than either kaolinite or montmorillonite (Edzwald et al., 1976). There are trends in phosphate adsorption among soil orders as well. In general, Vertisols have a stronger phosphate sorption capacity than most other soil orders, though sorption capacity is greatly varied at the order level (Burnham and Lopez-Hernandez, 1982). Non-calcareous soils may bind phosphate through forming the surface species $S{\equiv}HPO_4^-$ and $S{\equiv}PO_4^{2-}$, which form independently of soil pH (Goldberg and Sposito, 1984).

Local phosphate concentrations may be controlled through environmental management techniques in the environment using iron oxyhydroxides, such as goethite, as adsorbents, due to their strong affinity for phosphate anions (Chitrakar et al., 2006). The application of these iron oxides may increase the adsorption of phosphate by the

soils, thereby decreasing the amount of phosphate that will leach into the watershed. Phosphate adsorbs on the surfaces of goethite rapidly, but cannot enter inner-layer sites due to its large size (Chitrakar et al., 2006).

1.2.6 Desorption

Desorption of anions will occur from soil surfaces when a complex, either inner- or outer-sphere, breaks away from the edge site and enters the soil solution. As previously discussed in section 2.5, this process is largely driven by the concentration gradient of a specific anion between the adsorbed forms on the soil surfaces and the dissolved form in soil solution. Once, the reactive sites on mineral surfaces are saturated with phosphate, this deters future adsorption of phosphate, resulting in leaching of phosphate in soil profiles (Garcia-Rodeja and Gil-Sotres, 1995; Siemens et al., 2004). Desorption is due to the build-up of negative charge on the soil particle, causing repulsion between the negative soil surface and anions (Barrow, 1980). Figure 1.1b shows an inner-sphere complex of phosphate would need to overcome both the much higher energy of the reaction plus the activation energy in order to be reversed. The energy of reaction is much lower in outer-sphere complexes (McBride, 1994). Typically, when the adsorption of ligands is monodentate, the complex tends to be reversible. More stable attachments of ligands, such as multidentate ligands or ring structures, results in an irreversible adsorption complex (Hingston et al., 1974).

While the concentration gradient is the major driving force of phosphate desorption, chemisorbed phosphate ions often become labile, and are exchanged with

hydroxyl anions as they become more prevalent under alkaline conditions (McBride, 1994). In other words, phosphate retention on variable charge mineral surfaces decreases with increasing pH. The hydroxyl anion displays stronger attraction to metal cations in metal oxyhydroxide surfaces, such as iron, due to their low shared charge (1.0) (McBride, 1994). The share charge is determined by dividing the valence of the central atom by the number of bonded O atoms. The smaller shared charge, the greater the effective negative charge residing on each O atom, the stronger the metal-oxyanion ionic bond. Table 1.3 reviews shared charge of various oxyanions (McBride, 1994).

Phosphate, though its shared charge (1.25) is not as low as that of the hydroxyl anion, has a lower shared charge than many other common soil oxyanions. For this reason, it is often used in research to promote desorption of arsenate, sulfate, nitrate, etc. For example, Goldberg (2010) described how phosphate out-competed molybdenum for sorption sites on gibbsite, while sulfate had no effect on Mo(IV) sorption. Xu et al. (2008) observed this same occurrence when phosphate was able to displace arsenate on aluminum hydroxide soil surfaces, causing overall arsenate desorption and phosphate adsorption (Xu et al., 2008).

Until recently, dissolved P (e.g., molybdenum reactive P (MRP)) in solutions that were passed through 0.2-0.45μm filters was thought to control the desorption processes in soil minerals. However, recent studies indicated that filtrate of soil solutions contains not only dissolved P but also colloidal phosphate (i.e., colloids that retain phosphate) (e.g., Heathwaite et al., 2005). The colloidal phosphate might be as important as the MR-P in assessing the fate and transport of P in aquatic and terrestrial environment.

Kretzschmar et al. (1999) describe the importance of colloids as a mobile solid phase, onto which phosphate and other materials may sorb while still moving through the soil subsurface. Examples and a review of various desorption proceses are described in the subsections below.

Phosphate Desorption in Soils and Soil Minerals

Phosphate desorption is as important as its adsorption, as this represents a potential release of P back into water and biological systems. Desorption is also the process by which phosphate leaches into the surrounding fresh water systems, causing eutrophication in instances of over-application of phosphate-based fertilizers (Addiscott and Thomas, 2000). As reviewed in the previous sections, iron oxyhydroxides (e.g., goethite), common iron minerals in soils, showed almost instantaneous phosphate adsorption, but limited, if any, phosphate desorption at environmentally relevant conditions (Madrid and Posner, 1979), which highlights the strength of the association between the phosphate anion and the soil particle. Desorption is possible; however, it is a much more difficult process. Nearly irreversible sorption processes of phosphate have been observed in the biphasic desorption process and the hysteresis effect.

Many studies reported the biphasic phosphate desorption processes (a fast initial desorption followed by slow desorption) from soils and soil components. Two studies examined P desorption on goethite and ferrihydrite using batch replenishment techniques (diluting the reacted samples at a constant ionic strength) (Madrid and Posner, 1979; Ryden and Syers, 1977). The batch desorption data should be carefully interpreted since a period of overall re-adsorption may follow after the initial desorption (Barrow, 1979).

Desorption phenomena were biphasic, a fast reaction for a few hours was followed by a slow reaction for over 100 hours (Madrid and Posner, 1979; Ryden and Syers, 1977). Biphasic P desorption phenomena were also observed for kaolinite using a similar batch technique (Bar-Yosef and Kafkafi, 1978).

In some of early P kinetic research, Australian researchers compared P adsorption and desorption processes on soils and soil components, investigating the hysteresis effect, in which an adsorption isotherm curve does not coincide with a desorption isotherm curve. Using a batch equilibrium study, Barrow (1983) showed the slight shifts between adsorption and desorption isotherm curves on an Australian sandy loam. Ryden and Syers (1977) utilized the same experimental approaches to compare the phosphate hysteresis effect on soils and ferrihydrite. Desorption isotherm curves on the soils and ferrihydrite were greatly shifted from adsorption isotherm curves, and ferrihydrite showed greater irreversibility than the soils (Ryden and Syers, 1977). The concentration effect on hysteresis was also investigated. A wide range of initial P ($[P]_{total}$= 0.001 – 1mM) was reacted with kaolinite, and then the desorption was investigated using isotopic exchange (Kafkafi et al., 1967). A hysteresis effect was observed over all concentration ranges.

The slow release of phosphate from variable charge mineral surfaces and in soils can be enhanced by changes in ionic strength, the presence of competitive anions, residence time, and temperature.

Ionic strength is important in determining the degree of phosphate desorption. For example, high amounts of calcium chloride will hinder the phosphate desorption process, while magnesium chloride and especially sodium chloride have much less of an effect

(Barrow and Shaw, 1979). Phosphate desorption may also occur as the result of competitive sorption of other anionic species, including arsenate. At very high concentrations, arsenate could remove and displace adsorbed phosphate on mineral surfaces, though not as much as sodium hydroxide (Barrow, 1974). In some cases, however, phosphate will displace arsenate, especially on aluminum hydroxides (Xu et al., 2008).

In areas of high P saturation, for example, highly fertilized agricultural lands, the desorption process is much more likely to occur. Phosphate desorption will be more likely to occur in areas where there is sufficient phosphate available (Barrow, 1983). In addition, phosphate is easier to desorb if it has not been sorbed to the soil surface for prolonged periods of time (Barrow, 1983). Incubation time highly influences the reversibility of adsorbed P from soils and soil components. Barrow reported that P desorption from Australian loamy soils was rapid when aging time was short (<24 hours), but the desorption process became much slower when aging time was longer (>24 hours) (Barrow, 1979; Barrow and Shaw, 1975). Madrid and Posner (1979) also observed similar irreversible P desorption from goethite. P desorption decreased with increasing aging time from 1 hour to 23 hours. High temperatures, especially over 40º C, also increase phosphate desorption, as the solution species is favored in these conditions, making its adsorption an exothermic reaction (Barrow and Shaw, 1975).

Colloid-Facilitated Phosphate Desorption

Although the definition of colloid size may be disputed, their environmental importance is not. Colloidal particles are defined as having a diameter between 1 and

1000 nm (Heathwaite et al., 2005; Hens and Merckx, 2001; Kretzschmar et al., 1999) in some cases, or between 1 – 10 nm and 2 – 10 μm (Buffle and Leppard, 1995; Stumm, 1992) in others. Colloidal particles play an important role in the transport of phosphate and other nutrients throughout soil solutions. Phosphorus is transferred from soil to water in both particulate and dissolved forms (Heathwaite et al., 2005). Colloidal particles can be thought of as a continuum between the dissolved and particulate forms of phosphate in soil solution (Hens and Merckx, 2002). Additionally, small particles of soil may break loose through physical weathering to form mobile colloidal sediments; this may also happen with manures and wastes spread as fertilizer (McGechan and Lewis, 2002). In this way, colloids may act as a vehicle for the transfer of colloidal P from agriculturally amended soils to watersheds (Heathwaite et al., 2005). These colloidal particles serve as a contrast to what is commonly thought of as stationary sediments. They may be thought of as a mobile solid phase.

Various soil conditions affect solubility of P over various fractions of particle size. Water flowing through sub-surface environments may act as a driver of colloidal- P release from soils, as it tends to initiate their desorption (Heathwaite et al., 2005). Additionally, ionic strength, soil solution pH, overall soil water content, and macropore flow further influence colloid interactions (Siemens et al., 2008). Soil type also has an influence. Sandy soil may be more affected by the dissolved P leaching, while other soils are more affected by colloidal P leaching (Siemens et al., 2008). Finally, seasonal variability and cultivation practices may also affect leaching of particulate and dissolved

P due to variation in precipitation and soil moisture throughout the year (Schelde et al., 2006).

High ionic strength may, in fact, impede colloidal leaching (Siemens et al., 2008). A high level of electrical conductivity, or ionic strength, reduces colloid mobility and also reduces the amount of particulate P that may be transported (Zhang, 2008). This relationship is so pronounces that Heathwaite et al. (2005) employed it to determine the amount of colloidal P in soils by adjusting the ionic strength of the solution.

Rainfall events may have an effect on the amount of colloidal versus dissolved P released from soils. In general, large rainfall events cause a large amount of P, especially less than 0.45 μm, to be released from soils (Preedy et al., 2001). The combination of this, along with the loss of other necessary plant nutrients, is often detrimental for farmers. Accumulation of P in soils increases the risk that P already sorbed onto colloids will leach out when large rain events pass through the soil column , which is especially pronounced where there are few background electrolytes present in the soil solution (Siemens et al., 2004). Additionally, plowing increases the risk of particle-facilitated and dissolved P leaching after large rain events (Schelde et al., 2006).

In regions of sandy soils, such as South Carolina, excess P in the soils has particularly harsh effects on the environment. When P adsorbs onto soil particles in these conditions, they cause the surfaces of the soil particles to become more negatively charged, which, in turn causes them to have a heightened electrostatic repulsion between the soil particles, sand grains, and colloidal particles present in the solution (Ilg et al., 2008). Therefore, addition of P in large amounts to soils could cause removal of not only

the dissolved P through leaching, but also the mobilization and leaching of colloidal P particles (Ilg et al., 2008). In high clay soils, it is known that colloidal P is readily released by detaching the bond between kaolinite particles and amorphous iron hydroxides (Swartz and Gschwend, 1998). When there is a high degree of P saturation, a large fraction is sorbed onto dispersed particles (Siemens et al., 2004), which may be related to the high surface area, and therefore, reactivity of colloids. It is hypothesized that this is due to the relatively large surface area to volume ratio of colloidal particles, as compared to the larger soil particles (Kretzschmar et al., 1999). A soil with a high degree of P saturation will cause the highest level of leaching by colloidal P particles (Siemens et al., 2008). Adding fertilizer P to soils in excess of the requirements of crops will create a saturated soil sorption capacity, and has the potential to mobilize P-colloids from soils (Siemens et al., 2004). In highly fertilized agricultural soils, there seems to be a complex set of reactions occurring involving colloidal P particles. Complexes form between the OM widely available in these soils, metals, and colloidal P (Hens and Merckx, 2001).

1.3 Silver in Soil/Water Environments

1.3.1. Introduction

Silver (Ag) is a transition metal with many anthropogenic uses in electronics, photographic processing, and as a precious metal. Due to its value, it is actively mined and used in industrial and commercial products. These activities lead to its deposition into aquatic and terrestrial environments. In general, natural concentrations in soils and waters are relatively low, except near large deposits of Ag minerals. Silver is typically

present in soils at around 0.5 mg/L (Emsley, 2001). In the oceans, Ag is typically present at 0.06 to 4 ng/L (Luoma and Rainbow, 2008). Freshwater may contain Ag in concentrations of 1 to 200 ng/L, when measurable (Kramer et al., 2002). In the atmosphere, Ag is only present in trace amounts (Emsley, 2001).

As recently as 2003, new uses have been found for Ag as a nanoparticle. These silver nanoparticles (AgNPs) are manufactured to be between 1 and 100 nm in diameter, and composed of zero-valent Ag (Ag(0)). Due to their extremely small size, nanoparticles have a very large surface area to volume ratio, leading to potentially highly reactive surfaces. Monovalent Ag (Ag(I)) has been used for centuries for its anti-microbial properties, and AgNPs also display unique anti-microbial characteristics. The rapidly increasing popularity of AgNPs for use in consumer products, however, has led to regulatory and environmental concerns.

1.3.2. Silver Chemistry

Silver is an element from Group IB on the periodic table. Its atomic number is 47, and atomic weight is 107.87 g/mol. The other metals of significance in group IB include copper (Cu) and gold (Au). Collectively, these are commonly known as the coinage metals, due to their historical uses as currency. All of these metals have the tendency to resist oxidation and remain in their relatively unreactive zero-valent form in the environment, though this trend increases moving down the group. In general, the oxidizability of group IB elements is as follows: Cu > Ag > Au (Greenwood and Earnshaw, 1984).

Silver(I) has an ionic radius of 0.115 nm and a coordination number of 6 (Shannon, 1976). Metallic Ag has an atomic radius of 0.144 nm (Ede, 2006), while Ag(II) has an ionic radius of 0.094 nm and Ag(III) has an ionic radius of 0.075 nm (Greenwood and Earnshaw, 1984). The first, second, and third ionization energies are 730.8, 2,072.6, and 3,359.4 kJ/mol, respectively (Greenwood and Earnshaw, 1984). Due to their very high ionization energies, Ag(II) and Ag(III) are extremely rare under environmental conditions. For this reason, we will focus only on Ag(0) and Ag(I). Common isotopes are ^{107}Ag, comprising 51.35% and ^{109}Ag, comprising 48.65%; neither of which are radioactive (Day, 1964). The electronic configuration of Ag is $[Kr]4d^{10}5s^{1}$.

In solution, Ag is most commonly found as Ag(I), and may be hydrated as the dehydrate species $[Ag(H_2O)_2]^+$ (Greenwood and Earnshaw, 1984). The Ag(I) ion is quite stable against reduction to Ag(0) in aqueous solution. Its potential is described by the following equation (Cotton, 1997):

$$Ag^{+}_{(aq)} + e^{-} \rightarrow Ag_{(s)} \qquad [1.1]$$
$$E^{0} = +0.779 \text{ V}$$

In its zero-valent state, Ag is stable in oxygen and water environments, though even trace amounts of S compounds in the environment will cause a black sulfide layer to form at the surface (Emsley, 2001). Silver(0) metal forms a 12-coordinate lattice with bond lengths Ag–Ag 2.89 Å (Cotton, 1997).

In the HSAB model (Pearson, 1963), Ag(I) is classified as a soft metal acid (Sparks, 2003), along with Au(I), Tl(I), Cu(I), Cd(II), and Hg(II), among others (Lippard

and Berg, 1994). These metal ions exhibit strong electronegativity and resistance to reduction or polarization (Sparks, 2003). Because of these properties, Ag(I) and other soft metal acids prefer to bind with soft bases, especially RS^- and R_2S, which are large and easily polarized (Lippard and Berg, 1994). Typically, Ag(I) will be found bound to S^{2-} groups in OM (e.g., humic acid, fulvic acid, and humin) due to their strong attraction (Bell and Kramer, 1999). A list of metals and ligands in the HSAB is shown in Table 1.4 (McBride, 1994).

1.3.3. Geochemical Occurrence and Mineralogy

Silver deposits were first mined in Turkey and Greece around 3000 BCE (Emsley, 2001). Although there is great variability in the concentration of Ag in sediments, the average concentration of Ag in the Earth's crust is 0.07 μg/g. Sandstone contains a rather large amount of Ag compared to other rock types at an average Ag concentration of 0.29 μg/g, while shale and limestone have lower average concentrations of 0.18 μg/g and 0.16 μg/g, respectively (Luoma and Rainbow, 2008).

Silver is notably absent from silicate minerals, due to its chalcophilic and siderophilic nature (Goldschmidt, 1958). Chalcophiles decline to bond with O species, but rather prefer S groups, and siderophiles also will not bind with O, but C and/or S groups instead. Soil OM containing S ligands inhibits Ag mineral dissolution, as shown in a laboratory study by Jacobson et al. (2005a). The main industrial sources of Ag are from Mexico, Peru, the US, and Australia, accounting for a total of 17,000 metric tons of Ag mined each year (Emsley, 2001). Most mined Ag is actually the by-product of other

metal mining: 40% comes from lead (Pb) or zinc (Zn) mining, 22% from Cu mining, and 13% from Au mining (Emsley, 2001). Galena minerals (PbS) are also a primary source of Ag ore, as large amounts of Ag(I) can remain trapped between sulfide groups in the crystal structure (Goldschmidt, 1958). A list of Ag minerals of importance can be found in Table 1.5 (Day, 1964; Emsley, 2001; Goldschmidt, 1958; Roberts, 1990).

1.3.4. Silver as a Metal Contaminant

Sources of Silver to the Environment

Silver may be released to the wastewater treatment system through industrial effluent from activities such as photoprocessing (Lytle, 1984). As of 2007, a total of 13 Gg of Ag is emitted to the environment each year, with the US emitting the most Ag of any nation in the world (Eckelman and Graedel, 2007). Silver removal from water is very efficient at wastewater treatment plants, since Ag binds so tightly to OM. Silver ion concentration is often measurable, 10^{-5} to 10^{-2} μg/L (Lytle, 1984), near municipal and industrial sewage outputs into surface water bodies, though the residence time is short in the aqueous form due to scavenging by humic substances (Sañudo-Wilhelmy and Flegal, 1992).

When present in aqueous solution, as in a soil environment, Ag(I) is most abundant as colloidal particles between 10 and 200 nm, and is often undetectable in solutions containing only particles <10 nm (Kramer et al., 1999). It is suggested that these Ag particulates are combinations of Ag(I) and OM rich in thiol groups. These colloidal-sized natural Ag particles were also studied by Wen et al. (1997). Their research

showed the Ag present in river water was made up of 33 – 89% colloids between 1 and 450 nm (Wen et al., 1997). In addition to these natural colloidal Ag particles, the advent of AgNPs to the marketplace has now created a new source of Ag to natural environments.

Wastewater treatment sludge is known to contain high levels of heavy metals (Logan and Chaney, 1983). Though it is highly variable, Ag concentrations in sewage sludge can be as high as 960 mg/L (Alloway, 1990). As sewage sludge is often used as an agricultural field amendment, this becomes an important source of Ag to the environment. Due to this fact, the US Environmental Protection Agency (US EPA) allows domestic sewage sludge to be applied to agricultural lands, but sets limits for the amount of certain heavy metals (e.g., Cu, Pb, Zn), not including Ag, which it can contain (USEPA, 1993). There are currently no regulations that limit the sludge application rate based on Ag loading level. Silver is not commonly deemed a pollutant of interest due to its strong binding abilities to chloride to form the precipitate $AgCl_{(s)}$ (Luoma et al., 1995), as discussed earlier.

Environmental Effects of Nanosilver

Silver nanoparticles pose special problems in the environment due to their small size and unpredictable reactions. The primary mechanism of nanoparticle release to the environments is through use of consumer products containing AgNPs, especially AgNP impregnated plastics and textiles (Blaser et al., 2008). Silver nanoparticle impregnated plastics may slowly leach Ag(I) when they are in contact with water (Kumar et al., 2005). Textiles enhanced with AgNPs (e.g., socks) may leach Ag(I) and nanoparticles as they

are washed (Benn and Westerhoff, 2008). These nanoparticles are either deposited directly to landfills, or are gradually washed away in household wastewater. As discussed earlier, AgNPs, similar to Ag(I), will partition to sludge in a wastewater treatment plant; and the sewage sludge may be applied as a land amendment to agricultural fields and urban landscapes.

Overview of Nanosilver Manufacturing and Uses

Silver nanoparticles are generated either through electrochemical reduction of Ag(I), such as $AgNO_{3(aq)}$, or irradiation of larger metallic Ag particles (Chen and Schluesener, 2008). Silver nanoparticles are typically manufactured to be between one and 100 nm in diameter, and contain approximately 20 to 15,000 Ag atoms (Oberdorster et al., 2005).

Many commercially available AgNPs are coated with capping agents, to increase nanoparticle stability and/or dispersibility in water, and to prevent aggregation. Several common capping agents include sodium borohydride, citric acid, and polyvinylpyrrolidone (PVP) (Tan et al., 2007). Often, the reactivity and fate of AgNPs in natural environments is more dependent on the capping agent than on other AgNP properties (El Badawy et al., 2010). For instance, acidic environments with high concentrations of divalent cations will favor AgNP aggregation, while environments high in chloride ion will favor AgNP stability (El Badawy et al., 2010). The PVP capping agent may increase AgNP mobility and ease of transport within aqueous environments (El Badawy et al., 2010).

Consumer use of AgNP products has continued to grow since their introduction in 2003. The Samsung corporation released the first commercially available AgNP-infused clothes washing machine in 2003 in Korea, which was advertised to kill 99.9% of bacteria (Samsung, 2003). In addition to consumer usage, AgNPs are also used in industry and medicine. Ionic Ag has long been used in medicine for wound dressings to prevent infection, and now AgNPs are also becoming more commonly used in medicine, especially to treat burn wounds (Rai et al., 2009).

Difficulties in Regulation of Nanosilver Products

Silver is regulated in US drinking water by the US EPA. The US EPA classifies it as a voluntarily enforced secondary contaminant, with a secondary maximum contaminant level for Ag in drinking water set at 0.1 mg/L (USEPA, 2011).

Silver nanoparticles and Ag(I) use as a pesticide or anti-microbial agent is regulated by the US EPA under the Federal Insecticide, Fungicide & Rodenticide Act (FIFRA) (Erickson, 2009). Since nanotechnology is such a new field of research, much is still yet to be discovered about the properties and activity of AgNPs and, indeed, all nanoparticles. In 2008 the International Center for Technology Assessment, along with other consumer advocacy groups, petitioned the US EPA to regulate AgNP and all nanomaterials separately from total metal concentration under FIFRA, and to halt production and sale of AgNP consumer products (Weiss, 2008).

As discussed above, as of early 2011, the US EPA does not differentiate between nano- and ionic-Ag in regulations for drinking water or use as a pesticide. However, these

particles may act very differently upon entering the environment, and have different effects on bacteria, plants, and animals.

Silver Toxicity

Silver has no beneficial role in biological systems, and is very toxic to microorganisms and viruses (Emsley, 2001). In cases of human over-exposure to Ag, a skin condition called argyria may result. Argyria can cause areas of the skin to produce a grayish-blue coloration, resulting from Ag granules depositing in the skin (Kim et al., 2009). In all terrestrial animals, Ag will partition to the liver and skin, but there are no serious medical consequences (Emsley, 2001). There have been several cases recently in which argyria was diagnosed after consumption of dietary supplements containing colloidal Ag recommended by alternative health groups (Brandt et al., 2005; Chang et al., 2006; Kim et al., 2009; White et al., 2003). Colloidal Ag is sold as a "cure-all" food supplement and is not classified as a medicine, but as a dietary supplement; therefore, it is unregulated by the US Food and Drug Administration (White et al., 2003).

Monovalent Silver Toxicity

In freshwater systems, the US EPA has set the chronic toxicity level for aquatic organisms for Ag(I) at 0.12 μg/L (USEPA, 1980). Silver ions are toxic primarily through binding to S-containing ligands within microbial cells, such as the thiol group on the amino acid cysteine (Liau et al., 1997). This antimicrobial effect can have prolonged inhibitory action to *Escherichia coli* organisms (Zhao and Stevens, 1998). Interestingly, some bacteria have developed resistance mechanisms to excess Ag(I) in their environment. *E. coli*, for instance, is able to decrease its uptake of Ag(I), thereby

reducing its exposure; *Pseudomonas* spp., on the other hand, has displayed no Ag(I) resistance (Russell and Hugo, 1994). Silver is used in a wide range of antimicrobial uses, especially in medical settings. This may lead to the advancement of more Ag-resistant bacteria in hospital environments (Silver, 2003).

Municipal sewage sludge is a major source of Ag to the environment in the US (Eckelman and Graedel, 2007). In studies of sewage sludge spiked with Ag_2S applied to soils, Ag_2S has the ability to slow and even completely halt microbial denitrification, as measured by N_2O evolution (Johansson et al., 1998; Throbäck et al., 2007). Interestingly, high Ag(I) concentrations in soil (up to 100 mg/kg) reduced the number of denitrifying bacteria, while increasing diversity of *nirK*, which encodes for nitrite reductase, along with novel *nirK* sequences (Throbäck et al., 2007).

Nanosilver Toxicity

Although Ag(I) has long been used as an antimicrobial agent, Sondi and Salopek-Sondi (2004) first demonstrated the antimicrobial effects of AgNPs against *E. coli* in 2004. Another landmark paper in AgNP toxicity to bacteria was published by Morones et al. (2005). These papers established several possibilities in AgNP toxicity: that AgNPs can bind to bacterial membranes, causing distress to the cell; and that AgNPs can, in some cases, penetrate cell membranes and cause cell death (Morones et al., 2005; Sondi and Salopek-Sondi, 2004). Navarro et al. (2008) found that AgNPs may, in fact, be more toxic to bacterial cells than Ag(I), for the reason that they are able to penetrate cell membranes when Ag(I) is unable to due to charge interactions.

The specific mechanism by which AgNPs are toxic to microorganisms is still under debate. One hypothesis is that AgNPs may bind to sulfur ligands once inside the cell in bacterial amino acids, similar to Ag(I) binding, which would cause protein denaturing and cell death (Wigginton et al., 2010). A recent paper by Xiu and coworkers (2012) suggests that AgNP can be entirely explained by their release of Ag(I).

Manufactured AgNPs are available for purchase in a coated form, either with a natural coating, such as calcium carbonate, or a polymer, such as PVP. Surface interactions cause a difference in binding between bare and coated nanoparticles. AgNPs are, by definition, composed of zero-valent, metallic Ag. However, they most likely contain some metal that has been oxidized to Ag(I) at the surface (Lok et al., 2007). This allows them to interact with the intracellular space, in part, as if they were Ag(I).

It has also been shown that AgNPs may partially oxidize at the surface after exposure to oxygen, and therefore, may bind similarly to Ag(I) in protein structures (Lok et al., 2007). Ionic Ag has been previously shown to associate with S-containing compounds inside *E. coli* cells (Feng et al., 2000); however, there have been very few studies on AgNP intracellular associations. Choi et al. (2009) showed that the addition of sulfide to a AgNP media greatly decreased AgNP toxicity to bacteria. However, they did not investigate AgNP binding to intracellular S groups.

1.3.5. Ion Exchange Reactions

Ion exchange processes in soils involve the rapid transfer of ions between those free in solution, and those attached to the charged surfaces of soil particles. The

maximum adsorption activity of ions at soil surfaces (e.g., easily exchangeable ions, outer-sphere complexes, and the diffuse ion swarm) determines the ion exchange capacity of a soil. An ion exchange reaction occurs primarily at the boundary layer between the soil particle and the soil solution, where a cloud of ions surrounds the oppositely charged soil surface. Both cation exchange capacity (CEC) and anion exchange capacity (AEC) are factors in ion exchange, and are important in determining the reactivity of ions in soil environments. Both of these factors are affected by the pH of the soil solution. As pH decreases, the CEC also decreases, while the AEC increases (Sparks, 2003). Cations, such as Ag(I), will have a lower affinity for soil surfaces under acidic conditions, and will therefore be more available to soil biota.

The chemical properties of soil components have an effect on the effective ion exchange capacity of the bulk soil. Most silicate clays possess a permanent negative charge. Those with a strongly negative permanent charge, such as smectite, maintain a large CEC over the environmental pH range (pH = 4 – 8), which will vary quite little (McBride, 1994). These clays have a larger portion of inner-sphere adsorbed ions. In comparison, silicate clays with little to no permanent charge, such as kaolinite, have a CEC dominated by pH, and dependent on variable charge edge sites (McBride, 1994). These clays will also have more rapid ion exchange than a clay such as smectite, due to the prevalence of outer-sphere adsorption (Sparks, 2003).

The ion exchange process is reversible, diffusion-controlled, stoichiometric, and in most cases, there is some selectivity of one ion over another at exchange sites. Since electrostatic forces are involved in the process, Coulomb's law can be used to explain this

selectivity. When ions with the same valence state are compared, the smallest hydrated radius is preferred (Sparks, 2003). The smaller the hydrated radius of the cation, the greater the polarization; the greater its valence, the greater its polarizing power. Helfferich (1962) proposed the following lyotropic series for some common cations: Ba^{2+} > Pb^{2+} > Sr^{2+} > Ca^{2+} > Ni^{2+} > Cd^{2+} > Cu^{2+} > Co^{2+} > Zn^{2+} > Mg^{2+} > Ag^{+} > Cs^{+} > Rb^{+} > K^{+} > NH_4^{+} > Na^{+} > Li^{+}. Among monovalent cations, Ag(I) has one of the smallest hydrated radii (2.77Å) (Parfitt and Smith, 1963), resulting in a greater polarizability. This indicates that Ag(I) is one of the most competitive monovalent cation exchangers in soil solutions. For this reason, when Ag(I) is present in soil solution, it will experience preferential exchange. This assumption was tested in a study by Top and Ülkü (2004) using a natural clinoptilolite. Ammonium-saturated clinoptilolite samples were exposed to Na^{+}, Ag^{+}, Zn^{2+}, and Cu^{2+} nitrates to assess the extent of exchange by each cation. Silver experienced the highest selectivity under all experimental conditions (Top and Ülkü, 2004), supporting the hydrated radius assumption.

1.3.6. Silver and Soft Metal Sorption on Soils and Soil Components

Since most clays and clay minerals possess a negative permanent and/or pH dependent charge, cation retention is generally favored above the PZC (McBride, 1994). As the pH of the soil increases, more cationic particles may sorb onto the soil mineral surface, as long as it is undersaturated with respect to solid phases (e.g., $Ag_2O_{(s)}$) (Sparks, 2003). Increasing pH additionally frees up negatively-charged sites on metal oxyhydroxide surfaces as hydrogen ions dissociate. Cation binding can occur at a variety

of sites, especially where Fe and Al are coordinated with OH^- or H_2O groups (McBride, 1994).

Metal cations may undergo the formation of inner-sphere and/or outer-sphere complexes at the soil mineral-water interfaces. Metal cations with high electronegativity form stronger covalent bonds to oxygen atoms within soil mineral structure, causing these cations to be favored for sorption (McBride, 1994). Monovalent cations, such as Ag(I), selectively associate with surfaces at the mineral water interface depending on their hydrated radius. Potassium(I) has relatively smaller hydrated radius (2.32 Å), and therefore, can be held close to the surface of a substrate; subsequently it is the tightest bound cation (Sparks, 2003). Larger cations such as Li(I) have a much higher specificity due to their large hydrated radius (3.40 Å).

Silver(I), like other metal cations, can function as a Lewis acid in solution by binding to a ligand and accepting its electrons. Silver(I) is classified as a soft acid due to the fact that it is a large, easily polarized atom of low charge (McBride, 1994). Soft acid metals will bind preferentially with soft ligands, such as sulfide. For a more complete listing of hard and soft acids and bases, please see Table 1.4.

Of the soft and borderline ligands, organic N and S are the most prevalent in natural environments. Organic S compounds range from 10^{-5} to 10^{-8} M in concentration in natural freshwater systems, and organic N compounds range from 10^{-4} to 10^{-6} M (Buffle, 1984), as shown in Figure 1.2.

Silver and Soft Metal Sorption on Clays and Clay Minerals

In general, the adsorption of Ag(I) onto mineral surfaces is dependent on the pH_{water} and the PZC of the mineral surfaces. When the pH of the soil solution is greater than the PZC of the minerals present, Ag(I) is attracted to mineral surfaces much more easily through outer-sphere complexes. Sorption can still occur at pH values below the PZC, though sorption tends to be dominated by inner-sphere complexation. Silver sorption on inorganic and organic soil components has not been as extensively studied as other soft and borderline metals, e.g., Pb(II), Cu(II), Cd(II), Hg(II). For this reason, a general overview of soft acid reactivity in minerals and organic components is summarized in the following sections (sections 6.1 through 6.3) along with our recent research findings of Ag geochemistry. Soft metal sorption onto phyllosilicates and metal oxyhydroxides should provide insight as to how Ag(I) might behave in soil environments.

Quartz (PZC~2) can attain maximum Hg(II) sorption near pH 4, and maintains high Hg(II) sorption up to pH 6 (Sarkar et al., 1999). The presence of inorganic ligands preferable to Hg(II), such as chloride or sulfate, greatly diminishes Hg(II) sorption onto quartz surfaces, suggesting the competitive sorption/precipitation reactions of ligands (Sarkar et al., 1999). In addition, competing cations such as Pb(II) and Ni(II) will also decrease Hg(II) sorption onto quartz surfaces (Sarkar et al., 1999).

Kaolinite (PZC = 4.7) displays similar pH dependent sorption behavior for Pb(II) and Cd(II). The metal sorption increases with increasing pH and decreasing ionic strength in kaolinitic systems (Puls et al., 1991; Schaller et al., 2009). Cadmium(II) and Pb(II)

sorption onto illite (PZC~8) also increases with pH, though sorption is affected by ionic strength and metal concentration (Echeverría et al., 2002; Echeverría et al., 2005). The proposed sorption mechanism features layered silicates that retain Cd(II) on aluminol functional groups at broken edge sites (Zachara and Smith, 1994). In the case of Pb(II), outer-sphere sorption mechanism was suggested, since the Pb(II) surface complexes maintained their hydrated sphere during the sorption. The theory was later re-visited by Strawn and Sparks (1999). They used Pb L_{III}-edge X-ray adsorption fine structure (XAFS) analysis to reveal the formation of Pb(II) inner-sphere and outer-sphere complexes on montmorillonite under low ionic strength and pH, while high ionic strength and pH resulted in the formation of only inner-sphere surface complexes (Strawn and Sparks, 1999).

Hayes and Leckie (1987) showed that Pb(II) and Cd(II) sorbed on goethite (PZC~9) surfaces primarily as inner-sphere surface complexes, and that there was minimal change in sorption with changing ionic strength. The lack of ionic strength dependency on Cd(II) sorption on hydrous ferric oxide was also reported by Schaller et al. (2009). They successfully modeled uptake data using the diffuse-layer model (Schaller et al., 2009). This indirect evidence of inner-sphere sorption mechanisms of Pb(II) has been supported by the results of XAFS analysis, which have shown Pb(II) to form trigonal pyramidal inner-sphere surface complexes in aluminum oxides (e.g., Al_2O_3) (Bargar et al., 1997).

Gibbsite (PZC~10), displays maximum Hg(II) sorption near pH 5, and maintains high levels of sorption up to pH 6 (Sarkar et al., 1999). Similar to quartz, the presence of

available inorganic ligands will decrease Hg(II) sorption, though the presence of competing cations Pb(II) and Ni(II) has much less effect on Hg(II) sorption to gibbsite than onto quartz (Sarkar et al., 1999).

Praus et al. (2008) investigated Ag(I) sorption on smectite minerals. Silver sorption on montmorillonite (PZC~2.5) can be described by the Langmuir isotherm (Praus et al., 2008). This sorption was primarily achieved through the formation of a monolayer coverage on the montmorillonite surface. Montmorillonite can achieve maximum Ag(I) sorption at a lower pH than many other minerals due to its lower PZC, which allows its surfaces to be mostly deprotonated, and therefore, attractive to cations, at environmentally relevant near neutral pH values.

Silver and Soft Metal Sorption on Humic Substances

Sulfur groups on humic matter are some of the most important binding sites for Ag(I) in soil systems. These groups work as soft bases to attract Ag(I) and other soft metal cations. The S groups in humic substances are either oxidized or reduced: oxidized sulfonates and bonded sulfates, or reduced organic sulfides or polysulfides (Vairavamurthy et al., 1997). Reduced sulfur groups have more soft base characteristics, and therefore, attract more soft metal cations.

The soft metal-soft ligand interactions between Ag cations and the S atom of thiol groups provide very strong complexes, which allow Ag to outcompete and replace other metal cations, such as Fe, for thiol binding (Manolopoulos, 1997). Humic acid desorbed less Ag cations the longer they had been sorbed originally, and the rates were slower overall (Li et al., 2004). Silver with a long residence time in humic acid could display a

lower toxicity to bacteria and other microorganisms due to its strong binding interactions (Li et al., 2004). Silver also complexes with N atoms in amine and ammonium molecules, to form linear compounds (Smith and Carson, 1997). The degree of Ag sorption by humic substances has been determined to be more a factor of N-based functional group concentration than of acidic functional groups (Sikora and Stevenson, 1988). Because of the strong sorption capacity of humic substances for Ag(I) in soils, when the overall dissolved Ag concentration is low, the vast majority of it remains complexed by these groups. Typically, less than 5% of Ag in soils is in a bioavailable form (Jones et al., 1984).

In general, soil OM will have a much higher sorption capacity than whole soil with regards to other heavy metals such as Pb(II) and Cu(II) (Guo et al., 2006). While Pb(II) and Cu(II) typically adsorb onto particulate OM as inner-sphere complexes with carboxyl and hydroxyl groups, Cd(II) generally forms outer-sphere complexes (Guo et al., 2006). This could be in part due to the fact that Cd(II) displays more soft acid characteristics than Pb(II) or Cu(II), as shown in Table 1.4. Because of the HSAB characteristics, it would be less attracted to the carboxyl and hydroxyl groups favored by the borderline metals. All three of these metals, however, display higher sorption to humic acid than to fulvic acid (Gondar et al., 2006). Sorption of Pb(II) onto humic and fulvic acids was greater than Cd(II) (Gondar et al., 2006). Copper(II) sorption also shows much stronger affinity for ombrotrophic peat than Cd(II) (Villaverde et al., 2009). Divalent Hg, another soft metal, will readily react with both thiol (R-SH) and disulfide

functional groups that are present in humic acid, as well as oxygen atoms (Xia et al., 1999).

Silver and Soft Metal Sorption on Soils

In an early study, Jones and co-workers (1984) described Ag sorption in soils using the Freundlich isotherm equation. They, however, could not predict the Ag(I) uptake well when the concentration of Ag was below 100 mg/L. It has been a challenge to predict the fate and transport of trace metals in soils at environmentally relevant concentration, a few parts per million. Unfortunately, Ag reactivity in different soils types which vary in OM content (e.g., Histosols vs. Aridisols) has not been extensively investigated. For this reason, we summarize the reactivity of other soft and borderline metals (e.g., Cd(II), Pb(II), and Hg(II), see Table 1.4) in various soils below.

Yin et al. (1996) studied Hg(II) adsorption on fifteen soils from New Jersey. The pH of these soils ranged from 5 to 6.4, indicating that they are weakly acidic. Organic matter content, however, varied from 2.2 to 10 mg/kg. In most of experiments, maximum Hg(II) adsorption was observed at pH 3-5, decreasing notably as pH increased (Yin et al., 1996). Soil sorption capacity for Hg(II) was linearly correlated with soil OM content. The sorption capacity increased from 5 to 20 μmol/g with increasing OM content from 0.2 to 20 g/kg.

Oxisols show pH-dependent Cd(II) sorption behavior (Kookana and Naidu, 1998; Soares et al., 2009). The uptake of Cd(II) by Oxisols generally increase with increasing pH (Kookana and Naidu, 1998). However, soil surfaces retain only a small quantity of Cd(II), as little as 0.07 mmol/kg. Interestingly, an increase in ionic strength effectively

decreases the uptake of Cd(II). The effect was more pronounced in soils that contain smectite minerals, due to their strong permanent charge (Kookana and Naidu, 1998; Naidu et al., 1994). The importance of smectite for Cd(II) sorption was also reported in Alfisols (Kookana and Naidu, 1998).

Shaheen (2009) compared the sorption of Pb(II) and Cd(II) in different soils types from Greece (i.e., Entisols, Vertisols, Mollisols, Histosols, Alfisols) and Egypt (Entisols and Aridisols). Batch adsorption data were successfully modeled using the Freundlich equation. In all soils, K_d values for Pb(II) were much greater than those for Cd(II). When soil types were compared with respect to metal reactivity, Egyptian Entisols showed the highest affinity for Pb(II) and Greek Histosols showed the highest affinity for Cd(II), while acidic Greek Alfisols showed the lowest affinity for both metals. Overall, metal sorption was correlated to clay content, CEC, and amorphous Al-oxide content. Other notable soil properties that affected metal sorption were 1) amorphous silica oxide content for Pb(II) and 2) OM, amorphous iron oxyhydroxide, and $CaCO_3$ content for Cd(II) (Shaheen, 2009).

1.3.7. Silver and Soft Metal Desorption on Soils and Soil Components

As in the previous sorption section, desorption of Ag and soft metals in the soil has been poorly investigated. Soil properties/conditions (e.g., residence time, OM content, soil acidity, ligand availability, ionic strength) that affect the desorption of Ag and soft metals are reviewed below.

Li et al. (2004) examined the effect of residence time on Ag desorption from organic substances (humic acid and charcoal) and from iron oxyhydroxides (synthesized goethite and ferrihydrite) using batch desorption techniques. The incubation experiments were first carried out for short term (4 day, T = 20ºC) and long term (40 day, T = 35ºC) residence times at pH 7. A 0.01 M $Ca(NO_3)_2$ solution was used as a desorptive solution to displace labile Ag from adsorbents during the experiment. They found that ferrihydrite desorbed Ag with no regard to the amount of time it had been reacted, while goethite did display an incubation time-dependent desorption reaction. The release of Ag decreased with increasing the residence time (Li et al., 2004).

In a study by Jacobson et al. (2005b), they investigated Ag desorption from illite-rich mineral soils with differing textures and an organic peaty-muck soil, from New York using a resin (Duolite G-73) containing a thiol functional group as a sink. The technique is suited to minimize the backward reaction (i.e., re-adsorption) during the desorption experiments; therefore, the extent of Ag release represents its bioavailability. Desorption was monitored for 1 hr and 4 weeks from soils that were reacted with Ag(I) for 24 hr (steady-state) or for up to 1 year. Less Ag was released with increasing the residence time, and only ~25% of total Ag sorption was reversible. Overall, more Ag desorbed from the sandy soil (pH 5.3) than from the peaty-muck soil (pH 5.1) or from mineral soils with higher clay contents (pH 6.6 – 7.1). However, within two weeks, Ag was mobilized from the peaty-muck soils, suggesting the potential transport mechanism of Ag(I) as Ag-humic aqueous complexes in soils (Jacobson et al., 2005b).

Wang et al. (2009) studied Cd(II) desorption from Chinese Oxisols and Ultisols using the stirred-flow method. The desorption rate was successfully modeled using a first order kinetic equation. They found Cd(II) desorption to be biphasic. An initial fast desorption was followed by a slow release of Cd(II) in both Oxisols (pH 5.61) and Ultisols (pH 4.57) (Wang et al., 2009). The rate coefficient increased from 0.013 to 0.023 in the Oxisols and from 0.021 to 0.056 in the Ultisols while pH decreased from 4.5 to 3.5, suggesting the proton-promoted desorption. The effect of pH on total Cd(II) release was also different between the two soils. Ultisols and Oxisols released 80-99% and 25-28% of total Cd(II), respectively.

Yuan and co-workers (2007) studied the desorption of Cu(II) and Cd(II) from artificially contaminated soils as a function of ionic strength, pH and organic ligands (EDTA, oxalic and tartaric acid). The soils were reacted with Cu(II) (0 to 14.17 mM) or Cd(II) (0 to 8.01 mM) at pH 6.4 – 10.7. The desorption of both Cu(II) and Cd(II) increased with increasing ionic strength or with decreasing pH. While EDTA (> 5 mM) enhanced the release of both metals, citric acid influenced the release of Cu(II) and Cd(II) differently. High citrate concentrations (up to 100 mM) increased the desorption of Cu(II) but had no effect on the desorption of Cd(II) (Yuan et al., 2007). Variations in organic acid promoted desorption was explained by the competitive complexation, precipitation, and sorption reactions.

A study by McLaren et al. (1983) investigated the Cu(II) desorption from several soil components (humic acid, soil oxide and montmorillonite). This study employed repeated washing of the soils with Cu-free electrolyte solutions. Interestingly, the

replenishment method did not promote the desorption of Cu(II) from the soil by any appreciable amount, which indicates that Cu(II) sorption in these adsorbents is irreversible, especially in humic acids (McLaren et al., 1983).

Eick and co-workers (1999) investigated Pb(II) desorption kinetics from goethite. The desorption was rapid, and achieved a maximum of >90% desorption within one hour. However, the desorption rate coefficient decreased as Pb(II) residence time increased (Eick et al., 1999). They suggested an increase in the irreversible fraction was due to the formation of stable, inner-sphere Pb(II) complexes over time. A similar aging effect on Pb(II)-iron oxyhydroxide was also reported in an earlier study by McKenzie (1980). When residence time of Pb(II) on hematite and goethite was increased from 24 hours to 28 weeks, total Pb(II) release was decreased by ~50% on hematite, and was completely halted on goethite (McKenzie, 1980). This provides further evidence for the residence time effect on Pb(II) sorption on iron-based minerals.

1.3.8. Dissolution of Silver Minerals and Nanoparticles

Chemical weathering, i.e., dissolution, of Ag minerals is one of major biogeochemical processes that control [Ag(I)] in soil solutions and pore waters. In the natural system, the dissolution process is generally slow and is controlled by: 1) mass transfer process of reactants/products and/or 2) surface processes associated with the detachment of reaction products (Stumm and Morgan, 1996). If the rate-determining step is controlled by transport processes through layers of minerals, the dissolution process is often defined by the parabolic rate law. Alternatively, when the surface reactions are

much slower than the mass transfer of reactants and reaction products, we often assume that the reaction is controlled at the mineral surfaces. Because of the slow steps, there will be a uniform concentration gradient of solutes at the mineral-water interface. The dissolution kinetics often follows a zero-order rate law when we assume the system has reached at steady state.

In the case of Ag minerals, including emerging AgNPs, the dissolution process is facilitated or retarded by the following mechanisms: 1) the mass transport of protons or ligands from the bulk solution to mineral surfaces, 2) surface complexation of ligands, and 3) electron transfer reactions (e.g., oxidative dissolution of Ag(0) nanoparticles).

Several researchers have investigated the proton promoted dissolution of AgNPs. In all studies, pH dependent dissolution of AgNPs was reported. Elzey and Grassian (2010) studied the pH dependent dissolution of uncapped 10 nm manufactured AgNPs (Nanostructure and Amorphous Materials, Inc., Houston, Texas). They reported that nearly 95% of total Ag was dissolved in nitric acid solutions at pH 0.5. The dissolution, however, was largely reduced from 95% to 1.2% with increasing pH from 0.5 to 3.5. This suggests that AgNPs are insoluble at environmentally relevant pH values (e.g., 5 – 7.5) (Elzey and Grassian, 2010). Stebounova et al. (2011) showed additional evidence of AgNP solubility. The dissolution of AgNPs in artificially created intestinal (Gamble's solution, pH 7.4) and lysosomal fluids (pH 4.5) was minimum. Less than 0.1% of total Ag was dissolved in both artificial fluids after 24 hr at 38^{o} C (Stebounova et al., 2011). While the pH dependent dissolution process is clear, some researchers have pointed out the effects of particle size on the rate of AgNP dissolution. Liu and co-workers (2010)

reported that the dissolution of citrate-capped AgNPs (mass ratio of citrate:Ag = 3:1). The batch experiments were conducted in acetate buffer solutions at pH 4 under air equilibrated condition. The rate of dissolution was proportional to particle size. The first order dissolution rate constant increased from 0.78 to 4.1 day^{-1} with decreasing particle size from 60 to 4.8 nm (Liu et al., 2010).

The dissolution of AgNPs is not only promoted by the activity of hydrogen ions, but also by the presence of soft base ligands such as cyanide. The dissolution of a Ag sulfide mineral, Ag_2S, is described in the following reaction (Xie and Dreisinger, 2007).

$$Ag_2S + 4CN^- \rightarrow 2Ag(CN)_2^- + S^2 \quad [1.2]$$
$$\Delta G^o = 52.5 \text{ kJ/mol}$$

However, under aerobic conditions, sulfide can readily oxidize to thiocyanate (SCN^-), making the dissolution of Ag_2S less effective. The rate of dissolution in the aerated cyanide solution is reported to be 0.38 μmole/hr. The modified reaction can be expressed as following.

$$2Ag_2S_{(s)} + 10CN^- + 2H_2O + O_2 \rightarrow 4Ag(CN)_2^- + 2SCN^- + 4OH^- \quad [1.3]$$
$$\Delta G^o = -388.42 \text{ kJ/mol}$$

The kinetic experiments indicated that both surface- and diffusion-controlled dissolution reactions were occurring during the reaction (Luña-Sanchez et al., 2003). In another Ag_2S dissolution study using a mixture of ferricyanide-cyanide ligand, an activation

energy of 6.7 kJ/mol was reported, suggesting a diffusion controlled reaction (Xie and Dreisinger, 2007). Although the cyanide promoted dissolution reaction is thermodynamically favorable, other soft ligands are known to suppress the dissolution of Ag minerals as well. Humic acids can suppress the dissolution of Ag_2S as much as 75% (Jacobson et al., 2005a). Cysteine and thiosulfate almost completely inhibited the dissolution of Ag minerals during long-term (22 days) dissolution experiment (pH 3.5 – 5) (Jacobson et al., 2005a). Similar results have been reported by Liu et al. (2010). The dissolution of 4.8 nm AgNPs, which were pre-treated with 0.4 mM Na_2S and 4 mM 11-mercaptoundecanoic acid, was nearly negligible in the pH 5.6 acetate buffer solution.

Oxidative dissolution of AgNPs was recently studied by several researchers. In air equilibrated distilled water at pH 5.68, dissolution of citrate capped AgNPs (4.8nm) was as high as 0.3 mg/L after 1 day, while there was negligible dissolution of AgNPs in deoxygenated solution. This suggests the following oxidative dissolution reaction of AgNPs.

$$2Ag_{(s)} + 0.5\ O_{2(aq)} + 2H^{+} \rightarrow 2Ag^{+} + H_2O_{(aq)} \qquad [1.4]$$
$$\Delta G^{o} = -91.3 \text{ kJ/mol}$$

Ho and co-workers (2010) investigated the oxidative dissolution of AgNPs (5 – 10 nm synthetic, citrate capped) by H_2O_2. The rate of dissolution (pH 7.4, I = 0.1 M) was proportional to the concentration of H_2O_2, with a maximum rate of 0.139 s^{-1} in an acetate buffer solution at pH 7.4. The rate was positively linearly correlated with both particle size and temperature. The chemically controlled rate limiting step was supported by an

activation energy of 35.1 kJ/mol. Interestingly, they showed the rate of dissolution was not dependent on ionic strength, suggesting that it is predominantly uncharged particles involved in the rate-limiting step. Dissolution experiments in the presence of ligands (i.e., 0 – 10 mM PVP and 0.05 – 5 mM chloride) show a decrease in the rate, suggesting that sorption of ligands on AgNP surfaces perturbed electron transfer reactions.

1.3.9. Areas for Future Research

It is apparent that there are several areas where the current scientific literature is lacking with regards to Ag, both in its ionic and nanoparticulate forms. Silver continues to be emitted to the environment from industry (e.g., photoprocessing effluents), mining, and natural mineral dissolution. It is important to fully grasp its reactivity in natural settings, especially as new technologies, such as AgNPs, emerge.

The toxicity of both Ag(I) and AgNPs was discussed in section 4.3. Soil bacteria of many species play vital roles in the biogeochemical cycling of N, P, Fe, and many other essential elements in soil-water environments. Silver's broad-spectrum antimicrobial properties may affect these bacteria even at the soil-water interface. It is essential to investigate AgNP toxicity mechanisms under environmentally relevant conditions.

Looking to analogs, such the soft metals Hg(II), Cd(II), and Tl(I) and borderline metals Ni(II), Cu(II), Zn(II), and Pb(II), provides some clues to Ag(I) sorption behaviors in soils and soil components. It is clear, however, as shown previously, that basic Ag(I) sorption literature is severely deficient. It will be important to study Ag(I) sorption, both

at the macro-scale, as well as the molecular scale. Spectroscopic evidence for Ag(I) sorption mechanisms have been used to some degree as pure minerals e.g., (Bell and Kramer, 1999), however, it is still not clear to what extent Ag(I) participates in inner-sphere and/or outer-sphere adsorption onto mineral surfaces, and how the sorption is influenced by ligands in soil solutions and pore waters. Furthermore, the distinction between Ag(I) and AgNPs becomes even more apparent at the molecular scale. Nanoparticles bear physical properties that differentiate them from dissolved components. The behavior of AgNPs in soil environments remains virtually untouched in the scientific literature. Both particle and chemical sorption of AgNPs must be considered in predicting the fate in soils and sediments.

1.4 References

Addiscott, T.M., and D. Thomas. 2000. Tillage, mineralization and leaching: Phosphate. Soil Till. Res. 53:255-273.

Afif, E., V. Barrón, and J. Torrent. 1995. Organic matter delays but does not prevent phosphate sorption by Cerrado soils from Brazil. Soil Sci. 159:207-211.

Alloway, B.J. 1990. Heavy Metals in Soils. John Wiley & Sons, New York.

Altschuler, Z.S. 1973. The weathering of phosphate deposits - Geochemical and environmental aspects, p. 33-96, *In* E. J. Griffith, et al., eds. Environmental Phosphorus Handbook. John Wiley & Sons, New York.

Anderson, M.A., and D.T. Malotky. 1979. The adsorption of protolyzable anions on hydrous oxides at the isoelectric pH. J. Colloid Interf. Sci. 72:413-427.

Arai, Y., and D.L. Sparks. 2001. ATR-FTIR spectroscopic investigation on phosphate adsorption mechanisms at the ferrihydrite-water interface. J. Colloid Interf. Sci. 241:317-326.

Arai, Y., and D.L. Sparks. 2007. Phosphate reaction dynamics in soils and soil components: A multiscale approach. Adv. Agron. 94:136-179.

Arai, Y., K.J.T. Livi, and D.L. Sparks. 2005. Phosphate reactivity in long-term poultry litter-amended southern Delaware sandy soils. Soil Sci. Soc. Am. J. 69:616-629.

Atkinson, R.J., R.L. Parfitt, and R.S. Smart. 1974. Infa-red study of phosphate adsorption on goethite. J. Chem. Soc. Farad. T. 1. 70:1472-1479.

Bache, B.W. 1964. Aluminium and iron phosphate studies relating to soils. II: Reactions between phosphate and hydrous oxides. J. Soil Sci. 15:110-116.

Bar-Yosef, B., and U. Kafkafi. 1978. Phosphate desorption from kaolinite suspensions. Soil Sci. Soc. Am. J. 42:570-574.

Bar-Yosef, B., U. Kafkafi, R. Rosenberg, and G. Sposito. 1988. Phosphorus adsorption by kaolinite and montmorillonite 1. Effect of time, ionic strength, and pH. Soil Sci. Soc. Am. J. 52:1580-1585.

Bargar, J.R., G.E. Brown, and G.A. Parks. 1997. Surface complexation of Pb(II) at oxide-water interfaces: I. XAFS and bond-valence determination of mononuclear and polynuclear Pb(II) sorption products on aluminum oxides. Geochim. Cosmochim. Acta. 61:2617-2637.

Barrow, N.J. 1974. On the displacement of adsorbed anions from soil. 2. Displacement of phosphate by arsenate. Soil Sci. 117:28-33.

Barrow, N.J. 1979. The description of desorption of phosphate from soil. J. Soil Sci. 30:259-270.

Barrow, N.J. 1980. Differences among some North American soils in the rate of reaction with phosphate. J. Environ. Qual. 9:644-648.

Barrow, N.J. 1983. On the reversibility of phosphate sorption by soils. J. Soil Sci. 34:751-758.

Barrow, N.J. 1985. Reactions of anions and cations with variable-charge soils. Adv. Agron. 38:183-230.

Barrow, N.J., and T.C. Shaw. 1975. The slow reactions between soil and anions: 5. Effects of period of prior contact on the desorption of phosphate from soils. Soil Sci. 119:311-320.

Barrow, N.J., and T.C. Shaw. 1979. Effects of ionic strength and nature of the cation on desorption of phosphate from soil. J. Soil Sci. 30:53-65.

Beek, J., and W.H. van Riemsdijk. 1982. Interactions of orthophosphate ion with soil, p. 259-284, *In* G. H. Bolt, ed. Soil Chemistry B, Physico-chemical Models. Elsevier, Amsterdam.

Bell, R.A., and J.R. Kramer. 1999. Structural chemistry and geochemistry of silver-sulfur compounds: Critical review. Environ. Toxicol. Chem. 18:9-22.

Benn, T.M., and P. Westerhoff. 2008. Nanoparticle silver released into water from commercially available sock fabrics. Environ. Sci. Technol. 42:4133-4139.

Bielmyer, G.K., R.A. Bell, and S.J. Klaine. 2002. Effects of ligand-bound silver on *Ceriodaphnia dubia*. Environ. Toxicol. Chem. 21:2204-2208.

Black, C.A. 1943. Phosphate fixation by kaolinite and other clays as affected by pH, phosphate concentration, and time of contact. Soil Sci. Soc. Am. J. 7:123-133.

Blaser, S.A., M. Scheringer, M. MacLeod, and K. Hungerbuhler. 2008. Estimation of cumulative aquatic exposure and risk due to silver: Contribution of nano-functionalized plastics and textiles. Sci. Total Environ. 390:396-409.

Bleam, W.F., P.E. Pfeffer, S. Goldberg, R.W. Taylor, and R. Dudley. 1991. A ^{31}P solid-state nuclear magnetic resonance study of phosphate adsorption at the boehmite/aqueous solution interface. Langmuir. 7:1702-1712.

Bloom, P.R. 1981. Phosphorus adsorption by an aluminum-peat complex. Soil Sci. Soc. Am. J. 45:267-272.

Borggaard, O.K. 1983. The influence of iron oxides on phosphate adsorption by soil. J. Soil Sci. 34:333-341.

Brady, N.C., and R.R. Weil. 2008. The Nature and Properties of Soils. 14th ed. Prentice Hall, Upper Saddle River, New Jersey.

Brandt, D., B. Park, M. Hoang, and H.T. Jacobe. 2005. Argyria secondary to ingestion of homemade silver solution. J. Am. Acad. Dermatol. 53:S105-S107.

Buffle, J. 1984. Natural organic matter and metal-organic interactions in aquatic systems, p. 165-221, *In* H. Sigel, ed. Metal Ions in Biological Systems. Dekker, New York.

Buffle, J., and G.G. Leppard. 1995. Characterization of aquatic colloids and macromolecules 1. Structure and behavior of colloidal material. Environ. Sci. Technol. 29:2169-2175.

Burkholder, J.M., and H.B. Glasgow. 1997. *Pfiesteria piscicida* and other *Pfiesteria*-like dinoflagellates: Behavior, impacts, and environmental controls. Limnol. Oceanogr. 42:1052-1075.

Burnham, C.P., and D. Lopez-Hernandez. 1982. Phosphate retention in different soil taxonomic classes. Soil Sci. 134:376-380.

Cathcart, J.B. 1980. World phosphate reserves and resources, p. 1-18, *In* F. E. Khasawneh, et al., eds. The Role of Phosphorus in Agriculture. American Society of Agronomy, Madison, Wisconsin.

Celi, L., G. De Luca, and E. Barberis. 2003. Effects of interaction of organic and inorganic P with ferrihydrite and kaolinite-iron oxide systems on iron release. Soil Sci. 168:479-488.

Chang, A.L.S., V. Khosravi, and B. Egbert. 2006. A case of argyria after colloidal silver ingestion. J. Cutan. Pathol. 33:809-811.

Chen, X., and H.J. Schluesener. 2008. Nanosilver: A nanoproduct in medical application. Toxicol. Lett. 176:1-12.

Chen, Y.S.R., J.N. Butler, and W. Stumm. 1973. Adsorption of phosphate on alumina and kaolinite from dilute aqueous solutions. J. Colloid Interf. Sci. 43:421-436.

Chitrakar, R., S. Tezuka, A. Sonoda, K. Sakane, K. Ooi, and T. Hirotsu. 2006. Phosphate adsorption on synthetic goethite and akaganeite. J. Colloid Interf. Sci. 298:602-608.

Choi, O., T.E. Cleuenger, B.L. Deng, R.Y. Surampalli, L. Ross, and Z.Q. Hu. 2009. Role of sulfide and ligand strength in controlling nanosilver toxicity. Water Res. 43:1879-1886.

Coleman, R. 1944. The mechanism of phosphate fixation by montmorillonitic and kaolinitic clays. Soil Sci. Soc. Am. J. 9:72-78.

Corbridge, D.E.C. 2000. Phosphorus 2000: Chemistry, Biochemistry & Technology. Elsevier, Amsterdam.

Cotton, S.A. 1997. Chemistry of Precious Metals. Blackie Academic & Professional, London.

Dalal, R.C. 1977. Soil organic phosphorus. Adv. Agron. 29:83-117.

Daniel, T.C., A.N. Sharpley, and J.L. Lemunyon. 1998. Agricultural phosphorus and eutrophication: A symposium overview. J. Environ. Qual. 27:251-257.

Day, F.H. 1964. The Chemical Elements in Nature. Reinhold Publishing Corporation, New York.

de Jonge, L.W., C. Kjaergaard, and P. Moldrup. 2004. Colloids and colloid-facilitated transport of contaminants in soils: An introduction. Vadose Zone J. 3:321-325.

Dodd, J.C., C.C. Burton, R.G. Burns, and P. Jeffries. 1987. Phosphatase activity associated with the roots and the rhizosphere of plants infected with vesicular arbuscular mycorrhizal fungi. New Phytol. 107:163-172.

Echeverría, J.C., E. Churio, and J.J. Garrido. 2002. Retention mechanisms of Cd on illite. Clay. Clay Miner. 50:614-623.

Echeverría, J.C., I. Zarranz, J. Estella, and J.J. Garrido. 2005. Simultaneous effect of pH, temperature, ionic strength, and initial concentration on the retention of lead on illite. Appl. Clay Sci. 30:103-115.

Eckelman, M.J., and T.E. Graedel. 2007. Silver emissions and their environmental impacts: A multilevel assessment. Environ. Sci. Technol. 41:6283-6289.

Ede, A. 2006. The Chemical Element: A Historical Perspective. Greenwood Press, Westport, Connecticut.

Edzwald, J.K., D.C. Toensing, and M.C.Y. Leung. 1976. Phosphate adsorption reactions with clay minerals. Environ. Sci. Technol. 10:485-490.

Eick, M.J., J.D. Peak, P.V. Brady, and J.D. Pesek. 1999. Kinetics of lead adsorption/desorption on goethite: Residence time effect. Soil Sci. 164:28-39.

El Badawy, A.M., T.P. Luxton, R.G. Silva, K.G. Scheckel, M.T. Suidan, and T.M. Tolaymat. 2010. Impact of environmental conditions (pH, ionic strength, and electrolyte type) on the surface charge and aggregation of silver nanoparticles suspensions. Environ. Sci. Technol. 44:1260-1266.

Ellinger, R.H. 1972. Phosphates as Food Ingredients. CRC Press, Cleveland.

Elzey, S., and V.H. Grassian. 2010. Agglomeration, isolation and dissolution of commercially manufactured silver nanoparticles in aqueous environments. J. Nanopart. Res. 12:1945-1958.

Emsley, J. 2001. Nature's Building Blocks. Oxford University Press, Inc., New York.

Erickson, B.E. 2009. Nanosilver pesticides. Chem. Eng. News. 87:25-26.

Feng, Q.L., J. Wu, G.Q. Chen, F.Z. Cui, T.N. Kim, and J.O. Kim. 2000. A mechanistic study of the antibacterial effect of silver ions on *Escherichia coli* and *Staphylococcus aureus*. J. Biomed. Mater. Res. 52:662-668.

Filippelli, G.M. 2002. The global phosphorus cycle, p. 391-425, *In* M. J. Kohn, et al., eds. Phosphates: Geochemical, Geobiological, and Materials Importance. The Mineralogical Society of America, Washington, DC.

FIPR. 2004. Phosphate Primer [Online]. Available by Florida Institute of Phosphate Research http://fipr1.state.fl.us/PhosphatePrimer (verified 9 July 2012).

Fontes, M.P.F., and S.B. Weed. 1996. Phosphate adsorption by clays from Brazilian Oxisols: Relationships with specific surface area and mineralogy. Geoderma. 72:37-51.

Franklin, R.E., L. Duis, and B.R. Smith. 2006. Mehlich extractable and total elemental concentrations in South Carolina soils. Commun. Soil Sci. Plan. 37:679-691.

Garcia-Rodeja, I., and F. Gil-Sotres. 1995. Laboratory study of phosphate desorption kinetics in soils of calicia (N.W. Spain). Commun. Soil Sci. Plan. 26:2023-2040.

Goldberg, S. 2010. Competitive adsorption of molybdenum in the presence of phosphorus or sulfur on gibbsite. Soil Sci. 175:105-110.

Goldberg, S., and G. Sposito. 1984. A chemical model of phosphate adsorption by soils: II. Noncalcareous soils. Soil Sci. Soc. Am. J. 48:779-783.

Goldberg, S., and G. Sposito. 1985. On the mechanism of specific phosphate adsorption by hydroxylated mineral surfaces: A review. Commun. Soil Sci. Plan. 16:801-821.

Goldberg, S., and R.A. Glaubig. 1987. Effect of saturating cation, pH, and aluminum and iron oxide on the flocculation of kaolinite and montmorillonite. Clay. Clay Miner. 35:220-227.

Goldschmidt, V.M. 1958. Geochemistry. Oxford University Press, London.

Gondar, D., R. López, S. Fiol, J.M. Antelo, and F. Arce. 2006. Cadmium, lead, and copper binding to humic acid and fulvic acid extracted from an ombrotrophic peat bog. Geoderma. 135:196-203.

Greenwood, N.N., and A. Earnshaw. 1984. Chemistry of the Elements. Pergamon Press, Inc., Elmsford, New York.

Guo, X.Y., S.Z. Zhang, X.Q. Shan, L. Luo, Z.G. Pei, Y.G. Zhu, T. Liu, Y.N. Xie, and A. Gault. 2006. Characterization of Pb, Cu, and Cd adsorption on particulate organic matter in soil. Environ. Toxicol. Chem. 25:2366-2373.

Gustafsson, J.P. 2001. Modelling competitive anion adsorption on oxide minerals and an allophane-containing soil. Euro. J. Soil Sci. 52:639-653.

Hansmann, D.D., and M.A. Anderson. 1985. Using electrophoresis in modeling sulfate, selenite, and phosphate adsorption onto goethite. Environ. Sci. Technol. 19:544-551.

Harrison, A.F. 1982. Labile organic phosphorus mineralization in relationship to soil properties. Soil Biol. Biochem. 14:343-351.

Hayes, K.F., and J.O. Leckie. 1987. Modeling ionic strength effects on cation adsorption at hydrous oxide-solution interfaces. J. Colloid Interf. Sci. 115:564-572.

Hayes, K.F., C. Papelis, and J.O. Leckie. 1988. Modeling ionic strength effects on anion adsorption at hydrous oxide/solution interfaces. J. Colloid Interf. Sci. 115:717-726.

Heathwaite, A.L. 1997. Sources and pathways of phosphorus loss from agriculture, p. 205-223, *In* H. Tunney and O. T. Carton, eds. Phosphorus Loss from Soil to Water. CAB International, Wallingford, UK.

Heathwaite, L., P. Haygarth, R. Matthews, N. Preedy, and P. Butler. 2005. Evaluating colloidal phosphorus delivery to surface waters from diffuse agricultural sources. J. Environ. Qual. 34:287-298.

Helfferich, F. 1962. Ion Exchange. McGraw Hill, New York.

Hens, M., and R. Merckx. 2001. Functional characterization of colloidal phosphorus species in the soil solution of sandy soils. Environ. Sci. Technol. 35:493-500.

Hens, M., and R. Merckx. 2002. The role of colloidal particles in the speciation and analysis of "dissolved" phosphorus. Water Res. 36:1483-1492.

Hingston, F.J., A.M. Posner, and J.P. Quirk. 1972. Anion adsorption by goethite and gibbsite. I. The role of the proton in determining adsorption envelopes. J. Soil Sci. 23:177-192.

Hingston, F.J., A.M. Posner, and J.P. Quirk. 1974. Anion adsorption by goethite and gibbsite. II. Desorption of anions from hydrous oxide surfaces. J. Soil Sci. 25:16-26.

Hingston, F.J., R.J. Atkinson, A.M. Posner, and J.P. Quirk. 1967. Specific adsorption of anions. Nature. 215:1459-1461.

Ho, C.-M., S.K.-W. Yau, C.-N. Lok, M.-H. So, and C.-M. Che. 2010. Oxidative dissolution of silver nanoparticles by biologically relevant oxidants: A kinetic and mechanistic study. Chem. Asian J. 5:285-293.

Hughes, J.M., and J. Rakovan. 2002. The crystal structure of apatite, $Ca_5(PO_4)_3(F,OH,Cl)$, p. 1-12, *In* M. J. Kohn, et al., eds. Phosphates: Geochemical, Geobiological, and Materials Importance. The Mineralogical Society of America, Washington, DC.

Hunter, R.J. 1981. Zeta Potential in Colloid Science. Academic Press, London.

Hussain, S.A., S. Demirci, and G. Özbayoğlu. 1996. Zeta potential measurements on three clays from Turkey and effects of clays on coal flotation. J. Colloid Interf. Sci. 184:535-541.

Ilg, K., P. Dominik, M. Kaupenjohann, and J. Siemens. 2008. Phosphorus-induced mobilization of colloids: Model systems and soils. Euro. J. Soil Sci. 59:233-246.

Jacobson, A.R., C.E. Martinez, M. Spagnuolo, M.B. McBride, and P. Baveye. 2005a. Reduction of silver solubility by hurnic acid and thiol ligands during acanthite (β-Ag_2S) dissolution. Environ. Pollut. 135:1-9.

Jacobson, A.R., S. Klitzke, M.B. McBride, P. Baveye, and T.S. Steenhuis. 2005b. The desorption of silver and thallium from soils in the presence of a chelating resin with thiol functional groups. Water Air Soil Pollut. 160:41-54.

Johansson, M., M. Pell, and J. Stenström. 1998. Kinetics of substrate-induced respiration (SIR) and denitrification: Applications to a soil amended with silver. Ambio. 27:40-44.

Jones, K.C., P.J. Peterson, and B.E. Davies. 1984. Extraction of silver from soils and its determination by atomic absorption spectrometry. Geoderma. 33:157-168.

Kafkafi, U., A.M. Posner, and J.P. Quirk. 1967. Desorption of phosphate from kaolinite. Soil Sci. Soc. Am. J. 31:348-353.

Kämpf, N., A.C. Scheinost, and D.G. Schulze. 2000. Oxide minerals, *In* M. E. Sumner, ed. Handbook of Soil Science. CRC Press, Boca Raton, Florida.

Kamprath, E.J. 1999. Changes in phosphate availability of Ultisols with long-term cropping. Commun. Soil Sci. Plan. 30:909-919.

Kim, Y., H.S. Suh, H.J. Cha, S.H. Kim, K.S. Jeong, and D.H. Kim. 2009. A case of generalized argyria after ingestion of colloidal silver solution. Am. J. Ind. Med. 52:246-250.

Kookana, R.S., and R. Naidu. 1998. Effect of soil solution composition on cadmium transport through variable charge soils. Geoderma. 84:235-248.

Kotak, B.G., S.L. Kenefick, D.L. Fritz, C.G. Rousseaux, E.E. Prepas, and S.E. Hrudey. 1993. Occurrence and toxicological evaluation of cyanobacterial toxins in Alberta lakes and farm dugouts. Water Res. 27:495-506.

Kramer, J.R., N.W.H. Adams, H. Manolopoulos, and P.V. Collins. 1999. Silver at an old mining camp, Cobalt, Ontario, Canada. Environ. Toxicol. Chem. 18:23-29.

Kramer, J.R., G. Benoit, K.C. Bowles, D.M. DiToro, R.T. Herrin, G.W.I. Luther, H. Manolopoulos, K.A. Robillard, M.M. Shafer, and J.R. Shaw. 2002. Environmental Chemistry of Silver, p. 1-25, *In* A. W. Andren and T. W. Bober, eds. Silver in the Environment: Transport, Fate, and Effects. Society of Environmental Toxicology and Chemistry, Pensacola, Florida.

Kretzschmar, R., M. Borkovec, D. Grolimund, and M. Elimelech. 1999. Mobile subsurface colloids and their role in contaminant transport. Adv. Agron. 66:121-193.

Kumar, R., S. Howdle, and H. Munstedt. 2005. Polyamide/silver antimicrobials: Effect of filler types on the silver ion release. J. Biomed. Mater. Res., Part B. 75B:311-319.

Larsen, J.E., G.F. Warren, and R. Langston. 1959. Effect of iron, aluminum and humic acid on phosphorus fixation by organic soils. Soil Sci. Soc. Am. J. 23:438-440.

Li, J., A.W. Rate, and R.J. Gilkes. 2004. Silver ion desorption kinetics from iron oxides and soil organic matter: Effect of adsorption period. Aust. J. Soil Res. 42:59-67.

Liau, S.Y., D.C. Read, W.J. Pugh, J.R. Furr, and A.D. Russell. 1997. Interaction of silver nitrate with readily identifiable groups: Relationship to the antibacterial action of silver ions. Lett. Appl. Microbiol. 25:279-283.

Lippard, S.J., and J.M. Berg. 1994. Principles of Bioinorganic Chemistry. University Science Books, Mill Valley, California.

Liu, J.Y., D.A. Sonshine, S. Shervani, and R.H. Hurt. 2010. Controlled release of biologically active silver from nanosilver surfaces. ACS Nano. 4:6903-6913.

Logan, T.J., and R.L. Chaney. 1983. Metals, p. 235-323, *In* A. L. Page, et al., eds. Utilization of Municipal Wastewater and Sludge on Land. University of California, Riverside, California.

Lok, C.N., C.M. Ho, R. Chen, Q.Y. He, W.Y. Yu, H. Sun, P.K.H. Tam, J.F. Chiu, and C.M. Che. 2007. Silver nanoparticles: Partial oxidation and antibacterial activities. J. Biol. Inorg. Chem. 12:527-534.

López-Piñeiro, A., and A.G. Navarro. 1997. Phosphate sorption in Vertisols of southwestern Spain. Soil Sci. 162:69-77.

Luña-Sanchez, R.M., I. Gonzalez, and G.T. Lapidus. 2003. A comparative study of silver sulfide oxidation in cyanide media - Evans diagrams vs. leaching studies. J. Electrochem. Soc. 150:D155-D161.

Luoma, S.N., and P.S. Rainbow. 2008. Metal Contamination in Aquatic Environments. Cambridge University Press, New York.

Luoma, S.N., Y.B. Ho, and G.W. Bryan. 1995. Fate, bioavailability and toxicity of silver in estuarine environments. Mar. Pollut. Bull. 31:44-54.

Lytle, P.E. 1984. Fate and speciation of silver in publicly owned treatment works. Environ. Toxicol. Chem. 3:21-30.

Madrid, L., and A.M. Posner. 1979. Desorption of phosphate from goethite. J. Soil Sci. 30:697-707.

Madrid, L., and P. De Arambarri. 1985. Adsorption of phosphate by two iron oxides in relation to their porosity. J. Soil Sci. 36:523-530.

Maguire, R.O., R.H. Foy, J.S. Bailey, and J.T. Sims. 2001. Estimation of the phosphorus sorption capacity of acidic soils in Ireland. Euro. J. Soil Sci. 52:479-487.

Manolopoulos, H. 1997. Silver mobility in the presence of iron sulfides under oxidizing conditions, p. 133-135, *In* A. W. Andren and T. W. Bober, eds. The 5th International Conference Proceedings: Transport, Fate, and Effects of Silver in the Environment. University of Wisconsin System, Madison, Wisconsin.

Martin, R.R., and R.S. Smart. 1987. X-ray photoelectron studies of anion adsorption on goethite. Soil Sci. Soc. Am. J. 51:54-56.

Martin, R.R., R.S.C. Smart, and K. Tazaki. 1988. Direct observation of phosphate precipitation in the goethite/phosphate system. Soil Sci. Soc. Am. J. 52:1492-1500.

Marx, R.E. 2008. Uncovering the cause of "phossy jaw" circa 1858 to 1906: Oral and maxillofacial surgery closed case files-case closed. J. Oral Maxillofac. Surg. 66:2356-2363.

McBride, M.B. 1994. Environmental Chemistry of Soils. Oxford University Press, Oxford.

McGechan, M.B., and D.R. Lewis. 2002. Sorption of phosphorus by soil, Part 1: Principles, equations and models. Biosyst. Eng. 82:1-24.

McKenzie, R.M. 1980. The adsorption of lead and other heavy metals on oxides of manganese and iron. Aust. J. Soil Res. 18:61-71.

McLaren, R.G., J.G. Williams, and R.S. Swift. 1983. Some observations on the desoprtion and distribution behavior of copper with soil components. J. Soil Sci. 34:325-331.

Morones, J.R., J.L. Elechiguerra, A. Camacho, K. Holt, J.B. Kouri, J.T. Ramirez, and M.J. Yacaman. 2005. The bactericidal effect of silver nanoparticles. Nanotechnology. 16:2346-2353.

Mozaffari, M., and J.T. Sims. 1994. Phosphorus availability and sorption in an Atlantic coastal plain watershed dominated by animal-based agriculture. Soil Sci. 157:97-107.

Muljadi, D., A.M. Posner, and J.P. Quirk. 1966. The mechanism of phosphate adsorption by kaolinite, gibbsite, and pseudoboehmite. Part I: Isotherms and effect of pH on adsorption. J. Soil Sci. 17:212-229.

Mullen, M.D. 2005. Phosphorus and Other Elements, p. 463-488, *In* D. M. Sylvia, et al., eds. Principles and Applications of Soil Microbiology, 2nd ed. Pearson Prentice Hall, Upper Saddle River, New Jersey.

Naidu, R., N.S. Bolan, R.S. Kookana, and K.G. Tiller. 1994. Ionic-strength and pH effects on the sorption of cadmium and the surface charge of soils. Euro. J. Soil Sci. 45:419-429.

Nair, V.D., D.A. Graetz, and K.R. Reddy. 1998. Dairy manure influences on phosphorus retention capacity of Spodosols. J. Environ. Qual. 27:522-527.

Navarro, E., F. Piccapietra, B. Wagner, F. Marconi, R. Kaegi, N. Odzak, L. Sigg, and R. Behra. 2008. Toxicity of silver nanoparticles to *Chlamydomonas reinhardtii*. Environ. Sci. Technol. 42:8959-8964.

Norfleet, M.L., A.D. Karathanasis, and B.R. Smith. 1993. Soil solution composition relative to mineral distribution in Blue Ridge Mountain soils. Soil Sci. Soc. Am. J. 57:1375-1380.

Oberdorster, G., E. Oberdorster, and J. Oberdorster. 2005. Nanotoxicology: An emerging discipline evolving from studies of ultrafine particles. Environ. Health Perspect. 113:823-839.

Parfitt, G.D., and A.L. Smith. 1963. Conductance of silver, potassium and lithium nitrates in ethanol-water mixtures. Trans. Faraday Soc. 59:257-267.

Parfitt, R.L. 1979. The nature of the phosphate-goethite (α-FeOOH) complex formed with $Ca(H_2PO_4)_2$ at different surface coverage. Soil Sci. Soc. Am. J. 43:623-625.

Parfitt, R.L. 1989. Phosphate reactions with natural allophane, ferrihydrite and goethite. J. Soil Sci. 40:359-369.

Parfitt, R.L., and R.J. Atkinson. 1976. Phosphate adsorption on goethite (α-FeOOOH). Nature. 264:740-742.

Parfitt, R.L., and J.D. Russell. 1977. Adsorption on hydrous oxides. 4. Mechanisms of adsorption of various ions on goethite. J. Soil Sci. 28:297-305.

Parfitt, R.L., R.J. Atkinson, and R.S.C. Smart. 1975. The mechanism of phosphate fixation by iron oxides. Soil Sci. Soc. Am. J. 39:837-841.

Patrick, W.H., S. Gotoh, and B.G. Williams. 1973. Strengite dissolution in flooded soils and sediments. Science. 179:564-565.

Pearson, R.G. 1963. Hard and soft acids and bases. J. Am. Chem. Soc. 85:3533-3539.

PEN. 2010. The Project on Emerging Nanotechnologies: Nanotechnology consumer products inventory [Online]. Available by Woodrow Wilson International Center for Scholars http://www.nanotechproject.org/inventories/consumer/ (verified 10 July 2012).

Persson, P., N. Nilsson, and S. Sjoberg. 1996. Structure and bonding of orthophosphate ions at the iron oxide-aqueous interface. J. Colloid Interf. Sci. 177:263-275.

Porter, P.S., and C.A. Sanchez. 1992. The effect of soil properties on phosphorus sorption by Everglades Histosols. Soil Sci. 154:387-398.

Praus, P., M. Turicova, and M. Valaskova. 2008. Study of silver adsorption on montmorillonite. J. Braz. Chem. Soc. 19:549-556.

Preedy, N., K. McTiernan, R. Matthews, L. Heathwaite, and P. Haygarth. 2001. Rapid incidental phosphorus transfers from grassland. J. Environ. Qual. 30:2105-2112.

Puls, R.W., R.M. Powell, D. Clark, and C.J. Eldred. 1991. Effects of pH, solid/solution ratio, ionic strength, and organic acids on Pb and Cd sorption on kaolinite. Water Air Soil Pollut. 57-58:423-430.

Rai, M., A. Yadav, and A. Gade. 2009. Silver nanoparticles as a new generation of antimicrobials. Biotechnol. Adv. 27:76-83.

Redfield, A.C. 1958. The biological control of chemical factors in the environment. Am. Sci. 46:230A-221.

Roberts, W.L. 1990. Encyclopedia of Minerals. 2nd ed. Van Nostrand, New York.

Russell, A.D., and W.B. Hugo. 1994. Antimicrobial activity and action of silver. Prog. Med. Chem. 31:351-370.

Ryden, J.C., and J.K. Syers. 1977. Desorption and isotopic exchange relationships of phosphate sorbed by soils and hydrous ferric oxide gel. J. Soil Sci. 28:596-609.

Ryden, J.C., J.K. Syers, and J.R. McLaughlin. 1977. Effects of ionic strength on chemisorption and potential-determining sorption of phosphate by soils. J. Soil Sci. 28:62-71.

Samsung. 2003. SAMSUNG Electronics introduces Korea's first silver sanitation washing machine. Samsung press release. Samsung Electronics Co. Ltd., Suwon, Korea.

Sañudo-Wilhelmy, S.A., and A.R. Flegal. 1992. Anthropogenic silver in the Southern California Bight: A new tracer of sewage in coastal waters. Environ. Sci. Technol. 26:2147-2151.

Sarkar, D., M.E. Essington, and K.C. Misra. 1999. Adsorption of mercury(II) by variable charge surfaces of quartz and gibbsite. Soil Sci. Soc. Am. J. 63:1626-1636.

Schaller, M.S., C.M. Koretsky, T.J. Lund, and C.J. Landry. 2009. Surface complexation modeling of Cd(II) adsorption on mixtures of hydrous ferric oxide, quartz and kaolinite. J. Colloid Interf. Sci. 339:302-309.

Schelde, K., L.W. de Jonge, C. Kjaergaard, M. Laegdsmand, and G.H. Rubaek. 2006. Effects of manure application and plowing on transport of colloids and phosphorus to tile drains. Vadose Zone J. 5:445-458.

Sei, J., J.C. Jumas, J. Olivier-Fourcade, H. Quiquampoix, and S. Staunton. 2002. Role of iron oxides in the phosphate adsorption properties of kaolinites from the Ivory Coast. Clay. Clay Miner. 50:217-222.

Shaheen, S.M. 2009. Sorption and lability of cadmium and lead in different soils from Egypt and Greece. Geoderma. 153:61-68.

Shannon, R.D. 1976. Revised effective ionic radii and systematic studies of interatomic distances in halides and chalcogenides. Acta Crystallogr., Sect. A: Cryst. Phys., Diffr., Theor. Gen. Crystallogr. 32:751-767.

Sharpley, A. 1995. RCA III fate and transport of nutrients: Phosphorus. Working Paper No. 8

Sharpley, A.N., and S. Rekolainen. 1997. Phosphorus in agriculture and its environmental implications, p. 1-53, *In* H. Tunney and O. T. Carton, eds. Phosphorus Loss from Soil to Water. CAB International, Wallingford, UK.

Sharpley, A.N., R.W. McDowell, and P.J.A. Kleinman. 2001. Phosphorus loss from land to water: Integrating agricultural and environmental management. Plant Soil. 237:287-307.

Siemens, J., K. Ilg, F. Lang, and M. Kaupenjohann. 2004. Adsorption controls mobilization of colloids and leaching of dissolved phosphorus. Euro. J. Soil Sci. 55:253-263.

Siemens, J., K. Ilg, H. Pagel, and M. Kaupenjohann. 2008. Is colloid-facilitated phosphorus leaching triggered by phosphorus accumulation in sandy soils? J. Environ. Qual. 37:2100-2107.

Sikora, F.J., and F.J. Stevenson. 1988. Silver complexation by humic substances: Conditional stability constants and nature of reactive sites. Geoderma. 42:353-363.

Silver, S. 2003. Bacterial silver resistance: Molecular biology and uses and misuses of silver compounds. Fems Microbiol. Rev. 27:341-353.

Sims, J.T., A.S. Andres, J.M. Denver, W.J. Gangloff, P.A. Vadas, and D.R. Ware. 1996. Assessing the impact of agricultural drainage on ground and surface water quality in Delaware: Development of best management practices for water quality protection. Delaware Department of Natural Resources and Environmental Control, Dover, Delaware.

Smith, I., and B. Carson. 1997. Silver. Ann Arbor Science Publishers, Ann Arbor, MI.

Snoeyink, V.L., and D. Jenkins. 1980. Water Chemistry. John Wiley & Sons, New York.

Soares, M.R., J.C. Casagrande, and E.R. Mouta. 2009. Effect of ionic strength and pH on cadmium adsorption by Brazilian variable-charge soils. Commun. Soil Sci. Plan. 40:2132-2151.

Sondi, I., and B. Salopek-Sondi. 2004. Silver nanoparticles as antimicrobial agent: A case study on *E. coli* as a model for gram-negative bacteria. J. Colloid Interf. Sci. 275:177-182.

Sparks, D.L. 2003. Environmental Soil Chemistry. 2nd ed. Academic Press, San Diego.

Sposito, G. 2008. The Chemistry of Soils. 2nd ed. Oxford University Press, New York.

Stebounova, L.V., A. Adamcakova-Dodd, J.S. Kim, H. Park, P.T. O'Shaughnessy, V.H. Grassian, and P.S. Thorne. 2011. Nanosilver induces minimal lung toxicity or inflammation in a subacute murine inhalation model. Part. Fibre Toxicol. 8.

Strawn, D.G., and D.L. Sparks. 1999. The use of XAFS to distinguish between inner- and outer-sphere lead adsorption complexes on montmorillonite. J. Colloid Interf. Sci. 216:257-269.

Stumm, W. 1992. Chemistry of the Solid-Water Interface. Processes at the Mineral-Water and Particle-Water Interface in Natural Systems. John Wiley and Sons, New York.

Stumm, W., and J.J. Morgan. 1996. Aquatic Chemistry. 3rd ed. John Wiley & Sons, Inc., New York.

Swartz, C.H., and P.M. Gschwend. 1998. Mechanisms controlling release of colloids to groundwater in a southeastern Coastal Plain aquifer sand. Environ. Sci. Technol. 32:1779-1785.

Tan, S., M. Erol, A. Attygalle, H. Du, and S. Sukhishvili. 2007. Synthesis of positively charged silver nanoparticles via photoreduction of $AgNO_3$ in branched polyethyleneimine/HEPES solutions. Langmuir. 23:9836-9843.

Taylor, R.M., and U. Schwertmann. 1974. Association of phosphorus with iron in ferruginous soil concretions. Aust. J. Soil Res. 12:133-145.

Tejedor-Tejedor, M.I., and M.A. Anderson. 1990. Protonation of phosphate on the surface of goethite as studied by CIR-FTIR and electrophoretic mobility. Langmuir. 6:602-611.

Throbäck, I.N., M. Johansson, M. Rosenquist, M. Pell, M. Hansson, and S. Hallin. 2007. Silver (Ag^{+}) reduces denitrification and induces enrichment of novel nirK genotypes in soil. FEMS Microbiol. Lett. 270:189-194.

Top, A., and S. Ülkü. 2004. Silver, zinc, and copper exchange in a Na-clinoptilolite and resulting effect on antibacterial activity. Appl. Clay Sci. 27:13-19.

Torbert, H.A., and K.N. Potter. 2004. Fertility management effects on runoff losses of phosphorus, p. 220-234 Environmental Impact of Fertilizer on Soil and Water, Vol. 872. American Chemical Society, Washington, DC.

Torrent, J., U. Schwertmann, and V. Barron. 1992. Fast and slow phosphate sorption by goethite-rich natural minerals. Clay. Clay Miner. 40:14-21.

Toy, A.D.F. 1987. Phosphorus Chemistry in Everyday Living. 2nd ed. American Chemical Society, Washington, DC.

USEPA. 1980. Ambient water quality criteria for silver. 440/5-80-071. US Environmental Protection Agency, Washington, DC.

USEPA. 1993. Standards for the use or disposal of sewage sludge 40:503. US Environmental Protection Agency, Washington, DC.

USEPA. 2011. Secondary Drinking Water Regulations: Guidance for Nuisance Chemicals, 816-F-10-079 [Online]. Available by US Environmental Protection Agency http://water.epa.gov/drink/contaminants/secondarystandards.cfm (posted January 2011; verified 16 July 2012).

USGS. 2012. Mineral Commodity Summaries, January 2012. U.S. Geological Survey, Reston, Virginia.

Vairavamurthy, M.A., D. Maletic, S.K. Wang, B. Manowitz, T. Eglinton, and T. Lyons. 1997. Characterization of sulfur-containing functional groups in sedimentary humic substances by X-ray absorption near-edge structure spectroscopy. Energy Fuels. 11:546-553.

Van Emmerik, T.J., D.E. Sandstrom, O.N. Antzutkin, M.J. Angove, and B.B. Johnson. 2007. ^{31}P solid-state nuclear magnetic resonance study of the sorption of phosphate onto gibbsite and kaolinite. Langmuir. 23:3205-3213.

van Riemsdijk, W.H., F.A. Weststrate, and J. Beek. 1977. Phosphates in soils treated with sewage water: III. Kinetic studies on the reaction of phosphate with aluminum compounds. J. Environ. Qual. 6:26-29.

Villaverde, P., D. Gondar, J. Antelo, R. Lopez, S. Fiol, and F. Arce. 2009. Influence of pH on copper, lead and cadmium binding by an ombrotrophic peat. Euro. J. Soil Sci. 60:377-385.

Wang, D.Z., X. Jiang, W. Rao, and J.Z. He. 2009. Kinetics of soil cadmium desorption under simulated acid rain. Ecol. Complex. 6:432-437.

Weiss, R. 2008. Groups petition EPA to ban nanosilver in consumer goods. The Washington Post, 2 May 2008, Washington, DC.

Wen, L.S., P.H. Santschi, G.A. Gill, C.L. Paternostro, and R.D. Lehman. 1997. Colloidal and particulate silver in river and estuarine waters of Texas. Environ. Sci. Technol. 31:723-731.

White, J.M.L., A.M. Powell, K. Brady, and R. Russell-Jones. 2003. Severe generalized argyria secondary to ingestion of colloidal silver protein. Clin. Exp. Dermatol. 28:254-256.

Wigginton, N.S., A. de Titta, F. Piccapietra, J. Dobias, V.J. Nesatyy, M.J.F. Suter, and R. Bernier-Latmani. 2010. Binding of silver nanoparticles to bacterial proteins depends on surface modifications and inhibits enzymatic activity. Environ. Sci. Technol. 44:2163-2168.

Willett, I.R., C.J. Chartres, and T.T. Nguyen. 1988. Migration of phosphate into aggregated particles of ferrihydrite. J. Soil Sci. 39:275-282.

Xia, K., U.L. Skyllberg, W.F. Bleam, P.R. Bloom, E.A. Nater, and P.A. Helmke. 1999. X-ray absorption spectroscopic evidence for the complexation of Hg(II) by reduced sulfur in soil humic substances. Environ. Sci. Technol. 33:257-261.

Xie, F., and D.B. Dreisinger. 2007. Leaching of silver sulfide with ferricyanide-cyanide solution. Hydrometallurgy. 88:98-108.

Xiu, Z.-M., Q.-B. Zhang, H.L. Puppala, V.L. Colvin, and P.J.J. Alvarez. 2012. Negligible particle-specific antibacterial activity of silver nanoparticles. Nano Lett. 12:4271-4275.

Xu, R.K., L.M. Kozak, and P.M. Huang. 2008. Kinetics of phosphate-induced desorption of arsenate adsorbed on crystalline and amorphous aluminum hydroxides. Soil Sci. 173:683-693.

Yao, W., and F.J. Millero. 1996a. Adsorption of phosphate on manganese dioxide in sea water. Environ. Sci. Technol. 30:536-541.

Yao, W.S., and F.J. Millero. 1996b. Adsorption of phosphate on manganese dioxide in seawater. Environ. Sci. Technol. 30:536-541.

Yin, Y.J., H.E. Allen, Y.M. Li, C.P. Huang, and P.F. Sanders. 1996. Adsorption of mercury(II) by soil: Effects of pH, chloride, and organic matter. J. Environ. Qual. 25:837-844.

Yuan, S.H., Z.M. Xi, Y. Jiang, J.Z. Wan, C. Wu, Z.H. Zheng, and X.H. Lu. 2007. Desorption of copper and cadmium from soils enhanced by organic acids. Chemosphere. 68:1289-1297.

Zachara, J.M., and S.C. Smith. 1994. Edge complexation reactions of cadmium on specimen and soil-derived smectite. Soil Sci. Soc. Am. J. 58:762-769.

Zamuner, E.C., L.I. Picone, and H.E. Echeverria. 2008. Organic and inorganic phosphorus in Mollisol soil under different tillage practices. Soil Till. Res. 99:131-138.

Zhang, M.K. 2008. Effects of soil properties on phosphorus subsurface migration in sandy soils. Pedosphere. 18:599-610.

Zhao, G.J., and S.E. Stevens. 1998. Multiple parameters for the comprehensive evaluation of the susceptibility of *Escherichia coli* to the silver ion. Biometals. 11:27-32.

Table 1.1. Common phosphate minerals

Mineral	Chemical Formula
Fluorapatite	$Ca_{10}(PO_4)_6F_2$
Chlorapatite	$Ca_{10}(PO_4)_6Cl_2$
Hydroxapatite	$Ca_{10}(PO_4)_6(OH)_2$
Brushite	$CaHPO_4 \cdot 2H_2O$
Monetite	$CaHPO_4$
Whitlockite	$Ca_3(PO_4)_2$
Berlinite	$AlPO_4$
Variscite	$AlPO_4 \cdot 2H_2O$
Augelite	$Al_2PO_4(OH)_3$
Crandallite	$Al_3Ca(PO_4)_2(OH)_5 \cdot 2H_2O$
Millisite	$Al_6NaCa(PO_4)_4(OH)_9 \cdot 3H_2O$
Wavellite	$Al_3(OH)_3(PO_4)_2 \cdot 5H_2O$
Strengite	$FePO_4 \cdot 2H_2O$

Table 1.2. Point of zero charge of common soil minerals

Mineral	Point of Zero Charge	Specific Surface Area ($m^2 g^{-1}$)
Kaolinite	7.3-7.8[a]	7-30
Montmorillonite	2.5	600-800
Muscovite	2-3[b]	60-100
Chlorite	3[c]	25-150
Allophane	6-7[d]	100-800
Aluminum oxides	9.1	100-220[e]
Iron oxides	6.5-6.7	70-250[e]
Manganese oxides	2.8-7.2	5-360[e]

a. Goldberg and Glaubig, 1987; b. Stumm and Morgan, 1996; c. Hussain et al., 1996; d. Gustafsson, 2001; e. Kämpf et al., 2000

Table 1.3. Shared charge of several anions

Oxyanion	Formula	Shared charge
Silicate	SiO_4^{4-}	3/4 = 0.75
Hydroxyl	OH^-	1/1 = 1.0
Phosphate	PO_4^{3-}	5/4 = 1.25
Arsenate	AsO_4^{3-}	5/4 = 1.25
Carbonate	CO_3^{2-}	4/3 = 1.33
Sulfate	SO_4^{2-}	6/4 = 1.5
Nitrate	NO_3^-	5/3 = 1.67

Table 1.4. Hard and soft acids and bases, reproduced from McBride, 1994.

Classification	**Acids**	**Bases**
Hard	H^+, Li^+, Na^+, K^+, Mg^{2+}, Ca^{2+}, Mn^{2+}, Fe^{3+}, Al^{3+}	NH_3, R–NH_2 (amines), H_2O, OH^-, O^{2-}, R–OH (alcohols), NO_3^-, PO_4^{3-}, SO_4^{2-}
Borderline	Fe^{2+}, Ni^{2+}, Cu^{2+}, Zn^{2+}, Pb^{2+}	aromatic amines, NO_2^-, SO_3^{2-}
Soft	Cu^+, Ag^+, Cd^{2+}, Hg^+, Hg^{2+}, Tl^+	CN^-, CO, S^{2-}, R–SH (sulfhydryl), R–S^-

Table 1.5. Common silver minerals

Mineral group	Examples	Chemical formula
Elemental silver	Amalgam	Ag,Hg (not fully characterized)
	Goldamalgam	(Au,Ag)Hg
Halides: Chlorargyrite group	Bromargyrite	AgBr
	Chlorargyrite	AgCl
	Iodargyrite	AgI
	Miersite	(Ag,Cu)I
Pnictides	Allargentum	$Ag_{1-x}Sb_x$
	Dyscrasite	Ag_3Sb
Selenides	Eucairite	AgCuSe
	Naumannite	Ag_2Se
Sulfates: Jarosite group	Argentojarosite	$AgFe_3(SO_4)_2(OH)_6$
Sulfides: Argentite group	Aguilarite	β-Ag_4SeS
	Argentite	Ag_2S
	Acanthite	β-Ag_2S
Argyrodite group	Argyrodite	Ag_8GeS_6
	Canfieldite	$Ag_8(Sn,Ge)S_6$
Pearceite group	Polybasite	$(Ag,Cu)_{16}Sb_2S_{11}$
	Pearceite	$Ag_{16}As_2S_{11}$
Proustite group	Proustite	Ag_3AsS_3
	Pyargyrite	Ag_3SbS_3
Tetrahedrite group	Freibergite	$(Ag,Cu,Fe)_{12}(Sb,As)_4S_{13}$
Other sulfide minerals	Argentopyrite	$AgFe_2S_3$
	Sternbergite	$AgFe_2S_3$
	Miargyrite	$AgSbS_2$
	Samsonite	$Ag_4MnSb_2S_6$
	Smithite	$AgAsS_2$
	Stephanite	Ag_5SbS_4
	Stromeyerite	AgCuS
Tellurides	Empressite	AgTe
	Hessite	Ag_2Te
	Stützite	$Ag_{5-x}Te_3$

(Day, 1964; Emsley, 2001; Goldschmidt, 1958; Roberts, 1990)

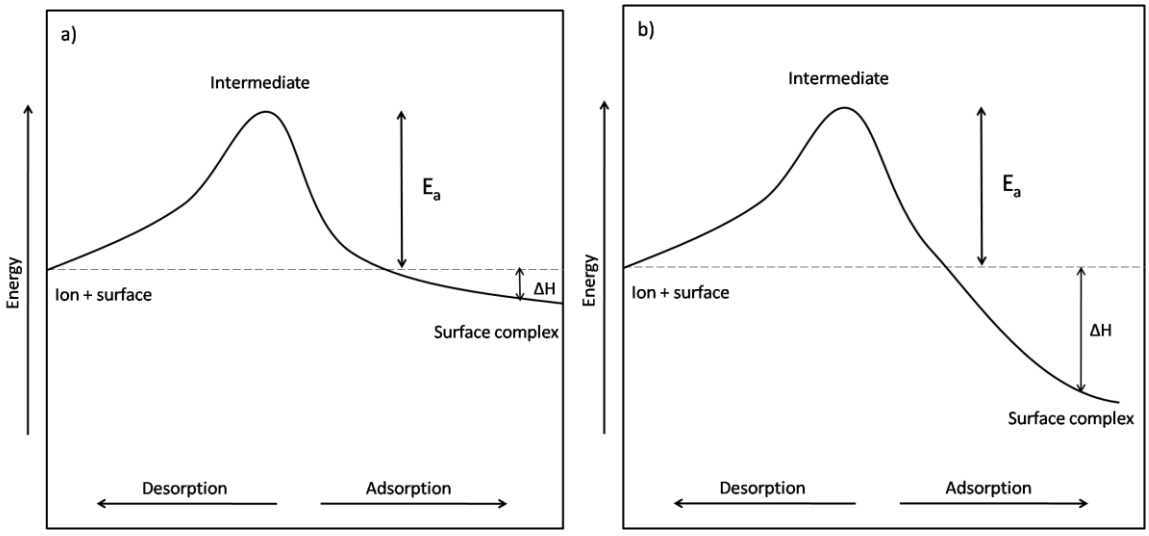

Figure 1.1. Differing energy profiles for: a) an easily reversible soil complex, and b) an almost irreversible soil complex (McBride, 1994).

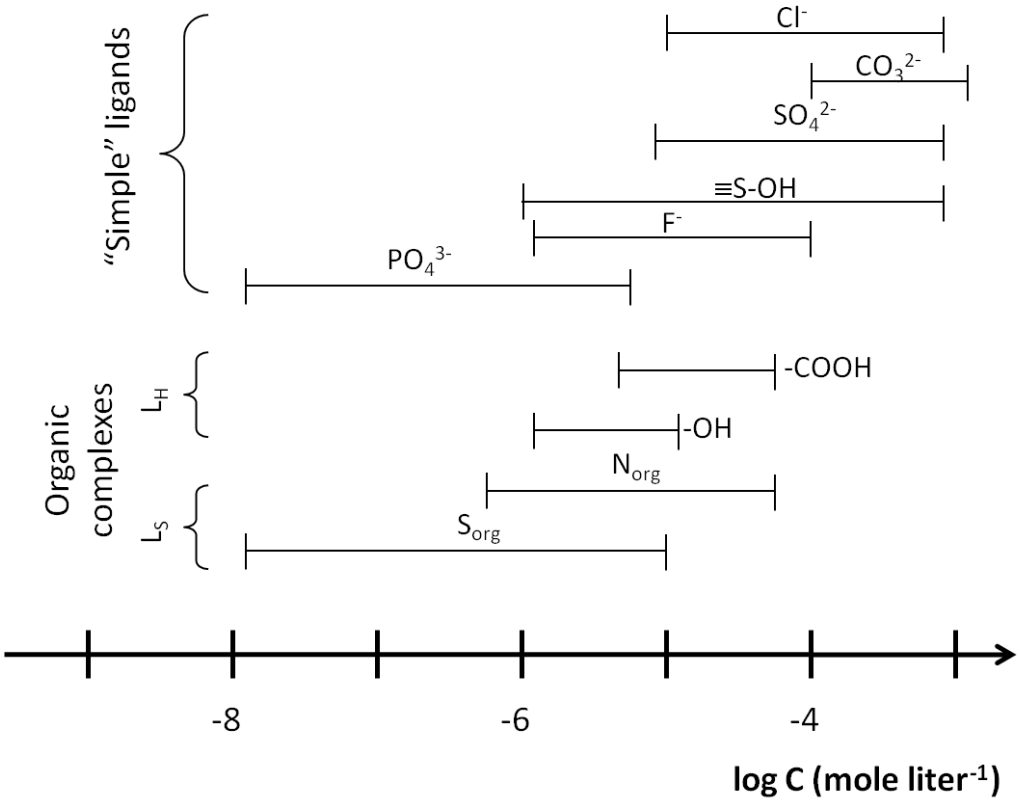

Figure 1.2. Concentration of common ligands in natural waters. Reproduced after Buffle (1984).

CHAPTER TWO

ROLE OF NATURAL NANOPARTICLES IN PHORPHORUS TRANSPORT PROCESSES IN ULTISOLS

2.1 Abstract

Labile phosphorus (P) is a well-recognized non-point source pollutant in agro-ecosystems. Predicting the fate and transport of P in watershed systems is critical in protecting water quality. In this case study, we investigated the role of soil nanoparticles in P release in South Carolina (SC) agricultural soils. Batch desorption experiments were coupled with scanning and transmission electron microscopy (SEM and TEM, respectively), and X-ray absorption spectroscopy (XAS) to better assess the reactivity of soil nanoparticles. The surface soils contain a total P concentration of 260 – 940 mg/kg, approximately 40 – 60% of which is ammonium oxalate extractable P. The 30 day desorption experiments showed that P desorption was initially rapid followed by a slow continuous release at pH 5.5 and 7. It was generally not correlated with the release of soil nanoparticles (operationally defined as 10 – 200 nm). Phosphorus was not readily retained on these nanoparticles at pH 4 – 7. These nanoparticles are rich in Si and S, and coated with Fe and C, and trace amounts of P, Ca, Na, Mg, and Al. The SEM images of nanoparticle morphology showed C-associated globular formations as well as assembled platelets and spherical nanoparticles. The colloid/nanoparticle facilitated P release has been often suggested as one of the important pathways for P transport in the soil-water

environment. However, this study presents a new aspect of nanoparticle reactivity in the soil environment: nanoparticles do not always contribute to the P transport processes.

2.2 Introduction

In the last several decades, excess labile P has been recognized as a point and non-point source pollutant throughout the United States due to long-term anthropogenic inputs such as industrial effluents and fertilizers (Abrams and Jarrell, 1995; Carpenter et al., 1998; Sharpley et al., 2001). Non-point P pollution impacts freshwater and seawater biogeochemical cycles. Eutrophication caused by large-scale P mobility causes problems in water supplies due to over-growth of algae and cyanobacteria and their resulting decomposition, which leads to a dissolved oxygen shortage (Lewitus et al., 2003). Exposure to and consumption of cyanobacteria contaminated water can be a serious health hazard to livestock and humans (Lawton and Codd, 1991). Over the last decade, harmful algal blooms by *Pfiesteria* spp. and *Kryptoperidinium* spp. have been discovered in SC coastal waters and estuaries from Georgetown to Hilton Head (Lewitus et al., 2002). These microscopic organisms produce toxins, killing various lower marine organisms (e.g., fish and crustaceans), and are also known to cause negative health symptoms in humans (Burkholder and Glasgow, 1997; Glasgow et al., 1995; Kempton et al., 2002). Given their widespread distribution and potential to adversely affect shellfish, the ecological and economic impacts of these blooms may be considerable in SC coastal water quality.

The P accumulation issue in SC agricultural soils was recently evaluated by our research group using the archive of soil testing data (over 360,000 soil samples) from 1997 to 2006. These data were provided by the Clemson Agricultural Service Laboratory. Approximately 55 – 62 % of SC soils have excess P (not requiring any P fertilization, and may act as sources of P water pollution) in all four regions of the state (Piedmont, Sandhill, Coastal Plain, and Lower Coastal Plain). Soils from the Lower Coastal Plain contain the largest excess. Several historic factors have contributed to the P accumulation in soils, including: (1) a long term amendment of "3-9-9" fertilizer, and (2) a lack of nutrient and land management in the last 30 years. Poultry litter application on agricultural soils remains a major source of soil P. Unfortunately, the distribution of poultry industry operations overlaps with the Savannah, Edisto, and Pee Dee River watersheds in SC. P runoff and leacheate from poultry operations could directly feed into these river watersheds, causing negative current and future impact on inland and coastal waters.

Predicting the fate and transport of P in SC coastal and inland watersheds is critical in protecting the water quality for SC citizens. Thus far, the molybdenum reactive P (MRP) concentration has been considered to be labile P, and used to predict the P transport processes. Phosphorus saturation index (SI), field scale runoff studies and many sorption/desorption laboratory studies have been established using the MRP value (Delgado and Torrent, 2001; Koopmans et al., 2006). However, recent research evidence suggests that nano- and/or colloidal-soil particulates in soil solutions could mask the MRP values in soil solution and in pore waters. The environmental role of these small

particles might be important in nutrient transport processes in aquatic and terrestrial environments (Kretzschmar et al., 1999). Colloid or nanoparticle facilitated transport generally requires that the contaminants be sorbed strongly onto the mobile small particles and desorb relatively slowly. These particles may then act as a vehicle for the transport of P particles to make their way through soils and into surface waterways (Heathwaite et al., 2005; Hens and Merckx, 2001). In this way, the small particles act as a mobile fraction of the solid phase of soil, and may even experience accelerated transport due to preferential flow in water systems (de Jonge et al., 2004a). Makris et al. (2006) found that colloids dispersed in the soil solution accounted for a good deal of the vertical subsurface flow of P. Additionally, they found that adding colloids to an agricultural soil resulted in an increase of MRP in the effluent (Makris et al., 2006).

In a field scale study, de Jonge et al. (2004b) found that approximately 75% of P was transported by colloids <0.24 µm. Also, Haygarth et al. (1997) found a large difference between the amount of MRP in filtrates at <0.45 µm and <0.10 µm. They also found that colloidal organic macromolecules may not be carriers of dissolved P, but inorganic materials, such as the products of mineral weathering, may play an important role (Haygarth et al., 1997). Others also reported dissolved P as MRP in association with inorganic colloidal particles (Bauer et al., 1996; Filella et al., 2006; Hens and Merckx, 2002). Many factors seem to influence the amount of P retained by these colloids, including their chemical composition and relative size (Filella et al., 2006).

Particles less than 0.45 µm are typically defined as dissolved (USEPA, 1983), and are, therefore, viewed as existing as a part of the soil solution. In reality, there is no

natural cutoff point between particulate and dissolved matter (Heathwaite et al., 2005). Some solid organic and inorganic forms of P may be present in the <0.45 μm solution (De Hann et al., 1984). Based on the previous research findings, we hypothesized that soil nanoparticles and/or colloids contribute to the P transport process in SC agricultural soils. We are especially interested in understanding the P-associated nanoparticle fraction, operationally defined as 10 – 200 nm, in soil solutions. Due to the iron oxyhydroxide rich mineralogy of Ultisols such as those in SC, it is possible that iron dominated nanoparticles (e.g., nano(n)-goethite, n-ferrihydrite and n-hematite) could serve as carriers for dissolved P in soil solutions.

In this study, we investigated the role of soil nanoparticles in P transport process in agricultural surface soils. Temporal effects on the nanoparticle facilitated P release were evaluated using batch desorption experiments. Physicochemical characterization of P-rich nanoparticles and soils were accomplished using chemical extraction, Fe K-edge XAS, and electron microscopy analysis.

2.3 Materials and Methods

2.3.1 Soil Descriptions and Characterization

Three long-term poultry litter amended (1 – 2 ton/acre·yr) top soils (0 – 20 cm) were collected from three watersheds in SC. These sites have been cultivated for over three decades. The soil samples were collected from well-drained soils: Cecil (CC) sandy loam (fine, kaolinitic, Typic Kanhapludults) and Lloyd (LD) sandy loam (fine, kaolinitic, thermic Rhodic Kanhapludults); and the moderately well-drained soil Goldsboro (GB)

sandy loam (fine-loamy, siliceous, thermic Aquic Paleudults). The soil samples were air-dried and passed through a 2 mm sieve prior to physicochemical analysis. The effects of air-drying on colloid dispersivity has been documented in the literature (e.g., Kjaergaard et al., 2004); considering the constant fluctuation of moisture content in agricultural surface soils, air drying the soils might stimulate environmental conditions.

Soil pH_{water} was determined using a soil/deionized water ratio of 1:1. Cation exchange capacity (CEC) was determined with an extraction method using unbuffered salt (Grove et al., 1982). To assess the agronomic soil P values in acidic, low CEC, SC soils, the Mehlich-1 extraction was used (Mehlich, 1978). Due to the Fe-rich nature of SC soils, we conducted sequential Fe oxyhydroxide extractions. An ammonium oxalate [$(NH_4)_2C_2O_4$] extraction was first performed in darkness to remove P associated with amorphous Fe from the soil samples (e.g., P sorbed ferrihydrite) to be measured (Loeppert and Inskeep, 1996). In this process, 0.5 g samples of soil were extracted in duplicates. The same set of samples was next placed through the dithionite-citrate-bicarbonate (DCB) extraction method, which was to sequentially extract P associated with crystalline Fe oxide fractions such as hematite and goethite (Mehra and Jackson, 1960). The supernatant from each extraction was saved for elemental analysis (P, K, Ca, Mg, S, Mn, Cu, Pb, Cr, Ni, Zn, Al, and Fe) using inductively coupled plasma atomic emission spectroscopy (ICP-AES).

2.3.2 Long-Term Phosphorus Desorption Experiments

We used two different desorption techniques to investigate the role of nanoparticles on dissolved P in soil solutions: batch and replenishment desorption methods. While the batch method keeps all reaction products in soil solutions, the replenishment method remove all reaction products at each sampling period. We expect to observe much greater release of nanoparticles and P in the replenishment method.

First, a batch method (suspension density 33 g/L, pH values 5.5 and 7, 22 ± 1^{o} C, and ionic strength (*I*) 0.065 M adjusted with $NaNO_3$) was used to investigate the P and nanoparticle desorption over 30 days. All experiments were conducted in duplicate tubes. To simulate the field pH before and after lime addition, pH values of 5.5 and 7 were chosen and controlled with organic buffers: 30 mM of 2-(N-morpholino)-ethanesulfonic acid (MES) and 3-(N-Morpholino)-2-hydroxypropanesulfonic acid (MOPSO) for pH 5.5 and pH 7, respectively. One gram of soil was used in 30 ml of solution. Samples were desorbed with P-free solutions containing 0.05 M $NaNO_3$ and 30 mM organic buffers, resulting in I = 0.065 M. No antimicrobial agents (e.g., sodium azide) were added. The soil suspensions were shaken on an end-over-end shaker at 20 rpm at 22 ± 1^{o} C for the duration of the experiment. Samples of 20 mL were analyzed for dissolved P and P-associated nanoparticles at each time point. No tubes were vented until the sampling time; however, the redox potential never reached <184 eV, which indicates that P release due to Fe reduction would be unlikely.

The particle size of nanoparticles is operationally defined using the following filtration and centrifugation methods. Soil suspensions were passed through 0.2 μm

polyvinylidene fluoride (PVDF) filters to obtain results on the total P present in the system. These same samples were then spun in an ultra-high-speed (UHS) centrifuge at 300,000 x *g* for 25 min to separate all nanoparticles > 10 nm. This, inclusively, is our operationally defined nanoparticle size of 10 – 200 nm. All nanoparticles were saved in suspensions for electron microscope and XAS analysis described below. Due to the use of the organic buffers MES and MOPSO, ICP-mass spectrometry (MS) was used to analyze the total dissolved P and other trace elements (e.g., Al and Fe). Scandium was used as an internal standard.

Second, the replenishment batch desorption experiments were conducted under the following reaction condition: suspension density 33 g/L, pH values 5.5 and 7 and I = 0.015 M. No additional electrolytes besides organic buffers (30 mM of MES and MOPSO) were added to facilitate the release of P and nanoparticles from soils. One gram of soil was introduced in 30 ml of P-free solution. Tubes were shaken at 20 rpm at 22^{o}C ±1 on an end-over shaker. At each sampling period, samples in 50 ml polycarbonate high-speed centrifuge tubes were centrifuged at 5045 x *g* for 10 min. The supernatant was decanted to recover the paste. The samples were re-suspended in 30 ml of P free desorption solutions at the same pH (5.5 or 7). The extraction procedures were repeated 5 times, at 1, 3, 7, 15, and 30 days. The separation of nanoparticles and dissolved P was employed using the same filtration and centrifugation method described above. The supernatants were analyzed for P and trace metals using ICP-MS.

2.3.3 Buffering Capacity Analysis on Soil Nanoparticle Suspensions

Soil-water solutions of LD, CC, and GB were prepared by shaking air dry soil samples (50 g) in 1 L of distilled deionized water for overnight. It is important to mention that no dispersion agent was used since we were interested in characterizing the soil nanoparticles in the natural state. The sedimentation method was used to separate the clay fraction from the rest. The clay suspensions were passed through 0.2 μm filters to collect the soil nanoparticles suspensions. In 20ml samples of suspensions, 10 – 300 μL of 0.1 – 1 M HNO_3 or NaOH was added to provide desired pH values. Tubes were shaken at 20 rpm on an end-over-end shaker overnight. After 24 hours, pH was measured in each sample.

2.3.4 Phosphorus Retention/Release in Soil Nanoparticles

Phosphorus retention in nanoparticles was investigated over the environmentally relevant pH values (4 – 7). The objective of this experiment is to understand the release of P from nanoparticles when nanoparticle suspensions at mildly acidic pH levels are transported into aquatic environments at near neutral pH. We used the same soil nanoparticle suspensions from the previous buffering capacity experiments. The pH of soil nanoparticles suspensions was adjusted using 0.1 to 1 M HNO_3 or NaOH. The suspensions were allowed to shake overnight on an end-over-end shaker at 20 rpm, and pH was measured after 24 hours. All samples were spun at 300,000 x *g* for 25 minutes using the UHS centrifuge. The nanoparticle suspensions and the supernatant of centrifuged samples were analyzed for P, Al, and Fe using ICP-MS. Prior to analysis, 2%

Suprapur HNO_3 (EM Science, Gibbstown, New Jersey) was added to each sample (volume ratio of sample to acid = 1:1) and allowed to equilibrate overnight. Due to the ^{40}Ar interference for Ca detection in ICP-MS analysis, we measured dissolved Ca concentration in selected desorption samples using ICP-AES.

2.3.5 Electron Microscopy Analysis

Soil nanoparticles collected from pellets formed by USH centrifugation in the desorption experiments were sonified, then placed on copper grids for viewing. Nanoparticles collected from across all desorption timepoints were combined for microscopy analysis. Scanning and transmission electron microscopy (SEM and TEM, respectively) was utilized for all three soil nanoparticle suspensions that were collected during the batch desorption study. Samples were examined uncoated. A scanning transmission electron microscope (STEM) Hitachi HD2000 outfitted with Oxford INCAEnergy energy dispersive X-ray spectroscopy (EDS) was utilized in SEM mode for some imaging, as well as chemical identification of nanoparticles. Quantitative analysis of elements (e.g., P, Ca, Fe, and Al) and the spatial distribution were evaluated in EDS elemental maps and spectra. A TEM-Hitachi H7600T was used for advanced imaging, as it provided higher resolution images.

2.3.6 Nanoparticle Characterization

Particle size was determined using a Wyatt Dawn Heleos-II particle separation system in batch mode. Baseline data were established using MilleQ water. Baseline and

all samples were read continuously for 5 minutes. Data were analyzed with ASTRA V software by Wyatt Technology. Approximately 25 ml of soil nanoparticle suspensions were analyzed for total organic carbon (TOC) through the acidify and sparge method using a Shimadzu TOC-5000A with high sensitivity catalyst.

2.3.7 Fe-K-edge X-ray Absorption Spectroscopic Analyses

All XAS sample preparation was carried out using the filtration and centrifugation methods described above. Due to extremely low suspension density of GB sample, it was not used for the XAS analysis. Samples were loaded in polycarbonate sample holders and sealed with Kapton tape (CHR Industries). Room temperature Fe K edge (7112 eV) fluorescence spectra were collected at beamline 4-1 at the Stanford Synchrotron Radiation Laboratory, Menlo Park, California, USA, using a Canberra 13-element Ge detector array equipped with a 3μx Mn filter. The spectra were collected in 0.5 to 10 eV steps between the pre-edge to extended regions. As an internal standard, a Fe foil, was run simultaneously with adsorption samples to check for potential energy shifts during the run. XAS data reduction and analyses were performed with SIXPACK/IFEFFIT interface (Webb, 2005) using the procedures described previously (Arai et al., 2004). The FEFF702 code reference was utilized to calculate single scattering theoretical spectra and phase shifts for Fe-O and Fe-Fe backscatters using an input file based on the structural refinement of hematite. During fitting, the values of coordination number (CN) and interatomic distance (R) of the Fe-O and Fe-Fe shells were allowed to vary, as well as a single E_0 for all sets of backscattering atoms. The Debye-Waller factors (σ^2) and CN of

the Fe-O/Fe/Si shells were floated unless otherwise mentioned. Errors of CN and R for the Fe-O/Fe shells were estimated by comparison of the extended X-ray absorption fine structure (EXAFS) fit results to the values given by O'Day et al. (2004). The accuracies were ± 12 % for R: Fe-O/Fe-Fe, ±10 % for CN: Fe-O, and ± 28 % for CN: Fe-Fe.

2.4 Results and Discussion

2.4.1 Physicochemical Characterization of Soils

Tables 2.1, 2.2, and 2.3 show the results of physiochemical characterization of three soils. All soils have sandy loam texture. Soil pH ranged from strongly (LD; 5.32) to moderately acidic (CC: 5.69) and (GB: 5.52) (Table 2.1). In all soils, cation exchange capacity was low (6.8 to 12.3 $cmol_c/kg$), as is typical of Ultisols (Kang et al., 1999; Karathanasis et al., 1986; Ludwig et al., 2001). Calcium was a dominant exchangeable cation in all. Quartz was found in sand and silt fractions of all soils. A major clay mineral was kaolinite in LD and CC, and the GB clay fraction did not have a predominance of any one clay mineral (Table 2.1).

The results of microwave digestion show a wide range of elemental and nutrient concentration (Table 2.2). While total P was nearly 900 mg/kg in CC and LD, only 263 mg/kg of P was measured in GB. Potassium, Ca, Mg, and S were highest in LD and followed by CC and GB. Manganese was a metal that showed its highest concentration in CC soil (720 mg/kg), and lowest in LD soil (19 mg/kg). The rest of trace metals (e.g., Cu, Pb, and Cr) were present in much lower concentrations (<50 mg/kg). Table 2.3 shows the results of Mehlich-1, ammonium oxalate, and DCB extractions. Al_{DCB} and Fe_{DCB} indicate

only crystalline forms due to the sequential extraction method (Table 2.3). Mehlich-1 extractable P was highest in LD, followed by CC and GB. The similar trend was seen in total P in Table 2.2. However, the P_{ox} values in CC were as high as in LD (370 – 490 mg/kg), followed by GB. These values correspond to 40 – 60% of total P in these soils. It is likely that P minerals such as apatite became soluble in acid solutions in microwave digestion and Mehlich 1 extraction (0.05N HCl and 0.025N H_2SO_4). Dithionite-citrate-bicarbonate extractable P was nearly 20 – 30% of total P in all soils. The high DCB extractable Fe concentration supports the presence of goethite and hematite in these weathered Ultisols. Overall, ammonium oxalate and DCB extractions indicate that P was predominantly associated with amorphous Fe and Al fractions, although the fractions of amorphous Fe and Al are low with respect to total Fe (2 – 15%) and total Al (2 – 5%).

2.4.2 Electron Microscopy Analysis

Figure 2.1 shows SEM images of soil nanoparticles (Figures 2.1a, 2.1d, 2.1g, and 2.1i), EDS spectra (Figures 2.1b, 2.1e and 2.1h), and TEM images (Figures 2.1c and 2.1f). We investigated 10 nanoparticles in each sample, and the results for each sample are consistent with the data presented in Figure 2.1. The particles range in size between approximately 400 – 600 nm, which is greater than the pore size of the filters (200 nm) that we used. This is probably due to the agglomeration of nanoparticles during the UHS centrifugation. It is important to mention that we did not observe any pure iron oxyhydroxide, Fe/Al phosphate or layered silicate phases in these three soil nanoparticle samples.

In the LD sample, a tricolor map of Si, C, and P is shown (Figure 2.1). Carbon coatings on a Si rich particle seem to retain P. However there is no noticeable concentration of P in the EDS analysis, suggesting that P is retained as sorbed rather than as precipitates. The distribution of Fe was at the upper edge of particles near carbon coatings (not shown). The major elemental composition is Si, followed by Mg, Ca, Na, Al, K, Ca, and Fe (Figure 2.1b). The TEM image of a LD particle (Figure 2.1c) displays the three distinct morphologies documented. Plate-like flat particles were surrounded by globular and fibrous matters. These particle morphologies of C rich materials are similar to the observation reported in the study by Myneni et al. (1999).

In the CC sample, a bicolor map of P and Fe is shown (Figure 2.1d). While P is distributed throughout the entire particle, Fe appeared as 10 – 20 nm nano-sized spherical dots (red dots in Figure 2.1d). The semi-qualitative analysis of P indicated approximately 4.53% by wt, suggesting that P might be present as precipitates. Considering that the major elemental composition is Si, (Figure 2.1e), the solid phase P is probably present as coatings on the Si rich particle. The minor elements are Mg, Ca, Na, Al, K, and Ca as seen in the LD sample. The TEM image (Figure 2.1f) clearly displays a globular particle that is an assemblage of several nanoparticles. The EDS spectrum of a CC sample shows the particles primary consists of Si and Ca with several minor concentrations of Mg, Na, and Al.

In the GB sample, it is clearly seen that Fe and C appear as coatings on Si rich particles (Figure 2.1g). The spatial distribution of Al was always within the core of particles with Si (not shown). The distribution of P on the particle was too low to show in

the XRF image. Unlike the other two samples, the GB sample contains high S, followed by Al, Si, and Fe (Figure 2.1h). The SEM image of GB particles shows many nanoparticles that are cemented forming a large cluster (Figure 2.1i).

Although there are variations in spatial distribution and elemental concentration, all particles contain Al and some Fe. The electron diffraction patterns indicated that all particles are amorphous (data not shown). Based on the low P counts (<1% wt) in these samples, P is likely to be present in sorbed phases except for in the CC sample. The CC sample contains ~4% P by wt, suggesting the presence of a solid phase P. We will use Fe and Al as markers of soil nanoparticles in the desorption study. Si will not be used as a maker because 1) Si can be interfered by the masses of O + C or N + N in the ICP-MS analysis, and 2) Si was not a dominant element in the GB sample.

2.4.3 Nanoparticle Characterization

Particle size varies slightly between samples. CC had the largest average particle size at 381.64 nm (standard deviation = 93.79 nm), while LD and GB had the smallest average particle sizes at 189.55 nm (standard deviation = 87.96 nm) and 172.35 nm (standard deviation = 37.22 nm), respectively. Aggregation is probably occurring in these samples, especially CC, since its average particle size was larger than the filter pore size. Electron microscope data, both of UHS centrifuged pellets and of whole samples, indicate that aggregation does occur in all samples.

Total organic carbon and nitrogen (TON) were both highest in the LD sample: 30.2 mg/L and 6.9 mg/L, respectively. Samples from CC also had relatively high

amounts, with 19.2 mg/L TOC and 6.9 mg/L TON. The smallest values were from GB, with 6.6 mg/L TOC and 1.1 mg/L TON.

2.4.4 X-ray Absorption Spectroscopy Analysis

The raw and fitted k^3-weighted χ functions for reference iron oxyhydroxides and soil nanoparticles are shown in Figure 2.2a. The corresponding radial structure functions (RSFs), obtained by Fourier-transformation of the χ functions, are shown in Figure 2.2b. It is clear that spectra of our sample soil nanoparticles are dissimilar to the reference spectra of iron oxyhydroxides, suggesting no pure nano-iron oxyhydroxide phases are present in these soil nanoparticles, which agrees with the previous (S)TEM observation.

The EXAFS spectra of second, third, and forth coordination shells are shown with interatomic distances in Table 2.4. In all spectra, the EXAFS are dominated by back-scattering from an O first-shell at 1.9Å in the RSF (uncorrected for phase shift), with additional contributions from 2 – 3 smaller shells at 2 – 4 Å (R + Δ Å). The fit for the reference iron oxyhydroxides agrees with the results reported in the previous literature (Combes et al., 1990; O'Day et al., 2004) as well as published X-ray diffraction data (Blake et al., 1966; Szytula et al., 1968). In goethite, we observed the interatomic distances of several Fe octahedral linkages. They are at 3.04 Å (corner sharing), 3.27 Å (face sharing), and 3.4 Å (corner sharing). In hematite, there are two Fe-Fe distances at 2.96 Å and 3.33 Å corresponding to edge sharing and corner sharing distances, respectively. In ferrihydrite, face-, edge- and corner-sharing Fe-Fe distances are observed at 2.88 Å, 3.03 Å, and 3.42 Å, respectively.

In the LD soil nanoparticles, there is a distinct Fe-Si shell at 3.25 Å. The similar interatomic distance has been reported in Fe k-edge XAS study on smectite and nontronite by O'Day and co-workers (2004). However, the overall fit was not similar to the structural parameters of smectite and nontronite, suggesting these phlyllosilicates are not present. The association of Fe with Si can be supported by our (S)TEM/EDS analysis shown in Figures 2.1a and 1b. CC soil nanoparticles contain not only the Fe-Si shell at ~3.2 Å but also two Fe-Fe distances at ~3.2 Å and 3.4 Å that correspond to face- and corner-sharing, respectively. The EXAFS analysis adds new information about the different Fe-Fe/Si coordination environment that the (S)TEM and EDS analysis could not reveal.

2.4.5 Phosphate and Nanoparticle Desorption Experiments

Figure 2.3 shows the results of batch P desorption experiments of soil nanoparticles. Each soil sample was desorbed at pH 5.5 and 7. The change in pH was minimal over 30 days (+/- 0.1 pH units) due to the use of organic buffers. The electrical conductivity (EC) values remain at ~3.0 using the empirical equation developed by Griffin and Jurinak (1974) based on I ($I = 0.0127EC_W$).

To distinguish "dissolved P" from "P associated nanoparticles", an UHS centrifugation method was used to separate the operationally defined nanoparticles (10 – 200 nm). In all figures, filled and open symbols represent total and dissolved concentration, respectively. If P is associated with nanoparticles, one should observe a large decrease in [P] after the UHS centrifugation. We also track the concentration of Fe

and Al as markers of nanoparticles. The previous (S)TEM analysis indicated that all soil nanoparticles contain Fe and or Al. The effect of centrifugation and pH on P, Al, and Fe desorption was summarized below.

In most cases, the release of P increases with increasing time (Figure 2.3). The concentration of dissolved P ranges from 340 – 2750 μg/L. The release of P in the three samples did not significantly change before and after the UHS centrifugation in each experiment. Although there are a few variations at later sampling periods (e.g., 30 days; LD, CC, and GB at pH 7), the total and dissolved P concentrations are within ±15%. The differences in elemental concentration before and after UHS centrifugation were much more pronounced for Fe and Al than for P. Specifically, the P concentration was, on average, 27 μg/L (range of differences = -204 to 342 μg/L) higher before UHS centrifugation than after (Figures 2.3a – 2.3f). In contrast, Fe and Al concentrations were, on average, 745 μg/L (range = 13 to 2534 μg/L) and 1190 μg/L (range = 111 to 5831 μg/L) higher before UHS centrifugation than after, respectively (Figures 2.3g – 2.3r). These averages include data across all samples and time points (1 to 30 days) for each element. While some P may be present as particulate matter, it appears that the majority of it did not settle under the centrifuged conditions. This suggests that 1) the majority of P is dissolved in solution and 2) the majority of Al and Fe was present as nanoparticles (10 – 200 nm).

The effect of pH can be clearly observed in the Fe and Al data in all samples (Figures 2.3g – 2.3i). All soils showed drastic differences in Fe and Al content by pH; Fe and Al was much more abundant in the samples at pH 7 than at pH 5.5 (e.g., filled

symbols in Figures 2.3o and 2.3p). The colloids and nanoparticles in LD, CC, and GB samples are primarily composed of ferric oxyhydroxides and SiO_2. Zhang et al. (2009) reported a negative zeta potential of n-SiO_2 and ferric oxyhydroxides at a mildly acidic pH. These charged properties should cause the repulsion from negatively charged soil mineral surfaces at pH 7, which results in an enhanced release of Fe and Al (Figures 2.3h, 2.3j, 2.3l, 2.3n, 2.3p, and 2.3r). An increased Fe and Al release might also be attributed to the formation of metal oxyhydroxides. Using the reaction conditions and dissolved [Fe] and [Al] values (i.e., open symbols in Figures 2.3h, 2.3j, 2.3l, 2.3n, 2.3p and 2.3r), ion activity product calculations were employed using the chemical speciation program Visual MINTEQ version 2.61 (Gustafsson, 2007). The formation of amorphous iron and aluminum oxyhydroxides was evaluated. The calculation indicated that the solutions were oversaturated with respect to ferrihydrite and gibbsite (SI = *log* IAP – *log* k_s, for ferrihydrite and gibbsite: 2.23 to 3.45 and 2.21 to 3.22, respectively), which couldcontribute to an increase in nanoparticulate Fe and Al concentrations.

pH also influenced the release of P. Phosphorus release decreased with increasing pH from 5.5 to 7 in the GB samples (Figures 2.3e and 2.3f). This trend was less pronounced for the LD sample (Figures 2.3a and 2.3b). As discussed above, an increase in the concentration of metal oxyhydroxide nanoparticles could increase the reactive sites for dissolved P, resulting in a decrease in [P] at pH 7 (Figures 2.3b, 2.3d, and 2.3f). The chemisorption of P on Fe and Al oxyhydroxide surfaces has been documented by several researchers (Arai and Sparks, 2001; Muljadi et al., 1966; Russell et al., 1974; van Riemsdijk and Lyklema, 1980). Unlike in the LD and GB samples, the effect of pH was

not pronounced in the CC sample. The concentration of P was nearly equal at pH 5.5 and 7 (Figures 2.3c and 2.3d). The (S)TEM analysis indicated that the CC sample contained solid phase P (~4% wt) coating on Si rich particles (Figure 2.1d). The slow dissolution of the solids could possibly contribute to small changes in the dissolved [P] at two pH values. Sulfonic acid based buffers, such as the ones used in these experiments, could sorb onto mineral surfaces, potentially acting as competitive anions for dissolved P. However, our preliminary experiments indicated that there was no trend in P release when comparing buffered and unbuffered soils. Additionally, sulfonic acid buffers have been shown to have negligible effects on P adsorption (Nowack and Stone, 1999), which indicates that our P release observations are not artifacts of the use of sulfonic acid buffers in our desorption experiments.

Besides simple desorption of P from mineral surfaces, we can also postulate the following two P release mechanisms: (1) microbial decomposition, and (2) hydroxyapatite dissolution. Microbial decomposition could result in the release of organic acids. Various organic acids are known to compete with P on variable charged mineral surfaces (e.g., Borggaard et al., 2005; Ohno and Erich, 1997). In moderately acidic soils, hydroxyapatite is not generally the major P fraction (e.g., Arai et al., 2005). We did not observe a clear trend in Ca release with P during the desorption experiment. Saturation indices for amorphous hydroxyapatite, $Ca_3(PO_4)_2$, (-18.05 to -10.54) indicate that it is undersaturated with respect to solids. Therefore, we cannot exclude the possibility that the dissolution of the apatite phase is controlling P release.

Figure 2.4 shows the result of the replenishment desorption experiment. The purpose of this experiment was to further remove nanoparticles in low *I* conditions without accumulating reaction products. The low *I* also thickens the diffuse double layer, promoting nanoparticle detachment. Therefore, one should expect more particle release in this experiment than in the previous batch desorption experiments. The release of P (Figures 2.4a – 2.4c) shows that P release is ~1.5 – 2 times greater than the values in the previous batch desorption experiments (Figures 2.3a – 2.3f). The total P release was as high as 6000 μg/L in one of CC samples (Figure 2.4b). In the replenishment experiment, it becomes much clearer that nanoparticles are not influencing the P transport process. The same trends observed in the batch desorption experiments outlined in Figure 2.3 were also observed in the replenishment desorption experiments. The total P (filled symbols) and dissolved P (open symbols) are nearly identical in all samples even if we consider the relative standard deviation (<5%) (Figures 2.4a – 2.4c). The release of total Fe and Al increased with increasing time, while dissolved Al and Fe are nearly negligible in all samples (Figures 2.4d – 2.4i). The open symbols, representing dissolved Fe and Al (Figures 2.4d – 2.4i) are all near zero, resulting in indistinguishable data points, which indicates that Fe and Al were closely associated with nanoparticles.

The release of Fe and Al was enhanced at higher pH values. Similar mechanisms that were discussed in the batch desorption section can be suggested to explain this trend. Charge repulsion between nanoparticles and soil mineral surfaces could enhance the nanoparticle detachment. The formation of metal oxyhydroxide precipitates at pH 7 can increase the total [Al] and [Fe] in the filtrate, which would enhance the P sorption,

resulting in [P] decreases at pH 7 in LD and GB samples (Figures 2.4a and 2.4c). Conversely, the CC sample shows insignificant changes in [P] at pH 5.5 and 7. A similar effect was observed in the previous batch desorption experiment. Minimum changes in [P] at two pH values might be attributed to the slow dissolution of the solid phase P coatings on Si rich particles.

It is also important to note that we cannot exclude the possibility of organic buffer (i.e., MES and MOPSO) induced particle dispersivity. Some studies (e.g., Cervini-Silva, 2004) suggest a decrease in the electrophoretic mobility values of metal oxide particles in the presence of sulfonic acid based buffers, which could facilitate particle dispersion due to the negatively charged mineral surfaces. However, when we tested the effects of the organic buffers on Fe- and Al-based nanoparticle release, there was no clear trend in buffer-induced nanoparticle release, which suggests that our observations of nanoparticle release in P desorption experiments were not artifacts of the use of organic buffers.

2.4.6 Buffering Capacity of Soil Nanoparticles

Figure 2.5 shows the pH titration curve of the three nanoparticle suspensions. All three samples display quite strong buffering capacity with the addition of base. It required approximately 0.003 mol/L of base to raise the pH from 5.5 to ~7.5 (i.e., 2 pH units). The soil samples had weaker buffering capacity with the addition of acid (Figure 2.5). It only required ~0.0015 mol/L of acid to decrease the pH from 5.5 to 3.5 (i.e., 2 pH units). The strong buffering capacity at pH 5.5 and 7.0 might be attributed to the total organic matter content in the samples. The buffering capacity is strongest in LD, followed by CC, and

finally GB. This order follows the organic matter of these samples: LD, 30.2; CC, 19.2; GB, 6.6; all units in mg/L. Soil organic matter is a strong buffering agent in soil solutions and pore spaces (Stevenson, 1982). The results of the titration curve shows unique buffering capacity that is contributed by the surface charge properties of nanoparticles and organic carbon content.

2.4.7 Phosphorus Retention and Release in Soil Nanoparticles

We used the UHS centrifugation method to investigate the P retention/release in 0.2 μm filtrate samples over various pH levels. Figures 2.6a, 2.6b, and 2.6c show the total P (filled symbols) and dissolved P (open symbols). All samples show that there are insignificant differences in total and dissolved P, which suggests that nanoparticles in the suspensions (i.e., 0.2 μm filtrates) were not reactive, as P was not sorbed onto them. This is in contrast to findings by other researchers, such as the work done by Siemens et al. (2004) who found that the majority of P in solution after passing through a 0.45 μm filter, was sorbed to colloidal-sized soil particles. An alternative presentation of the same data (Figures 2.6d – 2.6f) shows that % P sorption is as little as ~7 % in LD and GB samples. The CC sample shows the highest sorption of ~27 % at pH 7 (Figure 2.6e). Overall, the results of P retention/release experiments agree with the result of desorption experiments that nanoparticles are not as reactive as we predicted.

2.4.8. Conclusions

We investigated nanoparticle (10 – 200 nm) facilitated P release in moderately to strongly acidic SC agricultural soils that were collected from three watershed basins (i.e., Edisto, Savannah, and Pee Dee). As commonly documented in the literature (e.g., de Jonge et al., 2004b; Kretzschmar et al., 1999; Makris et al., 2006), we hypothesized the colloid/nanoparticle-facilitated transport processes of P in well-weathered Ultisols. Bulk chemical extractions, including Mehlich-1, indicated the P (40 – 60% of total P) may be associated with the amorphous Fe (5.29 – 15% of total Fe) and Al (2.5 – 5.4% of total Al) fractions. After 30 days of batch desorption experiments, the maximum total desorbable P was ~10% of total P for LD soil, ~20% for CC, and ~17% for GB. Contrary to our hypothesis, the release of labile P was not facilitated by soil nanoparticles. The batch P sorption in the soil nanoparticle suspensions also suggests lack of reactivity in soil nanoparticles at pH 4 – 7. These nanoparticles, which are rich in Si and S, have Fe and/or C coatings with trace amounts of Al and P. The EDS and XAS analysis showed that these particles are neither pure Fe oxyhydroxides nor phyllosilicate minerals.

Our findings contradict the findings of other researchers that that colloids facilitate P transport processes in soils. Most studies suggest that colloid facilitated transport occurs in the particles with a size between approximately 450 and 200 nm (e.g., Heathwaite et al., 2005; Makris et al., 2006; Siemens et al., 2004; Zhang, 2008). However, we found that nanoparticles (10 – 200 nm) are not as reactive as other researchers reported. Haygarth et al. (1997) previously reported a large difference between the amount of P in filtrates at <0.45 μm and <0.10 μm. The type of colloids or

nanoparticles might influence the P transport process in soil solutions. Colloidal organic macromolecules may not be carriers of dissolved P, but inorganic materials, such as the products of mineral weathering, may play an important role (Haygarth et al., 1997). Additionally, the difference in analytical methods could possibly yield different conclusions. While we used ICP-MS to measure [P], many researchers used the colorimetric method (e.g., molybdenum blue) to measure MRP (e.g, Bauer et al., 1996; Filella et al., 2006; Haygarth et al., 1997; Hens and Merckx, 2002). The interference of MRP in the presence of DOC, anions and colloids/nanoparticles must be carefully evaluated in each study prior to drawing any conclusions (Hutchison and Hesterberg, 2004; Sinaj et al., 1998).

Most literature predicting nutrient release extensively reports nanoparticles as carriers. Our findings show that it is not. Regardless of the contradicting results, the work presented in this work clearly showed a new aspect of soil nanoparticles. The key challenge in advancing our knowledge of environmental colloidal/nanoparticles might lie on 1) characterization of reactive nanoparticles and 2) unification in experimental and analytical methods that will allow us to better assess the nanoparticles reactivity in the soil-water environments.

2.5 References

Abrams, M.M., and W.M. Jarrell. 1995. Soil phosphorus as a potential nonpoint source for elevated stream phosphorus levels. J. Environ. Qual. 24:132-138.

Arai, Y., and D.L. Sparks. 2001. ATR-FTIR spectroscopic investigation on phosphate adsorption mechanisms at the ferrihydrite-water interface. J. Colloid Interf. Sci. 241:317-326.

Arai, Y., D.L. Sparks, and J.A. Davis. 2004. Effects of dissolved carbonate on arsenate and surface speciation at the hematite-water interface. Environ. Sci. Technol. 38:817-824.

Arai, Y., K.J.T. Livi, and D.L. Sparks. 2005. Phosphate reactivity in long-term poultry litter-amended southern Delaware sandy soils. Soil Sci. Soc. Am. J. 69:616-629.

Bauer, J.E., K.C. Ruttenberg, D.M. Wolgast, E. Monaghan, and M.K. Schrope. 1996. Cross-flow filtration of dissolved and colloidal nitrogen and phosphorus in seawater: Results from an intercomparison study. Mar. Chem. 55:33-52.

Blake, R.L., Hessevic.Re, T. Zoltai, and L.W. Finger. 1966. Refinement of hematite structure. Am. Miner. 51:123-&.

Borggaard, O.K., B. Raben-Lange, A.L. Gimsing, and B.W. Strobel. 2005. Influence of humic substances on phosphate adsorption by aluminium and iron oxides. Geoderma. 127:270-279.

Burkholder, J.M., and H.B. Glasgow. 1997. *Pfiesteria piscicida* and other *Pfiesteria*-like dinoflagellates: Behavior, impacts, and environmental controls. Limnol. Oceanogr. 42:1052-1075.

Carpenter, S.R., N.F. Caraco, D.L. Correll, R.W. Howarth, A.N. Sharpley, and V.H. Smith. 1998. Nonpoint pollution of surface waters with phosphorus and nitrogen. Ecol. Appl. 8:559-568.

Cervini-Silva, J. 2004. Alteration of the surface charge of aluminum goethites by a sulfonic acid buffer. J. Colloid Interf. Sci. 275:79-81.

Combes, J.M., A. Manceau, and G. Calas. 1990. Formation of ferric oxides from aqueous-solutions - A polyhedral approach by X-ray absorption spectroscopy 2. Hematite formation from ferric gels. Geochim. Cosmochim. Acta. 54:1083-1091.

De Hann, H., T. De Boer, J. Voerman, H. Kramer, and J. Moed. 1984. Size classes of 'dissolved' nutrients in shallow, alkaline, humic and eutrophic Tjeukemeer, The Netherlands, as fractionated by ultrafiltration. Verh. Internat. Verein Limnol. 22:876-881.

de Jonge, L.W., C. Kjaergaard, and P. Moldrup. 2004a. Colloids and colloid-facilitated transport of contaminants in soils: An introduction. Vadose Zone J. 3:321-325.

de Jonge, L.W., P. Moldrup, G.H. Rubaek, K. Schelde, and J. Djurhuus. 2004b. Particle leaching and particle-facilitated transport of phosphorus at field scale. Vadose Zone J. 3:462-470.

Delgado, A., and J. Torrent. 2001. Comparison of soil extraction procedures for estimating phosphorus release potential of agricultural soils. Commun. Soil Sci. Plan. 32:87-105.

Filella, M., C. Deville, V. Chanudet, and D. Vignati. 2006. Variability of the colloidal molybdate reactive phosphorous concentrations in freshwaters. Water Res. 40:3185-3192.

Glasgow, H.B., J.M. Burkholder, D.E. Schmechel, P.A. Tester, and P.A. Rublee. 1995. Insidious effects of a toxic estuarine dinoflagellate on fish survival and human health. J. Toxicol. Env. Health. 46:501-522.

Griffin, R.A., and J.J. Jurinak. 1974. Kinetics of the phosphate interaction with calcite. Soil Sci. Soc. Am. J. 38:75-79.

Grove, J.H., C.S. Fowler, and M.E. Sumner. 1982. Determination of the charge character of selected acid soils. Soil Sci. Soc. Am. J. 46:32-38.

Gustafsson, J.P. 2007. Visual MINTEQ [Online] http://www.lwr.kth.se/English/OurSoftware/vminteq/index.htm.

Haygarth, P.M., M.S. Warwick, and W.A. House. 1997. Size distribution of colloidal molybdate reactive phosphorus in river waters and soil solution. Water Res. 31:439-448.

Heathwaite, L., P. Haygarth, R. Matthews, N. Preedy, and P. Butler. 2005. Evaluating colloidal phosphorus delivery to surface waters from diffuse agricultural sources. J. Environ. Qual. 34:287-298.

Hens, M., and R. Merckx. 2001. Functional characterization of colloidal phosphorus species in the soil solution of sandy soils. Environ. Sci. Technol. 35:493-500.

Hens, M., and R. Merckx. 2002. The role of colloidal particles in the speciation and analysis of "dissolved" phosphorus. Water Res. 36:1483-1492.

Hutchison, K.J., and D. Hesterberg. 2004. Dissolution of phosphate in a phosphorus-enriched Ultisol as affected by microbial reduction. J. Environ. Qual. 33:1793-1802.

Kang, B.T., A.N. Atta-krah, and L. Reynolds. 1999. Alley Farming. Macmillan Education LTD, London.

Karathanasis, A.D., G.W. Hurt, and B.F. Hajek. 1986. Properties and classification of montmorillonite-rich hapludults in the Alabama coastal plains. Soil Sci. 142:76-82.

Kempton, J.W., J. Wolny, T. Tengs, P. Rizzo, R. Morris, J. Tunnell, P. Scott, K. Steidinger, S.N. Hymel, and A.J. Lewitus. 2002. *Kryptoperidinium foliaceum* blooms in South Carolina: A multi-analytical approach to identification. Harmful Algae. 1:383-392.

Kjaergaard, C., L.W. de Jonge, P. Moldrup, and P. Schjonning. 2004. Water-dispersible colloids: Effects of measurement method, clay content, initial soil matric potential, and wetting rate. Vadose Zone J. 3:403-412.

Koopmans, G.F., W.J. Chardon, P.H.M. Dekker, P. Romkens, and O.F. Schoumans. 2006. Comparing different extraction methods for estimating phosphorus solubility in various soil types. Soil Sci. 171:103-116.

Kretzschmar, R., M. Borkovec, D. Grolimund, and M. Elimelech. 1999. Mobile subsurface colloids and their role in contaminant transport. Adv. Agron. 66:121-193.

Lawton, L.A., and G.A. Codd. 1991. Cyanobacterial (blue-green algal) toxins and their significance in UK and European waters. J. Inst. Water Env. Man. 5:460-465.

Lewitus, A.J., K.C. Hayes, B.M. Willis, J.M. Burkholder, H.B. Glasgow, A.F. Holland, P.P. Maier, P.A. Rublee, and R. Magnien. 2002. Low abundance of the dinoflagellates, *Pfiesteria piscicida*, *P. shumwayae*, and *Cryptoperidiniopsis* spp., in South Carolina tidal creeks and open estuaries. Estuaries. 25:586-597.

Lewitus, A.J., L.B. Schmidt, L.J. Mason, J.W. Kempton, S.B. Wilde, J.L. Wolny, B.J. Williams, K.C. Hayes, S.N. Hymel, C.J. Keppler, and A.H. Ringwood. 2003. Harmful algal blooms in South Carolina residential and golf course ponds. Popul. Environ. 24:387-413.

Loeppert, R.H., and W.P. Inskeep. 1996. Iron, p. 639-664, *In* D. L. Sparks, ed. Methods of Soil Analysis. Part 3. Soil Science Society of America, Inc., Madison, WI.

Ludwig, B., P.K. Khanna, B. Anurugsa, and H. Folster. 2001. Assessment of cation and anion exchange and pH buffering in an Amazonian Ultisol. Geoderma. 102:27-40.

Makris, K.C., J.H. Grove, and C.J. Matocha. 2006. Colloid-mediated vertical phosphorus transport in a waste-amended soil. Geoderma. 136:174-183.

Mehlich, A. 1978. New extractant for soil test evaluation of phosphorus, potassium, magnesium, calcium, sodium, manganese and zinc. Commun. Soil Sci. Plan. 9:477-492.

Mehra, O.P., and M.L. Jackson. 1960. Iron oxide removal from soils and clays by a dithionite-citrate system buffered with sodium bicarbonate. Clay. Clay Miner. 7:317-327.

Muljadi, D., A.M. Posner, and J.P. Quirk. 1966. The mechanism of phosphate adsorption by kaolinite, gibbsite, and pseudoboehmite. Part I: Isotherms and effect of pH on adsorption. J. Soil Sci. 17:212-229.

Myneni, S.C.B., J.T. Brown, G.A. Martinez, and W. Meyer-Ilse. 1999. Imaging of humic substance macromolecular structures in water and soils. Science. 286:1335-1337.

Nowack, B., and A.T. Stone. 1999. Adsorption of phosphonates onto the goethite-water interface. J. Colloid Interf. Sci. 214:20-30.

O'Day, P.A., N. Rivera, R. Root, and S.A. Carroll. 2004. X-ray absorption spectroscopic study of Fe reference compounds for the analysis of natural sediments. Am. Miner. 89:572-585.

Ohno, T., and M.S. Erich. 1997. Inhibitory effects of crop residue-derived organic ligands on phosphate adsorption kinetics. J. Environ. Qual. 26:889-895.

Russell, J.D., R.L. Parfitt, A.R. Fraser, and V.C. Farmer. 1974. Surface structures of gibbsite, goethite and phosphated goethite. Nature. 248:220-221.

Sharpley, A.N., R.W. McDowell, and P.J.A. Kleinman. 2001. Phosphorus loss from land to water: Integrating agricultural and environmental management. Plant Soil. 237:287-307.

Siemens, J., K. Ilg, F. Lang, and M. Kaupenjohann. 2004. Adsorption controls mobilization of colloids and leaching of dissolved phosphorus. Euro. J. Soil Sci. 55:253-263.

Sinaj, S., F. Machler, E. Frossard, C. Faisse, A. Oberson, and C. Morel. 1998. Interference of colloidal particles in the determination of orthophosphate concentrations in soil water extracts. Commun. Soil Sci. Plan. 29:1091-1105.

Stevenson, F.J. 1982. Humus Chemistry. Dekker, New York.

Szytula, A., A. Burewicz, Dimitrij.Z, Krasnick.S, H. Rzany, Todorovi.J, A. Wanic, and W. Wolski. 1968. Neurtron diffraction studies of alpha-FeOOH. Phys. Status Solidi. 26:429-&.

USEPA. 1983. Methods for chemical analysis of water and wastes. US Environmental Protection Agency, Cincinnati, OH.

van Riemsdijk, W.H., and J. Lyklema. 1980. Reaction of phosphate with gibbsite ($Al(OH)_3$) beyond the adsorption maximum. J. Colloid Interf. Sci. 76:55-66.

Webb, S.M. 2005. SIXpack: a graphical user interface for XAS analysis using IFEFFIT. Physica Scripta. T115:1011-1014.

Zhang, M.K. 2008. Effects of soil properties on phosphorus subsurface migration in sandy soils. Pedosphere. 18:599-610.

Zhang, Y., Y.S. Chen, P. Westerhoff, and J. Crittenden. 2009. Impact of natural organic matter and divalent cations on the stability of aqueous nanoparticles. Water Res. 43:4249-4257.

Table 2.1. Physicochemical properties of long-term poultry litter amended P-rich South Carolina surface soils.

Soil Series	Texture	Sand and silt fractions	Clay fraction	pH_{water}	CEC*	Exchangeable cations		
						H^+ and Al^{3+}	Ca^{2+}	Mg^{2+}
					$cmol_c\ kg^{-1}$			
Lloyd (LD)	Sandy loam	Q	K	5.32	12.3	3.6	6.03	2.34
Cecil (CC)	Sandy loam	Q	K	5.69	7.7	3.2	3.47	0.69
Goldsboro (GB)	Sandy loam	Q	----	5.52	6.8	2.0	3.74	0.75

* CEC: Cation exchange capacity measure using an unbuffered salt extraction method (Grove et al., 1982).
Q: quartz, K: kaolinite.

Table 2.2. Total metal(loid) microwave digestion of long-term poultry litter amended P-rich South Carolina surface soils

Series	P	K	Ca	Mg	S	Mn	Cu	Pb	Cr	Ni	Zn	Al	Fe
	mg/kg											%	%
Lloyd	943	1264	1863	950	479	204	37	6.71	39	13	56	2.56	2.01
Cecil	921	462	714	488	186	720	20	4.80	6.18	3.10	63	1.58	1.13
Goldsboro	262	<0.37	629	307	84	19	5.25	5.99	11	2.66	13	0.88	0.39

Table 2.3. Inorganic P fractionation of long-term poultry litter amended South Carolina surface soils.

Series	Mehlich-1 P	P_{ox} ‡	Al_{ox} ‡	Fe_{ox} ‡	P_{DCB} §	Al_{DCB} §	Fe_{DCB} §
	mg/kg						
Lloyd	445 (47)	376 (40)	628 (2.45)	1,181 (5.88)	250 (27)	1,535 (5.99)	11,757 (59)
Cecil	144 (16)	485 (53)	546 (3.47)	596 (5.29)	165 (18)	608 (3.86)	5,108 (45)
Goldsboro	116 (44)	157 (60)	470 (5.37)	604 (15)	69.2 (26)	548 (6.26)	2,094 (53)

‡ Ammonium oxalate extractable (ox) P, Fe, and Al (P_{ox}, Al_{ox}, and Fe_{ox}, respectively)

§ Dithionite-citrate-bicarbonate extractable (DCB) P, Fe, and Al after oxalate extraction (P_{DCB}, Al_{DCB}, and Fe_{DCB}, respectively)

( ) = % fraction with respect to total inorganic P, Al, and Fe values of each soil shown in Table 1.

Within-column values are statistically different at the 0.05 probability levels.

Table 2.4. Least-squares analyses of Fe K-edge bulk XAS analysis of soil nanoparticles of Lloyd and Cecil sandy loam and reference iron oxyhydroxides.

Samples		O	Fe1	Fe2 or Si	Fe3	R-factor
Goethite	CN	6†	2(1)	4(1)	5(2)	0.029
	R(Å)	1.99(2)	3.04(2)	3.27(5)	3.40(4)	
	σ^2(Å^2)	0.011(1)	0.01*	0.005†	0.008†	
Hematite	CN	5(1)	3.7(5)	4(1)	-------	0.018
	R(Å)	1.98(2)	2.95(2)	3.33(2)		
	σ^2(Å^2)	0.012(3)	0.008†	0.0012†		
Ferrihydrite	CN	6†	0.8(5)	1.3(5)	1.6(6)	0.026
	R(Å)	1.96(2)	2.88(6)	3.03(4)	3.42(4)	
	σ^2(Å^2)	0.016(1)	0.01†	0.008†	0.01†	
Lloyd	CN	5.5(5)	-------	1.5(8)‡	-------	0.012
	R(Å)	1.991(7)		3.25(2)‡		
	σ^2(Å^2)	0.0093(1)		0.007(4)‡		
Cecil	CN	6.0†	4(2)	6(3)‡	2(1)	0.023
	R(Å)	1.98(1)	3.19(6)	3.21(5)‡	3.38(4)	
	σ^2(Å^2)	0.0078(9)	0.008†	0.007†‡	0.008†	

CN: Coordination number. R: Interatomic distance (Å). σ^2: Debye-Waller factor (Å^2). Fit quality confidence limit for parameters: Fe-O/Fe shells, CN: ±20 %, R ±0.02 Å †: Fixed parameter. ‡: Si shell

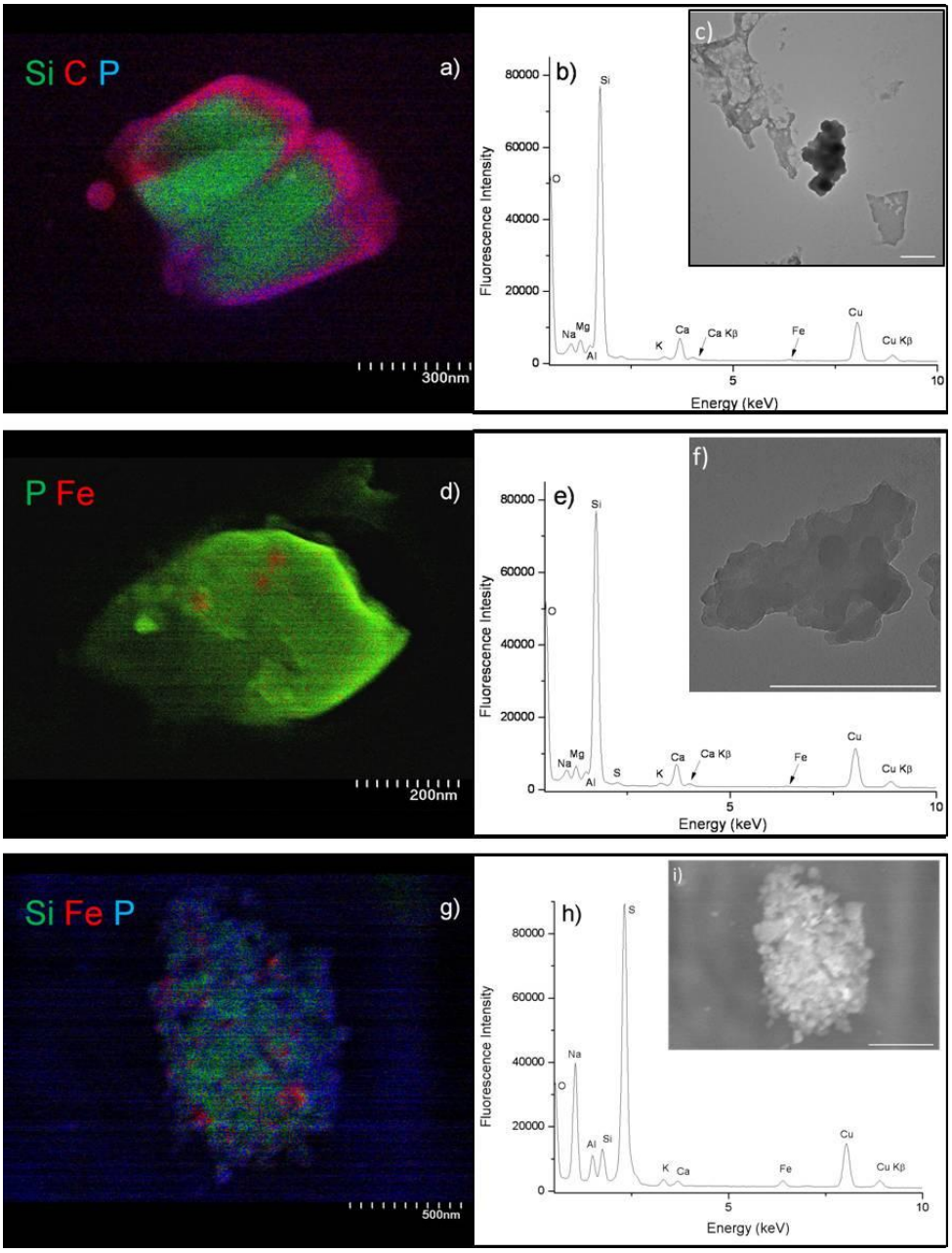

Figure 2.1. Scanning transmission electron microscopy (STEM), energy dispersive x-ray spectra (EDS), and transmission electron microscope (TEM) images of soil nanoparticles from Lloyd sandy loam (LD) (a – c), Cecil sandy loam (CC) (d – f), and Goldsboro sandy loam (GB) (g – i). STEM images with EDS mapping are displayed in a, d, and g. EDS spectra obtained from the whole field of STEM images are displayed in b, e, and h. TEM images are displayed in c and f. Figure 2.1i is an STEM image on GB. The white scale bar on these images represents 500 nm. TEM images were taken using a different instrument, and so are different particles than SEM images, but from the same sample.

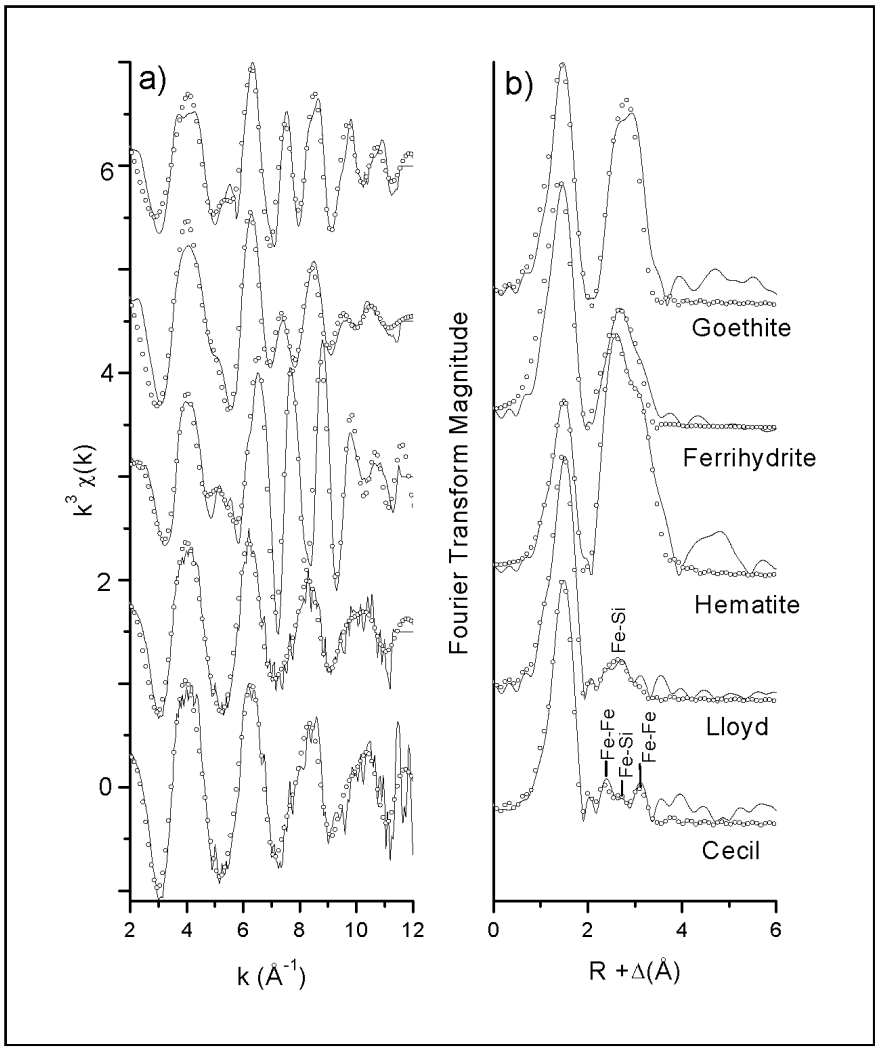

Figure 2.2. a) Normalized, background-subtracted k^3-weighted Fe K-edge EXAFS spectra of soil nanoparticles in Lloyd sandy loam (LD) and Cecil sandy loam (CC), and reference iron oxyhydroxides (hematite, goethite, and ferrihydrite). b) Fourier transformed k^3-weighted Fe K-edge EXAFS spectra of samples shown in Figure 2.2a). Solid lines are the experimental data and open circles represent the theoretical fit.

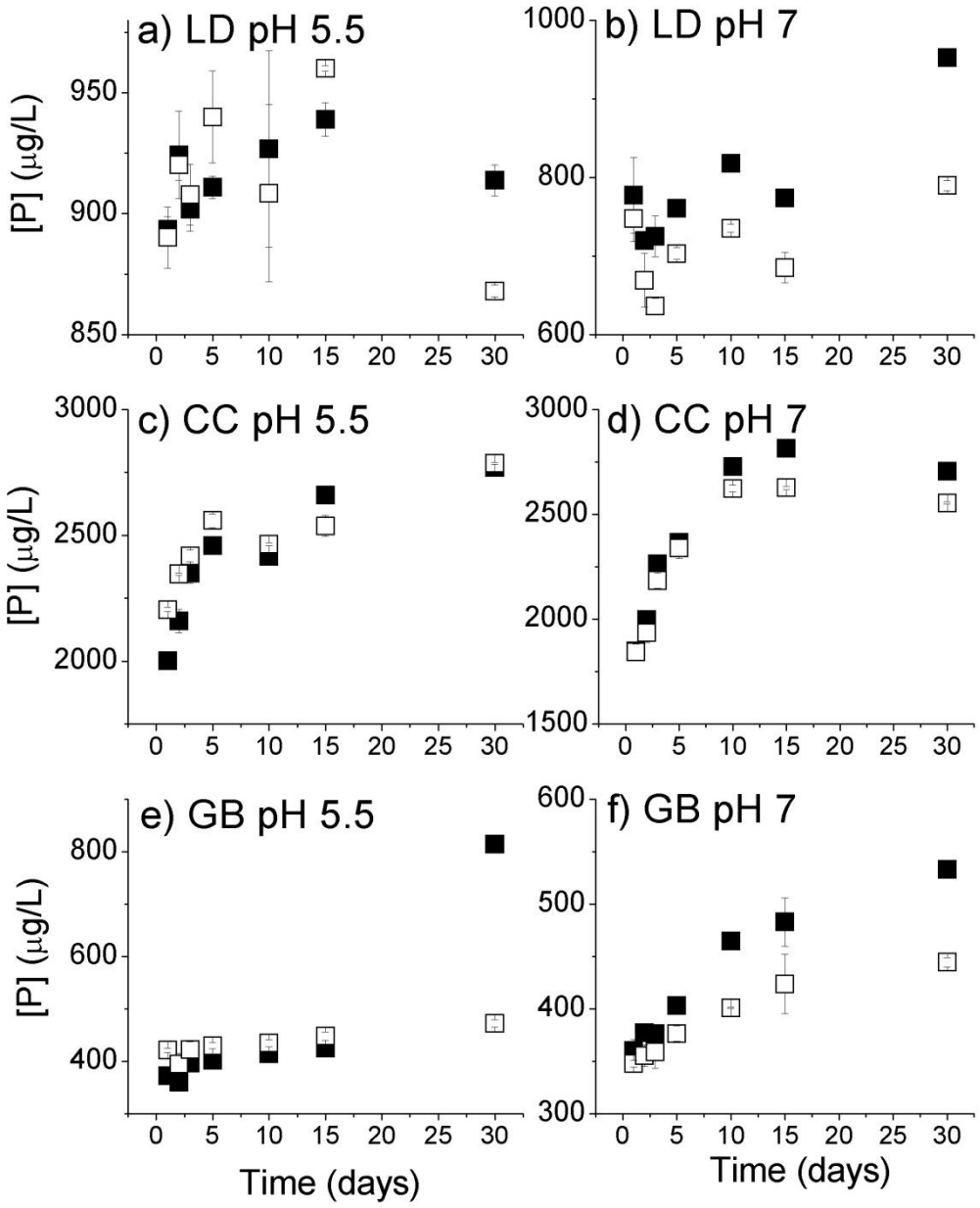

Figure 2.3. Batch desorption data of Lloyd sandy loam (LD), Cecil sandy loam (CC), and Goldsboro sandy loam (GB). All samples had solid/solution ratio = 1g in 30ml. Filled symbols represent total P, Fe, and Al concentration. Open symbols represent dissolved P, Fe, and Al concentration (<10 nm solution).

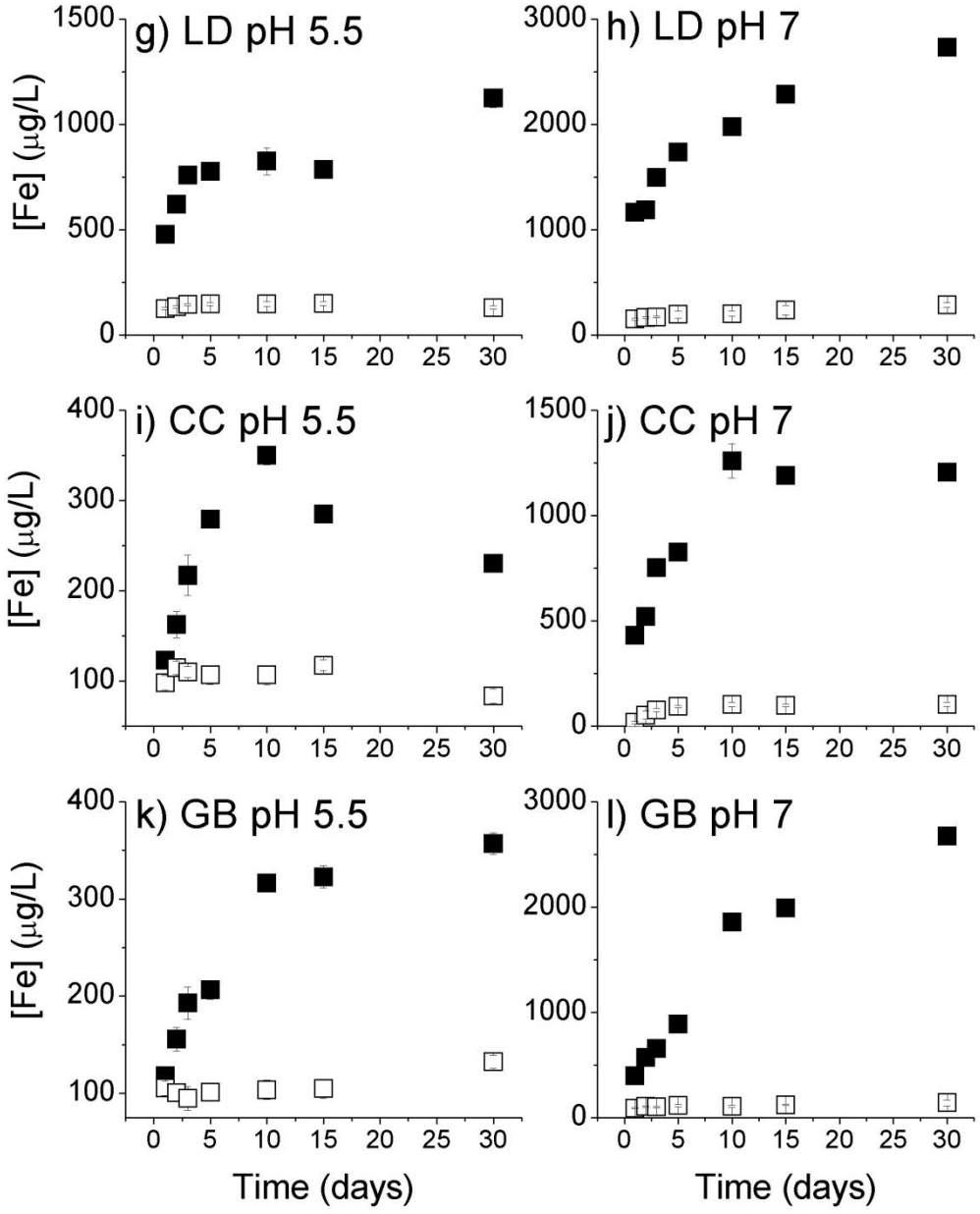

Figure 2.3. (continued)

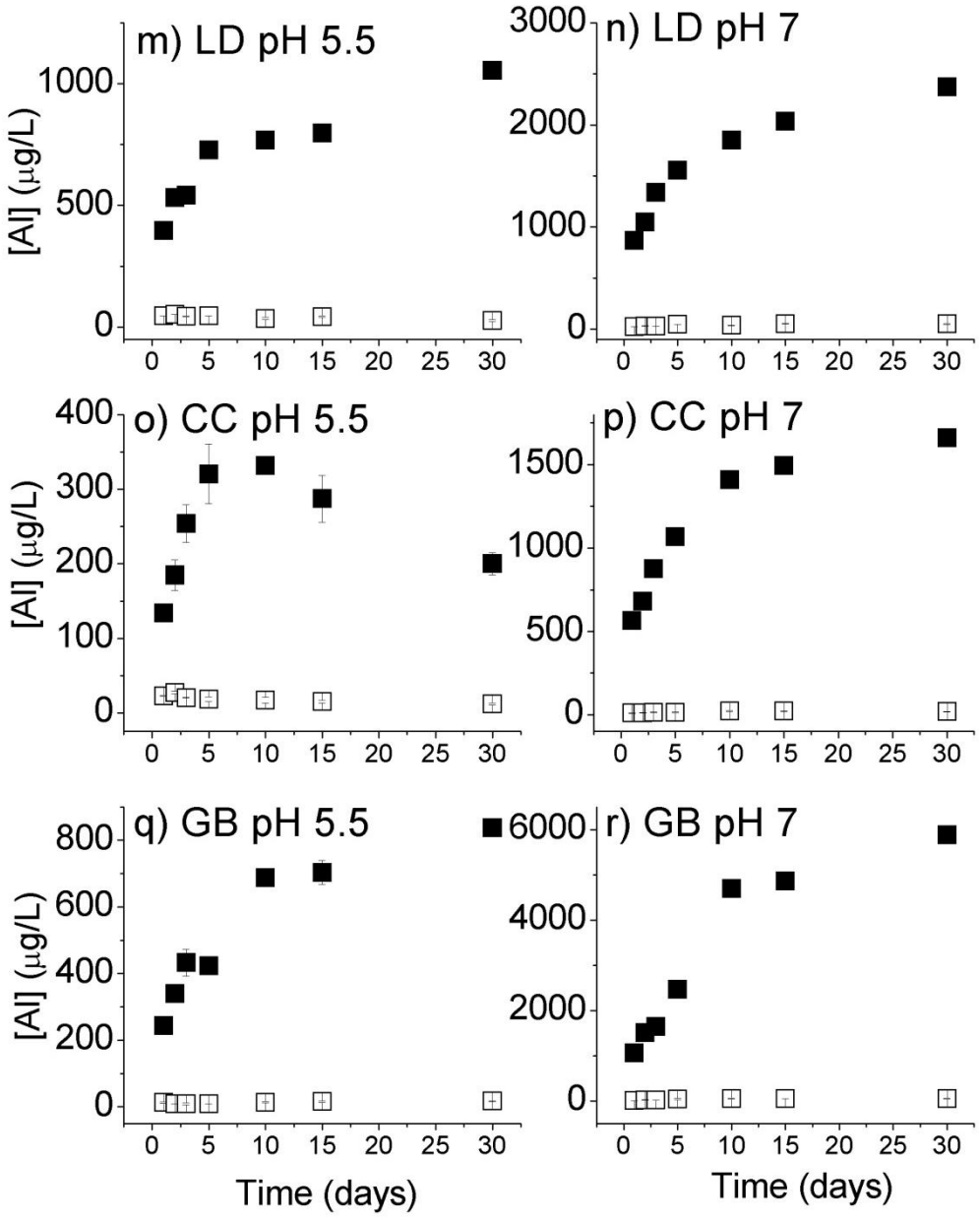

Figure 2.3. (continued)

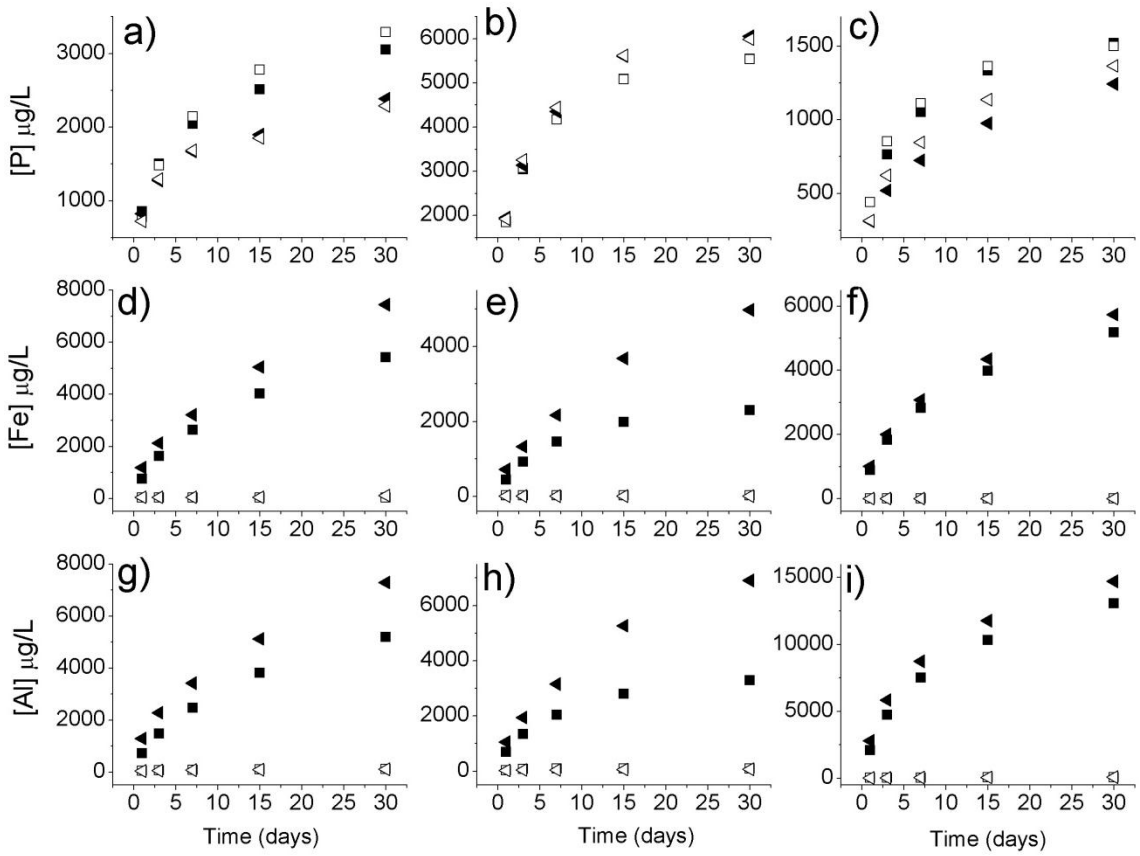

Figure 2.4. Batch replenishment desorption data of Lloyd sandy loam (LD)(a, d, and g), Cecil sandy loam (CC) (b, e, and h), and Goldsboro sandy loam (GB) (c, f, and i). All samples had solid/solution ratio = 1g in 30ml, and desorption is represented as the total cumulative desorption over the study time period in all cases. Square symbols and triangular symbols represent experiments performed at pH 5.5 and 7, respectively. Filled symbols represent total P, Fe, and Al concentration. Open symbols represent dissolved P, Fe, and Al concentration (<10 nm solution). %RSD is less than 5% for all values.

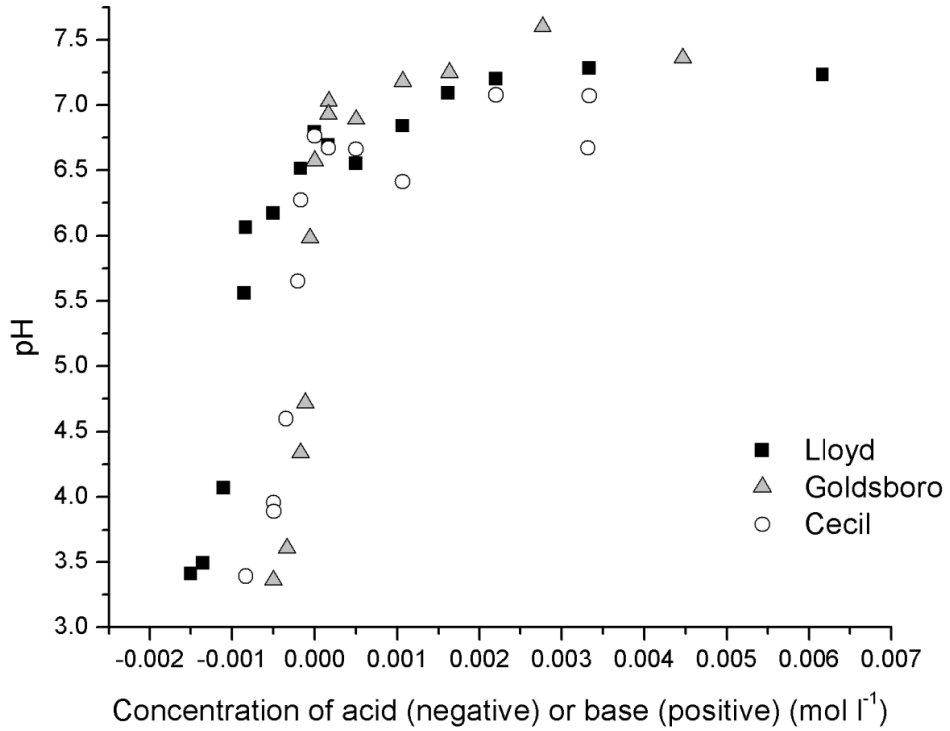

Figure 2.5. pH Titration curves of three soil nanoparticle suspensions in Lloyd sandy loam (LD), Cecil sandy loam (CC), and Goldsboro sandy loam (GB).

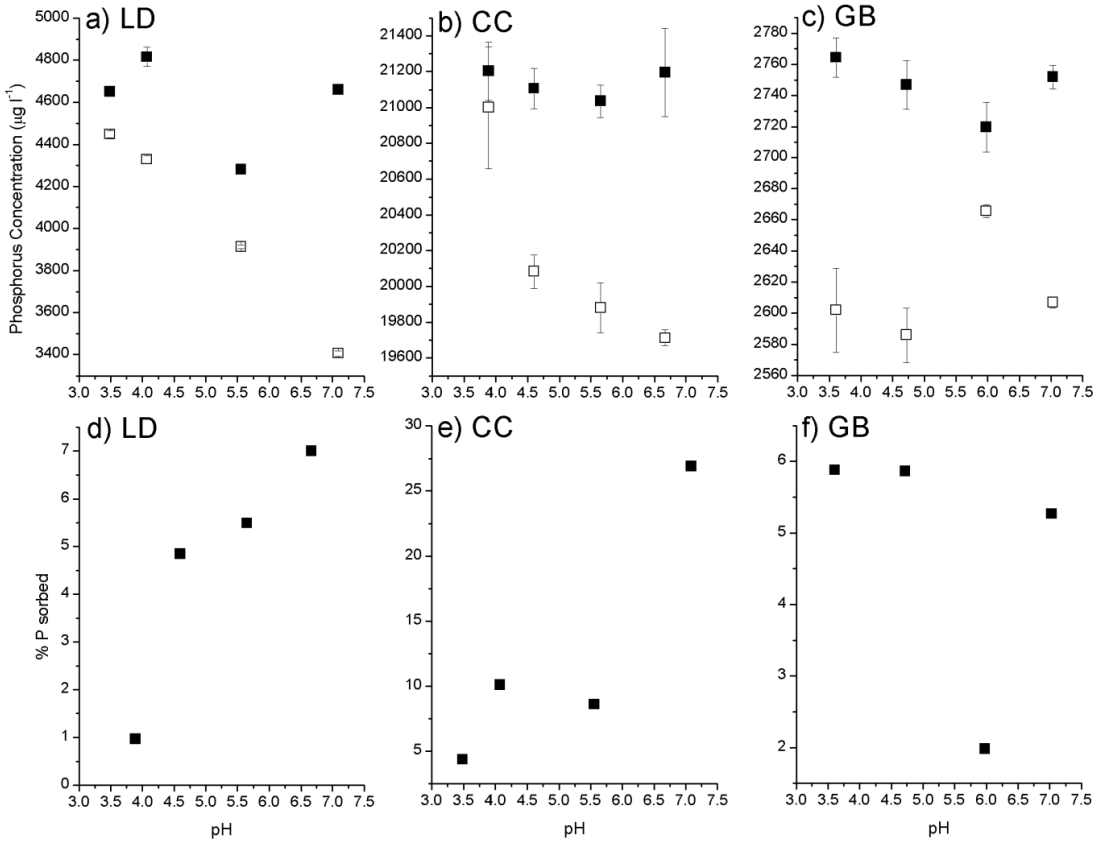

Figure 2.6. Phosphorus retention in soil nanoparticle suspensions as a function of pH. The suspensions were extracted from Lloyd sandy loam (LD), Cecil sandy loam (CC), and Goldsboro sandy loam (GB). Figures 2.6a – 2.6c show the effect of pH on dissolved P concentration. Filled symbols represent the total P concentration. Open symbols represent the dissolved P concentration. Figures 2.6d – 2.6f show % P sorption as a function of pH. %RSD was less than 5%. Black square symbols represent the total P sorption on nanoparticles in each sample.

CHAPTER THREE

REACTION CONDITIONS CONTROL SOIL COLLOID FACILITATED PHOSPHORUS RELEASE IN AGRICULTURAL ULTISOLS

3.1 Abstract

Colloid-facilitated phosphorus (P) transport in agricultural soils has received much research attention in recent decades due to its importance as a solid phase of mobile P, which may increase P runoff in some soils. Colloids are the very smallest portion of clay particles within the soil (typically <1 μm). The existing literature reports inconsistent results of colloidal P release as a percentage of total P in soil solution, separated by various centrifugation and/or filtration methods. It remarkably ranges from 0 to 95%. The cause of colloidal P release has been difficult to assess since their experimental/environmental conditions (e.g., soil type, pH) were different from each other. This case study aims to focus on three controllable reaction conditions: ionic strength (*I*), pH and added P concentration, to elucidate their effect on P colloid release. Our case study showed that these reaction conditions do not largely alter the release of colloidal P in Ultisols of the southeastern United States (US) (mildly acidic pH, low organic C). However, the availability of colloidal P was enhanced at near neutral pH in high [P] or high *I* (0.1 M) solutions. We further discussed these reaction conditions in selected literature studies to better assess the occurrence of colloid facilitated P transport in a wide variety of soil and conditions.

3.2 Introduction

It has been well established that labile P originating from long-term anthropogenic agricultural amendments, has severe impacts on freshwater and marine ecosystems, e.g., (Carpenter et al., 1998; Sharpley et al., 2001; Sims et al., 1998). Primarily, eutrophication fueled by mobile P has caused shortages of dissolved O_2 (Lewitus et al., 2003) and excessive cyanobacteria contamination, creating hazardous conditions for humans and livestock (Lawton and Codd, 1991). Nutrient (e.g., P and nitrogen)-enriched waters are also known to induce outbreaks of harmful algae (*Pfiesteria* spp. and or *Kryptoperidinium* spp.) blooms in estuaries and coastal waters from New York to Texas (Lewitus et al., 2002; Verity, 2010) and this has been linked to several massive fish kill incidents along the U.S. East coast, from Delaware to the Carolinas (Burkholder et al., 1992; Rublee et al., 1999; Rublee et al., 2001). The transport of excess P from agricultural fields into surface water is undesirable for both economic and environmental reasons.

Several transport processes (i.e., erosion, runoff, particulate-facilitated) are responsible for P non-point pollution. Successful prediction and management of mobile P is essential to protecting inland and coastal watersheds. While traditionally, all P remaining after filtration at 0.2 μm (or even 0.45 μm), was considered "dissolved," it has now been well-established that colloidal- and or nano- sized particles may be contributing to this portion of the soil P pool (e.g., Bauer et al., 1996; Filella et al., 2006; Haygarth et al., 1997; Hens and Merckx, 2002; Kretzschmar et al., 1999). While the proportion of molybdenum reactive phosphate (MRP) made up of colloidal-sorbed P (typically < 1 μm)

is highly variable, it may contribute up to 25% (Filella et al., 2006). The importance of particulate-facilitated transport, in particular, has been identified in recent years (Kretzschmar et al., 1999). Phosphate has the ability to be carried on particle-facilitated transport due to its strong sorption onto soil surfaces (Heathwaite et al., 2005; Hens and Merckx, 2001). Several case studies showed that colloid-facilitated transport processes were readily occurring under various environmental conditions (e.g., soil composition, hydrologic cycle, *I*, pH, and [P]).

A recent study by Zang et al. (2011) observed a greater than 25% increase in colloid-facilitated P transport in soils receiving manure applications over those with no manure addition. Meanwhile, in soils without manure additions, there was a strong correlation between colloidal P concentration and colloidal iron (Fe) concentration (Zang et al., 2011). Makris et al. (2006) also cited the importance of manure addition in the formation of soil colloids. Both artificially increasing the number of water-dispersible colloids and adding manure amendments to soils were found to increase colloidal inorganic P in approximately equal amounts (Makris et al., 2006).

The proportion of P transported through colloid-facilitated processes is also highly variable from month to month in the same region, as reported by Heathwaite and Dils (2000). This is primarily ascribed to seasonal weather changes, particularly rainfall, and indicates the importance of solution composition on colloidal-facilitated P transport processes (Heathwaite and Dils, 2000).

The influences of dispersion and aggregation imparted by *I* have an effect on the number and size of soil colloids present in soil solution. A dramatic example of this was

shown by Koopmans and coworkers in their 2005 paper. When *I* was low (< 1 mM), MRP was abundant in the colloidal fraction of soil solution (filtered at 0.45 μm), but when *I* was increased to > 0.5 M prior to filtration, MRP in the colloidal portion decreased by over 90% (Koopmans et al., 2005). This suggests that high *I* promoted intense flocculation to occur, producing particles > 0.45 μm in diameter; and that the soil colloids present in the dispersed (low *I*) sample contributed primarily to the MRP value. Work by Heckrath et al. (1995) showed that phosphate can easily be mobilized when Olsen-extractable P, including dissolved and colloidal P, is present in excess of 60 mg/kg, while it was effectively immobile at lower P concentrations. This relationship between P concentration and mobility/desorption was further investigated by Arai and co-workers in 2005. They reported that the addition of P to soil solution enhanced the release of P (i.e., dissolved P plus colloidal P via inductively coupled plasma-atomic emission spectroscopy (ICP-AES) analysis) beyond the addition concentration in P rich Ultisols (Arai et al., 2005), which suggests the effects of P ligand on total P release from soils. Ilg and coworkers (2008) hypothesized that excessive P inputs to soil systems may induce colloid-facilitated P transport processes.

While there is clear evidence of soil colloid-facilitated P transport processes, few recent studies indicated the absence of colloid facilitated P transport in soils. In our previous work, the occurrence of colloidal P was insignificant in weakly acidic agricultural soils (Rick and Arai, 2011). Another recent field-scale study by Fuchs et al. (2009) also observed a lack of colloid-facilitated P transport through both preferential and non-preferential flow paths in a natural setting under mildly acidic conditions.

The discrepancy in these studies leads us to question whether the colloid facilitated transport process is important in all soil systems. While differences in the methodology of particle separation could have resulted in different findings, we believe that the occurrence of colloid (e.g., >200 nm)-facilitated P transport processes is highly dependent on dispersibility and coagulation of soil nanoparticles (NPs) (e.g., <200 nm) that are influenced by environmental conditions. The greater the NP coagulation, the greater the formation of colloids, resulting in colloid facilitated transport. For example, at high *I,* compressed electrical double layer facilitates the coagulation of NPs (i.e., colloids). Anderson et al., (1985) reported that phosphate induced goethite coagulation in aqueous system. Unfortunately, the influence of these multi-variables (e.g., *I*, [P]) on the soil NP stability has been rarely tested together in a single case study. Therefore, it is difficult to validate the effect of reaction conditions on the occurrence of colloid facilitated P transport in heterogeneous systems like soils.

In this study, we hypothesize that colloid facilitated P transport is controlled by coagulation of NPs influenced by reaction conditions in agricultural soils. Based on the studies discussed above, the following reaction conditions, *I*, pH, and P concentration, were tested together in the same P rich agricultural soil. To test the hypothesis, experimental geochemistry (batch desorption experiments) was carried out in conjunction with zeta potential measurements, dynamic light scattering, and transmission electron microscopy.

3.3 Materials and Methods

3.3.1 Materials

A long-term poultry litter amended topsoil (0–20 cm), Cecil (CC) sandy loam (fine, kaolinitic, thermic Typic Kanhapludult), was collected in South Carolina. Physicochemical properties of soils are characterized and described in the work by Rick and Arai (2011). Operationally defined soil nano- (10 – 200 nm) and colloidal (200 – 400 nm) particles were collected using a combination of filtration and centrifugation method as described in the P desorption section. Crystalline kaolinite (KL) (KGa-1, Clay Mineral Society, Chantilly, Virginia), nano-hematite (HM) (99.5% purity, 30 nm diameter, purchased from US Research Nanomaterials, Inc. Houston, Texas), muscovite (MS) (Paris Hill, Maine), and lab synthesized goethite (GT) were used for zeta potential measurements and particle size distribution analysis. Characterization and chemical treatments (removal of carbonates and oxides) of KL are described in previous work by this research group (Arai, 2010). Muscovite flakes were ground using a dish and puck mill, and passed through a 2μm sieve. Goethite was synthesized according to the ferric nitrate method described by Schwertmann and Cornell (1991). These aluminosilicate and Fe oxyhydroxide minerals represent model minerals found in soil NPs via transmission electron microscopy (TEM) analysis, described later.

3.3.2 Phosphate Desorption Experiments

Desorption of phosphate from CC soil was measured via batch method using air-dried whole soil < 2 mm. For each batch method sample, 1.5 g CC soil was measured

into 35 mL polycarbonate Oakridge centrifuge tubes, along with 30 mL solution with 0.01 or 0.1 M *I*, adjusted with $NaNO_3$, and appropriate bicarbonate concentration for the desired final pH, as determined through a solubility calculation from Visual MINTEQ version 3.0 (Gustafsson, 2010). The samples were allowed to hydrate for approximately 24 hours, after which the pH was adjusted to the desired level (3 to 8) using NaOH and/or HNO_3. The samples were allowed to hydrate for an additional 24 hours, after which 0, 0.15 mL, or 1.5 mL of a 20 mM Na_2HPO_4 solution was added, resulting in a final P concentration of 0, 0.1, or 1 mM as P, respectively (referred to hereafter as "initial P" or P_i). After a 48 hour reaction time on an end-over-end shaker, all samples were centrifuged at 2,300 x g for 3 minutes, resulting in an aliquot containing only particles smaller than 0.41 µm in diameter. Of this aliquot, a portion was reserved for analysis using ICP-AES at the Clemson University Agricultural Services Laboratory ("total elements" or P_T, Fe_T, Al_T, or Ca_T hereafter). The rest of the sample was filtered at 0.2 µm through polyvinylidene fluoride (PVDF) filters; elemental analysis was again conducted with ICP-AES ("filtered elements" or P_f, Fe_f, Al_f, or Ca_f hereafter). Figure 3.1 displays a flow chart of this separation technique.

The colloidal contribution (P_C, Fe_C, Al_C, or Ca_C hereafter) to P_T, Fe_T, Al_T, and Ca_T was determined by subtracting the filtered element concentration value for each sample from its respective total element concentration value ($P_c = P_T - P_f$, etc.). Colloids are operationally defined in this study as soil particles between 0.41 and 0.2 µm in diameter.

The P sorption onto soil surfaces for the 0.01 M *I* samples was determined on a soil mass basis for both the total and filtered portions. Equation 1 below shows the calculation for P_T. The same equation was also used for P_f.

$$P_T \text{ sorption} = P_i - P_T \times \frac{\text{Volume (L)}}{\text{soil mass (kg)}} \quad [3.1]$$

The contribution of the colloidal particles towards P_T sorption was calculated for each data point by subtracting the P_f sorption value from the P_T sorption value.

3.3.3 Zeta Potential and Particle Size Characterization

Model mineral solutions were analyzed for zeta potential and particle size (via dynamic light scattering, DLS) using a Brookhaven Instruments particle separation system (Brookhaven Instruments, Holtsville, New York). Model minerals were prepared by hydrating for several days at pH 5.5 ± 0.2 in 0.01 M $NaNO_3$. One day before zeta potential and DLS measurements were performed, some samples were adjusted for ionic strength, up to 0.1 M $NaNO_3$. All samples were adjusted for pH, and achieved pH 5 or pH 7 with the use of HNO_3 and/or NaOH. These samples were within 0.2 pH units of the target level. Finally, phosphate solution was added to select samples to achieve 0.1 to 1 mM [P].

The pH range (pH = 5 and 7) was chosen to mimic the optimum pH range of soil NP release in preliminary experiments. Because of our interest in the effect of phosphate ligand, all samples were kept suspended in distilled deionized water (18 mΩ) prior to the addition of orthophosphate stock solution ([P] = 1.005 mM). Zeta potential and DLS

measurements were taken on CC colloid and model mineral samples with no added P, and again after the addition of 0.01 mL P stock solution to the 2 mL samples, resulting in a [P] of 0.1 mM. Zeta potential and particle size were measured for a third time after the further addition of 0.99 mL of P stock solution, resulting in the final [P] or 1 mM. Suspension density of model minerals is approximately 0.17 g/L for KL, 0.10 g/L for GT, and 0.21 g/L for HM. Baseline data were established using a reference of 92 nm latex spheres. Baseline and all samples were read continuously for 50 s. Data were analyzed using Brookhaven Instruments 90Plus Particle Sizing Software, ver. 4.14.

3.3.4 Transmission Electron Microscopy Analysis

TEM analyses were done on a CM 300 FEG operating at 297 kV. Soil NP suspensions were deposited on a Cu TEM grid. Particles of interest were chosen for conventional TEM, selected area electron diffraction (SAED), and fast Fourier transforms (FFT) of high-resolution images to determine the crystalline nature of the phases. X-rays were collected using a light element Oxford energy dispersive spectrometer (EDS) and processed by the software ESVision 4. Images were processed (FFT) using the Gatan Digital Micrograph software package.

3.4 Results and Discussion

3.4.1 Mineralogy and Chemical Properties of Soil Nanoparticles

High resolution (HR) TEM equipped with EDS revealed both morphological and elemental data of soil NPs. There was evidence of Al, Si, and Fe in these natural NPs (~5

– 150 nm) that contained only minor amounts of P, Ca, Ti, Cl, S, and Mg. Based on a number of TEM observations (several tens of micrographs), we identified the following three major types NPs: amorphous aluminosilicate materials, HM, and KL/MS.

Soil NPs are primarily composed of amorphous materials, which rich in Al and Si, and variable in composition (Figure 3.2a and 3.2b). SAED patterns of this material contained broad rings indicative of an amorphous structure mixed with variable amounts of sharp reflections indexed as an iron oxide (Figure 3.2d).

Hematite was found in small (~10 nm) electron dense particles containing high Fe concentrations. Figures 3.2b and 3.3a have clusters of HM nanocrystals (~7 to 15 nm in diameter). EDS analyses of the Fe NPs always contained Al, Si, P and Ca (Figure 3.2c, 3.3b). SAED patterns of these NPs index as HM, clearly indicating that the NPs are HM and not GT (Figure 3.2d). Fast Fourier transforms processing of several HRTEM images yielded reflections for HM. Often, these Fe NPs were mixed with amorphous Al-Si material (Figure 3.2b).

Several EDS spectra (e.g., Figure 3.4c) showed near equal intensity of Si and Al, inferring the presence of 1:1 or 2:1 layer silicate phase. In addition, the SAED pattern in Figure 3.4d can be indexed as the *hk*0 net of a phyllosilicate mineral such as KL. However, these reflections are not diagnostic of any one phyllosilicate mineral. The ratio of Al to Si is close to 1:1, and K and Na are present. Yet, these alkali elements are present everywhere on the grid, including the carbon support film. If K is structural, then the phyllosilicate would be a 2:1 layered silicate such as illite or MS, but if K is a contaminant, then the phase is KL. Both KL and illite are present is the soil so neither

phase can be ruled out.

Because of common occurrence of apatite based P fertilizer, in agricultural soils, the presence of hydroxyapatite was also investigated via EDS analysis. Phosphorus was usually associated with both the amorphous phases and HM. In these analyses, the intensity of Ca in 50% of the spot analyses was half the intensity of P. A Ca-P rich particle was found during the particle survey, suggesting that, although apatite-like NPs are present, they are not a primary contributor to the colloid facilitated P transport process. Overall, the results of HRTEM analyses suggested that P in soil solutions was predominantly associated with amorphous Al and Si rich NPs, along with nano-HM.

We also compared the zeta potential values of soil NPs, GT, and soil colloid components in 0.01 $NaNO_3$ solutions at pH 7. Soil NPs showed -27.02 (±1.17) mV. MS, KL, and HM, all showed negative potentials (-25.71 (±1.17) mV, -26.76 (±2.42) mV, -16.74 (±3.03) mV, respectively), supporting the findings of TEM that soil NPs consists of these minerals components. However, GT showed a slightly positive zeta potential value, 3.97(±2.84) mV.

To further investigate the mobility of P associated soil NPs, we studied the effect of ionic strength and P ligand on the release of soil colloids using zeta potential measurements, DLS, and batch desorption experiments.

3.4.2 Ionic Strength (I) Effect on Colloid Release Associated with P, Fe, and Al

Figure 3.5 shows the effect of *I* on colloid (200 – 410 nm) release at pH 3.5 – 7.5. Because of common association of P with Al that was found in the TEM analysis, the

release of P_C, Fe_C, and Al_C is individually shown in Figure 3.5a – 3.5c. To assure uncommon occurrence of Ca associated NP/colloids, we reported the release of Ca_C in Figure 3.5d. We conducted the experiment under constant [P] = 0.1 mM because this condition yields negligible effects on the release of Fe_C and Al_C at I = 0.01 M (Figures 3.5a and 3.5b). Therefore, the effect of I can be studied. It is interesting that samples at the lower I consistently showed small release of colloids in all elements. Higher I (0.1 M) promoted increased colloidal fractions over low I (0.01 M). Although the amount P is low (0.5 – 2 mg/L), it is high enough to trigger eutrophication in waterways. The typical eutrophication-inducible P level is as low as 0.04 mg/L (Sims et al., 1996). Ionic strength is known to affect diffused double layer thickness, resulting in coagulation and dispersion of NPs (Hiemenez, 1986).

Increasing the I of the soil solution reduces the thickness of the diffused double layer, which should promote coagulation of soil NPs (< 200 nm). In our previous investigation, Fe-rich aluminosilicate NPs were readily available in the same soil series (Rick and Arai, 2011). It is likely that the stability of dispersed NPs was affected by I. This coagulation was especially pronounced at pH $\geq$ 6.5 for P_C, Fe_C, and Al_C (Figures 3.5a – 3.5c). It is interesting that the release of P_C, Fe_C, and Al_C follows the same pH trend (Figure 3.5), suggesting that colloid-facilitated transport of P is associated with Al- and Fe-rich particles, such as amorphous aluminosilciates and nano-HM. This trend drastically increases with increasing pH from 3.5 to 6.5. On the contrary, the release of Ca_C was not pH dependent (Figure 3.5d). Because of weakly acidic soil pH, Ca-based colloids were not expected due to its high solubility (Figure 3.5d).

To observe the effect of *I* on particle size distribution, DLS measurements of soil components (HM and KL) and GT were compared at both low (0.01 M) and high (0.1 M) *I* levels at pH 7 (Figure 3.6). No data were collected for MS, due to its large average particle size (>100 μm), which was beyond the capabilities of the DLS instrument. For all samples, the average particle size at high *I* was approximately twice that of the particle size at low *I*. For GT, HM, and KL, it was 2.72, 2.21, and 2.38 times as high, respectively. Within each component, the difference in particle size between high and low *I* was > 1 standard deviation. In summary, these DLS data of NP components support *I*-dependent soil colloid release (Figure 3.5) that increasing ionic strength promotes the coagulation of soil nanoparticles strongly.

3.4.3 Effects of Phosphate on Colloid Release Associated with Fe. Al, and Ca

Figure 3.7 shows the effect of $[P_T]$ on colloid release from the soil at the constant background electrolyte solution, 0.01 M $NaNO_3$. The total concentration of Fe_C, Al_C, and Ca_C is individually presented in Figures 3.7a, 3.7b, and 3.7c, respectively. Varying P concentration greatly affected the release of Fe_C and Al_C. (Figures 3.7a and 3.7b). When soils were suspended in "P-free" solution, moderate colloid release (5 – 70 mg/L for Fe, 12 – 115 mg/L for Al) was observed across the pH spectrum (approx. pH 4 – 9) (Figure 3.7a). Interestingly, the addition of P (total P = 0.1 mM) reduced the release of colloid down to near negligible levels. A small quantity of Ca_C was observed in the low P concentration solution ($[P_T]$ = 0.1 mM) at pH >5 (Figure 3.7c). However, the amount of Ca-P colloids was two orders of magnitude less than those of Al_C and Fe_C. Colloidal Ca

release was not significantly affected by [P]. This was not a surprising result since the TEM analysis indicated rare occurrence of Ca_C in the soil extracts.

When we further increased the P addition to 1 mM, the release of soil colloids was enhanced. The release of colloids was much greater than that of the 0.1 mM P system, especially at near neutral pH values (160 mg/L for Fe_C and 350 mg/L for Al_C).

It is likely that specific adsorption of P in NPs facilitated the dispersion of colloids and/or the coagulation of NPs to > 0.41 μm. Several theories can be postulated to explain the coagulation. First, addition of 1 mM P resulted in greater *I* in the system comparing to the system with lower [P] (0 – 0.1 mM). The increased *I* resulted in a thinner diffuse double layer (DDL), resulting, in turn in the formation of colloids. Second, the potential of P sorbed NPs was near equal to the ISP at given soil pH, resulting in coagulation of NPs. Third, it is known that specific adsorption of PO_4 on goethite can bridge goethite particles to enhance the coagulation when P was added (Anderson et al., 1985).

To test the theory above, we measured 1) the changes in surface charge of soil NP components, Fe oxyhydroxide goethite, and phyllosilicate muscovite via zeta potential measurements, and 2) changes in particle size distribution during P sorption via DLS measurements for soil NP components HM and KL, along with Fe oxyhydroxide goethite.

Zeta potential or electrophoretic mobility (EM) measurements are a useful microscopic approach for determining surface charge properties of NPs and colloids. The shear plane is at the outer edge of the inner part of the double layer and near the outer

Helmholtz plane or the Stern layer, depending on the models to describe the interface (Hunter, 1981). Inner-sphere complexes, however, cause shifts in both EM and isoelectric point (IEP) (lowering zeta potential) due to specific ion adsorption inside the shear plane (Hunter, 1981). Figure 3.8 shows the zeta potential values of soil components HM and KL, along with phyllosilicate MS and Fe oxyhydroxide GT at 0.01 M *I* at 0, 0.1, and 1 mM P addition at both pH 5 and pH 7.

In nearly all cases, with the exception of MS at pH 7, the addition of 0.1 mM P caused a dramatic decrease in the zeta potential from the 0 mM P level, indicating more negatively charged particles. This decrease was more than one standard deviation below the 0 mM P value for all soil component samples, again, except MS at pH 7. The change in zeta potential was most dramatic for GT, which decreased by 49.5 mV at pH 5 and 50.7 mV at pH 7 with the addition of 0.1 mM P, followed by HM, which decreased by 20.3 and 11.5 mV at pH 5 and 7, respectively. This supports the hypotheses of inner-sphere P adsorption by GT, KL, and HM. A further addition of P to 1 mM concentration resulted in a much less pronounced decrease in zeta potential. Goethite and HM were again the components with the largest decrease in zeta potential from 0.1 to 1 mM [P]. For GT, the zeta potential dropped by 10.9 and 7.3 mV at pH 5 and 7, respectively. For HM, the zeta potential dropped by 13.9 and 5.0 mV at pH 5 and 7, respectively. While all other samples had a decrease in zeta potential by > 1 standard deviation between 0.1 and 1 mM P, KL at pH 7 actually saw a slight increase or near equal in zeta potential. Our findings of P specific adsorption on soil mineral colloids agree with several studies. Phosphate sorption on ferrihydrite, HM, GT, and boehmite (γ-AlOOH) is known to form

inner-sphere surface complexes due to charge reversal and a lower IEP with increasing P loading level (e.g., Anderson and Malotky, 1979; Arai and Sparks, 2001; Bleam et al., 1991; Elzinga and Sparks, 2007; Hansmann and Anderson, 1985; Tejedor-Tejedor and Anderson, 1990; Van Emmerik et al., 2007).

Next, we examined the effects of P specific sorption on particle size distribution in GT, HM, and KL (Figure 3.9). Yellow highlighted regions in Figure 3.9 indicate the particle size range of colloid (200 – 410 nm) that is defined in this study. As recalled from the previous discussion, the release of soil colloids fluctuated with changes in [P] (Figure 3.7). While colloids were not detectable at [P] = 0.1 mM at pH 5 to 7, they do became available when [P] is zero or increased to 1 mM. We find that the effect of P on the coagulation property is mineral specific. When [P] is zero, some HM particles are available at the 200 to 410 nm range, but KL is only available at pH 7. KL is not within the operationally defined colloid size at pH 5. Interestingly, GT particles are not within the range at either pH value. With increasing [P] to 0.1 mM, GT particles became dispersed to be within the defined colloid size range at both pH values. When we further increased [P] to 1mM, HM particles are only within this size range at pH 7. In the case of KL, the availability of colloids within the range increased with decreasing pH. Although we were unable to demonstrate DLS measurements on MS and amorphous aluminosilicate NPs, the release of soil colloid can be postulated by "mineral specific" coagulation properties of soil colloid components.

3.4.4 Effects of Phosphate on Colloidal Phosphorus Release

As discussed in the previous section, the P ligand could contribute to the coagulation of NPs. The concentration of dissolved P can be varied depending on timing of agricultural practices. While high [P] in runoff is expected in manure amended soils during storm events, (e.g., Addiscott and Thomas, 2000; Hollmann et al., 2008; Makris et al., 2006), low [P] in soil solutions is a likely scenario after the growing season, (e.g., Mayer and Jarrell, 1995). Therefore it is important to study the effect of P ligand on colloid facilitated P release. The P_C contribution over various [P_T] was analyzed by comparing MRP (<0.2 μm) to P_C over pH (Figure 3.10). In this figure, negative sorption corresponds to the release. The concentration of P associated colloid and MRP is shown in the dark blue area and light shaded area, respectively. The following sections consist of: 1) P_C release as a function of [P] and 2) a comparison between P_C and MRP.

Similar to overall colloid concentration, as determined by Fe_C and Al_C (Figure 3.7a – 3.7b), the P_C fraction was greatest at 1 mM added P (dark grey area in Figure 3.10a), followed by 0 mM added P, followed by 0.1 mM added P. When soils were suspended in "P free" solutions, the P_C fraction was largest (6.24 mg/kg) at pH=4.67, while with 0.1 mM added P, P_C only occurred at approximately 3.12 mg/kg at pH 6.2 (Figures 3.10a – 3.10b). Increasing the P addition to 1 mM caused P_C to be largest (36.25 mg/kg at pH 4.23, and 18.31 mg/kg at pH 7.07), with a decrease in the mildly acidic pH range.

In our system, the contribution of P_C is very small comparing to the MRP at respective pH values in each P treatment. At the largest P_C release in each system, the %

ratio of P_C: MRP is 6.85% when [P] = 0 mM, 2.65% when [P] = 0.1 mM, and 5.31% when [P] = 1 mM. This finding is consistent is our previous investigation that P_C release in this Ultisol is near negligible (Rick and Arai, 2011). Overall, there are substantial quantities of MRP release in each system. The [MRP] increases with increasing the addition of P. In the 0, 0.1, and 1 mM [P] systems, [MRP] was as high as ~250 mg/L at pH 7.2 (Figure 3.10a), ~240 mg/L at pH 3.5 (Figure 3.10b), and ~720 mg/L at pH 7.4 (Figure 3.10c), respectively. Overall, the MRP fraction showed a similar trend across the P additions, with the lowest MRP released in mildly acidic pH conditions, between pH 5.5 and 6.5 (Figure 3.10). This decrease is probably attributed to the formation of Ca/Mg phosphate solubility products. Overall, P release for both 0.1 mM and 1 mM was in great excess of the amount added (Figure 3.10b – 3.10c), especially below pH 4 and above pH 7 (Figures 3.10a and 3.10b). Considering the total P level in this P rich soil, it was likely that P sorption was already at the maximum sorption prior to the experiments. Our agronomic Mehlich-1 test suggested the level of P = 222.5 mg/kg, which is rated excessively high.

3.4.5 Significance of Colloid Facilitated Phosphorus Transport in Soils

This study, as well as previous work by our research group (Rick and Arai, 2011), showed very little contribution of P_C in the same soil series. Several other studies also recorded little to no observation of P_C (e.g., Fuchs et al., 2009; Liang et al., 2010; Siemens et al., 2008). This was particularly apparent in the study by Fuchs et al. (2009). While P_C was not the primary P form in these studies, experiments conducted under

different setting and environmental condition produced a wide range of results. We believe that the lack of colloid-facilitated transport, including the case study information provided here, can be attributed to the following physicochemical parameters: 1) total P level in native soils, 2) % organic matter (OM) content in soils, 3) soil pH, and 4) *I* of soil solutions. To facilitate the evaluation of these physicochemical parameters, the following colloid facilitated P transport studies were selected and the results were carefully summarized in Table 3.1. The studies are arranged by degree of P_C observation, decreasing down the column.

A low level of native P (33 mg/kg) in the soil, especially apparent in the Fuchs et al. (2009) study, may lead to overall P sorption in bulk soil minerals, instead of P release with particulates. Because of the strong chemisorption of P in soils, the input (100 mg/L) of P ligands may not contribute sufficiently to surface charge properties of NPs or solubility products. If P saturation has not yet been reached in a soil, the soil surfaces themselves may be providing a sink for overall P sorption.

Our investigations including this manuscript and the previous work (Rick and Arai, 2011) have been conducted in a soil with low organic C content (<0.5%). This is typically the case for other soils lacking P_C contributions as well (Fuchs et al., 2009; Siemens et al., 2008). In the literature surveyed, studies conducted in high organic C soils had much higher rates of P_C content (de Jonge et al., 2004; Koopmans et al., 2005; Shand et al., 2000; Siemens et al., 2004). Taking this a step further, artificially enhancing the organic C of the soil (e.g., adding manure fertilizer) has been shown to increase the colloidal fraction of P even further. Similar research findings (i.e., organic carbon

enhanced colloidal P release) were also reported in several other studies not included in Table 3.1 (e.g., Makris et al., 2006; Zang et al., 2011). Organically bound P and or organic P (e.g., inositol phosphate) in humic substances might be more susceptible to solute movement than orthophosphate bound to inorganic mineral fractions in soils.

When the results of studies that were reviewed in Table 3.1 were compared, we found the importance of soil pH on P_C release, especially in the absence of high levels of organic C. Mildly acidic pH appeared to impede P association with colloids in all studies considered (Fuchs et al., 2009; Liang et al., 2010; Rick and Arai, 2011; Siemens et al., 2008). It seems, as in several cases, that high organic C levels can promote P_C formation even in unfavorable pH conditions (Ilg et al., 2005; Mayer and Jarrell, 1995; Shand et al., 2000; Siemens et al., 2004). Likewise, it also appears that high pH can promote colloidal P formation even in the absence of large amounts of OM (Heathwaite et al., 2005; Turner et al., 2004). The increase of P_C at neutral to high pH values could be due, in part, to the charge characteristics of soil minerals. Many aluminum and iron (oxy)hydroxides experience their point of zero charge (PZC) between pH 6.5 and 8.5 (Stumm and Morgan, 1996), promoting flocculation and coagulation of particles when pH is near or equal to PZC, likely in the colloidal size range. This sudden increase in available colloidal-sized particles above pH 6.5 could facilitate the P_C transport process.

Finally, *I* also appears to play a role in soil colloid formation and P association. The trend is not as clear as that of native [P], organic C, or pH. Several studies reviewed in Table 3.1 exhibit a large amount of P_C observation after the addition of excessive amounts of mineral fertilizers (Heathwaite et al., 2005; Ilg et al., 2005; Shand et al.,

2000; Siemens et al., 2004). While electrolytes may not have been added to these studies with the intention of increasing *I*, the excessive addition of fertilizer will cause the same effect. Increasing *I* along with the addition of P causes a compression of the diffuse double layer, leading soil particles to coagulate. This is likely the mechanism by which P_C formed in these case studies.

In summary, it is important to note that the current general perceptions in the field of geo/soil chemistry may overstate the importance of colloid-facilitated transport of P. While P_C is clearly the predominant form of P in some studies conducted in high native [P] soils, high pH, high OM, and/or high fertilization/*I* conditions (de Jonge et al., 2004; Heathwaite et al., 2005; Ilg et al., 2005; Koopmans et al., 2005; Shand et al., 2000; Siemens et al., 2004; Turner et al., 2004), it is not the predominant form of P under other conditions (Fuchs et al., 2009; Liang et al., 2010; Mayer and Jarrell, 1995; Rick and Arai, 2011; Siemens et al., 2008). While there has been much evidence to support colloidal-facilitated P transport in the last few decades, the contribution of P_C with respect to "non-point pollution" should be carefully evaluated based on environmental conditions in assessing the environmental risk from P rich agricultural lands.

3.5 References

Addiscott, T.M., and D. Thomas. 2000. Tillage, mineralization and leaching: phosphate. Soil Till. Res. 53:255-273.

Anderson, M.A., and D.T. Malotky. 1979. The adsorption of protolyzable anions on hydrous oxides at the isoelectric pH. J. Colloid Interf. Sci. 72:413-427.

Anderson, M.A., M.I. Tejedor-Tejedor, and R.R. Stanforth. 1985. Influence of aggregation on the uptake kinetics of phosphate by goethite. Environ. Sci. Technol. 19:632-637.

Arai, Y. 2010. Effects of dissolved calcium on arsenate sorption at the kaolinite-water interface. Soil Sci. 175:207-213.

Arai, Y., and D.L. Sparks. 2001. ATR-FTIR spectroscopic investigation on phosphate adsorption mechanisms at the ferrihydrite-water interface. J. Colloid Interf. Sci. 241:317-326.

Arai, Y., K.J.T. Livi, and D.L. Sparks. 2005. Phosphate reactivity in long-term poultry litter-amended southern Delaware sandy soils. Soil Sci. Soc. Am. J. 69:616-629.

Bauer, J.E., K.C. Ruttenberg, D.M. Wolgast, E. Monaghan, and M.K. Schrope. 1996. Cross-flow filtration of dissolved and colloidal nitrogen and phosphorus in seawater: Results from an intercomparison study. Mar. Chem. 55:33-52.

Bleam, W.F., P.E. Pfeffer, S. Goldberg, R.W. Taylor, and R. Dudley. 1991. A ^{31}P solid-state nuclear magnetic resonance study of phosphate adsorption at the boehmite/aqueous solution interface. Langmuir. 7:1702-1712.

Burkholder, J.M., E.J. Noga, C.H. Hobbs, and H.B. Glasgow. 1992. New 'phantom' dinoflagellate is the causative agent of major estuarine fish kills. Nature. 358:407-410.

Carpenter, S.R., N.F. Caraco, D.L. Correll, R.W. Howarth, A.N. Sharpley, and V.H. Smith. 1998. Nonpoint pollution of surface waters with phosphorus and nitrogen. Ecol. Appl. 8:559-568.

de Jonge, L.W., P. Moldrup, G.H. Rubaek, K. Schelde, and J. Djurhuus. 2004. Particle leaching and particle-facilitated transport of phosphorus at field scale. Vadose Zone J. 3:462-470.

Elzinga, E.J., and D.L. Sparks. 2007. Phosphate adsorption onto hematite: An in situ ATR-FTIR investigation of the effects of pH and loading level on the mode of phosphate surface complexation. J. Colloid Interf. Sci. 308:53-70.

Filella, M., C. Deville, V. Chanudet, and D. Vignati. 2006. Variability of the colloidal molybdate reactive phosphorous concentrations in freshwaters. Water Res. 40:3185-3192.

Fuchs, J.W., G.A. Fox, D.E. Storm, C.J. Penn, and G.O. Brown. 2009. Subsurface transport of phosphorus in riparian floodplains: Influence of preferential flow paths. J. Environ. Qual. 38:473-484.

Gustafsson, J.P. 2010. Visual MINTEQ [Online]. Available by KTH, Department of Land and Water Resources Engineering http://www.lwr.kth.se/English/OurSoftware/vminteq/index.htm (verified 20 July 2012).

Hansmann, D.D., and M.A. Anderson. 1985. Using electrophoresis in modeling sulfate, selenite, and phosphate adsorption onto goethite. Environ. Sci. Technol. 19:544-551.

Haygarth, P.M., M.S. Warwick, and W.A. House. 1997. Size distribution of colloidal molybdate reactive phosphorus in river waters and soil solution. Water Res. 31:439-448.

Heathwaite, A.L., and R.M. Dils. 2000. Characterising phosphorus loss in surface and subsurface hydrological pathways. Sci. Total Environ. 251:523-538.

Heathwaite, L., P. Haygarth, R. Matthews, N. Preedy, and P. Butler. 2005. Evaluating colloidal phosphorus delivery to surface waters from diffuse agricultural sources. J. Environ. Qual. 34:287-298.

Heckrath, G., P.C. Brookes, P.R. Poulton, and K.W.T. Goulding. 1995. Phosphorus leaching from soils containing different phosphorus concentrations in the Broadbalk Experiment. J. Environ. Qual. 24:904-910.

Hens, M., and R. Merckx. 2001. Functional characterization of colloidal phosphorus species in the soil solution of sandy soils. Environ. Sci. Technol. 35:493-500.

Hens, M., and R. Merckx. 2002. The role of colloidal particles in the speciation and analysis of "dissolved" phosphorus. Water Res. 36:1483-1492.

Hiemenez, P.C. 1986. Principles of Colloid and Surface Chemistry 2nd ed. Marcel Dekker, Inc., New York.

Hollmann, M., K.F. Knowlton, M.R. Brosius, M.L. McGilliard, and G.L. Mullins. 2008. Phosphorus runoff potential of varying sources of manure applied to fescue pastures in Virginia. Soil Sci. 173:721-735.

Hunter, R.J. 1981. Zeta Potential in Colloid Science. Academic Press, London.

Ilg, K., J. Siemens, and M. Kaupenjohann. 2005. Colloidal and dissolved phosphorus in sandy soils as affected by phosphorus saturation. J. Environ. Qual. 34:926-935.

Ilg, K., P. Dominik, M. Kaupenjohann, and J. Siemens. 2008. Phosphorus-induced mobilization of colloids: Model systems and soils. Euro. J. Soil Sci. 59:233-246.

Koopmans, G.F., W.J. Chardon, and C. van der Salm. 2005. Disturbance of water-extractable phosphorus determination by colloidal particles in a heavy clay soil from the Netherlands. J. Environ. Qual. 34:1446-1450.

Kretzschmar, R., M. Borkovec, D. Grolimund, and M. Elimelech. 1999. Mobile subsurface colloids and their role in contaminant transport. Adv. Agron. 66:121-193.

Lawton, L.A., and G.A. Codd. 1991. Cyanobacterial (blue-green algal) toxins and their significance in UK and European waters. J. Inst. Water Env. Man. 5:460-465.

Lewitus, A.J., K.C. Hayes, B.M. Willis, J.M. Burkholder, H.B. Glasgow, A.F. Holland, P.P. Maier, P.A. Rublee, and R. Magnien. 2002. Low abundance of the dinoflagellates, *Pfiesteria piscicida*, *P. shumwayae*, and *Cryptoperidiniopsis* spp., in South Carolina tidal creeks and open estuaries. Estuaries. 25:586-597.

Lewitus, A.J., L.B. Schmidt, L.J. Mason, J.W. Kempton, S.B. Wilde, J.L. Wolny, B.J. Williams, K.C. Hayes, S.N. Hymel, C.J. Keppler, and A.H. Ringwood. 2003. Harmful algal blooms in South Carolina residential and golf course ponds. Popul. Environ. 24:387-413.

Liang, X.Q., J. Liu, Y.X. Chen, H. Li, Y.S. Ye, Z.Y. Nie, M.M. Su, and Z.H. Xu. 2010. Effect of pH on the release of soil colloidal phosphorus. J. Soils Sediments. 10:1548-1556.

Makris, K.C., J.H. Grove, and C.J. Matocha. 2006. Colloid-mediated vertical phosphorus transport in a waste-amended soil. Geoderma. 136:174-183.

Mayer, T.D., and W.M. Jarrell. 1995. Assessing colloidal forms of phosphorus and iron in the Tualatin River Basin. J. Environ. Qual. 24:1117-1124.

Rick, A.R., and Y. Arai. 2011. Role of natural nanoparticles in phosphorus transport processes in ultisols. Soil Sci. Soc. Am. J. 75:335-347.

Rublee, P.A., J.W. Kempton, E.F. Schaefer, J.M. Burkholder, H.B. Glasgow, and D.W. Oldach. 1999. PCR and FISH detection extends the range of *Pfiesteria piscicida* in estuarine waters. Va. J. Sci. 50:325-336.

Rublee, P.A., J.W. Kempton, E.F. Schaefer, C. Allen, J. Harris, D.W. Oldach, H. Bowers, T. Tengs, J.M. Burkholder, and H.B. Glasgow. 2001. Use of molecular probes to assess geographic distribution of *Pfiesteria* species. Environ. Health Perspect. 109:765-767.

Schwertmann, U., and R.M. Cornell. 1991. Iron Oxides in the Laboratory. 2nd ed. Wiley, Weinheim, Germany.

Shand, C.A., S. Smith, A.C. Edwards, and A.R. Fraser. 2000. Distribution of phosphorus in particulate, colloidal and molecular-sized fractions of soil solution. Water Res. 34:1278-1284.

Sharpley, A.N., R.W. McDowell, and P.J.A. Kleinman. 2001. Phosphorus loss from land to water: Integrating agricultural and environmental management. Plant Soil. 237:287-307.

Siemens, J., K. Ilg, F. Lang, and M. Kaupenjohann. 2004. Adsorption controls mobilization of colloids and leaching of dissolved phosphorus. Euro. J. Soil Sci. 55:253-263.

Siemens, J., K. Ilg, H. Pagel, and M. Kaupenjohann. 2008. Is colloid-facilitated phosphorus leaching triggered by phosphorus accumulation in sandy soils? J. Environ. Qual. 37:2100-2107.

Sims, J.T., R.R. Simard, and B.C. Joern. 1998. Phosphorus loss in agricultural drainage: Historical perspective and current research. J. Environ. Qual. 27:277-293.

Sims, J.T., A.S. Andres, J.M. Denver, W.J. Gangloff, P.A. Vadas, and D.R. Ware. 1996. Assessing the impact of agricultural drainage on ground and surface water quality in Delaware: Development of best management practices for water quality protection. Delaware Department of Natural Resources and Environmental Control, Dover, Delaware.

Stumm, W., and J.J. Morgan. 1996. Aquatic Chemistry. 3rd ed. John Wiley & Sons, Inc., New York.

Tejedor-Tejedor, M.I., and M.A. Anderson. 1990. Protonation of phosphate on the surface of goethite as studied by CIR-FTIR and electrophoretic mobility. Langmuir. 6:602-611.

Turner, B.L., M.A. Kay, and D.T. Westermann. 2004. Colloidal phosphorus in surface runoff and water extracts from semiarid soils of the western United States. J. Environ. Qual. 33:1464-1472.

Van Emmerik, T.J., D.E. Sandstrom, O.N. Antzutkin, M.J. Angove, and B.B. Johnson. 2007. ^{31}P solid-state nuclear magnetic resonance study of the sorption of phosphate onto gibbsite and kaolinite. Langmuir. 23:3205-3213.

Verity, P.G. 2010. Expansion of potentially harmful algal taxa in a Georgia Estuary (USA). Harmful Algae. 9:144-152.

Zang, L., G. Tian, X. Liang, J. Liu, and G. Peng. 2011. Effect of water-dispersible colloids in manure on the transport of dissolved and colloidal phosphorus through soil column Afr. J. Agric. Res. 6:6369-6376.

Table 3.1. Summary of selected coll. P literature. Studies arranged in descending order of observance of coll. P.

Soil Type	pH	Org. C (%)	Total P (mg/kg)	Settings of study	*I* (M)	Part. size definition	Coll.-P as % of Total P	Notes	Ref.
Heavy clay from Waarden-burg, the Nether-lands	6.7 to 7.7	5.4% at surf.	747 at surf.	Lab-based	0.03M w/ $CaCl_2$, adj. to 0.51M w/ NaCl	>0.45 μm	Refilt. samples had avg. 94% more coll. P	0.45 μm low-*I* filtrates given 0.51 M NaCl, then refilt..	(Koopmans et al., 2005)
Sandy loam near Røgen, Denmark	6.42 to 8.16	1.5%	734	Column study	0.0088	0.24 to 2 μm	75%	Downward part. transp. in columns; structure impt.	(de Jonge et al., 2004)
Fine sandy soils near Münster, Germany	5.5 to 6.2 at surf., 7.1 to 8.2 below 4 m	1.1 to 2.5% at surf., dec. w/ depth	610 to 884 at surf., dec. w/ depth	Column study	No added elect.	<0.01 to 0.45 μm	Highly var., from approx. 0 to 95%	Artific. inc. [P] may promote coll. P form., esp. at low *I*	(Siemens et al., 2004)
Peaty podzol from northeast Scotland	5.0	High, due to peat present	3356, additional from P mineral fertilizers	Lab-based	0.03 M w/ $CaCl_2$, adj. further to 0.1 M w/ NaCl	Multi-filt. at 1.6, 1.2, 0.45, and 0.22 μm	MRP: 55% >1.2 μm, 19% >0.45, 4% >0.22 μm; OP: 34% >1.2 μm, 39% >0.45 μm, 7% >0.22 μm	MRP assoc. w/ large soil coll., while OP assoc. w/ smaller coll. in high OM soils	(Shand et al., 2000)

Table 3.1. continued

Soil Type	pH	Org. C (%)	Total P (mg/kg)	Settings of study	*I* (M)	Part. size definition	Coll.-P as % of Total P	Notes	Ref.
Silt loam soils from the NW US	7.7 to 8.1	0.54 to 0.9%	Olsen P: 4 to 145	Field study of surf. runoff	No added elect.	0.001 to 1 μm	Up to 56% in calcar-eous soils	[Coll.] highest w/ high pH and [$CaCO_3$], low [OM]	(Turner et al., 2004)
Several UK soils ranging from silt loam to clay from	Ranges from 5.3 to 8.1	Ranges from 0.13 to 0.37%	Ranges from 461 to 1373	Both lab and field studies	Varies from 0 added to 0.03 M w/ NaCl and $CaCl_2$	Size cutoffs at 2, 0.8, 0.45, 0.22, and 0.001 μm	Highly var. between size fractions and P add.	Coll. P increased w/ fert. P additions, esp. on coll. >0.45 μm in size	(Heathwaite et al., 2005)
Sand and sandy loam from Northwest Germany	Top soil 6.1 to 7.2, below 30 cm 4.7-6.8	Not given, but inc. w/ addition of org. fert.	Available P 47 to 140. Various min. and/or org. P fertilizers used	Lab-based column study	0 added and 0.01 M KCl	Approx. 0.01 to 1.2 μm	Around 28% for top 30 cm, up to 94% below 30 cm depth	Coll. P release fac. by low *I*	(Ilg et al., 2005)

Table 3.1. continued

Soil Type	pH	Org. C (%)	Total P (mg/kg)	Settings of study	*I* (M)	Part. size definition	Coll.-P as % of Total P	Notes	Ref.
Fine silty to clay soils from Tualatin Basin, NW Oregon	5.0 to 5.8	"high levels"	660 to 2304	Field testing data	No added elect.	0.05 to 1 μm	Ranges from 0 to 48%, especially high imm. after rain events	Coll. P may be affected by seasonal var. and/or rainfall	(Mayer and Jarrell, 1995)
Loamy sands from Branden-burg, Germany	4.0 to 6.1	0.39 to 0.83%	Both sites fertilized, one w/ mineral P and one w/ manure	Field study	None in field, 0.01 M w/ KCl for lab expt.	<1.2 μm, lower cutoff via cent. (approx. 0.02 μm from calc.)	1 to 37% (most <10%)	Coll. P minor fraction of total P under these cond.	(Siemens et al., 2008)
Silty loam near Hang-zhou, China	Soil pH 6.0, adj. to var. levels from 1.4-9.9 expt.	1.74%	1720	Lab-based	No added elect.	Approx. 0.01 to 1 μm	<5% between pH 4 and 7; 25.5% at pH 7.6	Coll. P greatest below pH 4 and above pH 7	(Liang et al., 2010)

Table 3.1. continued

Soil Type	pH	Org. C (%)	Total P (mg/kg)	Settings of study	*I* (M)	Part. size definition	Coll.-P as % of Total P	Notes	Ref.
Sandy loam soil from upstate South Carolina	5.32 to 5. 69	<0.5%	262 to 900	Lab-based	0.065 M adj. w/ $NaNO_3$	0.01 to 0.2 μm	Neg., <15%	P not associated w/ small coll. in acidic, sandy, low OM soils	(Rick and Arai, 2011)
Gravelly loam near Tahlequah, Oklahoma	Mildly acidic charact-eristic of region	Low (0.5-1%) charact-eristic of region	33 in top 15 cm, no fertilizer for several years	100 mg/L P injected const. trench sites in field	No added elect.	Filt. at 0.45 μm; coll. vs. diss. det. through analytical methods	Neg.	Essent. no coll. P under pref. or non-pref. flow paths	(Fuchs et al., 2009)
George-town, South Carolina sediment, 95% quartz	5.2 in ground-water	0.1%	0 to 120 mg/L P added	Column study	0.0004 M in ground-water	>0.03 μm	Not meas.	Addition of 0.5 mM P + 0.5 mM ascorbic acid resulted in highest coll. release (meas. by turbidity)	(Swartz and Gschwend, 1998)

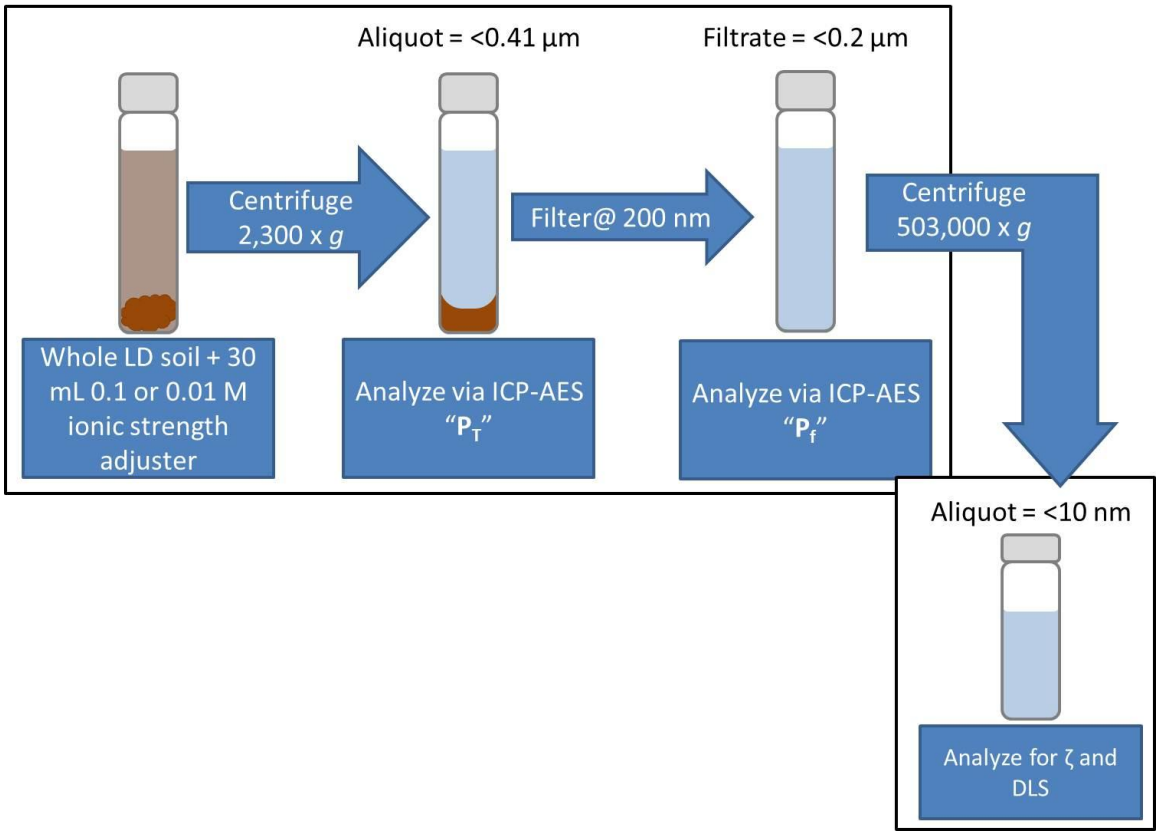

Figure 3.1. Flow chart of particle separation by size using centrifugation and filtration methods.

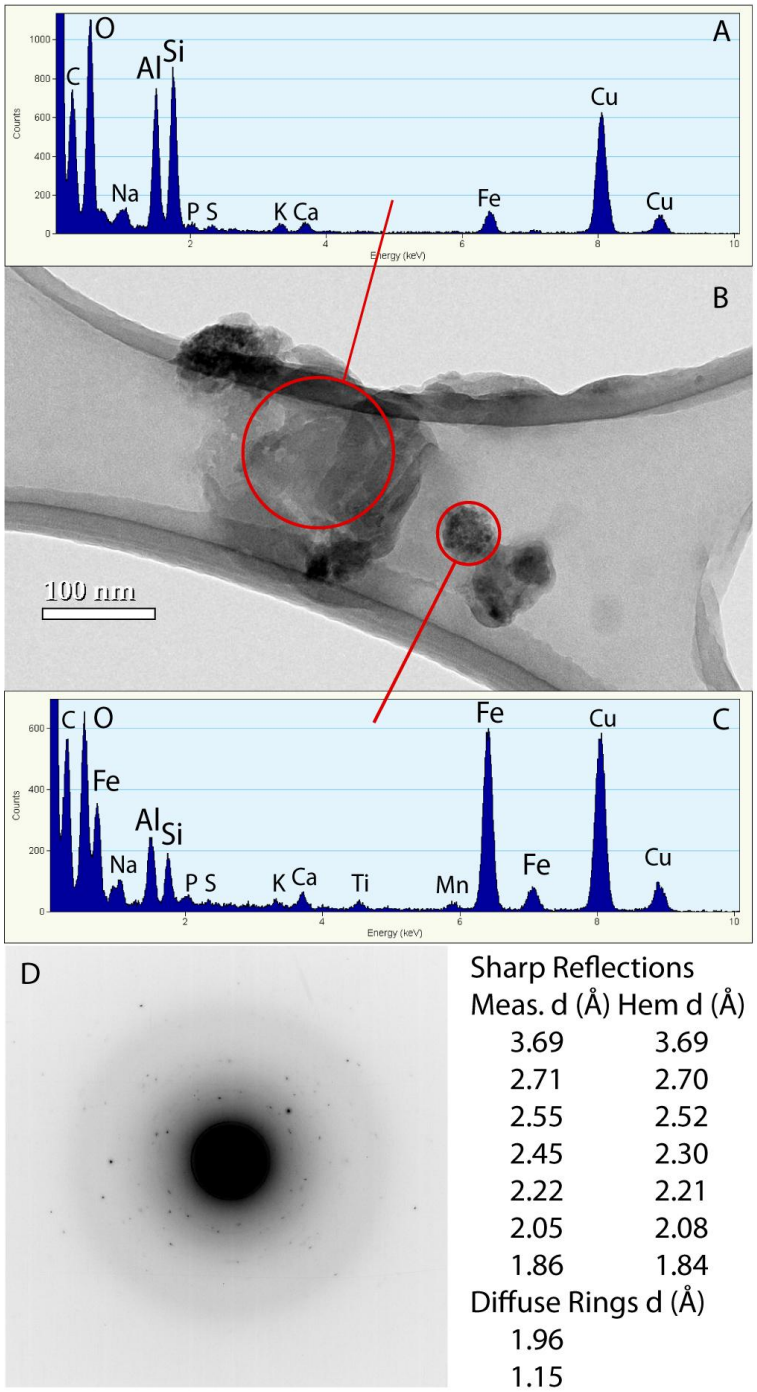

Figure 3.2. Transmission electron microscopic analysis of Cecil soil nanoparticles (d = 0.01 to 0.2 μm) a) EDS analysis of amorphous material. Cu and C originate from the grid holder and support film; b) TEM image of amorphous Al-Si-rich material and nano-hematite; c) EDS of nano-hematite mixed with some amorphous Al-Si-rich material; d) SAED of b) and matching of reflections with hematite.

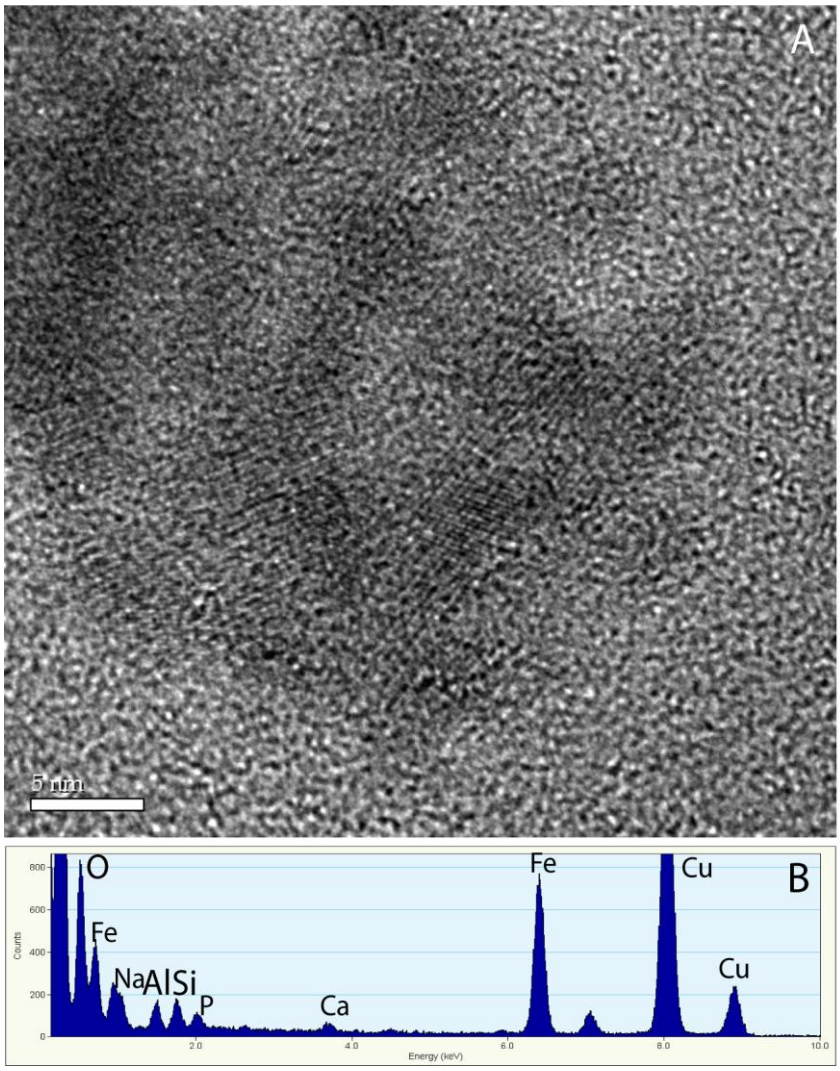

Figure 3.3. Transmission electron microscopic analysis of Cecil soil nanoparticles (d = 0.01 to 0.2 μm). a) HRTEM image of nano-hematite particles ranging from 7 to 15 nm in diameter; b) EDS of nano-hematite cluster.

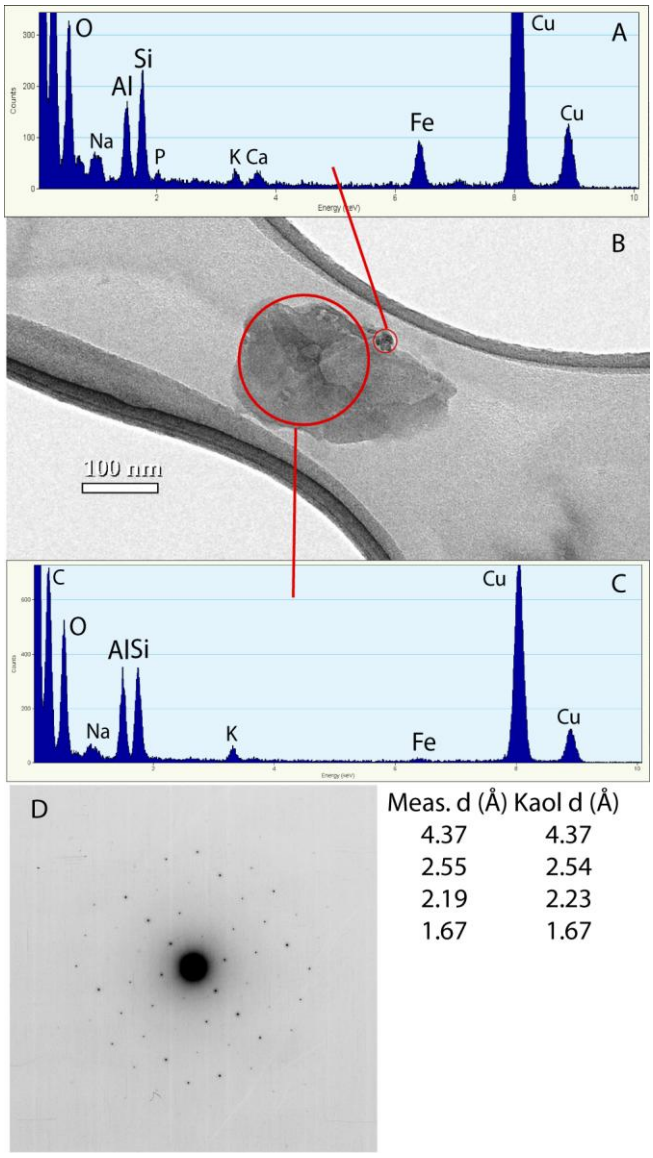

Figure 3.4. Transmission electron microscopic analysis of Cecil soil nanoparticles (d = 0.01 to 0.2 μm). a) EDS of nano-hematite cluster; b) TEM image of phyllosilicate with an associated nano-hematite cluster; c) EDS of phyllosilicate; d) SAED of phyllosilicate and matching of measured reflections with kaolinite.

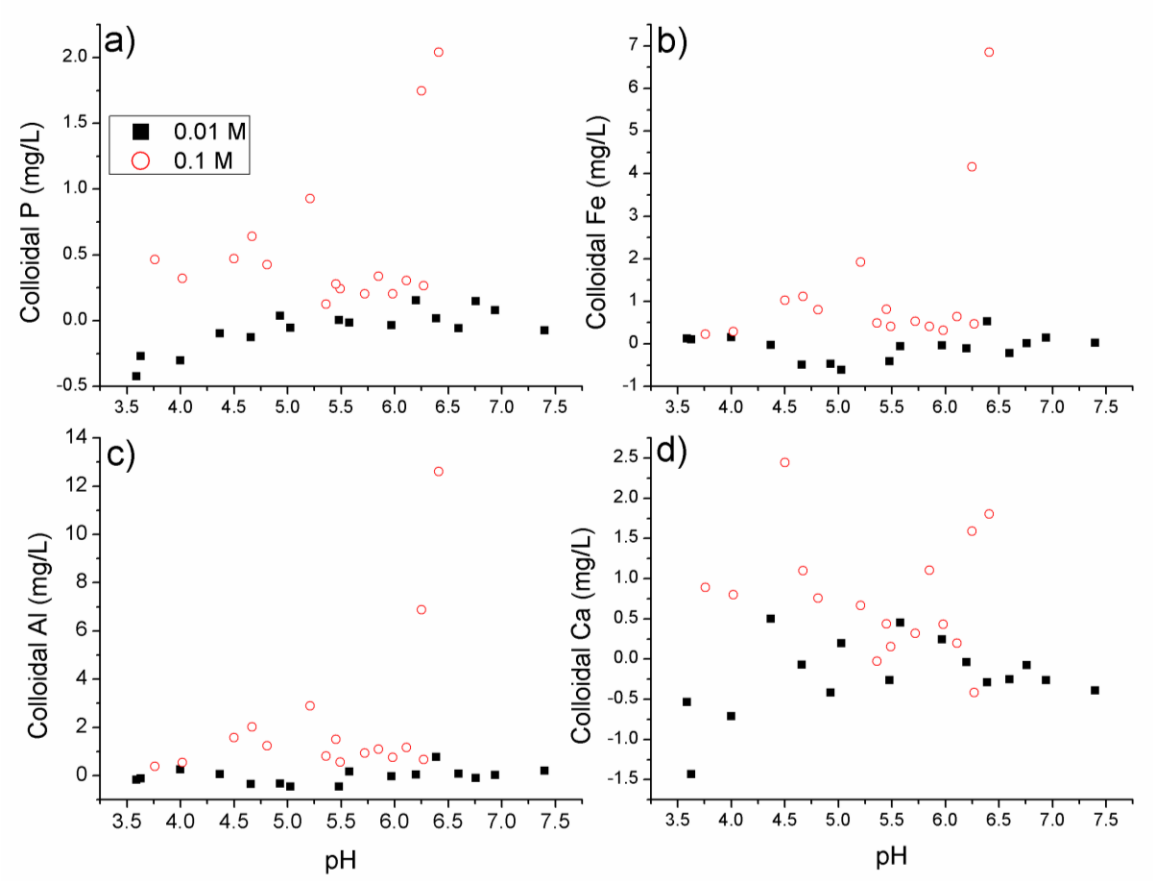

Figure 3.5. pH dependent release of soil colloids (d: 0.2-0.4 µm) associated with phosphorus (a), iron (b), aluminum (c), and calcium (d) as a function of ionic strength (0.01 and 0.1 M $NaNO_3$). All experiments were conducted in the presence of 0.1 mM NaH_2PO_4.

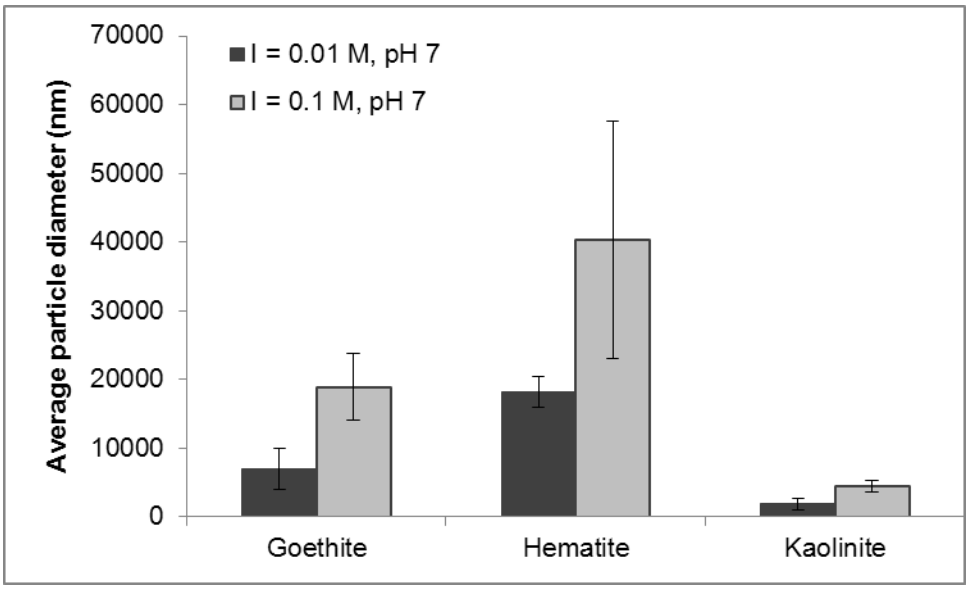

Figure 3.6. Average particle diameter of goethite and two soil components (hematite and kaolinite) as determined by dynamic light scattering measurements at pH 7 in 0.01 or 0.1 M $NaNO_3$ solutions.

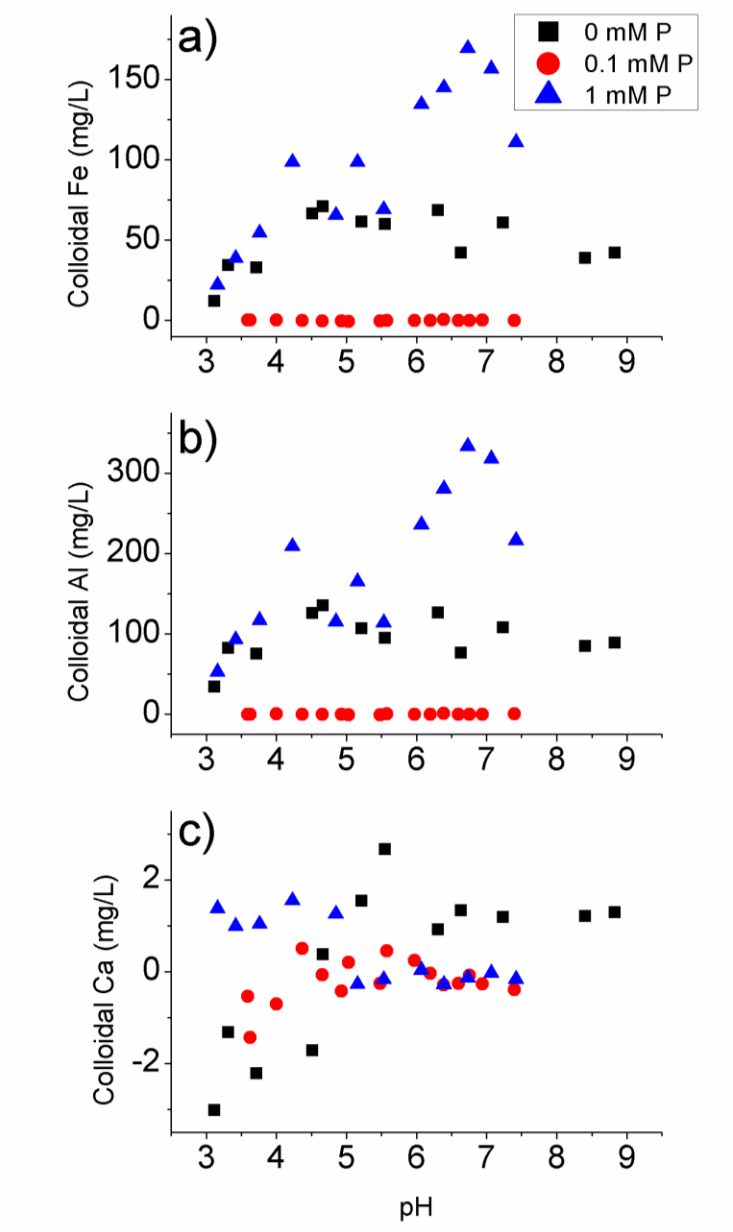

Figure 3.7. pH dependent release of soil colloids (d: 0.2-0.4 µm) associated with iron (a), aluminum (b), and calcium (c) as a function of [P]: 0, 0.1, and 1 mM NaH_2PO_4.

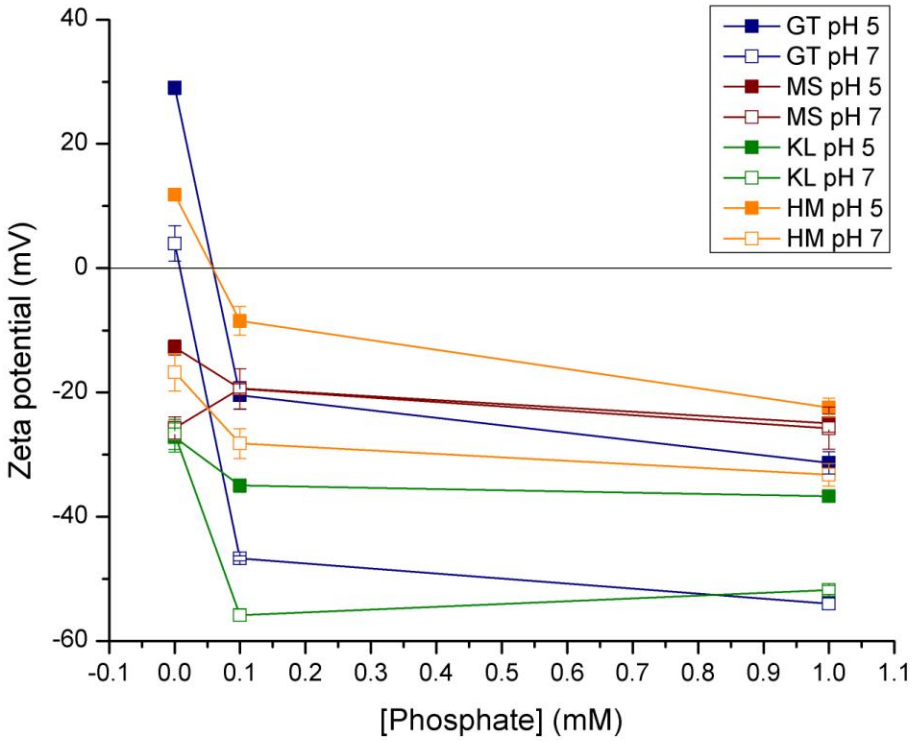

Figure 3.8. Zeta potential of soil components muscovite (MS), kaolinite (KL), and hematite (HM); and goethite (GT) at ionic strength = 0.01 M $NaNO_3$. The reaction condition was varied at pH 5 or 7 and total [P] = 0, 0.1 or 1 mM.

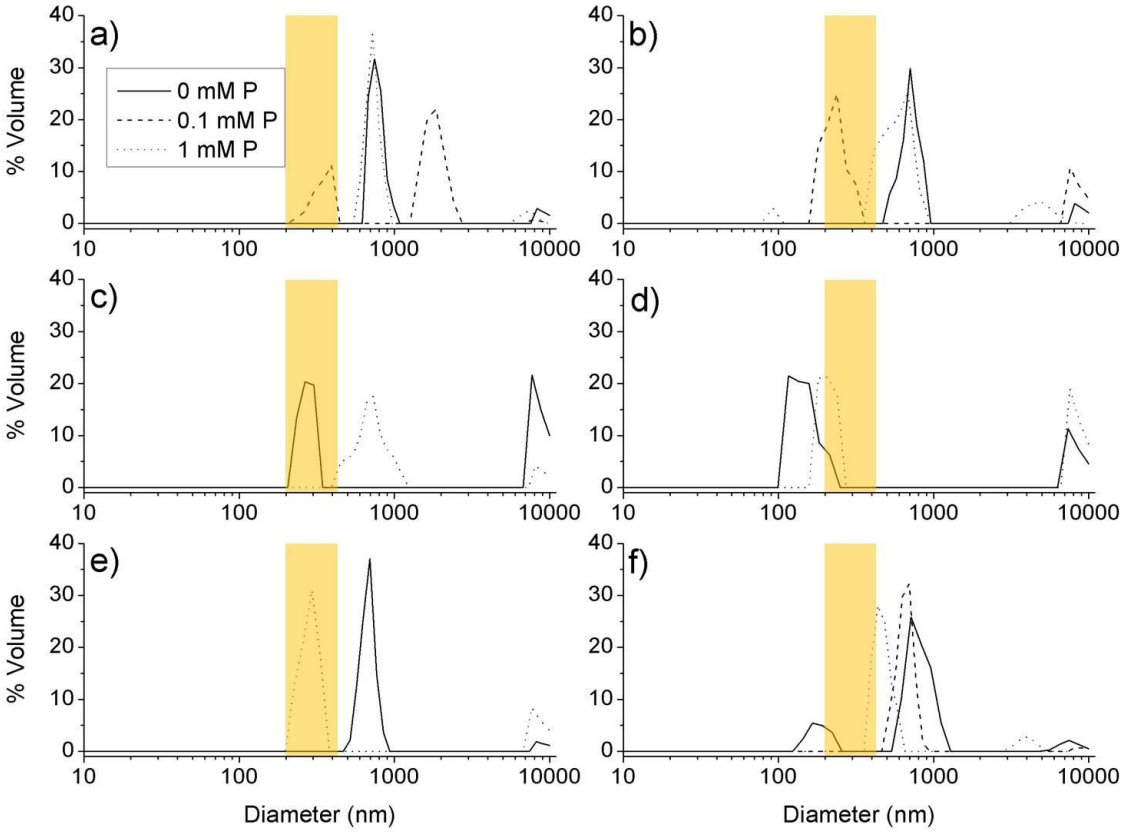

Figure 3.9. Particle size as determined by dynamic light scattering of goethite and soil nanoparticle components at ionic strength = 0.01 M $NaNO_3$ as a function of [P] = 0, 0.1 or 1 mM and pH 5 and 7: a) goethite (GT) at pH 5; b) GT at pH 7; c) hematite (HM) at pH 5; d) HM at pH 7; e) kaolinite (KL) at pH 5; f) KL at pH 7. Shaded regions represent the operationally defined soil colloid definition of 0.2 to 0.41 µm (=200 – 410 nm). Several lines not displayed (i.e., HM 0.1 mM P at pH 5 and 7, KL 0.1 mM P at pH 5, and all muscovite samples) due to all particles in these samples being >9900 nm in diameter.

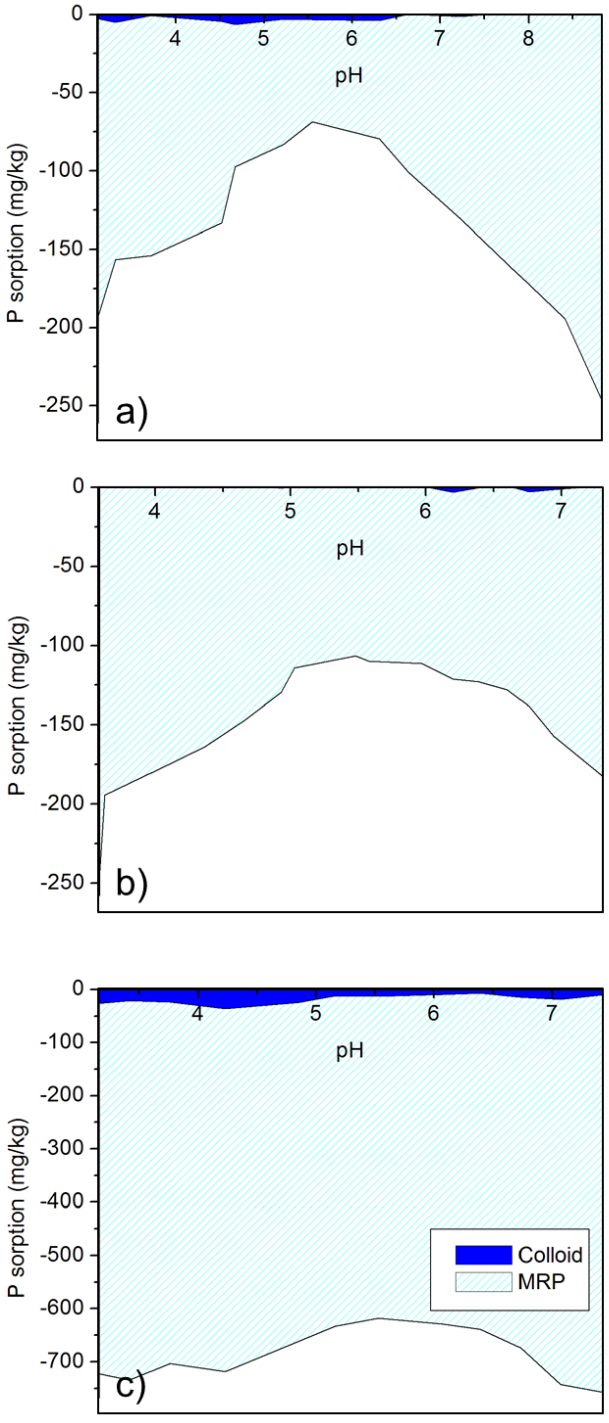

Figure 3.10. Negative phosphate sorption (P release) envelope on Cecil sandy loam as a function of [P]: (a) 0, (b) 0.1, and (c)1 mM NaH_2PO_4. All experiments were conducted in 0.1 M $NaNO_3$. Light grey shaded areas indicate dissolved P concentration, while dark grey shaded area indicate colloidal P concentration.

CHAPTER FOUR

PARTICLE SPECIFIC CHEMICAL FATE OF NANOSILVER IN REDUCING SOILS

4.1 Abstract

The chemical fate of manufactured silver nanoparticles (AgNPs) (15-90 nm and with and without polyvinylpyrrolidone (PVP) coating) was investigated in agricultural soils under reducing redox conditions using experimental geochemistry (batch dissolution and sorption isotherm) and X-ray absorption near edge structure spectroscopy (XANES) analysis, including linear combination (LC) of reference compound fit and principal component analysis (PCA). While dissolution of AgNPs increased with decreasing particle size, we found that all AgNPs were readily retained (>97% sorption) in soils over the course of 48 hr. After 30 days, all AgNPs persisted to a certain extent (~22-82%); however, there was particle specific chemical transformation that was kinetically limited. Sulfidation was more pronounced in PVP coated AgNPs whereas the humic acid (HA) fraction was dominant in uncoated AgNPs. Partitioning of AgNPs in soils and particle specific reactivity of AgNPs should be accounted for when predicting the fate of AgNPs in reducing heterogeneous environments.

4.2 Introduction

Nanotechnology is emerging as one of the primary technological advances of our day. Silver nanoparticles in particular, have gained commercial popularity through their

use as a reliable antimicrobial agent, and have been adapted for a wide variety of uses as such (Benn et al., 2010; Benn and Westerhoff, 2008). As the commercial and home usage of AgNP products and technologies increases in the future, so will AgNP release to the environment. Although ionic silver (Ag(I)) has long been used as an antimicrobial agent, Sondi and Salopek-Sondi (2004) first demonstrated the antimicrobial effects of AgNPs against *Escherichia coli* in 2004. While the exact method of toxicity to microorganisms has not been established, AgNPs can work through several pathways to cause cellular toxicity: binding to bacterial membranes, causing distress to the cell; and penetrating cell membranes, causing cell death (Morones et al., 2005; Sondi and Salopek-Sondi, 2004). Navarro et al. (2008) found that AgNPs may, in fact, be more toxic to bacterial cells than Ag(I). The toxicity of AgNPs to bacteria, algae, small aquatic invertebrates, and fish in pure culture systems has been well documented in the scientific literature (e.g., Chae et al., 2009; Choi et al., 2008; Griffitt et al., 2008; Navarro et al., 2008; Sondi and Salopek-Sondi, 2004). A number of studies have demonstrated AgNP bacterial toxicity found in pure culture and/or aqueous systems (e.g., Choi and Hu, 2009; Feng et al., 2000). However, there are only few available reports that specifically describe the antimicrobial effect of AgNPs in heterogeneous systems such as soils and sediments (e.g., Scheckel et al., 2010; Shoults-Wilson et al., 2011a; Shoults-Wilson et al., 2011b). Ionic silver has been shown to have a toxic effect on soil bacteria at 100 mg/kg (Throbäck et al., 2007), though the availability of AgNPs to soil bacteria is still under investigation. The effects of AgNPs on these and other organisms under environmental conditions, especially in soils and sediments, however, is still in need of much study. As AgNPs enter the

environment, there is great risk for AgNPs to adversely affect beneficial bacteria communities in the soil-water environment, perturbing the biogeochemical cycle of nutrients and trace metals. Furthermore, there is potential for increased AgNP usage to promote antibiotic resistance by potentially harmful bacteria.

Silver nanoparticles may act very differently from dissolved silver upon entering the environment, and have different effects on bacteria, plants, and animals. While the effect of AgNPs on bacteria in natural environments is still under investigation, environmental regulating agencies have taken particular interest in the fate of AgNPs as they enter natural systems. Much is yet to be discovered about the reactivity and fate of AgNPs in aquatic and terrestrial environments. Silver nanoparticle usage in commercial products as an antimicrobial agent is currently regulated as total silver in the United States (US) under the Federal Insecticide, Fungicide & Rodenticide Act by the US Environmental Protection Agency (EPA) (USEPA, 2011). Separately, under the current EPA regulation, any metals (i.e., colloidal and dissolved) that pass through 0.2 μm filters are considered "total dissolved metals" and are regulated as such. This would include any substances < 200 nm such as AgNPs (USEPA, 2012).

Manufactured AgNPs are often available for purchase in coated forms, either with a natural coating, such as calcium carbonate, or a polymer such as PVP. Surface interactions are influenced by the presence or absence of coating on AgNPs. AgNPs are, by definition, composed of zero-valent, metallic Ag. However, they most likely contain some metal that has been oxidized to Ag(I) at the surface (Lok et al., 2007). Xiu and coworkers (2011) showed that AgNPs were up to five times more toxic to *E. coli* bacteria

after being oxidized by ambient conditions for 10 days. For this reason, we will be observing the fate and reactivity of manufactured AgNPs, both bare and PVP-coated.

The fate and toxicity of AgNPs should be greatly affected by changes in redox condition in soil-water environment. Overall, an extensive search of the literature failed to uncover the fate of AgNPs in heterogeneous media. Our research group has shown that these AgNPs (Table 4.1) have a high affinity for soils when placed in a soil-water environment (>97% on soil surfaces), even greater than the affinity for soils shown by $AgNO_3$ (>34%) for soil surfaces (VandeVoort and Arai, 2012). Federal agencies are seeking new scientific evidence in formulating new regulations for AgNPs that can be applied to agricultural and food systems (e.g., Tolaymat et al., 2009; USEPA, 2011). The objective of this study is to observe phase transformations to AgNPs aging in a soil environment under reducing conditions, which may affect their bioavailability to soil bacteria.

4.3 Materials and Methods

Surface soils (top 10-30 cm) of Toccoa sandy loam (coarse-loamy, thermic typic Udifluvents) were collected from a Clemson University organic farm in South Carolina. Soils were air dried and passed through a 2 mm sieve, and then characterized for physicochemical properties (cation exchange capacity (CEC), organic matter (OM) content, pH, texture) and mineralogy according to the methods described by VandeVoort and Arai (2012).

Three different types of manufactured AgNPs were chosen for this study (Table 4.1). These AgNPs differ in size (15 – 90 nm) and the presence or absence of PVP coating. They are identified in this paper based on their approximate size and presence/absence of PVP coating. Particle size was determined through high resolution (HR) transmission electron microscopy (TEM) analysis of over 100 individual particles per AgNP type (Ma et al., 2012). Zeta potential measurements were conducted using a PALS Zeta Potential Analyzer Ver. 3.57, Brookhaven Instruments Corp. (Holtsville, NY). Measurements were performed in Milli-Q water and 2-(*N*-morpholino)ethanesulfonic acid (MES) buffer solution adjusted to pH 5.0±0.2 to simulate the native soil pH.

4.3.1 Batch Dissolution Studies of AgNPs

To test bioavailability of Ag(I) in the AgNP reacted soils, AgNP dissolution experiments were conducted in oxidized and reduced aqueous systems. These conditions simulate conditions during the incubation of AgNP spiked sub-anoxic soils. Both experiments were performed at $[Ag]_{Total}$ 500 mg/L. Our preliminary experiments indicated that the suspension density was required to generate [Ag(I)] > 0.01 mg/L, the detection limit of the silver ion specific electrode (ISE). Ionic strength was maintained with 0.005 M Na_2SO_4, and pH was maintained at 5 ± 0.1 using 0.02 M sodium acetate. Solutions were kept in 50 mL Oak Ridge Nalgene polycarbonate centrifuge tubes and shaken on an end-over-end shaker at 15 rpm for 2, 10, and 30 days. At each sampling period, AgNPs were separated from the bulk solution with an ultra-high-speed

centrifugation method. Using an adapted version of Stokes' law (Jackson, 1985), settling rate was calculated. The pAg15 AgNP spiked samples were spun at approximately 500 000 x *g* for 12 minutes using a Beckman 70Ti rotor ultra-high-speed centrifuge (Beckman Coulter, Inc., California). The Ag20 and Ag50 AgNP samples were spun at approximately 16 000 x *g* for 18 minutes and 10 minutes, respectively, on a Marathon 21K high speed centrifuge (Fischer Scientific, Inc., Pennsylvania). The aliquot was removed and acidified in 1.6M HNO_3 and analyzed for dissolved Ag using inductively-coupled plasma-atomic emission spectroscopy (ICP-AES). We also accounted for the adhesion of AgNPs in tubes. Acid digestion analysis indicated a negligible amount (i.e., below the detection limit of ICP-AES) of AgNPs in the tubes.

Hydrated AgNPs were saved for micro- (μ-)XANES analysis. For reduced systems, degassed Milli-Q water (18.2 MΩ) was pre-equilibrated in an argon filled glove bag for 30 days prior to the preparation of reagents. All reagents were prepared and handled in the glove bag.

4.3.2 Microfocused X-ray Absorption Near Edge Structure Spectroscopy Analysis

X-ray microprobe measurements of dissolution samples were performed at beamline (BL) X27A at the National Synchrotron Light Source (NSLS), Upton, New York. The purpose of this measurement was to understand Ag valence state in dissolution samples. The micron-sized beam can be effectively used to locate AgNP aggregates in sample holders. Polycarbonate sample holders (2 x 4 cm and 2 mm thick) that have 2 pin holes (1-2 mm in diameter) were fabricated. Silver nanoparticles were mixed with

degased Vaseline®, packed in the pin holes, and sealed with Kapton tape in an anaerobic glove bag. The use of Vaseline minimized the contact with oxygen prior to the measurements. Preliminary X-ray fluorescence (XRF) measurement tests indicated that Vaseline® was free of trace metals. To better understand changes in Ag speciation in aged AgNPs, LC of reference compound fit analysis was performed using the following reference compounds: 30 mM $AgNO_3$ solution at pH 5±0.1 for outer-sphere Ag surface species, AgCl(s), Ag_2O(s), and respective AgNPs in original powder form. The µ-XRF compositional maps of Ag were conducted above the Ag K absorption edge (25.55 keV) using a Canberra SL30165 Si(Li) detector. Spectra were collected up to 50-200 eV above the Ag K-edge absorption energy in fluorescence mode using a Canberra 9-element Ge Array detector. Minimizing the self-absorption effect, µ-XANES spectra were collected at diffused areas with a beam size of ~20 by 15 µm. These reference spectra were also compared with respective bulk XANES data collected in transmission mode to assure the minimum self-absorption effect.

4.3.3 Ionic Silver and AgNP Adsorption Isotherm Experiments

Adsorption isotherm experiments (suspension density: 33 g/L, $[Ag]_T$ for Ag(I): 1-50 mg/L, $[Ag]_T$: 10 - 500 mg/L for AgNP, ionic strength: 000.5 M Na_2SO_4) were conducted under ambient conditions. The Ag(I) experiments were used to assess the retention capacity of dissolved Ag from AgNPs. The use of a sulfate based electrolyte was to minimize the interference for a nitrate ISE. Solutions were mixed in 50 mL Oak

Ridge polycarbonate centrifuge tubes and placed on an end-over-end shaker for approximately 48 hr.

Ionic silver samples were first spun for 10 min in a centrifuge at 10 000 x *g* to separate large particles, and then filtered at 0.2 μm Millex-GV filters (Millipore Corp., Bedford, MA) to remove soil particulates. Total [Ag] in the filtered sample was analyzed with ICP-AES. An ultra-high-speed centrifugation technique was used for the AgNP samples to separate unreacted AgNPs in solution from soil particles, as described above. Filtration was not used for any AgNP samples, due to the affinity of AgNPs for the carbon composing the filter paper.

4.3.4 Bulk X-ray Absorption Spectroscopy Analysis

Using the methods described in the isotherm section, AgNP reacted soil samples were prepared in an argon filled glove bag. To facilitate the microbial consumption of oxygen to achieve a reduced environment, 10,000 mg/L glucose was added to the system. An additional chemical constituent, 50 mg/L of nitrate, was added to monitor the antimicrobial effects of AgNP on denitrifying bacteria (due to the scope this study, chemical fate of AgNP in soils, the results of denitrification are not discussed here). In the anaerobic glove box, bottle caps remained loose to allow the release of $N_2(g)$ during nitrification. We periodically monitored the changes in redox potentials.

Using a colorimetric method (Cline, 1969), [$S^{2-}(aq)$] was measured in the anaerobic glove box. Soil suspension subsamples of 10 mL volume were passed through 0.2 μm polyvinylidene fluoride (PVDF) Millex-GX filters (Millipore Corp., Bedford,

MA). Sulfide standard solutions were prepared using degased Milli-Q water. Aliquots and standards were reacted with 68.2 mM N,N-dimethyl-*p*-phenylenediamine sulfate and 88.8 mM ferric chloride in a 50% by volume conc. hydrochloric acid solution. Their absorbance at 670 nm was measured using a Milton Roy (Warminster, PA) Spectronic 20+ spectrophotometer. The detection limit of analysis is approximately 0.1 mg/L.

The soil paste was collected after 1 and 30 days via filtration and packed into polycarbonate sample holders in anaerobic environment, and kept moist until analysis. X-ray absorption spectroscopy was performed at BL 4-1, Stanford Synchrotron Light Source, Menlo Park, CA; and at BL X18B, NSLS. To better understand changes in Ag speciation in aged AgNPs, LC of reference compound fit analysis were performed using the reference spectra described below (Arai et al., 2006a; Arai et al., 2006b). Due to the crystal glitches in some spectra of model compounds, our analysis was limited to the XANES region (25,400-25,700 eV). The XANES spectra of the following ACS grade reference compounds (Alpha Aesar, Ward Hill, MA): Ag_2S(s), Ag_2CO_3(s), AgCl(s), Ag_2SO_4(s), Ag_2O(s), and a 30 mM solution of $AgNO_3$ (Fisher Chemical, Fair Lawn, NJ) solution at pH 5±0.1, were collected in transmission mode. In addition, Ag(I) was reacted with Pahokee Peat reference HA (International Humic Substances Society, St. Paul, MN) and prepared using the method described by Xia et al. (1997). Silver reacted HA solution (600 mg/L HA: pH 6, ionic strength maintained with 0.001 M $NaNO_3$, $[Ag]_T$ 0.05 mM) that had near 98% Ag sorption, determined via Ag ISE, was freeze dried. To further verify change in Ag chemical speciation, PCA was conducted using spectra of AgNP-reacted soils at 1 and 30 days.

4.4 Results and Discussion

4.4.1 Soil and Nanoparticle Characterization

The results of the physiochemical characterization of the soil are summarized in Table 4.2. It has a sandy loam texture and CEC of 7.4 $cmol_c$/kg. The moderately acidic pH of the soil (5.2 ± 0.2) is attributed to ~70% acid saturation. Calcium was a dominant exchangeable cation. Quartz was predominant in sand and silt fractions, and kaolinite, hydroxyl interlayer vermiculite, gibbsite, and hematite, goethite were identified in the clay fraction. Organic matter content was 1.5%.

Particle size analysis via TEM showed slightly larger size than the reported values by the manufacturers, except for pAg15. Zeta potential values showed negatively charged particles for all AgNPs except for pAg15, which had a slight positive charge, and is heavily coated with PVP (Table 4.1).

4.4.2 Batch Dissolution Studies

Figure 4.1 shows a summary of batch dissolution data under both aerobic and anaerobic conditions. These conditions simulate the changing redox conditions during the denitrification experiments. The pAg15 sample displayed the highest degree of Ag(I) release/dissolution of all AgNP samples (Figure 4.1c). It reached a maximum Ag of 26 mg/L after 10 days under aerobic conditions, and a maximum Ag of 25 mg/L (±0.1) after 2 days under anaerobic conditions. This was substantially higher than the maximum Ag release of pAg50: 1.5 mg/L after 30 days (aerobic) and 1.0 mg/L after 2 days (anaerobic) (Figure 4.1b), or the maximum [Ag(I)] release of uAg50: 2.9 mg/L after 30 days

(aerobic) and 1.7 mg/L after 2 days (anaerobic) (Figure 4.1a). Overall, all samples had an initial dissolution of at least 1 mg/L of Ag(I) after day 2. Dissolution under aerobic conditions remained fairly constant over time (Figures 4.1a to 4.1c); anaerobic dissolution did not follow the same trend. All AgNPs had the highest Ag(I) release within 2 days. The AgNPs released less Ag(I) with increasing time. Dissolved silver represents <1% of $[Ag]_T$ under both aerobic and anaerobic conditions for uAg50 and pAg50. In the pAg15 condition, however, [Ag(I)] represents as much as 5.3% of $[Ag]_T$ under aerobic conditions and 6.3% of $[Ag]_T$ under anaerobic conditions. Similarly, Sotiriou and Pratsinis (2010) demonstrated high amounts of Ag(I) release from small AgNPs (approximately 5-15 nm).

4.4.3 Microfocused X-ray Absorption Near Edge Structure Spectroscopy Analysis

Figure 4.2 shows normalize XANES spectra of dissolution samples and reference compounds. When the spectra of reference compounds are compared, there are clear differences in post-edge features of Ag(0) foil, AgCl(s), Ag_2O(s), and $AgNO_3$(aq). The Ag foil spectrum displays two distinctive post-edge regions, denoted by arrows on Figure 4.2. These features are absent on both the Ag_2O(s) and $AgNO_3$(aq) spectra. Instead, the $AgNO_3$(aq) spectrum displays much shaper edge jump comparing to other reference materials. The Ag_2O(s) spectrum displays some moderate post edge features, though they are not similar to either the foil spectrum or the $AgNO_3$(aq) spectrum. Due to the fact that Ag only changes by one oxidation state from its metallic form, Ag(0), to its oxidized form, Ag(I), there is no discernible edge shift in the XANES spectra of AgNPs. The day

0 dissolution sample spectra of all three AgNPs display similar post edge features to the Ag(0) foil spectrum. Additionally, the day 30 dissolution sample spectra bear similarities to the day 0 sample spectra for all AgNPs.

To gain insight in the Ag chemical speciation in the AgNPs during dissolution, LC of reference compound least squares fit analyses were performed on the 30 days dissolution samples under both reduced and oxidized conditions (Figure 4.3 and Table 4.3). The spectra features for each 30 day AgNP dissolution sample were simulated using the spectra from its corresponding 0 days dissolution sample, $AgNO_3$(aq), AgCl(s), Ag_2CO_3(s), and Ag_2O(s). The uAg50 30 days spectra under reduced and oxidized conditions (Figure 4.3a and 3b and Table 4.3) was able to be constructed from nearly 100% of unreacted AgNP, suggesting negligible changes in solid state speciation of Ag in uAg50. Conversely, there were some changes in the other two AgNPs. After 30 days under oxic and reduced conditions, pAg50 retained 2.2-4.4% of AgO_2(s) in addition to >95% of unreacted pAg50. The pAg15 dissolution samples under reduced condition (Figure 4.3e, Table 4.3) had approximately 82% pAg15 0 days, 17% Ag_2O, and 1% $AgNO_3$(aq) while 30 days AgNP in the oxic system produced ~82% pAg15 0 days and 11 % $AgNO_3$(aq). The presence of aqueous $AgNO_3$ in pAg15 30d is a direct reflection of the contribution of dissolved oxygen and/or pre-dissolution oxidation. In the case of pAg15 dissolved under oxidized conditions, presence of dissolved oxygen in the water may cause an oxidation reaction at the surface of the AgNPs, resulting in the formation of Ag(I). Under reduced conditions, this Ag(I) component is likely the result of an already partially oxidized AgNP, as supported by the relatively high [Ag(I)] in the second day of

the dissolution studies (Figure 4.1c). Previous studies have shown Ag(I) adsorbing onto AgNP surfaces (Liu and Hurt, 2010), explaining the presence of these Ag(I) species during XANES analysis. It is interesting that Ag_2O(s) was retained in the reduced systems. Manufactured AgNPs generally contain $Ag(0, +1)_2O$ impurity (Xiu et al., 2011; Yin et al., 2002). One should expect that oxic condition drives the dissolution process of $Ag(0, +1)_2O$ faster than the reduced condition, resulting in the near negligible quantity of Ag_2O(s) remained under the oxidized condition.

4.4.4 Adsorption Isotherms

Adsorption isotherm data (Figure 4.4) show C-curves for all AgNPs and an L-curve for Ag(I). In general, AgNPs (Figures 4.4b – 4.4d) showed a greater affinity for soil surfaces than ionic Ag (Figure 4.4a). Among all AgNPs, pAg15 has the lowest affinity for soil surfaces, though at its lowest [Ag] (500 mg/L), it showed at least 97% sorption onto soil surfaces. Both uAg50 and pAg50 showed nearly 100% sorption onto soil surfaces at all [Ag] (10 – 500 mg/L). While pAg15, which had a positive zeta potential, could have undergone hydrophilic interaction with negatively charged soil constituents at pH ~5 (Anderson et al., 1973; Jacobson et al., 2005a), AgNPs with negative zeta potential values (pAg50 and uAg50) could potentially interact with soil humic substances via hydrophobic interactions. Hydrophobic polymer coatings on AgNP is known to facilitate the adhesion to hydrophobic surfaces (Song et al., 2011). The sorption of Ag in Ag(I) systems (Figures 4.4b – 4.4d) increases with increasing $[Ag]_T$.

While nearly 90% of Ag(I) was sorbed when $[Ag]_T \leq 50$ mg/L, only ~55% of sorption was achieved when soils were reacted with $[Ag]_T = 500$ mg/L.

4.4.5 Bulk X-ray Absorption Spectroscopy Analysis

Bulk XANES spectra of AgNP reacted soils at 1 and 30 days and reference materials are shown in Figure 4.5. The absorption edge energy position of Ag K-edge XANES data is not as sensitive as that of redox sensitive metalloids (e.g., arsenic) to evaluate the sorbed/precipitate phases. Instead, our observation was focused on the spectra feature at whiteline and post edge regions. The post-edge features of Ag foil (two oscillations identified in μXANES analysis) are clearly observed in uAg50 and pAg50 samples whereas the features nearly disappeared after 30 days in pAg15 samples. The whiteline features in $AgNO_3$(aq), Ag_2CO_3, and AgCl(s) are much sharper than that in the rest of samples. Spectra of Ag_2S and Ag(I) reacted HA showed smooth post edge features. However, post edge oscillations are slightly more pronounced in the HA sample. The Ag-HA spectrum is noticeably different from both the Ag reference foil spectrum and the AgNP reference spectra. This suggests that Ag(I) was not reduced by HA to form AgNPs. While AgNP formation via HA exposure this has been reported by Akaighe et al. (2011), we find that this is not the case in our system. We have seen no spectral resemblance with our HA reacted Ag(I). To better elucidate changes in chemical speciation, we conducted the LC of reference compound fit and PCA.

The results of LC fit analysis (Figure 4.6 and Table 4.4) displayed a continuum of aging over a 30 day time period in an anaerobic soil environment. The degree of

transformation over 30 days increased from pAg50 to uAg50 to pAg15. The LC fit of uAg50 revealed a notable change between the 1 day and 30 day spectra (Figure 4.6a and -6b and 1st and 2nd rows in Table 4.4). The 1 day spectrum is composed 91% of the original uAg50 and a small quantity (<9%) of AgCl(s) and Ag_2O. At <24hr, the system was not completed reduced (Eh: 70-80 mV). It is likely that oxidative dissolution and precipitation reactions were simultaneously occurring in soils. After 30 days, the spectrum retains only 63% of the original uAg50 and ~36% Ag-reacted HA (Figure 4.6d and Table 4.4). Considering the soft acid characteristics of ionic silver, it makes sense to observe Ag complexation by soil OM. The stability constant of Ag(I) with a humic functional group, cysteine, is log K_f = 11.9 (Bell and Kramer, 1999). The retention of Ag(I) in humic rich soils and HA has been reported by several researchers (Jacobson et al., 2005b; Liu and Hurt, 2010). It is important to note that it was not possible to incorporate the Ag_2S spectrum in the LC fit. Attempts to fit this spectrum with Ag_2S alone, or with only the reference AgNP spectrum, resulted in much larger red. χ^2 values. The addition of the Ag_2S spectrum to the current fit resulted in a contribution of $<10^{-7}$% of the final fit. For these reasons, the Ag_2S spectrum was omitted from this final fit. Lack of sulfidation in our experimental systems was further discussed below. It seemed that Ag_2S precipitation reaction was out-competed by the HA complexation in this instance.

The PCA of six soil samples at 1 and 30 days showed that the variance in the samples was captured with three or less components, with only minor improvement with the addition of additional components (Table 4.5). The uAg50 AgNP required three components to reconstruct the spectrum of the 30 day aged sample. This supports the

evidence provided by the LC fit: that the chemical speciation of uAg50 is growing increasingly complex as it resides in an anaerobic soil-water environment.

The LC fit analysis on the pAg50 samples showed that the original pAg50 was still largely intact (>91% similarity) after 1 day (Figure 4.6c and 2nd row in Table 4.4). A small quantity (<10%) of Ag_2O(s) and Ag_2CO_3(s) was present after 1 day. During this first day, the system was not completed reduced (Eh: 211-262 mV). Aerobic microorganisms were actively converting glucose to bicarbonate (as high as 176 mg/L), facilitating the precipitation of Ag_2CO_3(s). Because of the solubility of Ag_2CO_3 (K_{sp}: 8.46 x 10^{-12}), it rapidly degraded after 30 days. During the 30 days incubation period, oxidative dissolution of AgNPs was simultaneously occurring. After 30 days, the contribution of Ag_2O(s) grew to 8.8%, while the contribution of the original AgNP spectrum decreased to 82%. The remainder of the spectral reconstruction was comprised of ~1.3% $AgNO_3$(aq) and ~7.4% Ag_2S(s). Although the Ag sorbed HA spectrum was included along with the Ag_2S(s) spectrum in the initial LC fit analysis, the fit did not yield any measurable presence of the Ag sorbed HA fraction, suggesting that the precipitation of Ag_2S(s) and Ag_2O(s) outcompeted for the HA complexation.

The PCA reveals the greatest differences between uAg50 and pAg50. Spectral reconstructions of aged pAg50-reacted soils are shown in Figure 4.7c and 4.7d. Only one component was sufficient to reconstruct the spectra features of pAg50 at both time points. This further supports the evidence that this AgNP is the least changed over time and least complex after 30 days in an anaerobic soil-water environment. This might be due to its lack of susceptibility for oxidative dissolution. The dissolution data (Figure 4.1b)

indicated that pAg50 released the least free Ag(I) during both aerobic and anaerobic dissolution experiments. This is the largest of all three AgNPs, and contains a small amount of PVP as a coating agent (Table 4.1). Although uAg50 displayed similar sorption to pAg50 in the isotherm data, these AgNPs (pAg50 and uAg50) behave differently in terms of the chemical fate. Differences in 1) the extent of dissolution and 2) partitioning mechanisms (e.g., hydrophilic vs. hydrophobic) might have resulted in the different chemical transformation paths

Lastly, pAg15 was by far the most transformed from the original AgNP after 30 days. This smallest and most heavily PVP-coated AgNP (Table 4.1) displayed dissolution at almost ten times the extent of the other two AgNPs (Figure 4.1). After 1 day, pAg15 rapidly underwent dissolution and precipitation processes, yielding approximately 5.8% of Ag_2O, 8.5% of Ag_2CO_3, and 15% $AgNO_3$(aq). It was evident in the dissolution study that pAg15 contained an Ag_2O impurity. It seemed that some of Ag_2O was still remaining in the system after 1 day. During the initial sub-anoxic condition (Eh: +222-264 mV), aerobic microorganisms rapidly converted glucose to CO_2/bicarbonate, possibly precipitating dissolved Ag(I) as Ag_2CO_3. Some Ag(I) seemed to reside on the surface of soil components as outer-sphere surface species. After 30 days, the XANES spectrum resembles the original AgNP powder by only ~22%. Instead, the bulk of the spectrum is comprised of near-equal portions of Ag_2S(s) and Ag sorbed HA phases. Because of high solubility of Ag_2CO_3, it was no longer present after 30 days.

The PCA required three components to reconstruct the spectrum of 30 days pAg15 sample, supporting the complexity of Ag chemical speciation that was observed in

the LC fit analysis. Ma et al. (2012) reported that solubility of AgNP can be predicted by TEM derived AgNP particle size. We have observed that solubility of PVP coated AgNPs increases with decreasing particle size. In fact, the dissolution of pAg15 (Figure 4.1c) was the highest (as high as 25 mg/L) of all three AgNPs. If one extrapolates the isotherm data (Figure 4.4) to assess the affinity of Ag(I) at ~25 mg/L, nearly 95% Ag(I) is sorbed. This supports our observation that all of the dissolved Ag(I) was complexed in the soil humic fraction and precipitated out as $Ag_2S(s)$.

4.4.6 Competitive Effects of Humic Substances in Reducing Soils

It was surprising to see minimal sulfidation in reducing soils, and the reaction products were varied in AgNPs and kinetically limited. We believe AgNP partitioning with soil components (e.g., humic substances) might have contributed to the results.

In the 1 day samples, it was unlikely that AgNPs were able to undergo the sulfidation process due to a lack of dissolved sulfide and Ag(I). The Eh was >+80 mV for all samples after 1 day. This sub-oxic condition would not promote the reduction of sulfate to sulfide. However, oxidative dissolution of AgNPs was likely as evidenced in our dissolution data. Dissolved Ag(I), which was very low (below the detection limit of ISE measurements: 0.01 mg/L), is likely to partition in humic components in soils (Jacobson et al., 2005a; VandeVoort and Arai, 2012). The strong affinity of Ag(I) can be supported by the adsorption isotherm data of Ag(I) (Figure 4.4a). When 10 mg/L of Ag(I) was reacted with soil, nearly 100% sorption was achieved.

In 30 days samples, we only observed some degree of sulfidation in PVP coated AgNPs (pAg50 and pAg15) (Table 4.4). Sulfidation process in PVP-coated AgNPs has been previously reported by Levard and coworkers (2011). Interestingly, sulfidation was not the dominant chemical process in the bare AgNP, uAg50. uAg50 has the largest negative zeta potential value of all AgNPs (Table 4.2), which may have facilitated partitioning in humic components in soils. Once AgNPs are partitioned in soils, these humic components further retard the oxidative dissolution process. Humic/fulvic acid is known to suppress the dissolution process of AgNPs (Liu and Hurt, 2010). In addition, the anoxic condition (Eh: <-500mV) did not promote oxidative dissolution. It is difficult to promote the sulfidation under the low sulfide environment (Liu et al., 2011). Under the anoxic condition, we only measured a maximum [S^{2-}(aq)] of 0.022 mM (~2 mg/L) in all systems.

4.4.7 Implications for the Environmental Fate of AgNPs

Although aqueous geochemical research of AgNPs has been extensively conducted in the last decade, the results often lack in critical information under environmentally relevant conditions (e.g., presence of adsorbents). It is poorly known how physicochemical properties of AgNPs (e.g., chemical transformation, partitioning in soil/sediment constituents, aggregation, and dispersibility) are altered once they are introduced into the heterogeneous environment. Any research findings in these areas should be of interest to risk assessors to regulate the commercial and industrial usages, applications, and productions of AgNPs. Our study showed that 1) strong partitioning of

AgNPs in soils and 2) particle specific chemical transformation of AgNPs in reducing soils. Several transport studies have previously reported the deposition (or partitioning) of engineered AgNPs (e.g., nano-TiO_2, nano-ZVI, and quantum dots) in SiO_2 mineral packed columns (e.g., Quevedo and Tufenkji, 2009; Zhan et al., 2008). This is one of few studies reporting the strong partitioning of AgNPs in soils. The affinity of AgNPs in soils was strong in all AgNPs regardless of size or quantity of PVP capping agents. Smaller AgNPs with large amounts of PVP (pAg15) underwent rigorous dissolution, resulting in the chemical transformation from Ag(0) to Ag_2S and or Ag-humic phases. Based on the equilibrium based thermodynamic chemical speciation models, it is reasonable to assume the sulfidation controlled fate in aquatic systems (e.g., Kim et al., 2010; Levard et al., 2011; Liu et al., 2011). However, the results of our study provide new insight in predicting the fate and transport of AgNPs in soils and sediments. Humic substances and soils might serve as important sinks for AgNPs as well as the reaction product (i.e., dissolved Ag(I)) in heterogeneous media.

Wastewater treatment plants generally remove suspended organic rich solids as well as sediments. It is likely that AgNPs are retained in solid phases that retard their further chemical transformation. To better assess the risk of AgNPs in the aquatic-terrestrial environment, it might be important to consider the persistency of AgNPs at the sediments/soil-water interface.

4.5 References

Akaighe, N., R.I. MacCuspie, D.A. Navarro, D.S. Aga, S. Banerjee, M. Sohn, and V.K. Sharma. 2011. Humic acid-induced silver nanoparticle formation under environmentally relevant conditions. Environ. Sci. Technol. 45:3895-3901.

Anderson, B.J., E.A. Jenne, and T.T. Chao. 1973. Sorption of silver by poorly crystallized manganese oxides. Geochim. Cosmochim. Acta. 37:611-622.

Arai, Y., M. McBeath, J.R. Bargar, J. Joye, and J.A. Davis. 2006a. Uranyl adsorption and surface speciation at the imogolite-water interface: Self-consistent spectroscopic and surface complexation models. Geochim. Cosmochim. Acta. 70:2492-2509.

Arai, Y., A. Lanzirotti, S.R. Sutton, M. Newville, J. Dyer, and D.L. Sparks. 2006b. Spatial and temporal variability of arsenic solid-state speciation in historically lead arsenate contaminated soils. Environ. Sci. Technol. 40:673-679.

Bell, R.A., and J.R. Kramer. 1999. Structural chemistry and geochemistry of silver-sulfur compounds: Critical review. Environ. Toxicol. Chem. 18:9-22.

Benn, T., B. Cavanagh, K. Hristovski, J.D. Posner, and P. Westerhoff. 2010. The release of nanosilver from consumer products used in the home. J. Environ. Qual. 39:1875-1882.

Benn, T.M., and P. Westerhoff. 2008. Nanoparticle silver released into water from commercially available sock fabrics. Environ. Sci. Technol. 42:4133-4139.

Chae, Y.J., C.H. Pham, J. Lee, E. Bae, J. Yi, and M.B. Gu. 2009. Evaluation of the toxic impact of silver nanoparticles on Japanese medaka (*Oryzias latipes*). Aquat. Toxicol. 94:320-327.

Choi, O., K.K. Deng, N.J. Kim, L. Ross, R.Y. Surampalli, and Z.Q. Hu. 2008. The inhibitory effects of silver nanoparticles, silver ions, and silver chloride colloids on microbial growth. Water Res. 42:3066-3074.

Choi, O.K., and Z.Q. Hu. 2009. Nitrification inhibition by silver nanoparticles. Water Sci. Technol. 59:1699-1702.

Cline, J.D. 1969. Spectrophotometric determination of hydrogen sulfide in natural waters. Limnol. Oceanogr. 14:454-458.

Feng, Q.L., J. Wu, G.Q. Chen, F.Z. Cui, T.N. Kim, and J.O. Kim. 2000. A mechanistic study of the antibacterial effect of silver ions on *Escherichia coli* and *Staphylococcus aureus*. J. Biomed. Mater. Res. 52:662-668.

Griffitt, R.J., J. Luo, J. Gao, J.C. Bonzongo, and D.S. Barber. 2008. Effects of particle composition and species on toxicity of metallic nanomaterials in aquatic organisms. Environ. Toxicol. Chem. 27:1972-1978.

Jackson, M.L. 1985. Soil Chemical Analysis. 2nd ed. Parallel Press, Madison, Wisconsin, US.

Jacobson, A.R., M.B. McBride, P. Baveye, and T.S. Steenhuis. 2005a. Environmental factors determining the trace-level sorption of silver and thallium to soils. Sci. Total Environ. 345:191-205.

Jacobson, A.R., C.E. Martinez, M. Spagnuolo, M.B. McBride, and P. Baveye. 2005b. Reduction of silver solubility by hurnic acid and thiol ligands during acanthite (β-Ag_2S) dissolution. Environ. Pollut. 135:1-9.

Kim, B., C.S. Park, M. Murayama, and M.F. Hochella. 2010. Discovery and characterization of silver sulfide nanoparticles in final sewage sludge products. Environ. Sci. Technol. 44:7509-7514.

Levard, C., B.C. Reinsch, F.M. Michel, C. Oumahi, G.V. Lowry, and G.E. Brown. 2011. Sulfidation processes of PVP-coated silver nanoparticles in aqueous solution: Impact on dissolution rate. Environ. Sci. Technol. 45:5260-5266.

Liu, J.Y., and R.H. Hurt. 2010. Ion release kinetics and particle persistence in aqueous nano-silver colloids. Environ. Sci. Technol. 44:2169-2175.

Liu, J.Y., K.G. Pennell, and R.H. Hurt. 2011. Kinetics and mechanisms of nanosilver oxysulfidation. Environ. Sci. Technol. 45:7345-7353.

Lok, C.N., C.M. Ho, R. Chen, Q.Y. He, W.Y. Yu, H. Sun, P.K.H. Tam, J.F. Chiu, and C.M. Che. 2007. Silver nanoparticles: Partial oxidation and antibacterial activities. J. Biol. Inorg. Chem. 12:527-534.

Ma, R., C. Levard, S.M. Marinakos, Y.W. Cheng, J. Liu, F.M. Michel, G.E. Brown, and G.V. Lowry. 2012. Size-controlled dissolution of organic-coated silver nanoparticles. Environ. Sci. Technol. 46:752-759.

Malinowski, E.R. 1991. Factor Analysis in Chemistry. John Wiley, New York.

Morones, J.R., J.L. Elechiguerra, A. Camacho, K. Holt, J.B. Kouri, J.T. Ramirez, and M.J. Yacaman. 2005. The bactericidal effect of silver nanoparticles. Nanotechnology. 16:2346-2353.

Navarro, E., F. Piccapietra, B. Wagner, F. Marconi, R. Kaegi, N. Odzak, L. Sigg, and R. Behra. 2008. Toxicity of silver nanoparticles to *Chlamydomonas reinhardtii*. Environ. Sci. Technol. 42:8959-8964.

Quevedo, I.R., and N. Tufenkji. 2009. Influence of solution chemistry on the deposition and detachment kinetics of a CdTe quantum dot examined using a quartz crystal microbalance. Environ. Sci. Technol. 43:3176-3182.

Scheckel, K.G., T.P. Luxton, A.M. El Badawy, C.A. Impellitteri, and T.M. Tolaymat. 2010. Synchrotron speciation of silver and zinc oxide nanoparticles aged in a kaolin suspension. Environ. Sci. Technol. 44:1307-1312.

Shoults-Wilson, W.A., O.I. Zhurbich, D.H. McNear, O.V. Tsyusko, P.M. Bertsch, and J.M. Unrine. 2011a. Evidence for avoidance of Ag nanoparticles by earthworms (*Eisenia fetida*). Ecotoxicology. 20:385-396.

Shoults-Wilson, W.A., B.C. Reinsch, O.V. Tsyusko, P.M. Bertsch, G.V. Lowry, and J.M. Unrine. 2011b. Role of particle size and soil type in toxicity of silver nanoparticles to earthworms. Soil Sci. Soc. Am. J. 75:365-377.

Sondi, I., and B. Salopek-Sondi. 2004. Silver nanoparticles as antimicrobial agent: A case study on *E. coli* as a model for gram-negative bacteria. J. Colloid Interf. Sci. 275:177-182.

Song, J.E., T. Phenrat, S. Marinakos, Y. Xiao, J. Liu, M.R. Wiesner, R.D. Tilton, and G.V. Lowry. 2011. Hydrophobic interactions increase attachment of gum arabic- and PVP-coated Ag nanoparticles to hydrophobic surfaces. Environ. Sci. Technol. 45:5988-5995.

Sotiriou, G.A., and S.E. Pratsinis. 2010. Antibacterial activity of nanosilver ions and particles. Environ. Sci. Technol. 44:5649-5654.

Throbäck, I.N., M. Johansson, M. Rosenquist, M. Pell, M. Hansson, and S. Hallin. 2007. Silver (Ag^{+}) reduces denitrification and induces enrichment of novel nirK genotypes in soil. FEMS Microbiol. Lett. 270:189-194.

Tolaymat, T.M., A.M. El Badawy, A. Genaidy, K.G. Scheckel, T.P. Luxton, and M. Suidan. 2009. An evidence-based environmental perspective of manufactured silver nanoparticle in syntheses and applications: A systematic review and critical appraisal of peer-reviewed scientific papers. Sci. Total Environ. 408:999-1006.

USEPA. 2011. Control of nanoscale materials under the Toxic Substances Control Act [Online]. Available by US Environmental Protection Agency http://www.epa.gov/opptintr/nano/ (posted 29 April 2011; verified 17 July 2012).

USEPA. 2012. Secondary drinking water regulations: Guidance for nuisance chemicals 816-F-10-079 [Online]. Available by US Environmental Protection Agency http://water.epa.gov/drink/contaminants/secondarystandards.cfm (posted 21 May 2012; verified 17 July 2012).

VandeVoort, A.R., and Y. Arai. 2012. Environmental chemistry of silver in soils: Current and historic perspectives, p. 59, *In* D. L. Sparks, ed. Adv. Agron., Vol. 114. AGRON UK Academic Press, London.

Xia, K., W. Bleam, and P.A. Helmke. 1997. Studies of the nature of Cu^{2+} and Pb^{2+} binding sites in soil humic substances using X-ray absorption spectroscopy. Geochim. Cosmochim. Acta. 61:2211-2221.

Xiu, Z.-M., J. Ma, and P.J.J. Alvarez. 2011. Differential effect of common ligands and molecular oxygen on antimicrobial activity of silver nanoparticles versus silver ions. Environ. Sci. Technol. 45:9003-9008.

Yin, Y., Z.-Y. Li, Z. Zhong, B. Gates, Y. Xia, and S. Venkateswaran. 2002. Synthesis and characterization of stable aqueous dispersions of silver nanoparticles through the Tollens process. J. Mater. Chem. 12:522-527.

Zhan, J., T. Zheng, G. Piringer, C. Day, G.L. McPherson, Y. Lu, K. Papadopoulos, and V.T. John. 2008. Transport characteristics of nanoscale functional zerovalent iron/silica composites for *in situ* remediation of trichloroethylene. Environ. Sci. Technol. 42:8871-8876.

Table 4.1. Characteristics of silver nanoparticles.

AgNP ID	Source (reported part. size)	Silver purity	*Average particle size (nm)	ζ (mV)	Capping agent
uAg50	Inframat Advanced Materials (40-90 nm)	99.95%	48 ± 14	-35.85 ± 1.50	None
pAg50	Nanostructured & Amorphous Materials, Inc. (20 nm)	99.7%	53 ± 21	-27.63 ± 1.71	0.3% PVP (by wt)
pAg15	Nanostructured & Amorphous Materials, Inc. (15 nm)	10%	13 ± 5	4.66 ± 3.00	90% PVP (by wt)

Particle size, zeta potential (ζ), and capping agent obtained from manufacturer information. Nanoparticle identification given based on average particle size and/or abundance of capping agent. *Average particle size estimated through TEM analysis

Table 4.2. Texture, physicochemical properties, organic matter, and clay mineralogy of Toccoa sandy loam surface soil.

pH	Clay	% OM	CEC	Acidity	Exchangeable Cations		
					K	Ca	Mg
5.2	K, HIV, H, G	1.53	7.4	5.2	0.22	1.62	0.37

CEC, acidity, and exchangeable cations are in $cmol_c/kg$. K= kaolinite, HIV = hydroxyl interlayer vermiculite, G= goethite, H= hematite

Table 4.3. Results of linear combination of reference compound fit of μ-XANES spectra of AgNP dissolution samples shown in Figure 3.

Sample	Respective 0 d AgNP	Ag_2O	$AgNO_{3(aq)}$	Red. χ^2
uAg50 30 d red.	0.9990 ± 0.0002	-	-	2.225×10^{-4}
uAg50 30 d ox.	1.0000 ± 0.00001	-	-	2.308×10^{-4}
pAg50 30 d red.	0.9558 ± 0.0062	0.0442 ± 0.0062	-	1.854×10^{-4}
pAg50 30 d ox.	0.9785 ± 0.0145	0.0215 ± 0.0145	-	9.879×10^{-4}
pAg15 30 d red.	0.8230 ± 0.0054	0.1654 ± 0.0064	0.0116 ± 0.0045	1.877×10^{-4}
pAg15 30 d ox.	0.8928 ± 0.0045	-	0.1072 ± 0.0045	3.326×10^{-4}

Table 4.4. Linear combination fitting of bulk XAS spectra collected from AgNPs aged in Toccoa sandy loam for 1 or 30 days under reducing conditions at pH 5.2.

Sample	Respective ref. AgNP	AgCl	Ag_2O	Ag_2CO_3	$AgNO_{3(aq)}$	Ag_2S	Ag-HA	Red. χ^2
uAg50 1 day	0.9114 ± 0.0022	0.0270 ± 0.0017	0.0616 ± 0.0024	-	-	-	-	1.501×10^{-5}
uAg50 30 days	0.6347 ± 0.0058	-	-	-	-	-	0.3653 ± 0.0058	1.088×10^{-4}
pAg50 1 day	0.9084 ± 0.0027	-	0.0573 ± 0.0031	0.0343 ± 0.0022	-	-	-	2.334×10^{-5}
pAg50 30 days	0.8245 ± 0.0015	-	0.0881 ± 0.0019	-	0.0134 ± 0.0013	0.0743 ± 0.0023	-	5.378×10^{-6}
pAg15 1 day	0.7075 ± 0.0026	-	0.0580 ± 0.0030	0.0845 ± 0.0046	0.1501 ± 0.0059	-	-	1.983×10^{-5}
pAg15 30 days	0.2245 ± 0.0035	-	-	-	-	0.3414 ± 0.0078	0.4340 ± 0.0065	2.827×10^{-5}

For each sample, the proportion of that spectrum recreated by the combination of reference spectra is listed. The respective reference AgNP column represents spectra collected from unaged powder AgNP samples spread on Kapton tape.

Table 4.5. Results of the principal component analysis performed on bulk XAS spectra collected from AgNPs aged in Toccoa sandy loam for 1 or 30 days under reducing conditions at pH 5.2.

Component, *n*	Eigen value	Variance explained (%)	Cumulative variance	IND functions
1	78.298	64.9	64.9	0.4216
2	18.980	15.7	80.7	0.4366
3	12.163	10.0	90.8	0.4412
4	5.733	4.7	95.5	0.6712
5	3.015	2.5	98.0	2.3072
6	2.307	1.9	100	n/a

IND function is indicator error function proposed by Malinowski (1991).

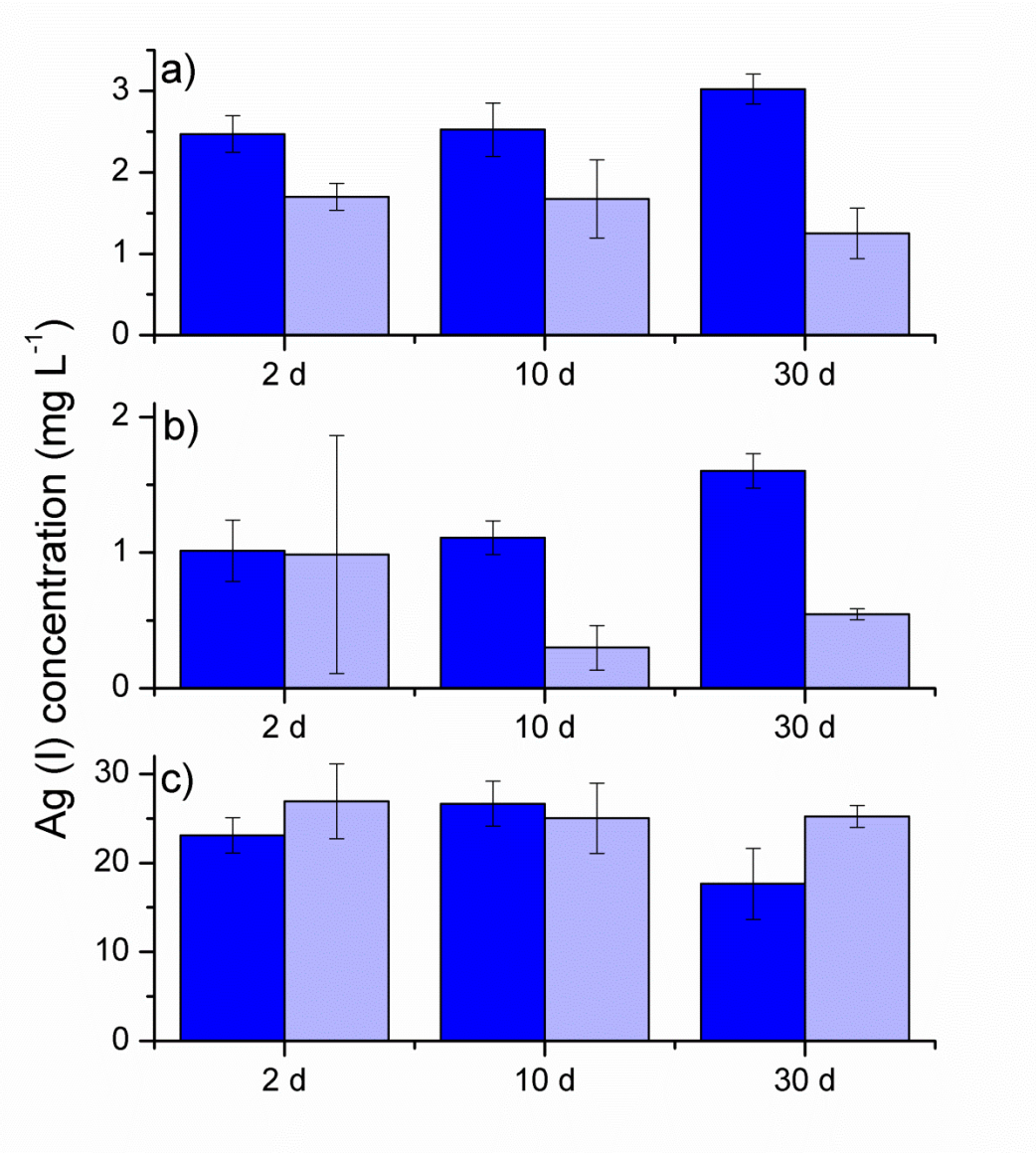

Figure 4.1. Batch dissolution data of AgNPs (Reaction time: 2, 10, and 30d, pH 5.2 ± 0.2 maintained using 0.05 mM acetate buffer): a) uAg50, b) is pAg50, and c) is pAg15. The dark blue bars represent oxidized conditions and the light blue bars represent reduced conditions. Error bars indicate one standard deviation above and below value.

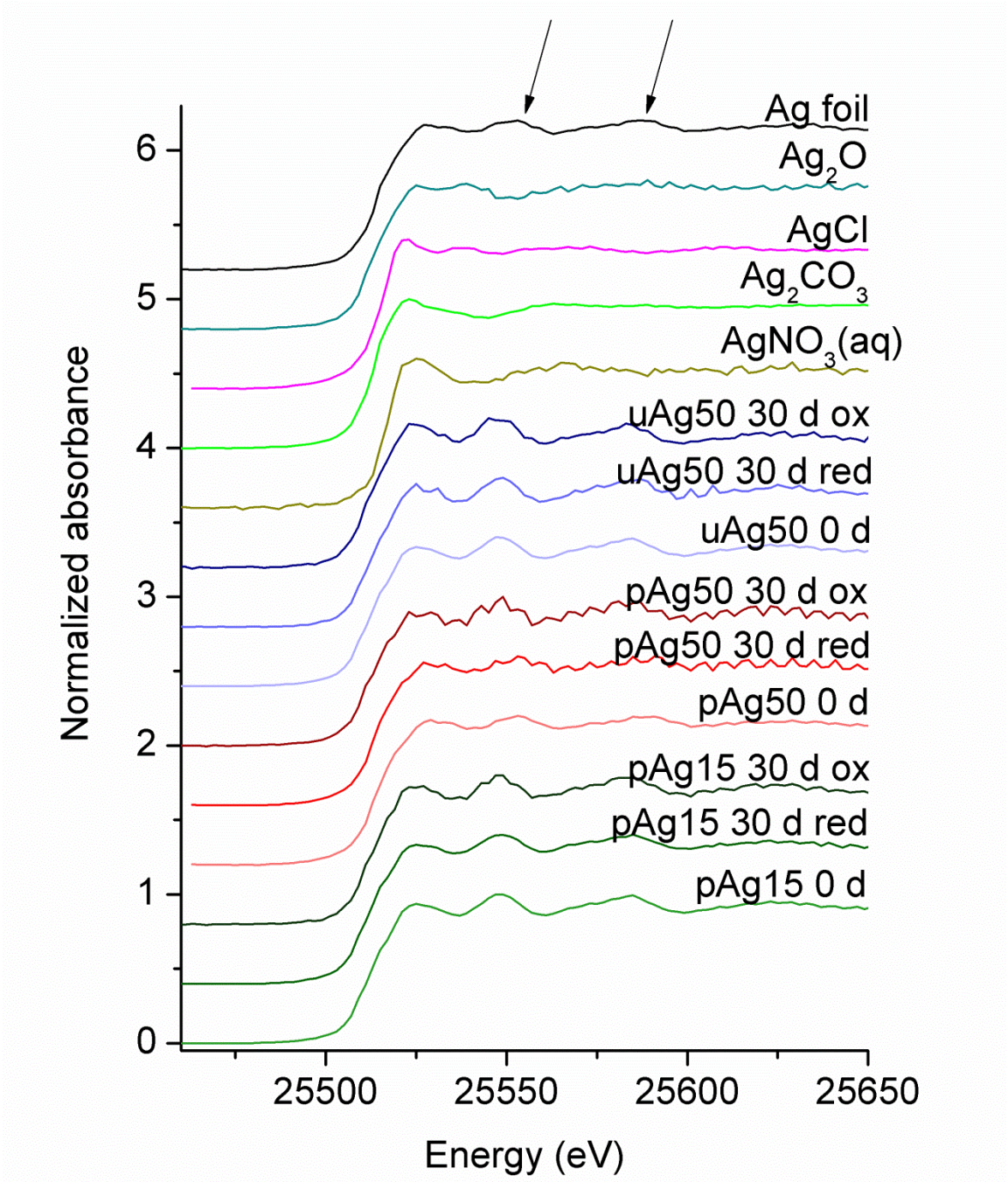

Figure 4.2. Microfocused(μ) XANES spectra of AgNPs dissolutions samples under oxidized (ox) or reduced (red) conditions at 0 and 30 days and selected μXANES reference compounds.

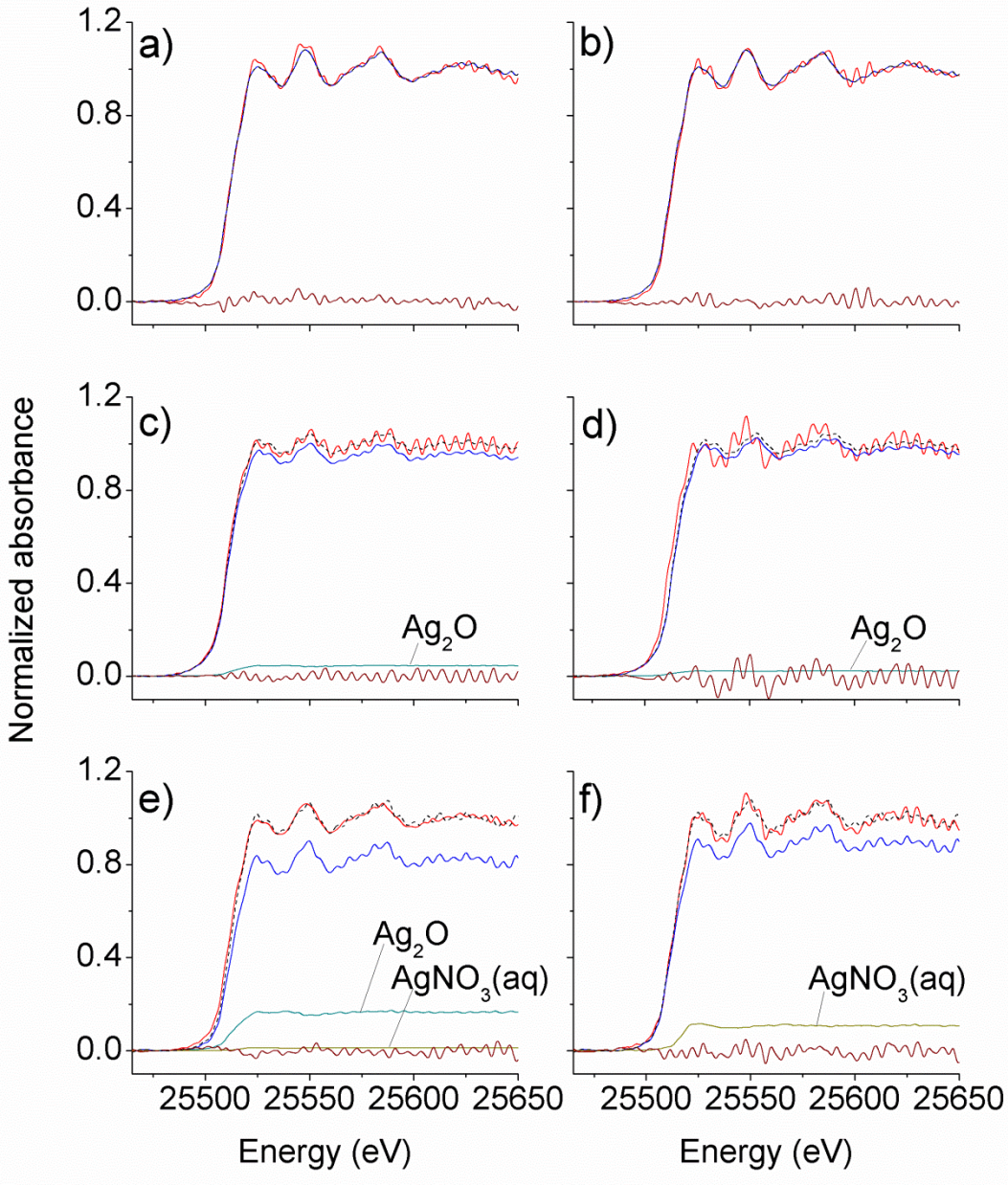

Figure 4.3. Linear combination of reference compound fit of μXANES spectra of AgNP dissolution samples at 30 days. a) uAg50 reduced, b) uAg50 oxidized, c) pAg50 reduced, d) pAg50 oxidized, e) pAg15 reduced, f) pAg15 oxidized. In all panels, normalized data, overall fit, respective 0 day AgNP spectra, and residual spectra are shown as red, black dashed, dark blue, and brown, respectively. Any other spectra included in fit are labeled.

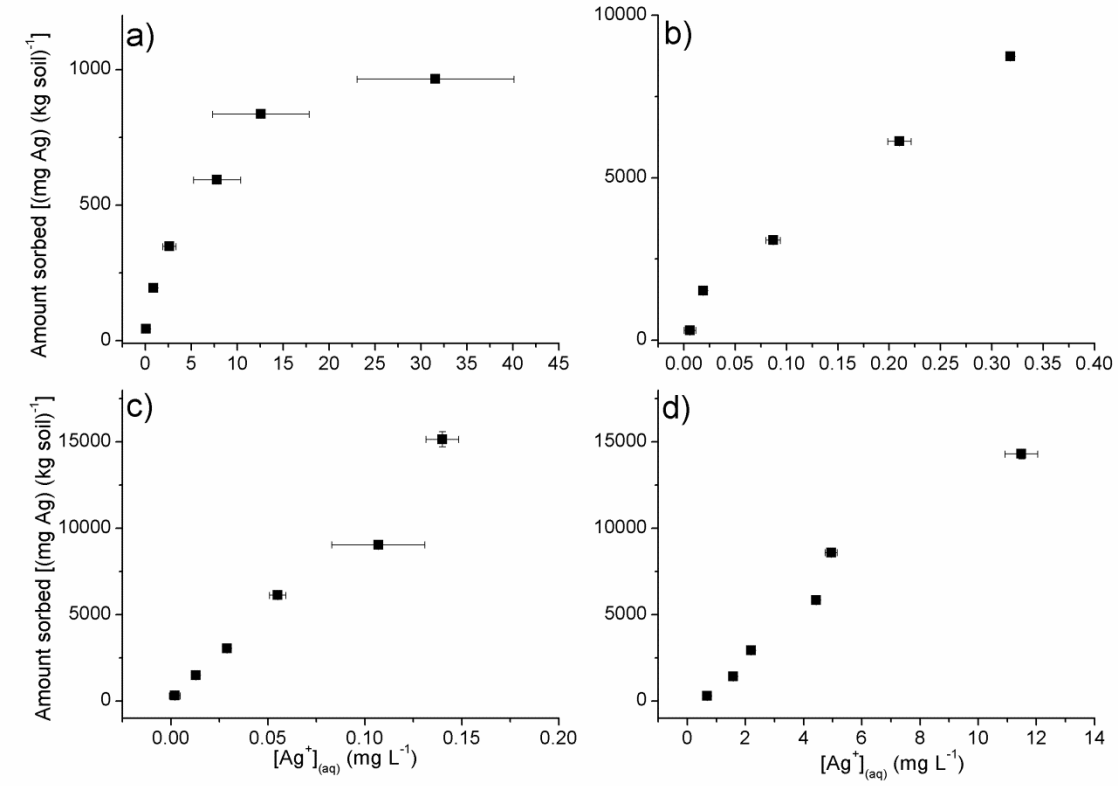

Figure 4.4. Adsorption isotherm data for Ag(I) and AgNPs in Toccoa sandy loam soil for a) $AgNO_3$, b) uAg50, c) pAg50, and d) pAg15. Error bars indicate one standard deviation above and below value.

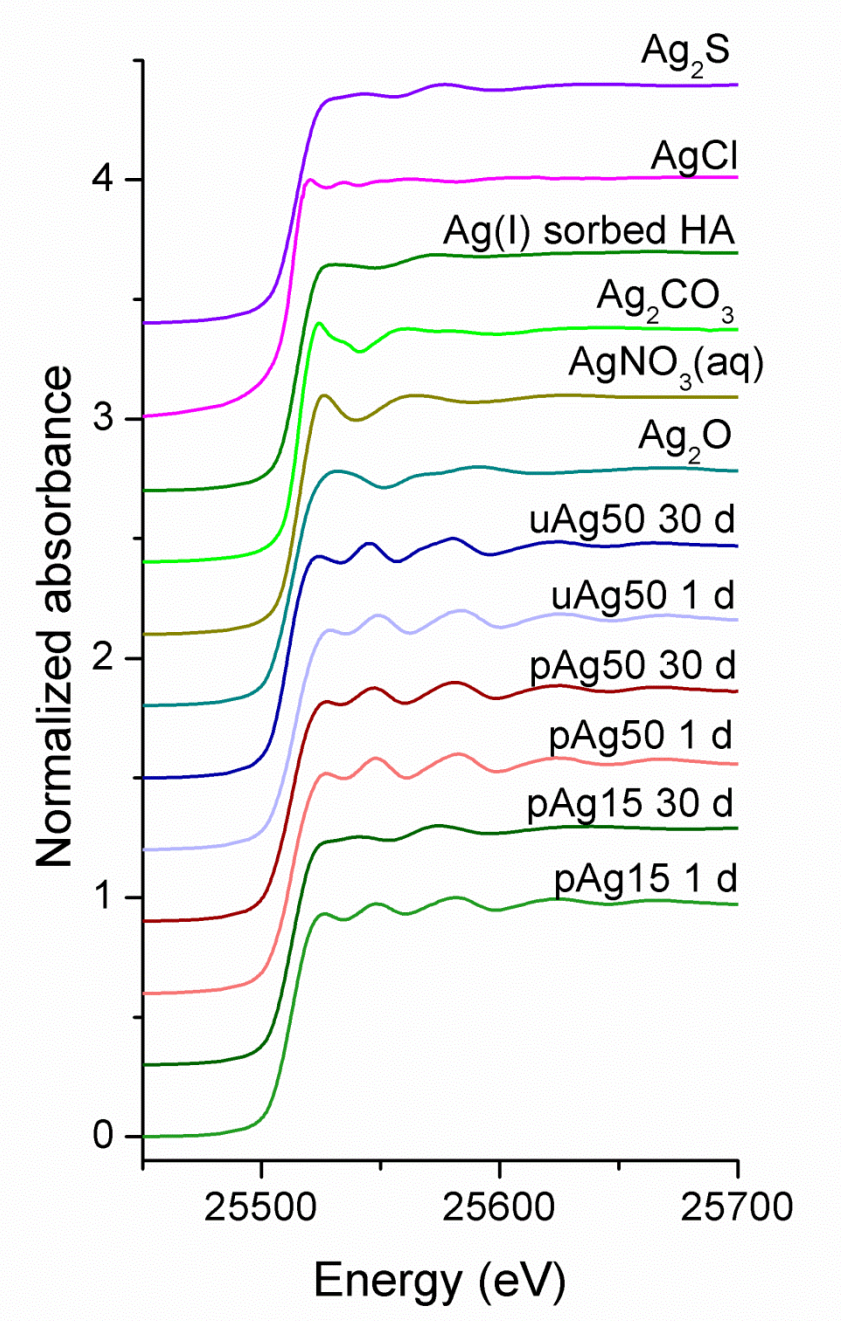

Figure 4.5. Normalized bulk Ag K-edge XANES spectra of AgNPs reacted Toccoa sandy loam soils under anaerobic conditions for 1 or 30 days at pH 5.2, along with selected reference compounds.

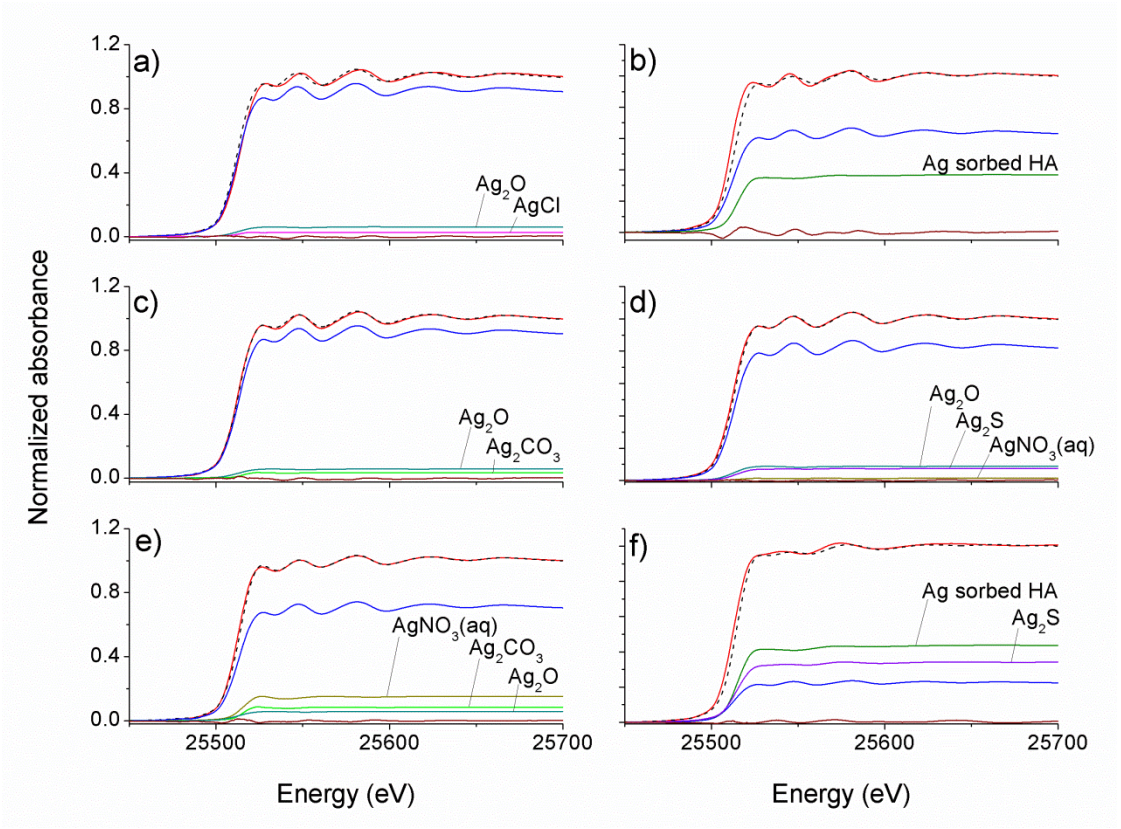

Figure 4.6. Linear combination of reference compound fit of bulk XANES spectra of AgNPs reacted with Toccoa sandy loam soils under anaerobic conditions at pH 5.2: a) uAg50 1 day, b) uAg50 30 days, c) pAg50 1 day, d) pAg50 30 days, e) pAg15 1 day, f) pAg15 30 days. In all panels, normalized data, overall fit, respective 0 day AgNP spectra, and residual spectra are shown as red, black dashed, dark blue, and brown, respectively. Any other spectra included in fit are labeled.

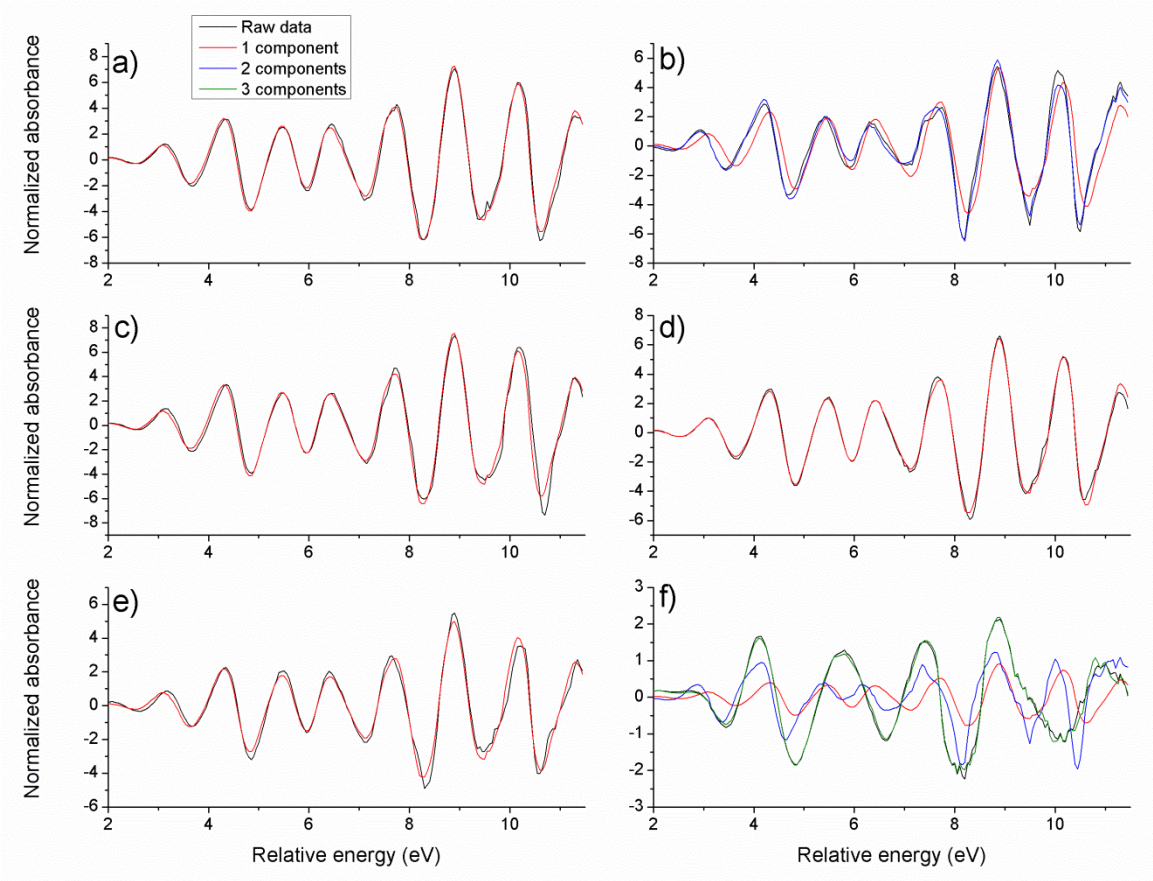

Figure 4.7. Principal component analysis and spectra reconstruction of bulk XANES spectra of AgNPs reacted with Toccoa sandy loam under anaerobic conditions at pH 5.2: a) uAg50 1 day, b) uAg50 30 days, c) pAg50 1 day, d) pAg50 30 days, e) pAg15 1 day, f) pAg15 30 days

CHAPTER FIVE

SPATIAL DISTRIBUTION OF SILVER NANOPARTICLES IN REDUCING SOIL ENVIRONMENTS AND THEIR EFFECT ON DENITRIFYING BACTERIA

5.1 Abstract

A large increase in the commercial and home usage of silver nanoparticle (AgNP) products and technologies is expected in the future. While several sources cite soils and sediments as the predominant sink for AgNPs once they enter the natural environment, few studies contribute to the risk assessment of AgNPs in terrestrial environments. In this study, the effect of AgNPs (total [Ag]: 1 – 100 mg/kg, 15 – 50 nm size with/without polyvinylpyrrolidone (PVP) capping agent) on native soil denitrifying bacteria was investigated using bench-scale biogeochemical kinetic experiments, synchrotron-based microprobe techniques, and scanning electron microscopy equipped with electron dispersive spectroscopy. Although the effects on denitrification kinetics and pseudo-equilibrium end-points were variable among the AgNPs, a distinct limitation of denitrification kinetics was observed under certain conditions (e.g., PVP-coated AgNPs ≥ 10 mg/kg). This is one of the first studies to demonstrate AgNP toxicity to bacterial organisms in soil environments. In general, AgNP toxicity in our soil environment was decidedly less than what was observed by other researchers studying AgNP toxicity under pure culture environments. This suggests the AgNPs may be residing at the soil-water interface as sorbed-AgNP aggregates or -Ag(I) species.

5.2 Introduction

Use of silver nanoparticles is a relatively new technology, which has continued to increase in popularity in consumer products since AgNP antimicrobial properties were first applied to commercial appliances: the Silver Nano Health System washing machine, manufactured by Samsung in 2003 (Samsung, 2003). As of 2012, the Project on Emerging Nanotechnologies consumer products inventory currently lists 97 separate products commercially available for purchase in the United States (US) containing AgNPs, including clothing, food storage containers, cleaning products, cosmetics, children's toys, and dietary supplements (PEN, 2012). The usage of these products inherently leads to the release of AgNPs into landfills, sewage treatment plants, the atmosphere, and directly into the environment (Gottschalk et al., 2009). A study by Benn and Westerhoff (2008) showed that the release of AgNPs into municipal wastewater treatment systems was likely to occur during typical home washings of commercially-available AgNP-impregnated socks. They demonstrated the release of total Ag would yield as high as 1,300 μg/L in wash water from these socks during their first washing (Benn and Westerhoff, 2008). A further study found Ag to be released from various consumer products, including: medical supplies, detergent, towels, humidifiers, etc. (Benn et al., 2010). According to a probabilistic material flow analysis model proposed by Gottschalk et al. (2009), 30.3 tons of AgNPs could be released to the environment per year. Of this, 10.7 tons per year are deposited into soils, making it the sink for approximately 35% of the total AgNP release. Landfills remain the primary sink for AgNPs (49% of total release) (Gottschalk et al., 2009). A separate modeling scenario

composed by Blaser et al. (2008) estimates that 80 to 190 tons of Ag_{Total} are being applied to agricultural fields each year via sewage sludge, up to 15% of which originated from the biocidal products described above. The unexpectedly high Ag inputs to terrestrial environment raises concerns about the effects on beneficial soil microbial communities.

Although mechanisms of AgNP induced antimicrobial effect are not well defined, it has been conclusively shown that AgNPs are toxic to bacteria in pure culture systems (e.g., Morones et al., 2005; Rai et al., 2009; Sondi and Salopek-Sondi, 2004). In early research, the effect of particle size/capping agents was extensively investigated (e.g., Choi and Hu, 2008; Griffitt et al., 2008; Morones et al., 2005; Pal et al., 2007; Sondi and Salopek-Sondi, 2004). The results, however, are varied in different strains of bacteria (e.g., gram positive and negative) (Kim et al., 2007; Ruparelia et al., 2008; Yoon et al., 2007), leaving difficulties in interpreting the dose-response relationship. More recently, reaction products of AgNPs, reactive oxygen species and free radicals, were suggested as alternative causes of antimicrobial toxicity (Choi and Hu, 2008; El Badawy et al., 2010; Hwang et al., 2008; Kim et al., 2007; Sondi and Salopek-Sondi, 2004). Furthermore, ionic Ag (Ag(I)) as dissolution products of AgNPs is also responsible for its bactericidal effect (Hwang et al., 2008; Lok et al., 2007; Miao et al., 2009; Navarro et al., 2008). AgNPs are known to release only a few percent of total [Ag] as Ag(I) in oxic aqueous suspensions (Fabrega et al., 2009; Griffitt et al., 2008; Navarro et al., 2008). However, this low concentration is sufficient to poise the microbial activity (Griffitt et al., 2008). It is apparent that both AgNPs and Ag(I) are toxic to bacteria communities in the environment (Choi et al., 2008; Hänsch and Emmerling, 2010; Lok et al., 2007; Sondi

and Salopek-Sondi, 2004), suggesting the potential threat to the biogeochemical cycles of trace metals and nutrients (e.g., nitrogen, N).

In this study, we are especially interested in studying the effect of AgNPs on the denitrifying group of bacteria. Denitrification occurs by the bacteria transformation of nitrate (NO_3^-) into nitrite (NO_2^-); and subsequently NO_2^- into nitrogen gas (N_2) and other gaseous forms of N (i.e., nitric oxide, NO(g), and nitrous oxide, N_2O(g)). The denitrification process plays an important role in the N cycle, removing excess NO_3^- and NO_2^- from anaerobic environments (e.g., waterlogged soils and wetlands). While denitrification supports the steady flux of gaseous nitrogen in atmosphere, it is also essential to protect human and ecosystem health. Denitrification reduces surface and groundwater contamination of NO_3^- that will prevent eutrophication as well as reduce the risk of methemoglobinemia in infants (Kross et al., 1992). The denitrification process in soils is performed by a host of bacteria, including *Flavobacterium spp.*, *Pseudomonas spp.*, and *Bacillus spp.*, all commonly found in soil environments (Wang and Skipper, 2004). Although it was previously shown in Chapter 4 of this text that AgNPs bind strongly to humic acid functional groups within the soil matrix, it is still reasonable to assume that they may still show toxic effects to soil organisms.

To test the hypothesis, we investigated the effect of manufactured AgNPs on the denitrification process in an anaerobic soil environment. The AgNPs had a size range of 15 – 50 nm, and were tested with and without a capping agent, PVP. The reactivity and bioavailability of AgNPs in heterogeneous systems such as soils are largely unknown. Toxicity in a soil environment depends on the bioavailability of AgNPs, the chemical

speciation of Ag(0)/Ag(I) and the spatial distribution of Ag within the soil matrix. To better interpret the denitrification kinetic data, changes in chemical speciation and spatial distribution of AgNPs in soils were investigated using synchrotron based microfocused-X-ray fluorescence (μ-XRF) analysis and scanning electron microscopy (SEM) coupled with electron dispersive spectroscopy (EDS).

5.3 Materials and Methods

5.3.1 Silver Nanoparticle Characterization

Four manufactured AgNPs were chosen for this study, and three of them are described in Chapter 4, Table 4.1. One AgNP was added to this study, and will be identified as uAg35 (US Research Nanomaterials, Inc., Houston, Texas; reported diameter = 20 nm, 99.99% Ag, density = 10.49 g/cm^3). This AgNP was chosen for its small size, relative to uAg50, and its absence of any surface coating. Transmission electron microscopy (described in Chapter 4, Section 4.3 of this work) revealed particles to be an average of 35 nm in diameter (± 21 nm).

All four AgNPs differ in size (13 – 53 nm) and the presence or absence of a capping agent: PVP. These parameters give the abbreviations used for each particle throughout this paper: uAg50 (uncoated, approximately 50 nm in size), pAg50 (coated with 0.3 % PVP by wt., approximately 50 nm in size), pAg15 (coated with 90% PVP by wt., approximately 15 nm in size), and uAg35. Silver nitrate (Fisher Chemical; Fair Lawn, New Jersey) was used as a source of Ag(I). Particle size was determined using dynamic light scattering (DLS) technology on a Brookhaven Instruments particle

separation system (Brookhaven Instruments, Holtsville, New York) in batch mode. Baseline data were established using a reference of 92 nm latex spheres. Baseline and all samples were read continuously for 50 s. Data were analyzed using Brookhaven Instruments 90Plus Particle Sizing Software, ver. 4.14.

5.3.2 Denitrification Kinetic Experiments.

A South Carolina Toccoa Entisol (coarse-loamy, thermic typic Udifluvents) from a local certified organic farm was chosen for the denitrification experiments. This site has not received any synthetic fertilizers or pesticides since its organic certification in 2005, so that any antimicrobial effects we observe in the experiments can be attributed to our Ag additions. Toccoa soil exhibits 1.53% organic matter, pH_{water} 5.2, 7.4 $cmol_c$/kg cation exchange capacity, and clay composed of kaolinite, hydroxyl-interlayer vermiculite, hematite, and goethite. The moisture content of soils was kept at field capacity (gravimetric water content approx. 10 g/g) and at ~3º C prior to denitrification experiments. Approximately 50 g of moist soil was placed into a 250 mL Nalgene polypropylene bottle for each denitrification batch. All bottles were kept in an argon-filled glove bag for the duration of the experiment to maintain an anaerobic environment. The following batch denitrification experiments were conducted in duplicate. All reagents were prepared using distilled deionized water (18MΩ).

For thecontrol system, 200 mL of solution was added to the soil for each treatment. The solution contained NO_3^- (as $NaNO_3$) at 50 mg/L as N. Our preliminary experiments suggested that this initial [NO_3^-] was sufficient to promote denitrification. To

maintain appropriate ionic strength, the solution contained 0.005 mol/L Na_2SO_4. We chose a sulfate-based electrolyte because it does not cause any interference with the nitrate-specific ion selective electrode (ISE) used. Finally, the solution contained 1% glucose solution as a carbon (C) source for the bacteria. A high amount of glucose ensures that electron acceptors, rather than soil C sources, will be the limiting factor in microbial growth. In addition, this high concentration will also act to speed up oxygen depletion by the facultative aerobic bacteria, decreasing the time needed for reducing environments to occur. Bottles were gently manually agitated daily in the glove bag. Denitrification was allowed to occur for two to eight days by the native bacteria present in the soil. Nitrate concentration was measured every four to ten hours via 5 mL samples taken from each bottle, filtered at 0.45 μm using syringe filters, and tested for [NO_3^-] using an ISE (detection limit: 0.4 mg/L NO_3^--N). During these sample times, pH and redox potential values were measured in the well-mixed soil suspensions using electrodes.

Silver toxicity to native denitrifying bacteria was measured through the addition of Ag(I) (in the form of $AgNO_3$) or various AgNPs described above to individual denitrification batches. The amount of NO_3^- added with the Ag(I) additions (<1 mg/L as N) was insignificant with respect to the total amount of NO_3^- in the system (~50 mg/L as N). An adequate amount of a 5 mmol/L $AgNO_3$ stock solution was added to assure the total Ag concentration of 1 and 10 mg/L. A known mass of AgNPs was added to make the $[Ag]_{total}$ equivalent to that of the Ag(I) systems (i.e. 1 and 10 mg/L) to compare antimicrobial effects under the same $[Ag]_{total}$. We also repeated AgNP experiments with

100 mg/L total Ag. The experiments with higher [Ag] were conducted because our preliminary experiments suggested that AgNPs were much less toxic to denitrifying bacteria than Ag(I).

Denitrification kinetics was evaluated using a zero-order kinetic reaction model. A zero-order, or linear, kinetic model is commonly used for denitrification processes in soils and water systems due to the independence of the rate of NO_3^- depletion from the initial NO_3^- concentration (Boaventura and Rodrigues, 1997; Dawson and Murphy, 1972; van Haandel et al., 1981). In addition to NO_3^- depletion during denitrification, a linear model can also be used to measure the rates of NO_2^- production and depletion, and N_2O production during denitrification (Betlach and Tiedje, 1981). This further supports our use of a linear model for overall denitrification analysis. Denitrification kinetics can be determined using the following equation:

$$\frac{dN}{dr} = -KX \qquad [5.1]$$

where N = NO_3^- concentration as N (mg/L), $\frac{dN}{dr}$ = denitrification rate, X = concentration of soil solids (mg/L), and K = the specific denitrification constant (mg NO_3^--N · mg solids^{-1}· time^{-1}) (van Haandel et al., 1981). Since these experiments were performed in batch systems, the concentration of soil, X, remains constant over time. The values for K are determined through linear best fit analysis of graphs displaying NO_3^- concentration over time (Figure 5.1).

Initial measurements may be affected by lingering aerobic bacteria in the system. Under aerobic conditions, ammonium (NH_4^+) is easily oxidized to nitrite (NO_2^-) by common soil bacteria such as *Nitrosomonas* spp. This conversion is typically followed by the oxidation of NO_2^- to NO_3^-, performed by common soil bacteria of the genus *Nitrobacter* (Myrold, 2005). For this reason, the highest NO_3^- concentration measured may be slightly greater than 50 mg/L, due to nitrification action by the native aerobic soil bacteria. In the linear equation fit analysis, the following data range was used: the starting point was assigned to the highest measured NO_3^- concentration (range = 47.0 to 77.1 mg/L NO_3^--N), and *K* calculation data concludes with 90% NO_3^- depletion. At this point, some anaerobic bacteria may begin to use sulfate as an electron acceptor, converting it to sulfide, as sulfate oxidation is the next most energy-rich electron acceptor after NO_3^-. Sulfide is a known cause of interference in our ISE, and for this reason, 90% NO_3^- depletion was chosen as our endpoint.

5.3.3 Synchrotron-Based X-ray Microprobe Analysis

Synchrotron-based X-ray microprobe measurements of AgNP (uAg50, pAg15 and pAg50) spiked soil samples were performed at beamline X27A at the National Synchrotron Light Source, Upton, New York. Due to time constraints, X-ray microprobe measurements of uAg35 were not permitted. The purpose of this measurement was to understand changes in spatial variability of AgNPs in soils. Silver nanoparticle-reacted soils samples were used to prepare a thin section (30 μm) according to the method described by Arai et al. (2007). Spent denitrification batches were first filtered through

Watman-2 filters, and air-dried in the anaerobic glove bag for 2 weeks. This drying process was necessary for the Epotek 301 resin (Epoxy Technology, Inc. Billerica, Massachusetts) to cure at room temperature. To eliminate the background metal(loid) impurities, quartz slides, and super glue were used for this process, as these materials have proven to be near metal(loid) free, which is necessary for backing materials during the μ-XRF analysis. The μ-XRF compositional maps of Ag were conducted at above the Ag K absorption edge (25.55 keV) using a Canberra SL30165 Si(Li) detector. At this high energy, additional elements in the sample that can be detected are limited. Using a XRF software (SNRLXRF) (Sutton et al., 2002), we qualitatively predicted the concentration of these two elements. In this approach, one calculates the fluorescence yield for two elements (e.g., Fe and Ag) at a particular monochromatic energy (i.e., 25.55 keV) and the sample geometry. It is assumed that some *a priori* information from bulk analysis exists for one of them (e.g., Fe @ 0.68 wt. %). The value was based on citrate-dithionite-bicarbonate extraction of the soil. By ratio of the fluorescence yields for these two elements, we arrived at an estimate of concentration for the unknown, Ag.

Within each thin section, microfocused X-ray absorption near-edge structure spectroscopy (μ-XANES) measurements at the Ag K edge were attempted near hotspots. All spectra analysis was performed using the SIXpack software packet (Webb, 2005).

5.3.4 Scanning Electron Microprobe Analysis

All three soil thin sections used in μ-XRF analysis were examined using SEM coupled with EDS. The samples were examined uncoated. A SEM-Hitachi SU6600

(Hitachi High-Technologies Corp., Tokyo) outfitted with Oxford INCA Energy (Oxford Instruments, Abingdon, United Kingdom) for EDS was used for imaging, as well as chemical identification of the nanoparticles. Quantitative analysis of elements (e.g., S, Ag, Fe, and Al) and their spatial distribution were evaluated in EDS elemental maps and spectra.

5.4 Results

5.4.1 Denitrification Kinetic Experiments

Results from the denitrification kinetics experiments are summarized in Figure 5.1, Figure 5.2, and Table 5.1. Figure 5.1 displays the denitrification data for one repetition of each treatment condition. The remaining repetition is not shown in figures, but was used in the statistical analysis discussed below. The kinetic rate (*k* value) for each condition was calculated from the negative slope of the linear best fit line. A student's t-test was performed on each *k* value, determining its validity. Since >90% of the t-test results were significant, the zero-order kinetic model is appropriate for these denitrification data, as supported by previous research (e.g., van Haandel et al., 1981). The average *k* value was obtained for each treatment, and a separate t-test was performed to compare the kinetic rate of each treatment to that of the control. These results are also listed in Table 5.1.

The control condition (Figure 5.1a) displayed a relatively rapid depletion of NO_3^-, achieving 90% depletion in 49 hr (± 4 hr) on average. The average *k* value is 1.486 ± 0.289 (Table 5.1). Ionic Ag in both 1 and 10 mg/L (e.g., Figure 5.1b and 5.1c,

respectively) concentrations resulted in a significantly slower *k* value than the control condition ($p < 0.1$): 0.748 ± 0.019 and 0.881 ± 0.224, respectively, showing the toxicity of Ag(I) to denitrifying bacteria. The t-test showed that the *k* values of the two Ag(I) concentrations are not, however, significantly different from each other. Therefore, we observe an absence of concentration dependent toxicity for Ag(I) in the reaction rate at given reaction conditions. Interestingly, there are differences between the Ag(I) concentrations at the pseudo-equilibrium end point. Ionic Ag at 1 mg/L achieved 90% NO_3^- depletion in 64 hr (± 11 hr), while the 10 mg/L concentration took 132 hr (± 17 hr) for the same effect (Figure 5.2).

The first AgNP, uAg50 (Figures 5.1d through 5.1f), did not have *k* values significantly different from the control condition at $[Ag]_{total}$ = 1 or 10 mg/L. At $[Ag]_{total}$ = 100 mg/L, however, the *k* value for NO_3^- depletion is significantly lower than the control at 0.939 ± 0.063 (Table 5.1). There are differences between the various uAg50 concentrations at the end point of experiments. The uAg50 conditions at $[Ag]_{total}$ = 1, 10, and 100 mg/L took 47 hr ± 1 hr, 56 hr ± 1 hr, and 71 hr ± 1 hr, respectively, to achieve 90% NO_3^- depletion (Figure 5.2). All *k* values within the uAg50 condition were significantly different from each other. This indicates a concentration dependence of toxicity in the reaction rate and the pseudo-equilibrium end point.

The pAg50 (Figures 5.1g through 5.1i) AgNP did not show significant differences in *k* values for NO_3^- depletion rate from the control condition at any concentration (Table 5.1), nor were the *k* values for each concentration ($[Ag]_{total}$ = 1, 10, and 100 mg/L) significantly different from each other. The effect of concentration was insignificant for

the reaction rate for this type of AgNP. Contrarily, there are differences in the pseudo-equilibrium end point. At $[Ag]_{total}$ = 1 and 10 mg/L, the amount of time to achieve 90% NO_3^- depletion was essentially the same: 67 hr ± 16 hr and 68 hr ± 22 hr, respectively (Figure 5.2). At $[Ag]_{total}$ = 100 mg/L, 91 hr ± 28 hr was required for 90% NO_3^- depletion.

The smallest AgNP, pAg15 (Figures 5.1k through 5.1l), showed the greatest differences from the control condition in the reaction rate and at the end point. At $[Ag]_{total}$ = 1 mg/L, the *k* value for NO_3^- depletion rate was not significantly different than that of the control (Table 5.1), and it took 68 hr ± 1 hr to achieve 90% NO_3^-depletion. Both the $[Ag]_{total}$ = 10 and 100 mg/L had *k* values significantly slower than the control condition, at 0.581 hr ± 0.069 hr and 0.425 hr ± 0.065 hr, respectively. While the *k* value for $[Ag]_{total}$ = 1 mg/L is significantly different from the *k* value for both $[Ag]_{total}$ = 10 and 100 mg/L, , their *k* values are not significantly different from each other. Again, interestingly, they do have different endpoint times. At $[Ag]_{total}$ = 10 mg/L, it took 111 ± 16 hr to achieve 90% NO_3^-depletion, while at $[Ag]_{total}$ = 100 mg/L, it took 194 hr ± 1 hr to achieve 90% NO_3^- depletion (Figure 5.2).

Finally, uAg35 (Figures 5.1m through 5.1o) did not show any significant differences from the control condition in terms of *k* values (Table 5.1) or time to reach end point (Figure 5.2). This held true for all Ag concentrations tested (1, 10, and 100 mg/L). All reaction vessels completed 90% NO_3^- depletion within 40 hrs (± 1 hr), which is slightly faster than the control condition (49 hrs ± 4 hrs).

5.4.2 Dynamic Light Scattering Analysis

Analysis via DLS revealed uAg50 to be the largest AgNP used in this set of experiments (Figure 5.3). The DLS measurements agreed reasonably well with the transmission electron microscopy (TEM) analysis described in Chapter 4 of this text, as well as the diameter reported by the manufacturer (50 nm). Approximately 90% by volume of the uAg50 particles were between 31.1 and 44.4 nm in diameter. The pAg50 particles appeared to have a bimodal particle size distribution. While 76% by volume of the particles were between 20.3 and 28.7 nm, another 18% were between 161 and 383 nm in diameter. The smaller sized particles for pAg50 agree reasonable well with the manufacturer data (diameter = 20 nm), while it is much larger than the TEM analysis results. The pAg15 particles were found by DLS to be much smaller than the diameter reported by the manufacturer (15 nm), and also smaller than the diameter determined through TEM analysis. Approximately 98% by volume of the pAg15 particles were between 2.0 and 3.6 nm in diameter. Likewise, the uAg35 AgNPs were also smaller than the reported diameter. Figure 5.3 shows that 83% of the uAg35 particles were between 11.1 and 13.2 nm in diameter, while another 8% were between 83.5 and 193.3 nm.

5.4.3 X-ray Microprobe Analysis

Figures 5.4a and 5.4b show μ-XRF maps of pAg50 and uAg50 spiked soil samples, respectively. They both show distinct "hotspots" of Ag within the heterogeneous soil matrix. The uAg50 sample shows several hotspots throughout the map (Figure 5.4a). In contrast, the pAg50 sample displays one concentrated spot. In addition

to these μ-XRF maps, several larger survey maps (not shown) were collected to locate micron size hot spots in both soil samples. Furthermore, the pAg15 μ-XRF map (Figure 5.4c) showed even more dilute, but evenly distributed Ag concentration throughout. While the hot spots were always located in every μ-XRF maps of uAg50 spiked soils, it was difficult to find the localized hot spots in pAg50 samples. While the uAg50 μ-XRF map displays a maximum [Ag] of 1000 mg/kg (Figure 5.4), pAg50 and pAg15 display maximum [Ag] values of only 100 and 300 mg/kg, respectively. To elucidate the chemical state of AgNPs in soils, μ-XANES measurements were attempted at hotspots (Figure 5.5). The distinct post edge features that are observed in the Ag foil can be observed in all spot μ-XANES. While areas of higher [Ag] should produce less noisy spectra, a lack of stability in electric supply to the beamline resulted in a lower signal to noise ratio for the uAg50 spot μ-XANES spectra. This was not experienced during the collection of pAg50 and pAg15 spectra. All spectra strongly resemble the Ag(0) foil spectrum in post edge features, while bearing little to no resemblance to oxidized Ag reference compounds such as $AgNO_3$ and Ag_2O.

5.4.4 Scanning Electron Microscopy Analysis

The same thin sections from which μ-XRF maps were made were analyzed under SEM outfitted with EDS capabilities. As shown in Figure 5.6, each thin section was analyzed for [Ag] under EDS to gain spatially resolved AgNP distribution in the soil matrix. Several spots of high [Ag] were found in the uAg50 thin section. The SEM micrograph shown in Figure 5.6a reveals a distinct hotspot of uAgNP particles,

approximately 20 μm across. The EDS spectra shown for spot 1 of this figure indicates that Ag is the predominant element present (50.1 wt. %). Spot 2 shows a nearby area of slightly more diffuse [Ag] (25.3 wt. %). The full elemental analysis from INCA indicated no measureable S at either location. As in the μ-XRF maps, it was much more difficult to find individual spots of high [Ag] in either pAg50 or uAg15. The EDS detection limit for Ag is approximately 100 mg/kg. One region of moderate [Ag], approximately 1.5 μm across, was observed in pAg50 (Figure 5.6b). Two EDS spectra were taken in the region. Both were of lower [Ag] than either uAg50 spot (19.5 and 21.9 wt. % for spots 1 and 2, respectively). Interestingly, both pAg50 spots 1 and 2 contained measureable S, at 0.07 and 0.06 wt. %, respectively. Only one area of measureable [Ag] was found in pAg15, approximately 1 μm across (Figure 5.6c). Spot 1 shows 0.17 wt. % Ag concentration, which is near the detection limit. This location displayed a similar amount of S (0.16 wt. %). This agrees with the previous findings presented in Chapter 4 of this text, that pAg50 and pAg15 associated with sulfide in the soil after 30 days aging time, while uAg50 shows no sulfide associations. These findings also suggest that the observations found in the μ-XRF maps hold true throughout the soil matrix.

5.5 Discussion

5.5.1 Denitrification Endpoint and Kinetics

The results of the denitrification experiments suggest that the antimicrobial effect of AgNPs was concentration dependent with regards to the pseudo-equilibrium endpoint for most AgNPs. uAg50, pAg50, and pAg15 all showed a significant difference from the

control condition in time to reach 90% NO_3^- depletion in at least the highest concentration. However, the zero-order kinetic model suggested, in general, that 1) the rates within the same AgNP were concentration dependent (i.e., the rate decreases with increasing $[Ag]_T$), and 2) the rates of the control system were statistically different from the high (100 mg/L) uAg50 system and the pAg15 systems at 1 – 100 mg/L. The small uncoated AgNP, uAg35, did not show a difference from the control in either kinetics (Table 5.1) or endpoint (Figure 5.2).

The toxicity of AgNPs to native soil bacteria is likely to be affected by chemical factors (e.g., sorption, complexation, dissolution, coating) and/or physical factors (e.g., size, spatial distribution, aggregation). Although other researchers have shown that AgNPs are more toxic to bacteria than Ag(I (e.g., Lok et al., 2007), these studies were not conducted in the presence of a natural substrate such as soil. Previous work has shown the strong affinity of AgNPs for soil surfaces through sorption processes (Chapter 4, this text), which may exhibit more complexity in describing subsequent toxicity to organisms. Based on the results of our spectroscopic investigation (described in Chapter 4 of this text) and spatially resolved analyses in this investigation, chemical and physical effects of AgNP toxicity in soils are discussed below.

5.5.2 Chemical Effects

The pseudo-equilibrium end point and kinetic rate of the denitrification clearly showed that Ag, in both the ionic (Ag(I)) and particulate (AgNP) form, displays toxicity to soil bacteria at high concentrations (Figure 5.2, Table 5.1). However, the method of

toxicity assessment remains convoluted since both Ag(I) and AgNPs undergo complex chemical processes (e.g., adsorption, dissolution, and ligand complexation) in soils. Our research group has previously shown that these AgNPs display near 100% sorption onto Toccoa soil surfaces at all concentrations used for the denitrification experiments (Chapter 4, Figure 4.4). In addition, pAg15, the most toxic AgNP to denitrifying bacteria of this study by both the kinetic model and the pseudo-equilibrium endpoint, exhibits the highest amount of Ag(I) release in a dissolution study under both oxidizing and reducing conditions, releasing 10 times the amount of Ag ions that either uAg50 or pAg50 do (Chapter 4, Figure 4.1). It has been suggested that Ag(I) ions originating from AgNPs are either released into solution or held on AgNP surface and may play an important role in AgNP toxicity (Lok et al., 2007).

No consensus has been made as to the exact mode of toxicity of AgNPs in soils from current scientific literature, whether primary toxicity occurs due to the presence of AgNPs themselves, or due to the Ag(I) released from these particles. However, it seems that the toxicity of Ag(I) is the most potent through all of our investigation. The denitrification data have shown Ag(I) at concentrations of both 1 and 10 mg/L to slow the denitrification kinetics more than uAg50, pAg50, or uAg35 did at all concentrations (Figure 5.1, Table 5.1). Ionic Ag primarily exhibits toxicity through binding to S-containing ligands within microbial cells, especially the thiol group on cysteine (Liau et al., 1997). This antimicrobial effect can have prolonged inhibitory action to *Eschericia coli* organisms (Zhao and Stevens, 1998). Ionic Ag has been previously shown to associate with S-containing compounds inside *E. coli* cells (Feng et al., 2000), however,

there have been very few studies on AgNP intracellular associations. In our study, Ag(I) should have contributed to observed toxicity as: 1) Ag(I)(aq) via dissolution of AgNPs, 2) surface sorbed Ag(I), and/or 3) formation of $Ag(I)_2O(s)$. The Ag(I) linked toxicity of AgNPs on microbes was previously suggested by several researchers. Sotiriou and Pratsinis (2010) demonstrated large amounts of Ag(I) release from small AgNPs (approx. 5 – 15 nm).

Our study found Ag(I) to be more toxic than any AgNP when controlled for concentration, which further supports the theory that Ag ions are the primary source of AgNP toxicity. In terms of kinetic rate, Ag(I) showed no significant concentration dependence (Figure 5.2). This could be because the Ag(I) toxicity threshold had already been reached. Bringmann and Kühn (1980) previously reported a Ag(I) toxicity threshold as low as 0.006 mg/L for *Pseudonomas putida* bacteria, which are known denitrifiers, supporting the results of our study. Because of the high toxicity, the rate was not affected with increasing total Ag levels.

In contrast, uAg50 and pAg15 did show concentration dependent toxicity. The presence of uAg50 and pAg15 retarded denitrification kinetics with increasing $[Ag]_T$. While there is no straightforward explanation for different toxicological effects, we suspect the toxicity of various AgNPs (pAg50, uAg50, pAg15, and uAg35) is dependent on their chemical properties that were altered during the incubation period. This was investigated previously by this research group. Under conditions identical to those of the denitrification experiments, pAg15 showed dramatic change in chemical state over time. X-ray absorption near edge spectroscopy revealed that pAg15 AgNPs were quite

chemically similar to Ag(0) after only one day of aging in reducing soil conditions, but became much more similar to Ag(I)-sorbed humic acid after 30 days under these conditions. This susceptibility to change suggests a more chemically active AgNP, which may increase bioavailability, and therefore, bacterial toxicity. While pAg50 showed the least change over time, it did show association with sulfide after aging for 30 days in the reducing soil environment. Choi et al. (2009) showed that the addition of sulfide to a AgNP media greatly decreased AgNP toxicity to bacteria, demonstrating how sulfide-AgNP complexes will form. It is possible that the S functional groups in soil with or without organic matter were suppressing the toxicity of Ag(I) in our study via ligand complexation on Ag(I), as well as AgNPs. As an already stable AgNP with little Ag(I) release, the association with sulfide may have further decreased the toxic properties of pAg50.

Finally, uAg35 showed no difference from the control in terms of either kinetic response (Table 5.1) or time to achieve endpoint (Figure 5.2). While the chemical speciation of this AgNP was not studied via XAS due to time constraints, the effects of lack of surface coating can still be addressed. Similar to uAg50, uAg35 lacks any surface coating, leaving bare Ag(0) exposed to the soil-water environment. Unlike PVP, bare Ag(0) is relatively hydrophobic. The lack of a surface coating leads to a less-stable AgNP in solution, increasing the likelihood for sedimentation (Kvitek et al., 2008). This means that these AgNPs may partition to soil-water interfaces and out of solution. A smaller diameter may also increase aggregation, unlike uAg50, further inhibiting antimicrobial properties. The size of uAg35 (Figure 5.3), which is smaller than uAg50 and pAg50,

allows for a greater amount of reactive surface area to come into contact with soil surfaces. Therefore, we hypothesize that the large surface area of uAg35, in combination with its lack of surface coating, resulted in strong adhesion to soil surfaces and a lack of bioavailability.

5.5.3 Physical Effects

While this study provides more evidence of Ag(I)-based AgNP toxicity to bacteria, it also shows that the toxicity is dependent on the physical properties of AgNPs at the soil mineral-water interface. Dissolution experiments coupled (Chapter 4, Figure 4.1) with SEM analysis (Figure 5.6) showed that more than 90% of particles were intact during the denitrification experiments. Nearly 100% of these particles readily retained in soils, as shown in the adsorption experiments (Chapter 4, Figure 4.4). Besides the Ag(I) based toxicity discussed above, the aggregation state of the particles (dispersed versus aggregated), particle size, and particle distribution across the soil matrix should be noted as contributors of antimicrobial effects. Discrepancies in particle size between DLS and TEM analyses were noted, especially for pAg15, which could be attributed to particle aggregation upon drying for TEM work. While TEM analysis requires a completely dry sample, DLS analysis is performed *in situ*, providing a potentially more accurate result. In the case of pAg50, the bimodal distribution of DLS particle size would have resulted in an average particle size somewhere between the two peaks. The pAg50 did display a large standard deviation of particle diameter under TEM analysis, supporting this theory.

The PVP-capped (90 wt. %) pAg15 has the smallest size from all of the characterization methods, and is the most dispersed AgNP of this experiment. Work by Kvitek et al. (2008) showed that the addition of PVP both increases particle stability and toxicity to bacteria. In our study, pAg15 has, by far, the most PVP of all AgNPs, and also displayed the strongest toxicity of all AgNPs. Nanoparticle size and dispersibility are among the most important physical characteristics to determine bioavailability, and hence, toxicity. Small, dispersed particles have the most available surface area, and are therefore most likely to diffuse into living cells (Hassellöv and Kaegi, 2009). The rate of denitrification in the presence of pAg15 at 10 mg/L was statistically similar to the rate of denitrification in the presence of Ag(I) at 10 mg/L, while both were statistically different from the control. With this evidence, it is clear that the particulate Ag must be having an effect on the denitrifying bacteria in the pAg15 sample. These particles only have, at most, 6% dissolution, yet show similar toxicity effects as the same concentration of Ag(I). Research such as that by Morones et al. (2005) has shown the particle-dependent form of AgNP toxicity. Most noticeably, particles may adhere to bacterial membranes due to the presence of S-containing ligands, causing membrane damage while also allowing for the easy passage for more AgNPs and/or Ag(I) directly into the cell (Morones et al., 2005). The results of particle size dependent toxicity on bacteria are in line with previous research (Elzey and Grassian, 2010). Although the particle size is slightly greater in pAg50, these same effects were not seen in this form of AgNP, which may be due to the small quantity of the PVP capping agent (0.3 wt. %) in the pAg50

particles (Table 5.1), resulting in aggregation of AgNPs. In the case of uAg50 that does not contain any capping agents, the aggregation was more prominent.

The state of AgNP aggregation was varied in the four AgNPs in stock solutions (Figure 5.3). The DLS data of AgNP stock solutions showed that AgNPs were least aggregated in pAg15 and most aggregated uAg50. uAg35 also showed little aggregation in the stock solution. The μ-XRF maps (Figure 5.4) show stark contrast of particle distribution between uAg50, pAg50 and pAg15 in incubated soils. The PVP coating may have helped the AgNPs from forming large aggregates, as displayed in Figures 5.4c and 5.6c. While it was easy to locate spots of intense Ag concentration in the uAg50 condition, it was nearly impossible to locate the areas of the same intensity for pAg15. This indicates a more even and dispersed condition across the soil matrix, and the potential for increased uptake by soil bacteria. Furthermore, it has been shown that small AgNPs are more toxic than larger AgNPs (Lok et al., 2007). This statement also holds true for these data. While no μ-XRF maps were attained for uAg35, it is likely that these AgNPs would behave similarly to uAg50 due to their lack of surface coating.

"Hotspots," or microenvironments, are common in soil environments, and have a large effect on microbial communities. This is particularly important for anaerobic processes such as denitrification. Denitrification may still occur, even while the majority of the soil is exposed to oxygen from the atmosphere, due to anaerobic zones, especially those within large soil aggregates (Myrold, 2005). The data presented here show that when AgNPs are only available in "hotspots," the remainder of the soil may support a

healthy denitrifying community. However, when AgNPs are more evenly dispersed (i.e., in the case of pAg15), Ag is bioavailable over a larger space, and more toxic overall.

To assess the state of aggregation in AgNP reacted soils via μ-XRF maps, the mass of Ag at hotspots (i.e., ≤1000 mg/kg for uAg50, or ≤300 mg/kg for pAg50 and pAg15) was compared with the theoretical mass of single AgNP in one kilogram of soils. The following assumptions were made in the calculation.

1. That the average particle size of AgNPs as determined via TEM held true in the soil
2. That all AgNPs and/or AgNP aggregates were spherical in shape

The following equation was derived to determine the mass of Ag per particle, where $\frac{m_{Ag}}{NP}$ is the mass of Ag per particle and ρ_{AgNP} is the density of each AgNP:

$$\frac{m_{Ag}}{NP} = \frac{\frac{4}{3}\pi \left(\frac{d \times \frac{1\text{ cm}}{10^7\text{nm}}}{2}\right)^3 \times \rho_{AgNP} \times \frac{1000\text{ mg}}{1\text{ g}}}{1\text{ kg}}$$

[5.2]

Based on the calculation, the mass per single AgNP for uAg50, pAg50, and pAg15 is 2.41 x 10^{-12} mg/kg, 4.71 x 10^{-12} mg/kg, and 6.68 x 10^{-14} mg/kg, respectively. If only a single AgNP is widely present in a pixel of the μ-XRF map, the scale of Ag fluorescence signal (i.e., concentration of Ag in the sample) should be significantly smaller than the data presented. However, this is not the case. μ-XRF maps of uAg50 and pAg50 consistently contain high fluorescence counts (i.e., AgNP aggregates). These

aggregates seemed to hold Ag(0) structure. μ-XANES analyses of all hotspots found distinct similarity to Ag(0) foil in all spectra in areas concentrated enough to produce readable μ-XANES, which indicates that aggregation may inhibit oxidation of AgNPs. The AgNP with the least concentrated aggregates (pAg15) also showed the highest amount of toxicity.

Work by Kvitek et al. (2008) showed that the addition of PVP both increases particle stability and toxicity to bacteria. In our study, pAg15 has, by far, the most PVP of all AgNPs, and also displayed the strongest toxicity of all AgNPs. The PVP coating may also keep AgNPs from forming large aggregates, as displayed in Figures 5.4 and 5.6. While it was easy to locate spots of intense Ag concentration in the uAg50 condition, it was nearly impossible to locate the areas of the same intensity for pAg15. This indicates a more even and dispersed condition across the soil matrix, and the potential for increased uptake by soil bacteria. Furthermore, it has been shown that small AgNPs are more toxic than larger AgNPs (Lok et al., 2007). This statement also holds true for these data.

This study of AgNP specific toxicity in soil microbes displays novel data on the impact of AgNPs in terrestrial environments. Since most previous AgNP toxicity assays have largely been performed in pure-culture systems and have rarely tracked the changes in temporal and spatial distribution of AgNPs, our study should add a new insight in assessing the impact to AgNPs in heterogeneous soil systems. This investigation revealed the importance of these variations in the physicochemical properties and toxicity of AgNPs in soils, which must be considered when enacting necessary regulations on these

modern nano-products. It is still an early significant study of the effects of AgNPs on microbially mediated nutrient cycles. As AgNP usage in commercial products increases, so will their release into the environment. Future studies using environmentally relevant reaction conditions (e.g., in the presence of soils and humic substances) will be essential to better establish the linkage between the fate of AgNPs and the ecotoxicity.

5.6 References

Arai, Y., M.A. Marcus, N. Tamura, J.A. Davis, and J.M. Zachara. 2007. Spectroscopic evidence for uranium bearing precipitates in vadose zone sediments at the Hanford 300-area site. Environ. Sci. Technol. 41:4633-4639.

Benn, T., B. Cavanagh, K. Hristovski, J.D. Posner, and P. Westerhoff. 2010. The release of nanosilver from consumer products used in the home. J. Environ. Qual. 39:1875-1882.

Benn, T.M., and P. Westerhoff. 2008. Nanoparticle silver released into water from commercially available sock fabrics. Environ. Sci. Technol. 42:4133-4139.

Betlach, M.R., and J.M. Tiedje. 1981. Kinetic explanation for accumulation of nitrite, nitric oxide, and nitrous oxide during bacterial denitrification. Appl. Environ. Microb. 42:1074-1084.

Blaser, S.A., M. Scheringer, M. MacLeod, and K. Hungerbuhler. 2008. Estimation of cumulative aquatic exposure and risk due to silver: Contribution of nano-functionalized plastics and textiles. Sci. Total Environ. 390:396-409.

Boaventura, R.A.R., and A.E. Rodrigues. 1997. Denitrification kinetics in a rotating disk biofilm reactor. Chem. Eng. J. 65:227-235.

Bringmann, G., and R. Kühn. 1980. Comparison of the toxicity thresholds of water pollutants to bacteria, algae, and protozoa in the cell multiplication inhibition test. Water Res. 14:231-241.

Choi, O., and Z. Hu. 2008. Size dependent and reactive oxygen species related nanosilver toxicity to nitrifying bacteria. Environ. Sci. Technol. 42:4583-4588.

Choi, O., K.K. Deng, N.J. Kim, L. Ross, R.Y. Surampalli, and Z.Q. Hu. 2008. The inhibitory effects of silver nanoparticles, silver ions, and silver chloride colloids on microbial growth. Water Res. 42:3066-3074.

Choi, O., T.E. Cleuenger, B.L. Deng, R.Y. Surampalli, L. Ross, and Z.Q. Hu. 2009. Role of sulfide and ligand strength in controlling nanosilver toxicity. Water Res. 43:1879-1886.

Dawson, R.N., and K.L. Murphy. 1972. The temperature dependency of biological denitrification. Water Res. 6:71-83.

El Badawy, A.M., T.P. Luxton, R.G. Silva, K.G. Scheckel, M.T. Suidan, and T.M. Tolaymat. 2010. Impact of environmental conditions (pH, ionic strength, and electrolyte type) on the surface charge and aggregation of silver nanoparticles suspensions. Environ. Sci. Technol. 44:1260-1266.

Elzey, S., and V.H. Grassian. 2010. Agglomeration, isolation and dissolution of commercially manufactured silver nanoparticles in aqueous environments. J. Nanopart. Res. 12:1945-1958.

Fabrega, J., S.R. Fawcett, J.C. Renshaw, and J.R. Lead. 2009. Silver nanoparticle impact on bacterial growth: Effect of pH, concentration, and organic matter. Environ. Sci. Technol. 43:7285-7290.

Feng, Q.L., J. Wu, G.Q. Chen, F.Z. Cui, T.N. Kim, and J.O. Kim. 2000. A mechanistic study of the antibacterial effect of silver ions on *Escherichia coli* and *Staphylococcus aureus*. J. Biomed. Mater. Res. 52:662-668.

Gottschalk, F., T. Sonderer, R.W. Scholz, and B. Nowack. 2009. Modeled environmental concentrations of engineered nanomaterials (TiO_2, ZnO, Ag, CNT, fullerenes) for different regions. Environ. Sci. Technol. 43:9216-9222.

Griffitt, R.J., J. Luo, J. Gao, J.C. Bonzongo, and D.S. Barber. 2008. Effects of particle composition and species on toxicity of metallic nanomaterials in aquatic organisms. Environ. Toxicol. Chem. 27:1972-1978.

Hänsch, M., and C. Emmerling. 2010. Effects of silver nanoparticles on the microbiota and enzyme activity in soil. J. Plant Nutr. Soil Sci. 173:554-558.

Hassellöv, M., and R. Kaegi. 2009. Analysis and characterization of manufactured nanopartices in aquatic environments, p. 211-266, *In* J. R. Lead and E. Smith, eds. Environmental and Human Health Impacts of Nanotechnology. John Wiley & Sons, Ltd., West Sussex, UK.

Hwang, E.T., J.H. Lee, Y.J. Chae, Y.S. Kim, B.C. Kim, B.-I. Sang, and M.B. Gu. 2008. Analysis of the toxic mode of action of silver nanoparticles using stress-specific bioluminescent bacteria. Small. 4:746-750.

Kim, J.S., E. Kuk, K.N. Yu, J.-H. Kim, S.J. Park, H.J. Lee, S.H. Kim, Y.K. Park, Y.H. Park, C.-Y. Hwang, Y.-K. Kim, Y.-S. Lee, D.H. Jeong, and M.-H. Cho. 2007. Antimicrobial effects of silver nanoparticles. Nanomed.-Nanotechnol. 3:95-101.

Kross, B.C., A. Ayebo, and L. Fuortes. 1992. Methemoglobinemia: Nitrate toxicity in rural America. Am. Fam. Physician. 46:183-188.

Kvitek, L., A. Panacek, J. Soukupova, M. Kolar, R. Vecerova, R. Prucek, M. Holecova, and R. Zboril. 2008. Effect of surfactants and polymers on stability and antibacterial activity of silver nanoparticles (NPs). J. Phys. Chem. C. 112:5825-5834.

Liau, S.Y., D.C. Read, W.J. Pugh, J.R. Furr, and A.D. Russell. 1997. Interaction of silver nitrate with readily identifiable groups: Relationship to the antibacterial action of silver ions. Lett. Appl. Microbiol. 25:279-283.

Lok, C.N., C.M. Ho, R. Chen, Q.Y. He, W.Y. Yu, H. Sun, P.K.H. Tam, J.F. Chiu, and C.M. Che. 2007. Silver nanoparticles: Partial oxidation and antibacterial activities. J. Biol. Inorg. Chem. 12:527-534.

Miao, A.J., K.A. Schwehr, C. Xu, S.J. Zhang, Z.P. Luo, A. Quigg, and P.H. Santschi. 2009. The algal toxicity of silver engineered nanoparticles and detoxification by exopolymeric substances. Environ. Pollut. 157:3034-3041.

Morones, J.R., J.L. Elechiguerra, A. Camacho, K. Holt, J.B. Kouri, J.T. Ramirez, and M.J. Yacaman. 2005. The bactericidal effect of silver nanoparticles. Nanotechnology. 16:2346-2353.

Myrold, D.D. 2005. Transformations of Nitrogen, p. 333-372, *In* D. M. Sylvia, et al., eds. Principles and Applications of Soil Microbiology, 2nd ed. Pearson Prentice Hall, Upper Saddle River, New Jersey.

Navarro, E., F. Piccapietra, B. Wagner, F. Marconi, R. Kaegi, N. Odzak, L. Sigg, and R. Behra. 2008. Toxicity of silver nanoparticles to *Chlamydomonas reinhardtii*. Environ. Sci. Technol. 42:8959-8964.

Pal, S., Y.K. Tak, and J.M. Song. 2007. Does the antibacterial activity of silver nanoparticles depend on the shape of the nanoparticle? A study of the gram-negative bacterium *Escherichia coli*. Appl. Environ. Microb. 73:1712-1720.

PEN. 2012. Nanotechnology Consumer Products Inventory [Online]. Available by The Project on Emerging Nanotechnologies http://www.nanotechproject.org/inventories/consumer/ (posted 2010 Aug 9; verified 27 June 2012).

Rai, M., A. Yadav, and A. Gade. 2009. Silver nanoparticles as a new generation of antimicrobials. Biotechnol. Adv. 27:76-83.

Ruparelia, J.P., A.K. Chatteriee, S.P. Duttagupta, and S. Mukherji. 2008. Strain specificity in antimicrobial activity of silver and copper nanoparticles. Acta Biomater. 4:707-716.

Samsung. 2003. SAMSUNG Electronics introduces Korea's first silver sanitation washing machine. Samsung press release. Samsung Electronics Co. Ltd., Suwon, Korea.

Sondi, I., and B. Salopek-Sondi. 2004. Silver nanoparticles as antimicrobial agent: A case study on *E. coli* as a model for gram-negative bacteria. J. Colloid Interf. Sci. 275:177-182.

Sotiriou, G.A., and S.E. Pratsinis. 2010. Antibacterial activity of nanosilver ions and particles. Environ. Sci. Technol. 44:5649-5654.

Sutton, S.R., P.M. Bertsch, M. Newville, M. Rivers, A. Lanzirotti, and P. Eng. 2002. Microflourescience and Microtomography Analyses of Heterogeneous Earth and Environmental Materials, *In* P. A. Fenter, et al., eds. Applications of synchrotron radiation in low-temperature geochemistry and environmental science. Reviews in Mineralogy and Geochemistry, Mineralogical Society of America, Chantilly, Virginia, US.

van Haandel, A.C., G.A. Ekama, and G.V. Marais. 1981. The activated sludge process - 3. Single sludge denitrification. Water Res. 15:1135-1152.

Wang, G., and H.D. Skipper. 2004. Identification of denitrifying rhizobacteria from bentgrass and bermudagrass golf greens. J. Appl. Microbiol. 97:827-837.

Webb, S.M. 2005. SIXpack: a graphical user interface for XAS analysis using IFEFFIT. Physica Scripta. T115:1011-1014.

Yoon, K.Y., J.H. Byeon, J.H. Park, and J. Hwang. 2007. Susceptibility constants of *Escherichia coli* and *Bacillus subtilis* to silver and copper nanoparticles. Sci. Total Environ. 373:572-575.

Zhao, G.J., and S.E. Stevens. 1998. Multiple parameters for the comprehensive evaluation of the susceptibility of *Escherichia coli* to the silver ion. Biometals. 11:27-32.

Table 5.1. Denitrification kinetics of native soil bacteria in an anaerobic environment.

Condition	Rep.*	N	*k* values‡	*k* t test	Average *k* value‡	Diff. from ctrl: t test	R^2
Ctrl	A	5	1.794 (0.269)	0.0023†	1.486 (0.289)	n/a	0.937
	B	5	1.444 (0.302)	0.0173†			0.884
	C	6	1.220 (0.125)	0.0006†			0.960
Ag^+_1	A	7	0.761 (0.234)	0.0226†	0.748 (0.019)	0.042†	0.679
	B	9	0.735 (0.130)	0.0008†			0.819
Ag^+_10	**A**	8	0.709 (0.088)	0.0002†	0.881 (0.244)	0.095†	0.915
	B	6	1.053 (0.176)	0.0039†			0.899
uAg50_1	A	5	1.473 (0.268)	0.0119†	1.517 (0.062)	0.897	0.909
	B	5	1.561 (0.238)	0.0072†			0.935
uAg50_10	A	6	1.325 (0.173)	0.0016†	1.309 (0.023)	0.472	0.936
	B	6	1.293 (0.164)	0.0014†			0.940
uAg50_100	**A**	7	0.983 (0.153)	0.0014†	0.939 (0.063)	0.087†	0.892
	B	7	0.894 (0.188)	0.0051†			0.818
pAg50_1	A	4	1.393 (0.558)	0.1298	1.182 (0.298)	0.337	0.757
	B	8	0.971 (0.152)	0.0007†			0.871
pAg50_10	**A**	6	1.364 (0.245)	0.0051†	1.136 (0.323)	0.292	0.886
	B	5	0.907 (0.219)	0.0256†			0.851
pAg50_100	**A**	5	1.032 (0.253)	0.0267†	1.027 (0.007)	0.123	0.847
	B	5	1.022 (0.257)	0.0284†			0.841
pAg15_1	A	4	1.235 (0.539)	0.1491	1.085 (0.212)	0.197	0.724
	B	6	0.935 (0.231)	0.0156†			0.803
pAg15_10	A	9	0.630 (0.103)	0.0005†	0.581 (0.069)	0.026†	0.842
	B	10	0.533 (0.053)	<0.0001†			0.927
pAg15_100	A	9	0.471 (0.058)	<0.0001†	0.425 (0.065)	0.017†	0.904
	B	14	0.380 (0.025)	<0.0001†			0.952
uAg35_1	A	5	1.415 (0.109)	0.0010†	1.380 (0.049)	0.659	0.976
	B	5	1.345 (0.103)	<0.0001†			0.977
uAg35_10	A	6	1.179 (0.135)	<0.0001†	1.288 (0.154)	0.453	0.937
	B	5	1.397 (0.058)	<0.0001†			0.993
uAg35_100	A	5	1.354 (0.356)	0.0319†	1.229 (0.177)	0.354	0.771
	B	5	1.104 (0.262)	0.0243†			0.808

*bolded value indicates repetition used for Figure 1; †indicates significant difference, $p < 0.1$; ‡values inside parentheses show one standard deviation

Kinetic rate (*k*) was calculated from linear fits of zero-order kinetic model, R^2 values correspond to goodness of fit for these models. Graphs of bolded repetitions can be found in Figure 5.1. Each item under the Condition column describes the type of silver (e.g. Ag^+, uAg50, etc.), followed by the concentration in mg/L (i.e. 1, 10, 100)

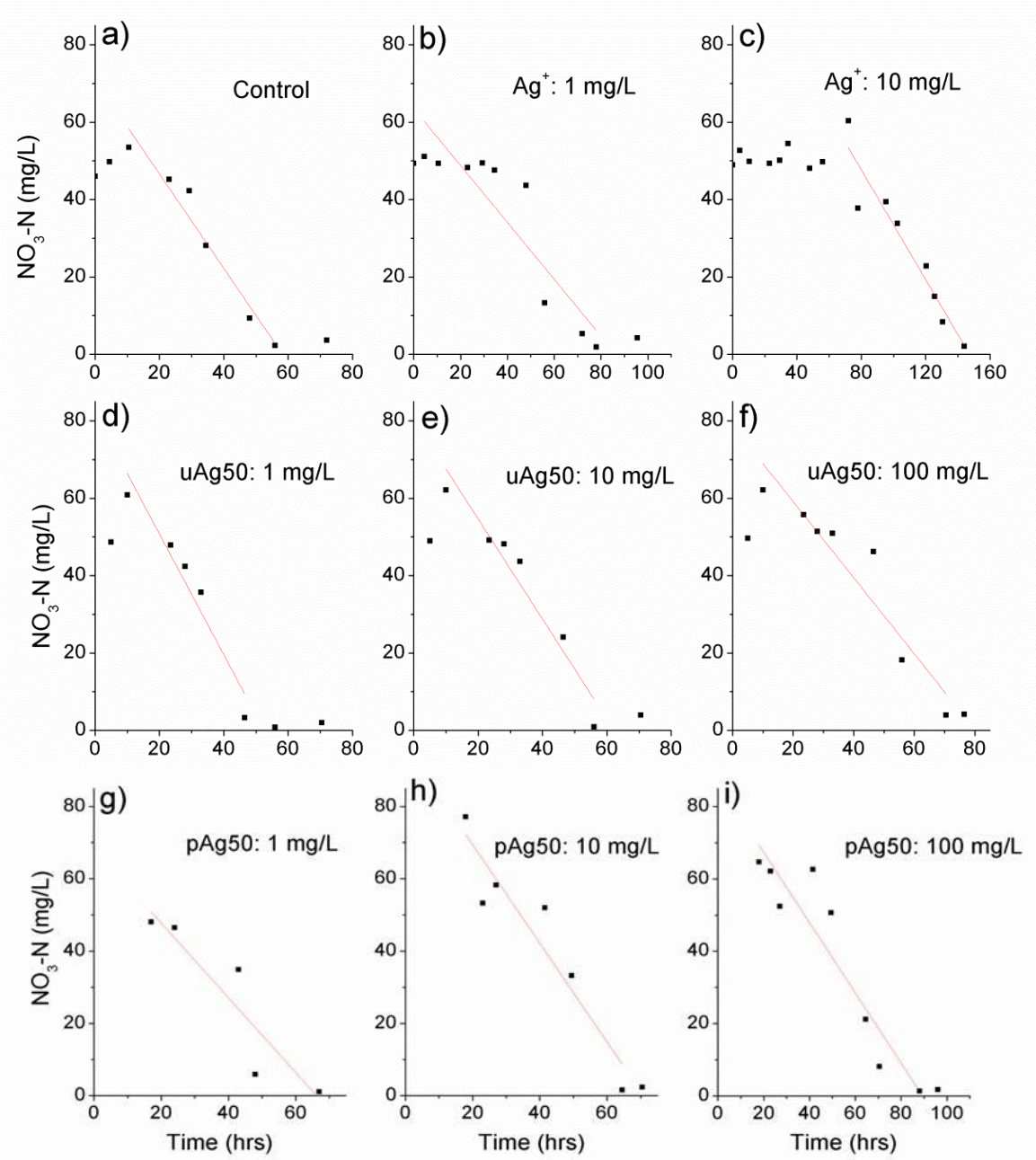

Figure 5.1. Denitrification kinetic data of native soil bacteria in an anaerobic environment. Each graph displays nitrate depletion over time for one batch per treatment condition. The line represents zero-order kinetic modeling, and corresponds to values listed in Table 1. Each graph represents a different reaction condition: a) control; b) Ag^+ at 1 mg/L; c) Ag^+ at 10 mg/L; d) through f) uAg50 at 1, 10, and 100 mg/L, respectively; g) through i) pAg50 at 1, 10, and 100 mg/L, respectively; j) through l) pAg15 at 1, 10, and 100 mg/L, respectively; and m) through o) uAg35 at 1, 10, and 100 mg/L, respectively.

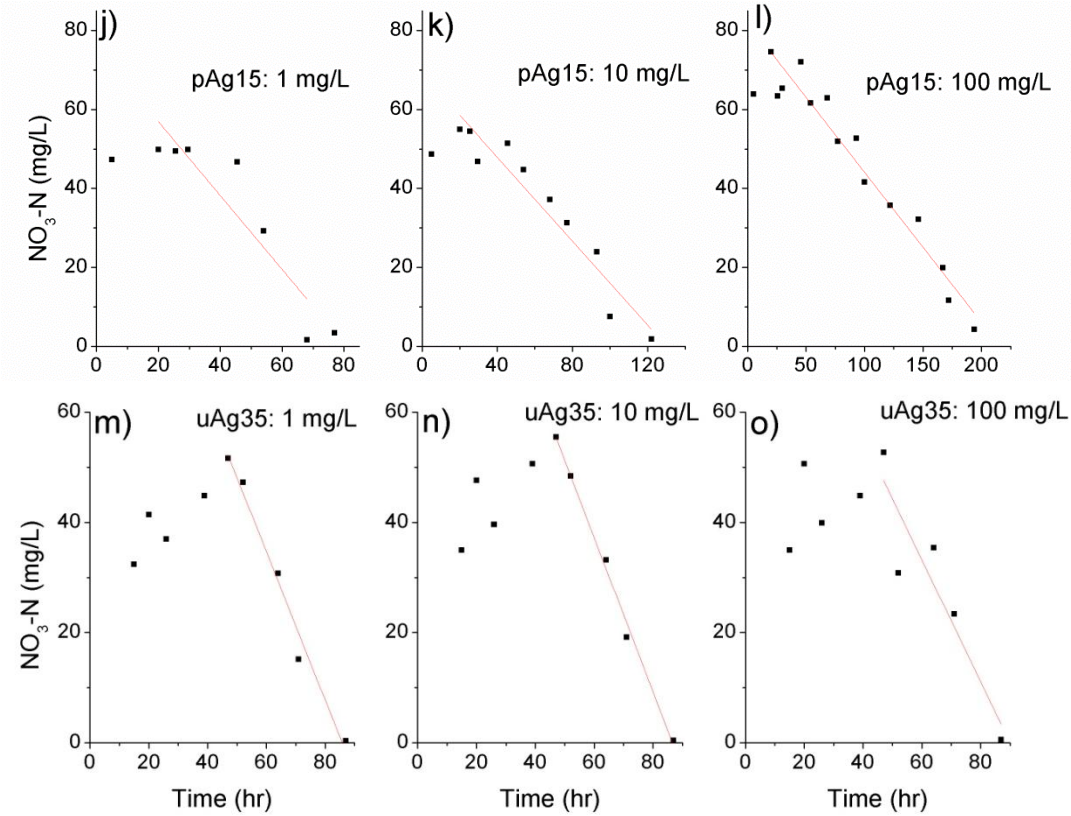

Figure 5.1. (continued)

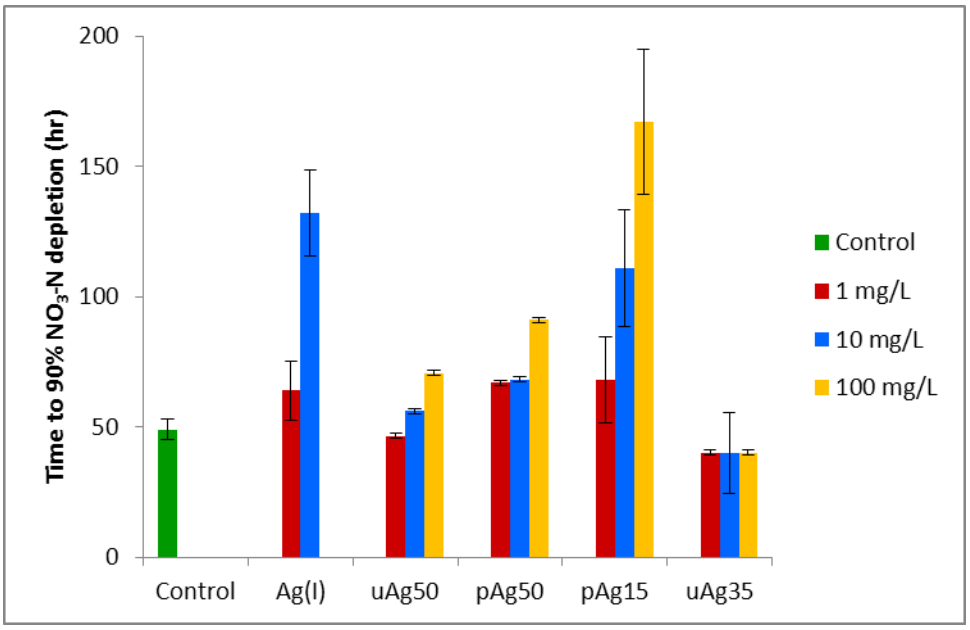

Figure 5.2. Histogram of denitrification activity in a Toccoa entisol. Time is measured from the point of maximum [nitrate] until [nitrate] decreases to <5 mg/L.

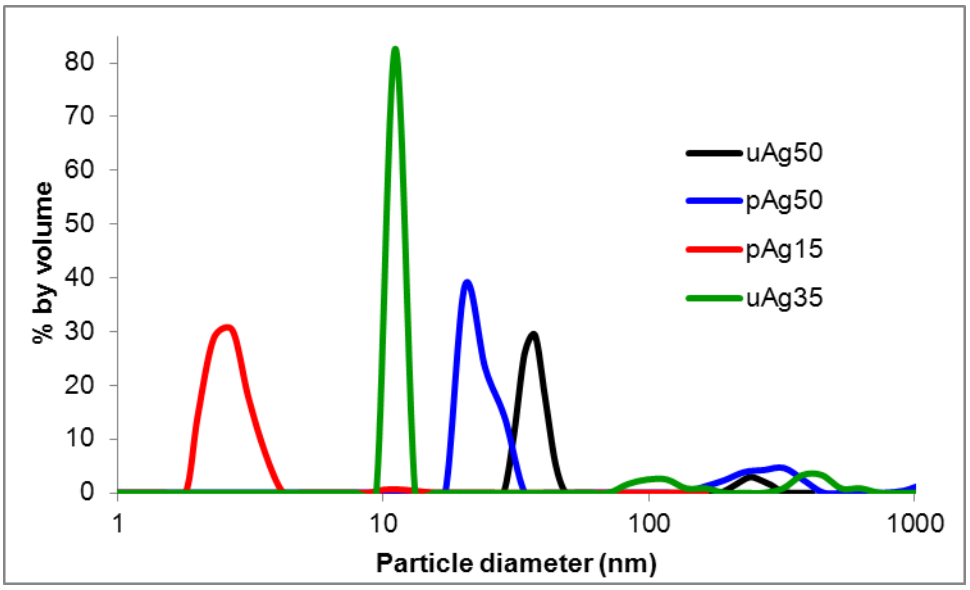

Figure 5.3. Particle diameter by volume collected through dynamic light scattering for each AgNP in 18 MΩ purified water at pH 4.5 to 5.

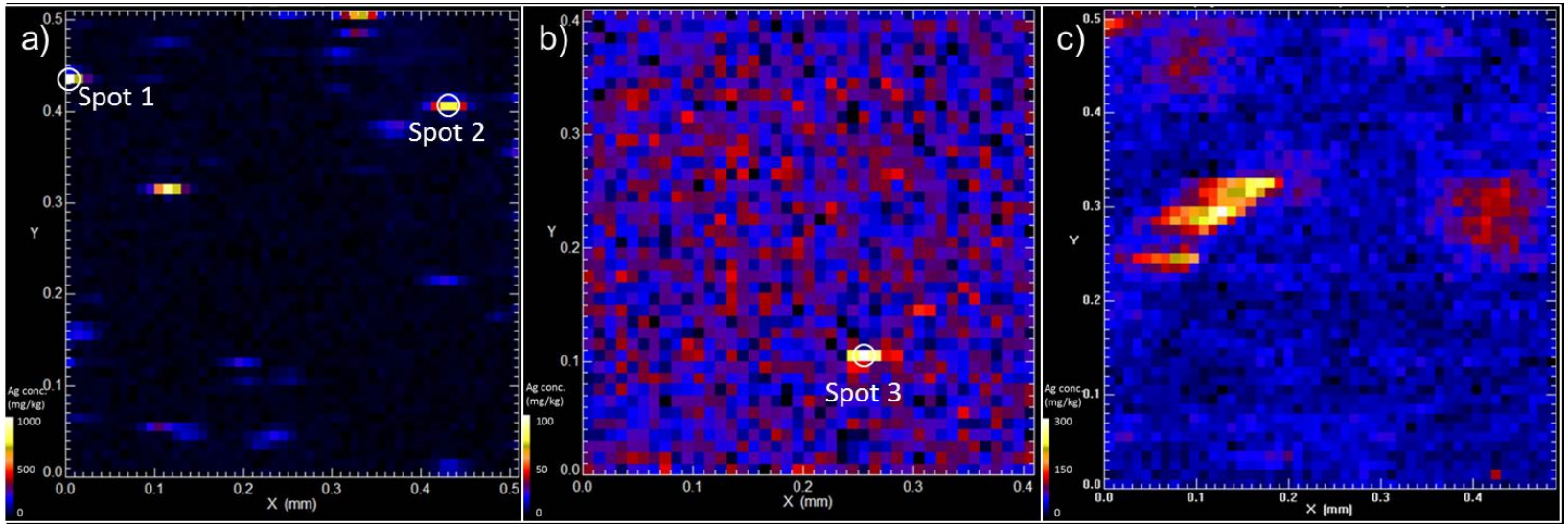

Figure 5.4. Microfocused(μ)-XRF maps of soil samples from the denitrification study. Soil samples were collected after the completion of nitrate depletion. a) uAg50, b) pAg50, and c) pAg15, all with $[Ag]_{total}$ = 100 mg L^{-1}.The color intensity of each pixel (see scale bar) represents the concentration of Ag (mg/kg) within that pixel. The conversion of fluorescence intensity to concentration is discussed in the method section. Spots 1-3 on the XRF maps indicate areas where μ-XANES were taken (displayed in Figure 5).

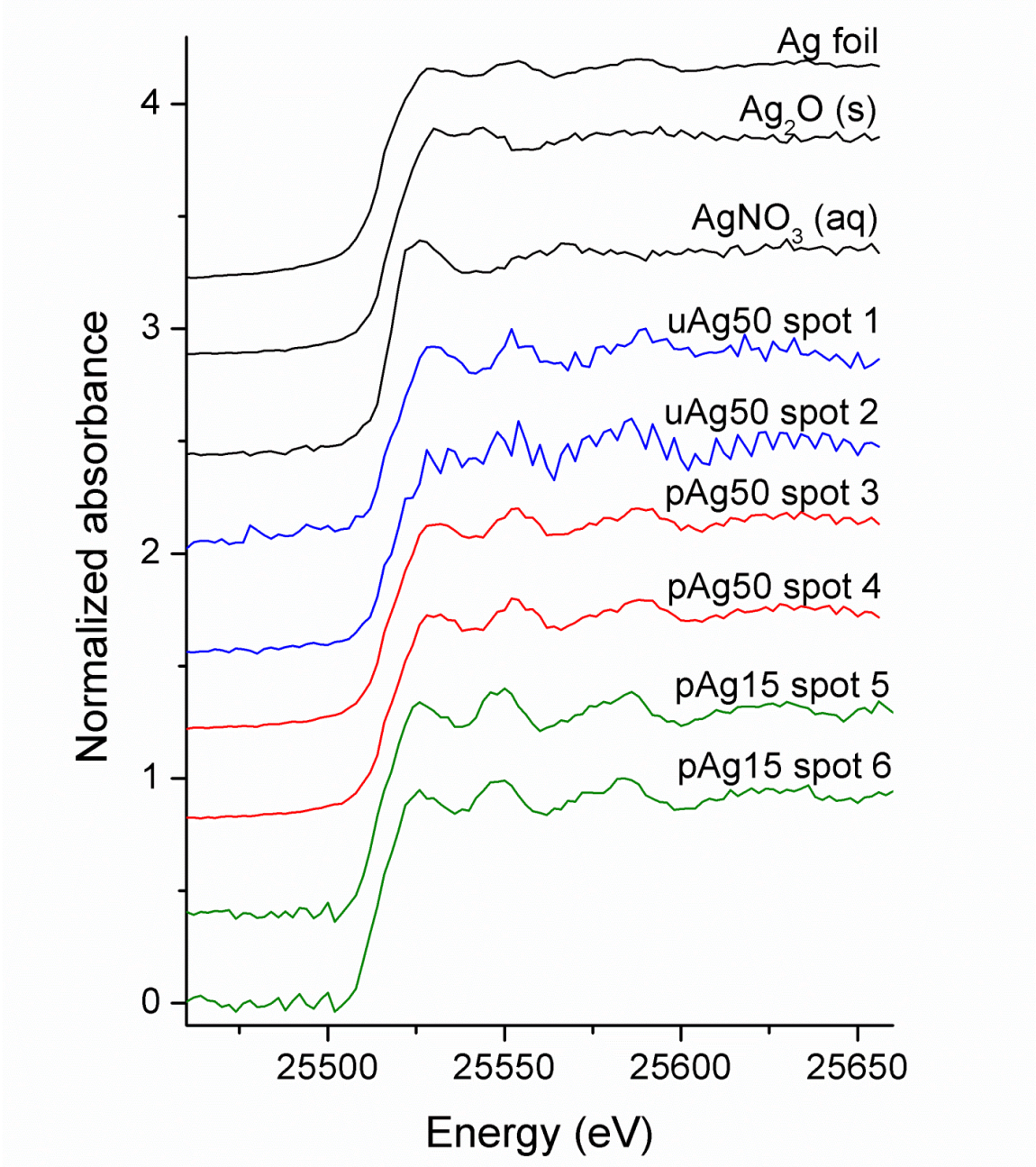

Figure 5.5. Normalized microfocused Ag K-edge XANES spectra of Ag reference compounds (Ag foil, $Ag_2O_{(s)}$, and 30 mM $AgNO_3$ solution) and selected spots from μ-XRF maps shown in Figure 4. uAg50 and pAg50 spots were taken from the points of highest [Ag] within each map (Figures 4a and 4b, respectively). Spectra at spots 4-6 were collected from different regions of the pAg50 and pAg15 thin sections (not shown).

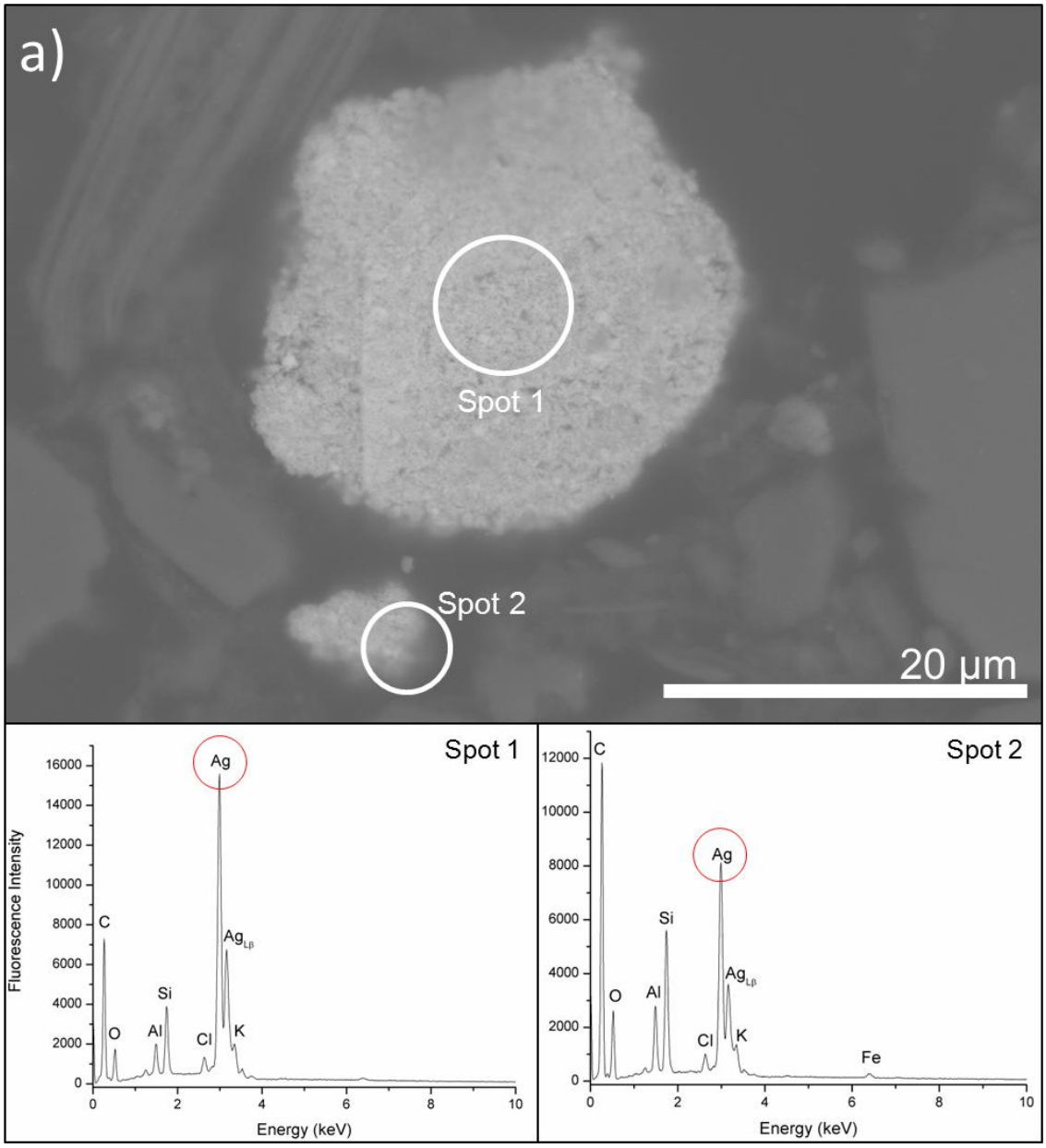

Figure 5.6. Scanning electron micrographs of a) uAg50, b) pAg50, and c) pAg15. Electron dispersive spectroscopy was conducted at two spots from each micrograph, displayed within each subfigure. Silver intensity is highlighted where measured.

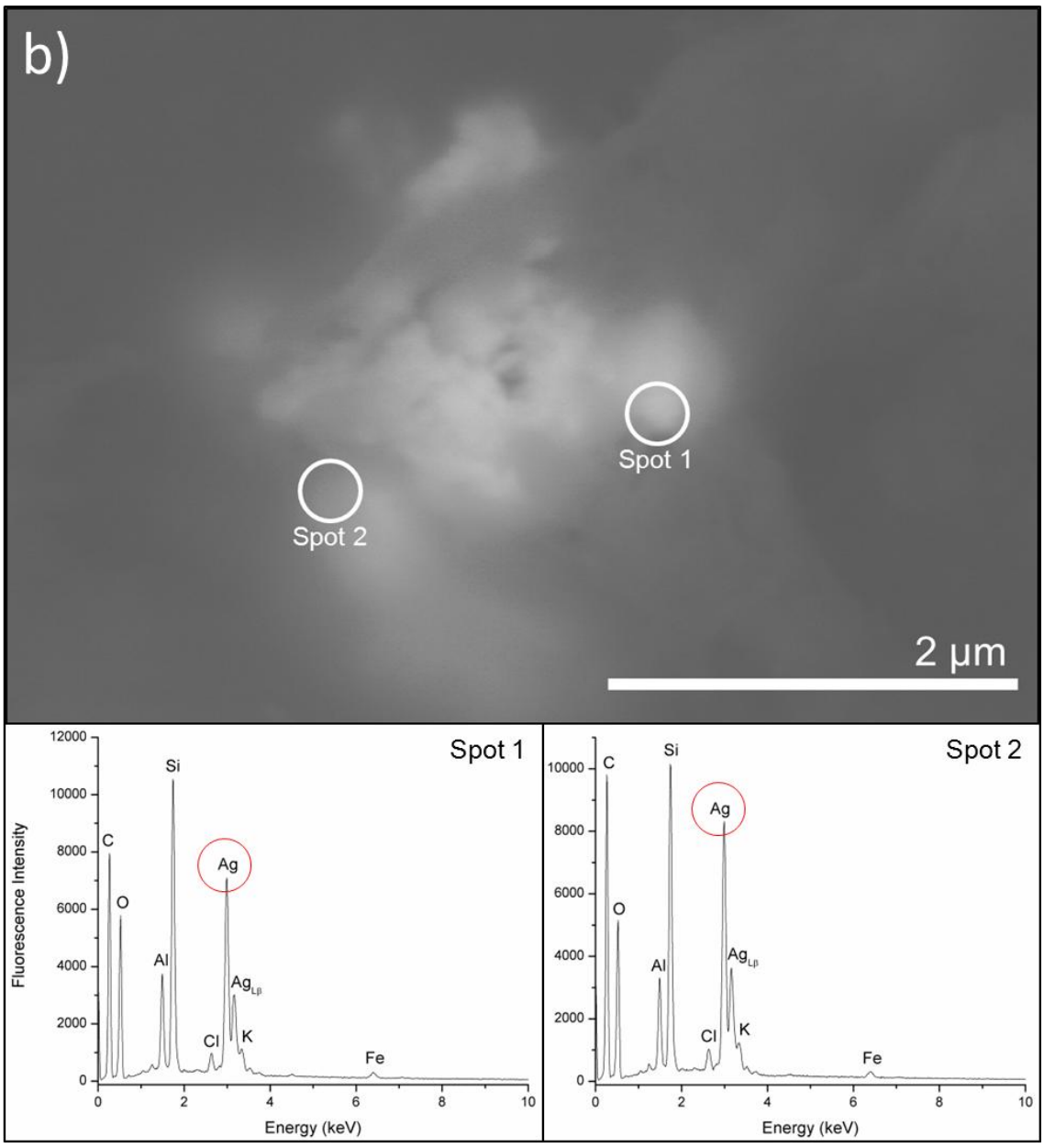

Figure 5.6. (continued)

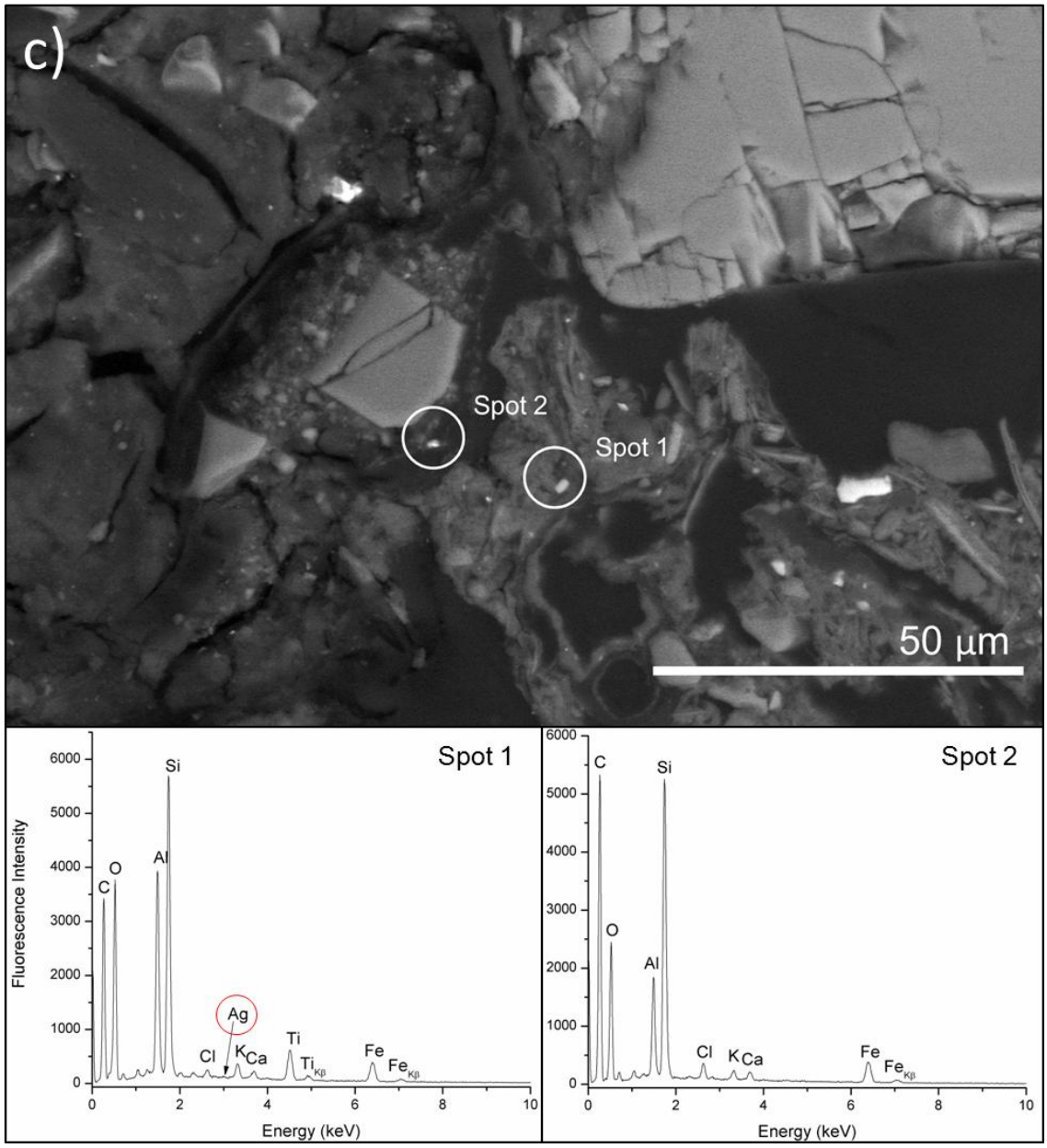

Figure 5.6. (continued)

CHAPTER SIX

CYSTEINE AFFECTED AQUEOUS-SILVER(I) AND –SILVER NANOPARTICLE SORPTION AT THE GOETHITE-WATER INTERFACE

6.1 Abstract

Thiol-based ligands are known to strongly complex soft acids, such as silver (Ag(I)), though little work has evaluated their influence on the Ag(I)/nanosilver (AgNP) partitioning on mineral surfaces. This work presents the macroscopic behavior of cysteine (un)affected Ag(I)/AgNP sorption on goethite surfaces at pH 3.5 to 8. Independently, both Ag(I) and AgNPs exhibited strong sorption onto goethite surfaces, as did cysteine. Likewise, Ag(I) showed a strong affinity for cysteine in aqueous systems, whereas the affinity of AgNPs for cysteine was notably lower than that of Ag(I). The presence of cysteine dramatically increased the sorption of Ag(I) in goethite, but it had little effect on the sorption of AgNPs. It is likely that the partitioning process of AgNPs in goethite is derived by hydrophobic interactions. The sorption of Ag(I) onto goethite does not largely alter zeta potential, nor is it affected by changes in ionic strength, suggesting the formation of inner-sphere surface species. Observed macroscopic behavior of Ag(I) and AgNPs with goethite in the presence of cysteine, along with well-documented specific sorption of carboxylic acid on goethite surfaces, lead to the conclusion that Ag(I)-cysteine aqueous complexes may undergo ligand exchange reactions on goethite surfaces to form cysteine-bridging inner-sphere ternary surface species and/or metal(Ag(I))-bridging inner-sphere ternary species.

6.2 Introduction

The reliable antimicrobial properties of AgNPs have increased the commercial popularity of their use in appliances and consumer products (e.g., Benn et al., 2010; Benn and Westerhoff, 2008). Because of the accelerated production and use of AgNPs, it is likely that the AgNP release to the environment will continue to increase, posing a threat to ecosystem health. In the last decade, most AgNP research has focused on toxicology. We are just beginning to understand how the toxicity, fate, and transport of AgNPs could be influenced by their chemical compositions, especially in aquatic-terrestrial environments. When coatings are added to bare AgNPs, their physicochemical properties change. These coating can either be added in the laboratory (commonly used coatings include citrate, polyvinylpyrrolidone, gum arabia, and more), or form as a result of chemical interactions in heterogeneous environments, especially through interaction with soil organic matter (SOM) and humic substances (HS) (Levard et al., 2012).

A few recent studies showed that AgNP interaction with soil HS might be important in the controlling the fate and toxicity, especially in terrestrial environments (e.g., Shoults-Wilson et al., 2011; VandeVoort et al., 2012) while others suggested the importance of sulfidation of silver nanoparticles in aquatic systems (e.g., Akaighe et al., 2011; Choi et al., 2009; Kim et al., 2010; Levard et al., 2011; Liu et al., 2011). It is known that manufactured Ag(0)NPs contain a Ag(+1) impurity (e.g., Xiu et al., 2011; Yin et al., 2002). This facilitates the (oxidative) dissolution of AgNPs under low temperature geochemical conditions, with varying results depending on time, temperature, size, coating, salt concentration (e.g., Chappell et al., 2011; Cornelis et al.,

2012; Elzey and Grassian, 2010; Griffitt et al., 2008; Ho et al., 2010; Kittler et al., 2010; Levard et al., 2011; Li et al., 2010; Liu and Hurt, 2010; Liu et al., 2011; Liu et al., 2010; Ma et al., 2012; Schnippering et al., 2008; VandeVoort and Arai, 2012; Yang et al., 2012).

One should also expect that AgNP defects/impurities of Ag(I) (soft acid) would enhance the complexation of soft basic ligands such as thiol functional groups in HS. The cysteine thiolate, which may bind one or two soft metal ions, is one of the most common metal-binding ligands of all amino acids (Lippard and Berg, 1994). In fact, according to thermodynamic stability constants, sulfide (either inorganic or as organic thiols) is among the most environmentally relevant ligands for Ag(I) (Bell and Kramer, 1999; Levard et al., 2012). The stability constant (log K_f) for Ag(I) and cysteine is 11.9, which makes it an extremely favorable ligand, even more so than dimethyl sulfide (log K_f = 3.7), another common form of sulfide in environmental systems (Bell and Kramer, 1999).

Humic substances in soils and water may largely affect the fate and transport of AgNPs in soils: 1) they may become less aggregated, and/or 2) the bond with HS may retard the dissolution of AgNPs. Humic acids prevented the aggregation of uncapped and capped (polyvinylpyrrolidone and gum Arabic) AgNPs (Croteau et al., 2011; Cumberland and Lead, 2009; Lin et al., 2012). It has been recently reported that natural organic matter/EDTA/cysteine effectively decreased the rate of oxidative dissolution of AgNPs and acanthite (β-Ag_2S) (Croteau et al., 2011; Jacobson et al., 2005a; Liu and Hurt, 2010).

While these studies provided fundamental knowledge in environmental geochemistry of HS-reacted AgNPs, it is not clear how dissolved HS influence the

partitioning of AgNPs in soils and sediments. In this study, we hypothesized the partitioning of AgNPs on variable charge mineral surfaces can be influenced by dissolved HS. Considering the HA/SB theory, it is likely that Ag(I) impurity in AgNPs will be chelated with thiol ligands (e.g., cysteine) in HS, resulting in the retardation or facilitated AgNP partitioning. The objective of this study is to understand the effect of cysteine on Ag(I)(aq) and AgNP (48 nm) sorption by an iron oxyhydroxide, goethite. Goethite was chosen because of its common occurrence in the low-temperature geochemical environment (Schwertmann and Cornell, 1991). Using experimental geochemistry, we investigated the affinity of AgNPs in goethite in the presence of cysteine, and changes in physicochemical properties of AgNPs using dynamic light scattering (DLS) and zeta potential measurements.

6.3 Materials and Methods

A manufactured AgNP (48 nm, uncoated) was chosen for this study because of its chemical stability during the incubation study in soils (VandeVoort and Arai, 2012). This AgNP is referred to in previous chapters as uAg50, and its physicochecmial characteristics are described in Chapter 4, Table 4.1. All AgNP solutions were prepared fresh from powder on the day of each experiment, and sonified for 30 seconds prior to use. Total silver concentration in these solutions was verified via inductively-coupled plasma atomic emission spectroscopy (ICP-AES). Silver sulfate was used as a source of ionic silver (Alfa Aesar Premion, Ward Hill, Massachusetts). Silver nitrate could not be used in this instance due to an interference in the cysteine determination method.

Cysteine was obtained from Alfa Aesar, Heysham, Lancaster, UK. Goethite was synthesized according to the ferric nitrate based methods described by Schwertmann and Cornell (1991). All silver and cysteine solutions were prepared using degassed water. Goethite suspensions were dialyzed for two weeks and kept in suspension prior to the sorption experiments described below. Goethite surface area was analyzed using BET theory via nitrogen (N_2) adsorption at 77 K using a physisorption analyzer (ASAP 2010, Micrometrics, Norcross, Georgia).

6.3.1 Zeta Potential and Particle Size Distribution Analyses

Zeta potential and DLS measurements were conducted using a PALS zeta potential analyzer ver. 3.57, Brookhaven Instruments particle separation system (Brookhaven Instruments, Holtsville, New York). Zeta potential measurements were conducted on goethite with and without 0.1 mM Ag(I) at 0.003 M Na_2SO_4, and again at 0.01 M $NaNO_3$, to achieve an ionic strength of 0.01 M. Measurements were conducted at a goethite suspension density of 0.1 g/L. pH was adjusted to various levels between 3 and 8.5 using NaOH and/or H_2SO_4. The critical coagulation concentration (CCC), or the minimum electrolyte concentration required to destabilize the nanoparticle suspension, is a good measure of how efficiently particles will remain in solution. Humic acid has been shown to increase the CCC of AgNPs, while having little effect on hydrodynamic radius (Zhang et al., 2012).

6.3.2 Ionic Ag and AgNP cysteine complexation experiments

The effect of cysteine concentration on AgNP availability was tested by combining a 0.2 mM of AgNP (as total Ag) with 0.1 or 0.2 mM cysteine for 24 hr on an end-over-end shaker. The 24 hr reaction time was chosen because our preliminary experiment suggested negligible oxidation of cysteine. Each sample was kept at 0.01 M ionic strength, adjusted with Na_2SO_4. Sodium sulfate was chosen as the background electrolyte for this study due to the oxidative properties of nitrate (Zepp et al., 1987). The presence of strong oxidizing agents causes the formation of a disulfide bridge between adjacent cysteine molecules, creating cystine. The use of sulfate, along with a short reaction time (<24 hours), prevented cystine formation. Appropriate amounts of bicarbonate buffer were added to appropriate pH values between 4 and 7. After 24 hours, pH was measured for all samples. All [Ag(I)] analysis was performed using an ion specific electrode (ISE) (det. limit 0.0001 mM Ag(I)), calibrated daily when in use with standards ranging from 0.0001 to 0.2 mM Ag and a 0.01 M Na_2SO_4 background.

Cysteine analysis was performed following the Gaitonde method (Gaitonde, 1967). Samples or standards of 1 mL were combined with 1.6 mL acetic acid, 0.4 mL HCl, and 0.025 g ninhydrin powder (AMRESCO, Solon, Ohio) in a glass cuvette, and covered and reacted in a boiling water bath for 10 minutes to allow color formation (Gaitonde, 1967). All samples or standards were cooled immediately, after which 4.5 mL 95% ethanol was added. Absorbance was measured at 560 nm using a Spec20 spectrophotometer (Thermo Fischer Scientific, Waltham, Massachusetts). The cysteine

concentration ([cys]) detection limit was 0.001 mM. The procedure was repeated using 0.2mM [Ag(I)].

Silver nanoparticle samples were first centrifuged at 10 000 x *g* for 10 minutes on a Marathon 21K high speed centrifuge (Fischer Scientific, Inc., Pennsylvania) to allow all AgNPs >42 nm in diameter to settle out of solution, according to a modified version of Stokes' Law (Jackson, 1985). Following this procedure, the aliquot of all samples were analyzed for pH, [Ag(I)] and [cys] as described above. A 1 mL sub-sample of each aliquot was removed prior to these analyses, and combined with 7 M HNO_3 for at least five days to digest AgNPs (Özmetin et al., 2000). Following acidification, all [Ag_{Total}] was measured via ICP-AES.

6.3.3 Ionic Ag and AgNP adsorption experiments

Adsorption edge experiments onto goethite (suspension density: 6.94 g/L, $[Ag(I)]_T$: 0.2 mM, $[Ag]_T$: 0.2 mM for AgNP, ionic strength: 0.01 mol L^{-1} adjusted with Na_2SO_4) were conducted in the presence of 0, 0.1, and 0.2 mM cysteine under ambient conditions. Solutions were mixed in 50 mL Oak Ridge polycarbonate centrifuge tubes and placed on an end-over-end shaker for approximately 24 hr, after which pH was recorded in mineral suspensions. Ionic Ag samples were first spun for 10 min in a centrifuge at 10 000 x *g* to separate large particles, and then filtered at 0.2 μm Millex-GX filters (Millipore Corp., Bedford, Massachusetts) to remove all goethite particulates. Following filtration, [Ag(I)], and [cys] were measured in each filtrate solution as

described above. Total Ag concentration in the filtered sample was analyzed using ICP-AES after acidification.

A high-speed centrifugation technique was used for the AgNP samples to separate unreacted AgNPs in solution from goethite particles. Filtration was not used for any AgNP samples, due to the affinity of AgNPs for the carbon composing the filter paper. Using an adapted version of Stokes' law (Jackson, 1985), settling rate was calculated. The AgNP samples were spun at approx. 10,000 x *g* for 6 minutes causing goethite particles >0.1 μm to settle out of solution, while leaving AgNPs <60 nm (i.e., those not reacted with goethite) in solution. Samples of these aliquots were removed and acidified with 7 M HNO_3, followed by [Ag] analysis via ICP-AES. Solutions were then vortexed and centrifuged again at the same speed for ten minutes, to cause all AgNPs to be removed from solution. [Ag(I)] and [cys] were also measured in the AgNP systems.

6.4 Results and Discussion

6.4.1 Effects of Cysteine on Ag(I) Sorption in Goethite

Sorption of Ag(I) was pH dependent. The total sorption increased from ~40% to ~65%. with increasing pH from 3.6 to 8.2 (Figure 6.1a, black squares). The addition of both 0.1 mM and 0.2 mM cysteine greatly increased the sorption of Ag(I). In the Ag(I) condition, the addition of 0.1 mM cysteine caused >90% sorption of Ag(I) over all pH levels. At pH 6.4 and above, Ag(I) sorption reached >99% sorption onto goethite surfaces. When 0.2 mM cysteine was added, both Ag-free and $Ag(I)_{cys}(aq)$ were below the detection limit at all pH levels. Cysteine-enhanced soft acid sorption onto mineral

surfaces has also been reported by other researchers. The sorption of mercury(II) was increased in kaolinite with the addition of cysteine (Senevirathna et al., 2011). Cysteine was also shown to decrease the desorption of previously sorbed Hg(II) from soils, indicating a strong affinity of the cysteine-soft-acid complex at the mineral water interface (Senevirathna et al., 2011). After testing the aliquot of the Ag(I) experiments in our study for the presence $Ag(I)_{cys}(aq)$, it was found to be limited in the 0.1 mM cysteine condition (max. 8.8% of Ag_{init} at pH 5.14), and negligible in the 0.2 mM cysteine condition (max. 0.20% of Ag_{init} at pH 3.27). This highlights the very strong sorption of soft-metal-cysteine complexes to soil components.

While there are few studies that investigated Ag(I) sorption in soils and soil components, there are even fewer studying AgNP sorption in soils and soil components. Work conducted previously by this research group documented ion exchange reactions between Ag(I) and K(I) and Ca(II) on a Toccoa Entisol (mineralogy primarily kaolinite, goethite, and hydroxyl interlayer vermiculite), which was described in Chapters 4 and 5 of this text (VandeVoort and Arai, 2012). The work showed that Ag(I) favorably bound to soil surfaces more so than K(I), and even more so than Ca(II). Jacobson and coworkers (2005a) have shown a similar preference for soil surfaces by Ag(I), when they documented <25% reversibility in sorption during desorption studies. They also reported a greater amount of Ag(I) desorption from sandy soils than from either peaty-muck or clayey soils, which might be suggesting the importance of inorganic soil components, such as clay, as a Ag(I) sink in soils. A series of Ag(I) desorption experiments by Li and coworkers (2004) on iron oxides (including goethite), showed that different iron oxides

have different affinities for Ag(I). While goethite retained more Ag(I) with increased reaction time, the length of reaction time had no effect on ferrihydrite Ag(I) retention (Li et al., 2004). Previous work by our research group also found strong sorption of AgNPs onto soil surfaces, even under low SOM conditions, as shown in Chapters 4 and 5 of this text.

6.4.2 Effects of Cysteine on AgNP Sorption in Goethite

The sorption of AgNPs onto goethite was also tested in the presence of 0.1 and 0.2 mM cysteine (Figure 6.1b). AgNPs showed a much stronger affinity for goethite than Ag(I). Under the same [Ag_{init}], AgNPs exhibited nearly 100% sorption, whereas Ag(I) sorption was as high as ~60%. (Figure 6.1a and 6.1b, black squares). This held true across the entire pH range (3 to 8.5).

In the AgNP-goethite system, retention of AgNPs onto soil surfaces (>99% at all pH conditions) slightly increased with both cysteine additions to essentially 100%. For both cysteine concentrations, the concentration of Ag was below the detection limit on both the ISE and ICP-AES, which indicates that both Ag_{free} and $Ag(I)_{cys}(aq)$ might be associated with goethite surfaces. This finding, strong interactions of AgNPs on minerals surfaces, follows the trend shown in Chapter 4 of this text where AgNPs also exhibited stronger sorption onto Toccoa soil than did Ag(I). Strong AgNP partitioning processes in a variety of soils were also observed by Cornelis and coworkers (2012), who reported median retential (K_r) values for AgNPs at 589 L/kg.

6.4.3 Postulated Molecule Configurations of Cysteine-Ag(I) and –AgNP Complexes on Goethite Surfaces

In the previous section, a strong retention of Ag(I) and AgNP on goethite surface was observed in the presence of cysteine. The following molecular configurations were postulated prior to concluding our findings. Figures 6.2a and 6.2b show two ionic Ag-cysteine ternary surface complexes on goethite surfaces. Ligand-bridging Ag-cysteine ternary surface species are coordinated to an Fe-OH group via the carboxylic functional group of cysteine in Figure 6.2a. Silver ions could undergo specific sorption onto goethite surfaces, and cysteine can be coordinated on the surface-sorbed Ag(I) through its thiol functional group (Figure 6.2b). In the case of AgNP sorption, we suspect that AgNPs could develop hydrophobic interaction with the surface of goethite due to its insoluble property in aqueous systems (Figure 6.2c). A cysteine molecule(s) could be simply attached to the Ag(I) surface impurity via its thiol functional group (Figure 6.2d). The impurity of Ag(I) in this manufactured AgNP is estimated at ~4% of total Ag via X-ray absorption near edge structure spectroscopy (XANES) analysis. If cysteine ligands can strongly bind to the surface of goethite through its carboxylic functional group, dangling thiol functional groups could be coordinated with the Ag(I) surface impurity of AgNPs (Figure 6.2e).

To elucidate the sorption mechanisms of Ag(I) and AgNP on goethite surfaces in the presence of cysteine, one must investigate the interaction between cysteine and Ag(I) or AgNPs in the absence of goethite. Complexation of cysteine ligands on these Ag components is discussed in the following sections.

6.4.4 Ag(I)(aq) and AgNP Interactions With Cysteine

The complexation of Ag(I) and cysteine was analyzed using known concentrations of Ag(I) and cysteine addition, and data collected from the Ag(I) ISE and the Gaitonde method of cysteine analysis. These chemical components are described in Table 6.1.

Figure 6.3 shows the molar ratio of chelated $Ag(I)_{cys}$ to $[Ag(I)]_{initial}$ in respective systems. When $[cys_{init}] > [Ag_{init}]$ (i.e., 0.73 mM Ag_{init} per 1 mM cys_{init}), thiol sites are prevalent compared to Ag(I) ions, however, when $[cys_{init}] < [Ag_{init}]$, thiol sites are rare compared to Ag(I) ions. When cys_{init} is increased from approximately 0.1 mM to 0.2 mM while Ag_{init} remains at constant 0.2 mM, the ratio of $[Ag(I)_{cys}]/[Ag_{init}]$ remains relatively constant at near 100% (range = 0.879 (0.2 mM cys, pH 3.83) to 0.991 (0.2 mM cys, pH 7.63)), which shows Ag(I) complexes with cysteine even when all of the preferential binding sites, i.e., the thiol groups, are occupied. A study by Andersson (1972) showed that when the pH is >7, a cysteine solution will complex an Ag(I) solution up to 1.5 times more concentrated by multiple Ag(I) binding on some cysteine molecules (Andersson, 1972). We observed a similar result, even at much lower pH values. At low cys_{init} (Ag_{init}/cys_{init} = 0.73), we observed >85% sorption at all levels from pH 3.90 to 6.16.

For these reasons, it is reasonable to assume that when $[Ag_{init}] < [cys_{init}]$, Ag(I) will preferentially bind to the thiol group on cysteine due to its favorable formation constant (Figure 6.2f). However, when excess $[cys_{init}]$ is available with respect to $[Ag_{init}]$, remaining Ag(I) ions may bind at less favorable sites. Binding may occur at the carboxylic group (Figure 6.2g), which is the only negatively charged site on cysteine

when the pH is between 2.1 and 8.3, as in these reaction conditions. Under both cysteine concentrations, it is clear that Ag(I) has a very high affinity for cysteine, which is consistent with many reports in the literature (e.g., Bell et al., 1997; Jacobson et al., 2005b; Liau et al., 1997; Shen et al., 2010). In addition, it has been shown that Ag(I) can form a repeating chain-like polymer with the thiol group of cysteine amino acids (Shen et al., 2010), which further supports our theory of non-linear Ag(I)-cys aqueous complexation. In general, as pH increases, cysteine and other HS binding with Ag(I) and other soft acids (such as Cu(II)), increases (VandeVoort and Arai, 2012; Xia et al., 1997). We have found this to be the case in these experiments, as the proportion of Ag made up of $Ag(I)_{cys}$ tended to increase with pH. This was especially true in the case of 0.2 mM Ag(I) reacted with 0.2 mM cys (Figure 6.3a).

Complexation of AgNPs with cysteine was also analyzed. All components in this system are defined in Table 6.2. AgNPs add a new level complexity to our system, due to the fact that they are primarily composed of Ag(0), but are known to have Ag(I) impurities, and to easily oxidize at the surface (Liu and Hurt, 2010; Liu et al., 2010; Lok et al., 2007). Using data previously collected for Chapter 4, the degree of Ag(I) impurity was assessed using microfocused (μ)- XANES. Table 4.3 from Chapter 4 of this text shows a linear combination fit of reference spectra for 30 day aged AgNPs under both oxidizing and reducing conditions. The same linear combination fit was performed on un-aged AgNPs using reference compounds. The test found that the Ag K-edge μ-XANES spectrum of un-aged uAg50 was composed of 96.0% Ag(0) foil and 4.0% Ag(I)Cl. This level of Ag(I) impurity from the AgNPs was accounted for by the $Ag(I)_{NP}$ component

listed in Table 6.2. Assuming that the impurity Ag(I) is present at the outer core of NP, one can estimate the Ag(I) complexation with cysteine.

At two different levels of cys_{init}, the complexation with AgNPs was quite varied. Figure 6.3b shows the ratio of $[Ag(I)_{cys}]/[Ag(I)_{NP}]$ between pH 4 and pH 7. When cys_{init} is low compared to Ag_{init} (i.e., $Ag_{int}/cys_{int} = 2.06$), the concentration of $Ag(I)_{cys}$ is at its highest, especially below pH 5, which could occur for several reasons. First, it has been shown that AgNP dissolution increases under acidic conditions (Liu and Hurt, 2010). While no Ag_{free} was detectable in any samples of the AgNP-cysteine complexation reactions, it is reasonably assumed that any Ag_{free} released from the AgNPs will be immediately complexed with cysteine, due to the high affinity observed in the Ag(I)-cysteine reactions. At low pH levels, the availability of Ag(I) may be the limiting factor for $Ag(I)_{cys}$ formation. Second, the relative abundance of AgNP compared to cysteine may also be a factor. Cysteine is known to prevent the dissolution of Ag(0) (Jacobson et al., 2005b). When cysteine is relatively scarce, it will have the least effect on Ag(0) dissolution, optimizing conditions for Ag(I) release and $Ag(I)_{cys}$ formation.

When $[cys_{init}]$ is increased to approximately the molar equivalent of Ag_{init}, the ratio of $[Ag(I)\cdot cys]/[Ag(I)_{NP}]$ is quite low (<0.003) at all pH levels. Under this condition, the ratio of $[Ag(I)_{cys}]/[Ag(I)_{NP}]$ also increases very slightly with increasing pH. Above pH 5.5, $[cys_{init}]$ appears to have very little effect on $Ag(I)_{cys}$ formation. It is likely that the slow/negligible dissolution of AgNPs, at near neutral pH levels is the limiting factor for $Ag(I)_{cys}$ formation.

6.4.5 Effects of ionic strength on Ag(I) sorption at the goethite-water interface

Sorption of Ag(I) was not pH dependent. Sorption is near 3800 mg/kg at pH 3 to 8.5. Sorption of Ag(I) was not strongly affected by changes in [$NaNO_3$], indirectly suggesting that inner-sphere sorption of Ag(I) (Figure 6.2j). Effects of ionic strength (adjusted with $NaNO_3$) on Ag(I) sorption on goethite surfaces are shown in Figure 6.4. As reviewed in Chapter 1 of this text, background electrolyte concentration can affect sorption of cations in several ways. High ionic strength can cause competition for available soil surface sites. Since outer-sphere adsorption (nonspecific), relies on electrostatic interactions to operate, it is sensitive to this competition, and will, therefore, occur less often in soil solutions of high ionic strength (Hayes and Leckie, 1987). The strong sorption of cations, through inner-sphere interactions, is not at all sensitive to changes in ionic strength (Hayes and Leckie, 1987). Due to the differences in sensitivity of inner-sphere and outer-sphere complexes to high ionic strength, this can be used to determine the amount of inner- vs. outer-sphere complexes formed by specific anions (Hayes and Leckie, 1987). While the method is commonly used in distinguishing the adsorption mechanism of cation sorption in soil minerals, the data should be also carefully interpreted based on 1) ionic strength effects on the diffused double layer thickness, 2) pH effect on ionic strength, and 3) interactions of cations with anions from the background electrolyte. Increasing the ionic strength of the soils solution reduces the thickness of diffused double layer, providing an easier access for ions to approach the mineral-water interface. Ionic strength is subject to change with increasing pH. Since alkaline systems (pH > 7) generally contain high bicarbonate concentrations (>

millimolar), it is difficult to maintain constant ionic strength at pH >7. For this reason, ionic strength studies are best performed under mildly acidic to acidic conditions or in the absence of CO_2.

6.4.6 Zeta Potential measurements of goethite suspensions in the presence of Ag(I)

Zeta potential measurements are a useful microscopic approach for not only determining the isoelectric point (IEP) of pure components but also for obtaining information that can be used to indirectly distinguish bulk surface complexes at colloidal/water interfaces. Non-specific ion sorption of different electrolytes at the outside of the shear plane (i.e., formation of outer-sphere complexes via van der Waals forces as in Figure 6.2i) generally does not affect the IEP, but it could cause shifts in the value of electrophoretic mobility (EM) if present at high concentration (Hunter, 1981). The shear plane is at the outer edge of the inner part of the double layer, near the outer Helmholtz plane or the Stern layer, depending on the models to describe the interface (Hunter, 1981). Inner-sphere complexes (e.g., Figure 6.2j), however, can cause shifts in both zeta potential and IEP due to specific ion adsorption inside the shear plane (Hunter, 1981). In other words, cation inner-sphere adsorption does decrease the net negative charge on the surface. With this knowledge, one can indirectly distinguish the predominant surface complexes on pure colloidal materials using EM measurements.

The zeta potential of goethite with and without 0.1 mM Ag(I) was measured in sodium nitrate and sodium sulfate solutions at pH 3 to 8 (Figure 6.5). The zeta potential of goethite suspensions in the absence of Ag(I) decreased with increasing pH, which is

due to the deprotonation of surface sites. This experiment showed the IEP of goethite solution to be between 7.5 and 8. The addition of 0.1 mM Ag(I) had a small effect on the zeta potential, especially between pH 5 and 6.5, which is the only region of the pH scale that showed significant differences between the zeta potential of the 0 mM and 0.1 mM Ag(I) samples. It seems that Ag(I) causes the zeta potential to remain higher than expected in this range, indirectly suggesting the formation of inner-sphere sorption of Ag(I) on goethite surfaces, especially at pH 5 to 6.5 (Figure 6.2j).

6.4.7 Cysteine sorption on goethite in the presence of Ag(I) or AgNPs

Figure 6.6 shows the results of cysteine sorption onto goethite. The experiment was conducted with no silver, in the presence of 0.2 mM Ag(I), and 0.2 mM AgNP (results of silver uptake were discussed above in sections 5.4.1 and 5.4.2). Cysteine sorption on goethite was pH dependent. It increased with increasing pH up to 7. At this pH range (3 to 7), only the carboxylic functional group is deprotonated ($pKa_{carbox.}$ = 2.05, pKa_{amino} = 10.25), while the surface functional groups of goethite are protonated (IEP = 7.5 to 8). One should expect that the deprotonated carboxylic acid group is interacting with hydroxyl group of goethite surfaces, possibly forming inner-sphere surface species (Figure 6.2k). During the experimentation phase, it was consistently observed that pH would drift upwards widely after < 24 hr, especially in the range of pH 4 to 6. At these pH levels well below the IEP of goethite, there is a prevalence of protonated edge sites on the goethite structure. It is possible that the carboxylate of cysteine is displacing –OH from the goethite structure, causing pH to increase. For this

reason, data points between pH 4 and 6 are somewhat sparse in conditions with high cysteine concentrations. Several researchers reported the importance of carboxylic functional groups of organic acids during their sorption onto goethite surfaces (Filius et al., 2000; Lindegren et al., 2009). They reported that the formation of inner-sphere surface complexes via carboxylic functional group became more important with decreasing pH at the goethite-water interface, which agrees with our macroscopic observation of cysteine sorption on goethite surfaces.

While cysteine sorption in the presence of AgNPs was very similar to cysteine sorption in the absence of Ag, it increased dramatically after the addition of Ag(I). In the Ag(I) systems, therefore, the formation of $Ag(I)_{cys}$ ternary surface complex is likely on goethite surfaces. This may be achieved either through complexation of Ag(I) by both the thiol group of cysteine and a hydroxide site on the goethite structure (Figure 6.2b), or through sorption of the carboxylic group of cysteine onto iron in goethite (Figures 6.2a).

In the system with 0.2 mM AgNP, 0.2 mM cysteine, and goethite, results are quite different. Essentially ~100% of Ag sorbed onto goethite surfaces, while cysteine sorption appears unchanged from the 0 mM Ag curve. For this reason, the ligand bridging AgNP sorption (Figure 6.2e) is unlikely. Instead, we propose the attachment of cysteine on AgNPs that have hydrophobic interaction with goethite surfaces (Figure 6.2d). As stated above, it is well-documented that AgNPs have a high affinity for mineral surfaces. It is possible that the goethite is making AgNPs unavailable to cysteine interactions under the conditions we studied.

Cysteine and silver form strong attractions to one another, and these could likely help predict the fate of Ag(I) and AgNPs in natural systems. Cysteine is a major source of the S-based ligands of humic substances in the aquatic and terrestrial environments. Based on our research findings, one could expect retardation in the Ag(I) transport process in humic-rich terrestrial environment due to the formation of ternary species on variable charged mineral surfaces in soils and sediments. Because of the strong retention of Ag(I) as ternary surface species, cysteine also likely has an effect on the bioavailability of Ag(I) to organisms in natural environments. In a Ag(I) toxicity study, it was shown that complexation with cysteine dramatically decreased the toxicity of silver nitrate for some bacteria (Liau et al., 1997).

Strong interactions between AgNPs and goethite were also found. Interestingly, cysteine did not largely affect the partitioning of AgNPs on goethite surfaces, which might suggest that humic substances may not directly control the sorption of AgNPs. However, thiol-containing organic molecules are known to complex with AgNPs, enhancing aggregation and/or suppress the dissolution of AgNPs. Several studies reported that these humic-AgNP interactions alter the toxicity of AgNPs to bacteria and other organisms (e.g, Bae et al., 2011; Dasari and Hwang, 2010; Fabrega et al., 2009).

As we reviewed, geochemical research of silver has not been extensively investigated in the past. Our investigation should provide a foundation in the environmental chemistry of silver in its ionic and nanoparticulate forms. To better predict the fate and transport of silver in humic rich aquatic and terrestrial environments,

interactions of organic ligands and silver should to be further investigated under environmentally relevant conditions (e.g., water treatment plants and agricultural soils).

6.5 References

Akaighe, N., R.I. MacCuspie, D.A. Navarro, D.S. Aga, S. Banerjee, M. Sohn, and V.K. Sharma. 2011. Humic acid-induced silver nanoparticle formation under environmentally relevant conditions. Environ. Sci. Technol. 45:3895-3901.

Andersson, L.-O. 1972. Study of some silver-thiol complexes and polymers: Stoichiometry and optical effects. J. Polym. Sci. A-1 Polym. Chem. 10:1963-1973.

Bae, E., H.-J. Park, J. Yoon, Y. Kim, K. Choi, and J. Yi. 2011. Bacterial uptake of silver nanoparticles in the presence of humic acid and $AgNO_3$. Korean J. Chem. Eng. 28:267-271.

Bell, R.A., and J.R. Kramer. 1999. Structural chemistry and geochemistry of silver-sulfur compounds: Critical review. Environ. Toxicol. Chem. 18:9-22.

Bell, R.A., S. Bennet, J.F. Britten, and M. Hu. 1997. Silver complexes of environmental and related thiols: Structural studies, p. 13-18, *In* A. W. Andren and T. W. Bober, eds. The 5th International Conference Proceedings: Transport, Fate, and Effects of Silver in the Environment. University of Wisconsin System, Madison, Wisconsin, US.

Benn, T., B. Cavanagh, K. Hristovski, J.D. Posner, and P. Westerhoff. 2010. The release of nanosilver from consumer products used in the home. J. Environ. Qual. 39:1875-1882.

Benn, T.M., and P. Westerhoff. 2008. Nanoparticle silver released into water from commercially available sock fabrics. Environ. Sci. Technol. 42:4133-4139.

Chappell, M.A., L.F. Miller, A.J. George, B.A. Pettway, C.L. Price, B.E. Porter, A.J. Bednar, J.M. Seiter, A.J. Kennedy, and J.A. Steevens. 2011. Simultaneous dispersion-dissolution behavior of concentrated silver nanoparticle suspensions in the presence of model organic solutes. Chemosphere. 84:1108-1116.

Choi, O., T.E. Cleuenger, B.L. Deng, R.Y. Surampalli, L. Ross, and Z.Q. Hu. 2009. Role of sulfide and ligand strength in controlling nanosilver toxicity. Water Res. 43:1879-1886.

Cornelis, G., C.D.M. Thomas, M.J. McLaughlin, J.K. Kirby, D.G. Beak, and D. Chittleborough. 2012. Retention and dissolution of engineered silver nanoparticles in natural soils. Soil Sci. Soc. Am. J. 76:891-902.

Croteau, M.-N.l., S.K. Misra, S.N. Luoma, and E. Valsami-Jones. 2011. Silver bioaccumulation dynamics in a freshwater invertebrate after aqueous and dietary exposures to nanosized and ionic Ag. Environ. Sci. Technol. 45:6600-6607.

Cumberland, S.A., and J.R. Lead. 2009. Particle size distributions of silver nanoparticles at environmentally relevant conditions. J. Chromatogr. A. 1216:9099-9105.

Dasari, T.P., and H.-M. Hwang. 2010. The effect of humic acids on the cytotoxicity of silver nanoparticles to a natural aquatic bacterial assemblage. Sci. Total Environ. 408:5817-5823.

Elzey, S., and V.H. Grassian. 2010. Agglomeration, isolation and dissolution of commercially manufactured silver nanoparticles in aqueous environments. J. Nanopart. Res. 12:1945-1958.

Fabrega, J., S.R. Fawcett, J.C. Renshaw, and J.R. Lead. 2009. Silver nanoparticle impact on bacterial growth: Effect of pH, concentration, and organic matter. Environ. Sci. Technol. 43:7285-7290.

Filius, J.D., D.G. Lumsdon, J.C.L. Meeussen, T. Hiemstra, and W.H. Van Riemsdijk. 2000. Adsorption of fulvic acid on goethite. Geochim. Cosmochim. Acta. 64:51-60.

Gaitonde, M.K. 1967. A spectrophotometric method for the direct determination of cysteine in the presence of other naturally occurring amino acids. Biochem. J. 104:627-633.

Griffitt, R.J., J. Luo, J. Gao, J.C. Bonzongo, and D.S. Barber. 2008. Effects of particle composition and species on toxicity of metallic nanomaterials in aquatic organisms. Environ. Toxicol. Chem. 27:1972-1978.

Hayes, K.F., and J.O. Leckie. 1987. Modeling ionic strength effects on cation adsorption at hydrous oxide-solution interfaces. J. Colloid Interf. Sci. 115:564-572.

Ho, C.-M., S.K.-W. Yau, C.-N. Lok, M.-H. So, and C.-M. Che. 2010. Oxidative dissolution of silver nanoparticles by biologically relevant oxidants: A kinetic and mechanistic study. Chem. Asian J. 5:285-293.

Hunter, R.J. 1981. Zeta Potential in Colloid Science. Academic Press, London.

Jackson, M.L. 1985. Soil Chemical Analysis. 2nd ed. Parallel Press, Madison, Wisconsin, US.

Jacobson, A.R., S. Klitzke, M.B. McBride, P. Baveye, and T.S. Steenhuis. 2005a. The desorption of silver and thallium from soils in the presence of a chelating resin with thiol functional groups. Water Air Soil Pollut. 160:41-54.

Jacobson, A.R., C.E. Martinez, M. Spagnuolo, M.B. McBride, and P. Baveye. 2005b. Reduction of silver solubility by hurnic acid and thiol ligands during acanthite (β-Ag_2S) dissolution. Environ. Pollut. 135:1-9.

Kim, B., C.S. Park, M. Murayama, and M.F. Hochella. 2010. Discovery and characterization of silver sulfide nanoparticles in final sewage sludge products. Environ. Sci. Technol. 44:7509-7514.

Kittler, S., C. Greulich, J. Diendorf, M. Koller, and M. Epple. 2010. Toxicity of silver nanoparticles increases during storage because of slow dissolution under release of silver ions. Chem. Mater. 22:4548-4554.

Levard, C., E.M. Hotze, G.V. Lowry, and G.E. Brown. 2012. Environmental transformations of silver nanoparticles: Impact on stability and toxicity. Environ. Sci. Technol. 46:6900-6914.

Levard, C., B.C. Reinsch, F.M. Michel, C. Oumahi, G.V. Lowry, and G.E. Brown. 2011. Sulfidation processes of PVP-coated silver nanoparticles in aqueous solution: Impact on dissolution rate. Environ. Sci. Technol. 45:5260-5266.

Li, J., A.W. Rate, and R.J. Gilkes. 2004. Silver ion desorption kinetics from iron oxides and soil organic matter: Effect of adsorption period. Aust. J. Soil Res. 42:59-67.

Li, X., J.J. Lenhart, and H.W. Walker. 2010. Dissolution-accompanied aggregation kinetics of silver nanoparticles. Langmuir. 26:16690-16698.

Liau, S.Y., D.C. Read, W.J. Pugh, J.R. Furr, and A.D. Russell. 1997. Interaction of silver nitrate with readily identifiable groups: Relationship to the antibacterial action of silver ions. Lett. Appl. Microbiol. 25:279-283.

Lin, S., Y. Cheng, J. Liu, and M.R. Wiesner. 2012. Polymeric coatings on silver nanoparticles hinder autoaggregation but enhance attachment to uncoated surfaces. Langmuir. 28:4178-4186.

Lindegren, M., J.S. Loring, and P. Persson. 2009. Molecular structures of citrate and tricarballylate adsorbed on α-FeOOH particles in aqueous suspensions. Langmuir. 25:10639-10647.

Lippard, S.J., and J.M. Berg. 1994. Principles of Bioinorganic Chemistry. University Science Books, Mill Valley, California.

Liu, J.Y., and R.H. Hurt. 2010. Ion release kinetics and particle persistence in aqueous nano-silver colloids. Environ. Sci. Technol. 44:2169-2175.

Liu, J.Y., K.G. Pennell, and R.H. Hurt. 2011. Kinetics and mechanisms of nanosilver oxysulfidation. Environ. Sci. Technol. 45:7345-7353.

Liu, J.Y., D.A. Sonshine, S. Shervani, and R.H. Hurt. 2010. Controlled release of biologically active silver from nanosilver surfaces. ACS Nano. 4:6903-6913.

Lok, C.N., C.M. Ho, R. Chen, Q.Y. He, W.Y. Yu, H. Sun, P.K.H. Tam, J.F. Chiu, and C.M. Che. 2007. Silver nanoparticles: Partial oxidation and antibacterial activities. J. Biol. Inorg. Chem. 12:527-534.

Ma, R., C. Levard, S.M. Marinakos, Y.W. Cheng, J. Liu, F.M. Michel, G.E. Brown, and G.V. Lowry. 2012. Size-controlled dissolution of organic-coated silver nanoparticles. Environ. Sci. Technol. 46:752-759.

Özmetin, C., M. Copur, A. Yartasi, and M.M. Kocakerim. 2000. Kinetic investigation of reaction between metallic silver and nitric acid solutions. Chem. Eng. Technol. 23:707-711.

Schnippering, M., H.V. Powell, M.Q. Zhang, J.V. Macpherson, P.R. Unwin, M. Mazurenka, and S.R. Mackenzie. 2008. Surface assembly and redox dissolution of silver nanoparticles monitored by evanescent wave cavity ring-down spectroscopy. J. Phys. Chem. C. 112:15274-15280.

Schwertmann, U., and R.M. Cornell. 1991. Iron Oxides in the Laboratory. 2nd ed. Wiley, Weinheim, Germany.

Senevirathna, W.U., H. Zhang, and B.H. Gu. 2011. Effect of carboxylic and thiol ligands (oxalate, cysteine) on the kinetics of desorption of Hg(II) from kaolinite. Water Air Soil Pollut. 215:573-584.

Shen, J.-S., D.-H. Li, M.-B. Zhang, J. Zhou, H. Zhang, and Y.-B. Jiang. 2010. Metal–metal-interaction-facilitated coordination polymer as a sensing ensemble: A case study for cysteine sensing. Langmuir. 27:481-486.

Shoults-Wilson, W.A., B.C. Reinsch, O.V. Tsyusko, P.M. Bertsch, G.V. Lowry, and J.M. Unrine. 2011. Role of particle size and soil type in toxicity of silver nanoparticles to earthworms. Soil Sci. Soc. Am. J. 75:365-377.

VandeVoort, A.R., and Y. Arai. 2012. Environmental chemistry of silver in soils: Current and historic perspectives, p. 59, *In* D. L. Sparks, ed. Adv. Agron., Vol. 114. AGRON UK Academic Press, London.

VandeVoort, A.R., R. Tappero, A. Lanzirotti, and Y. Arai. 2012. Particle specific chemical fate of nanosilver in reducing soils. Environ. Sci. Technol. *in review*.

Xia, K., W. Bleam, and P.A. Helmke. 1997. Studies of the nature of Cu^{2+} and Pb^{2+} binding sites in soil humic substances using X-ray absorption spectroscopy. Geochim. Cosmochim. Acta. 61:2211-2221.

Xiu, Z.-M., J. Ma, and P.J.J. Alvarez. 2011. Differential effect of common ligands and molecular oxygen on antimicrobial activity of silver nanoparticles versus silver ions. Environ. Sci. Technol. 45:9003-9008.

Yang, X.Y., A.P. Gondikas, S.M. Marinakos, M. Auffan, J. Liu, H. Hsu-Kim, and J.N. Meyer. 2012. Mechanism of silver nanoparticle toxicity is dependent on dissolved silver and surface coating in *Caenorhabditis elegans*. Environ. Sci. Technol. 46:1119-1127.

Yin, Y., Z.-Y. Li, Z. Zhong, B. Gates, Y. Xia, and S. Venkateswaran. 2002. Synthesis and characterization of stable aqueous dispersions of silver nanoparticles through the Tollens process. J. Mater. Chem. 12:522-527.

Zepp, R.G., J. Hoigne, and H. Bader. 1987. Nitrate-induced photooxidation of trace organic chemicals in water. Environ. Sci. Technol. 21:443-450.

Zhang, H., J.A. Smith, and V. Oyanedel-Craver. 2012. The effect of natural water conditions on the anti-bacterial performance and stability of silver nanoparticles capped with different polymers. Water Res. 46:691-699.

Table 6.1. Chemical components and their abbreviations in the Ag(I)-cysteine complexation system.

Chemical component	Definition
Ag_{init}	Conc. Ag(I) added as Ag_2SO_4
cys_{init}	Conc. cysteine added
Ag_{free}	Ag(I) free in solution, measured by ISE
cys_{Gait}	Cysteine measured by Gaitonde method: $cys_{Gait} = cys_{free} + Ag\ I\ _{cys}$
$Ag(I)_{cys}$	Calculated from ISE value: $Ag\ I\ _{cys} = Ag_{init} - Ag_{free}$
cys_{free}	Calculated from Gaitonde: $cys_{free} = cys_{Gait} - Ag\ I\ _{cys}$

All concentrations are in mM.

Table 6.2. Chemical components and their abbreviations in the AgNP-cysteine complexation system.

Chemical component	Definition
Ag_{init}	Conc. AgNP added as sonified mixture, confirmed via ICP-AES
$Ag(I)_{NP}$	Ag(I) impurity in unaged AgNPs. Determined via XAS to be 4.0% of Ag_{init} $$Ag(I)_{NP} = Ag_{init} \times 0.04$$
cys_{init}	Conc. cysteine added
Ag_{free}	Ag(I) free in solution, detected by ISE (negligible in all instances)
cys_{Gait}	Cysteine meas. by Gaitonde method: $$cys_{Gait} = cys_{free} + Ag\ I_{\ cys}$$
cys_{AgNP}	Cysteine sorbed to AgNPs, calc. from Gaitonde: $$cys_{AgNP} = cys_{init} - cys_{Gait}$$
$Ag(I)_{cys}$	Measured via ICP-AES after centrifugation of AgNPs (due to neg. amounts of Ag(I) free from ISE meas.)
cys_{free}	Calculated from Gaitonde method: $$cys_{free} = cys_{Gait} - Ag\ I_{\ cys}$$
AgNP	Conc. Ag remaining as nanoparticle (not free in solution). Calculated from ICP value: $$AgNP = Ag_{init} - Ag\ I_{\ cys}$$

All concentrations are in mM.

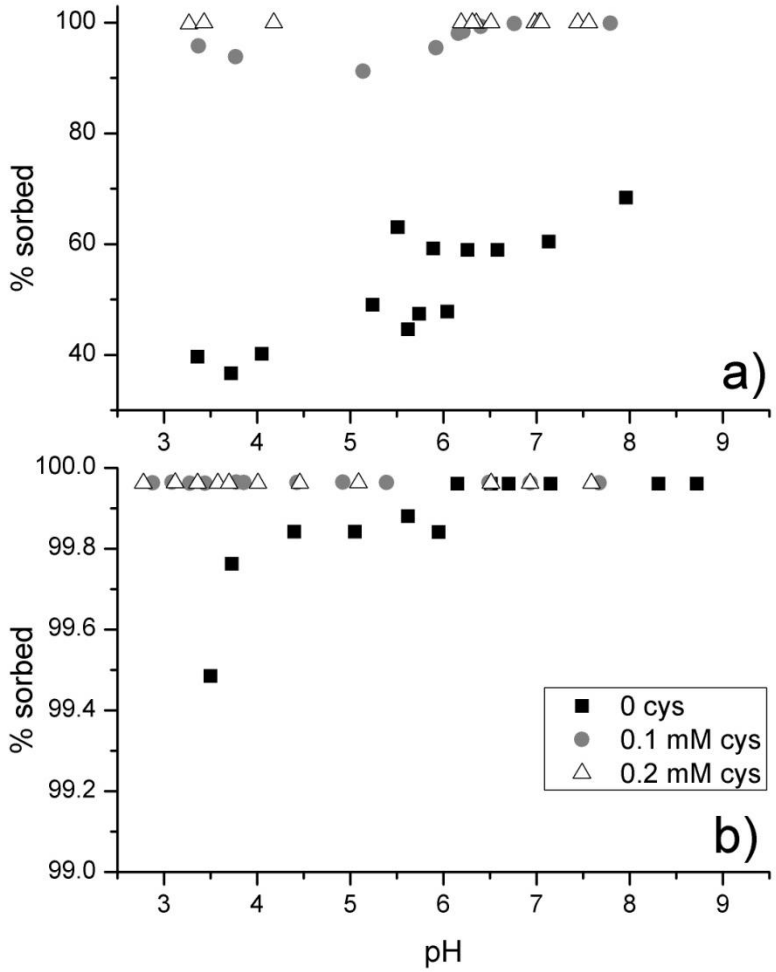

Figure 6.1. pH-dependent sorption of silver(I) (a) or AgNP (b) in goethite as a function of cysteine concentration (0, 0.1, or 0.2 mM). All experiments were conducted in 0.003 M Na_2SO_4.

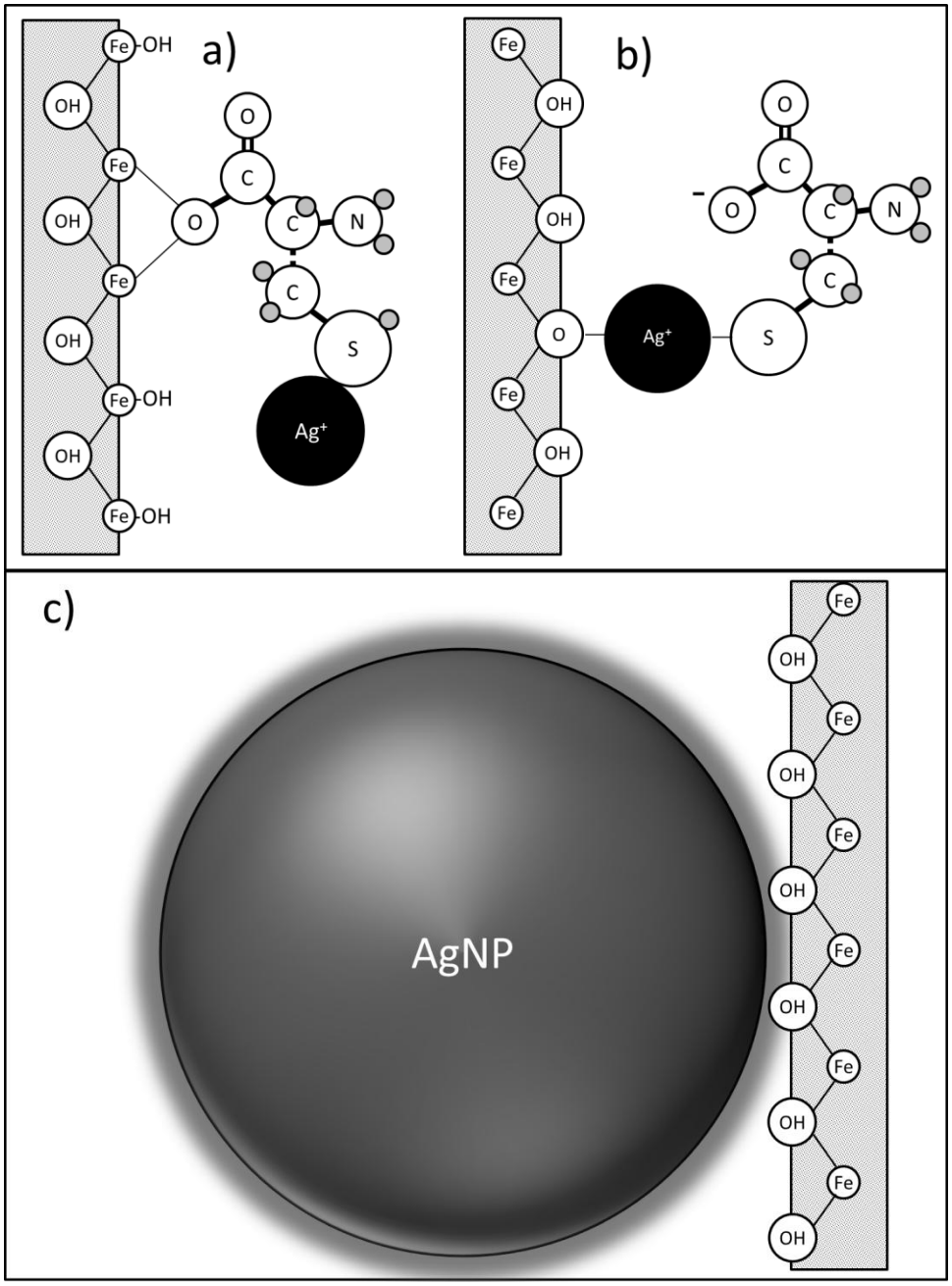

Figure 6.2. Ball and stick figures of potential molecular configurations of silver (Ag(I) and AgNPs) aqueous and surface complexes in this study: a) ligand (cysteine) bridging inner-sphere ternary surface complex of Ag(I) on goethite surfaces and b) metal (Ag(I)) bridging inner-sphere ternary surface complex of cysteine on goethite surfaces; c) hydrophobic interaction of silver nanoparticles (AgNP) on goethite surfaces.

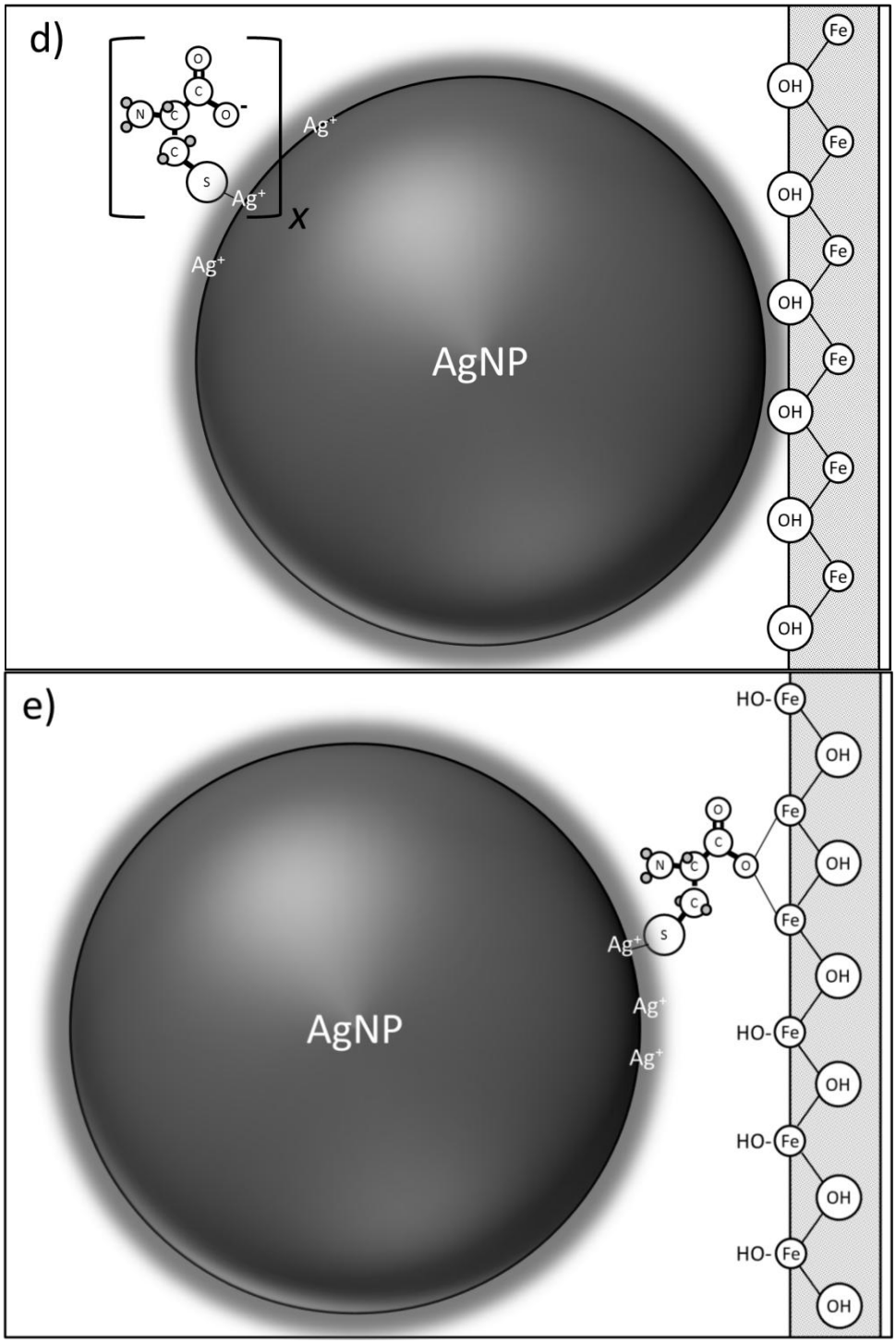

Figure 6.2. (continued) d) Cysteine sorbed AgNPs attached to goethite surfaces via hydrophobic interaction and e) ligand (cysteine) bridging AgNP sorption on goethite surfaces.

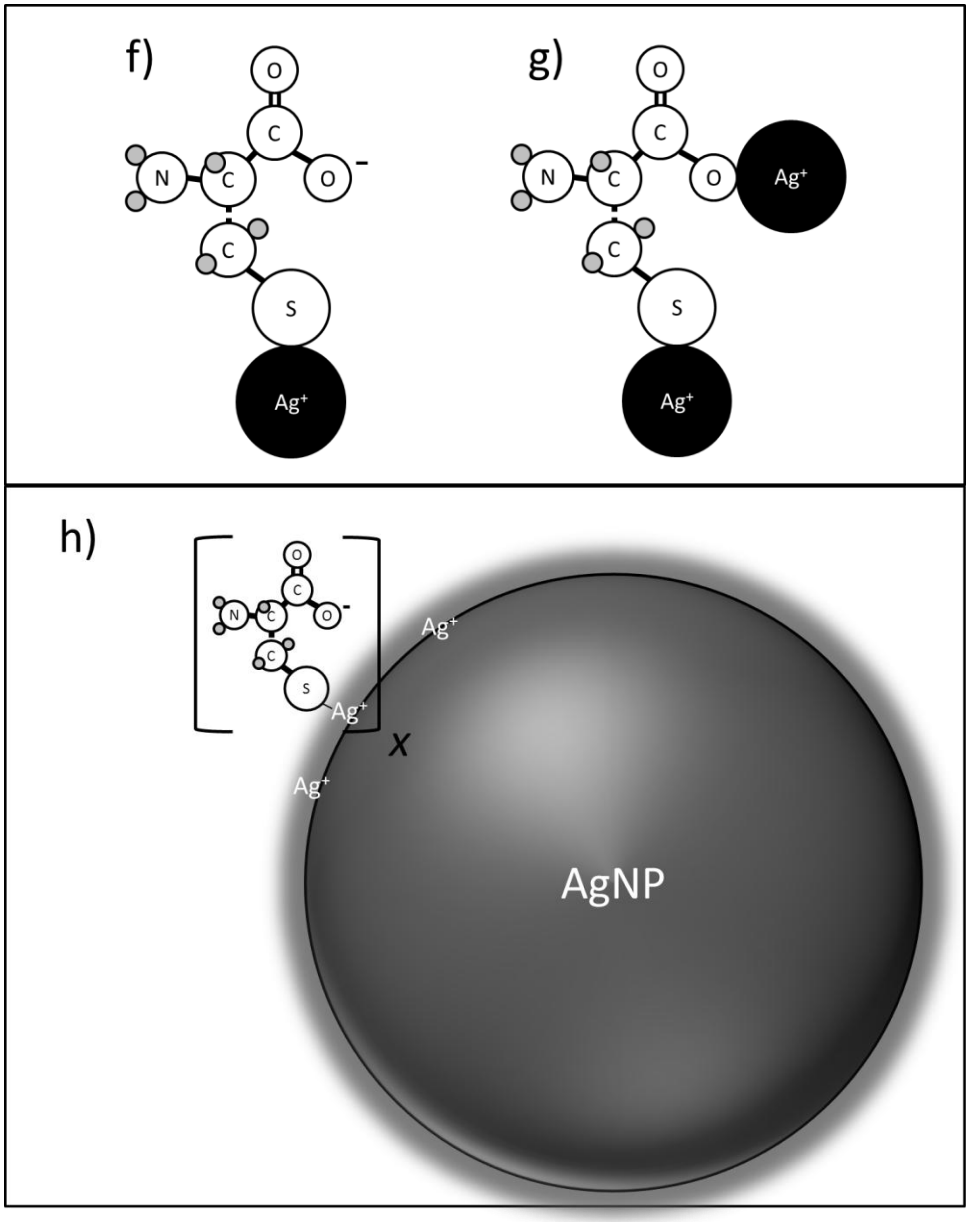

Figure 6.2. (continued) f) Ag(I)-cysteine aqueous complex via thiol functional group and g) Ag(I)-cysteine aqueous complex via carboxylic and thiol functional group; h) aqueous AgNP-cysteine complex via thiol functional group;

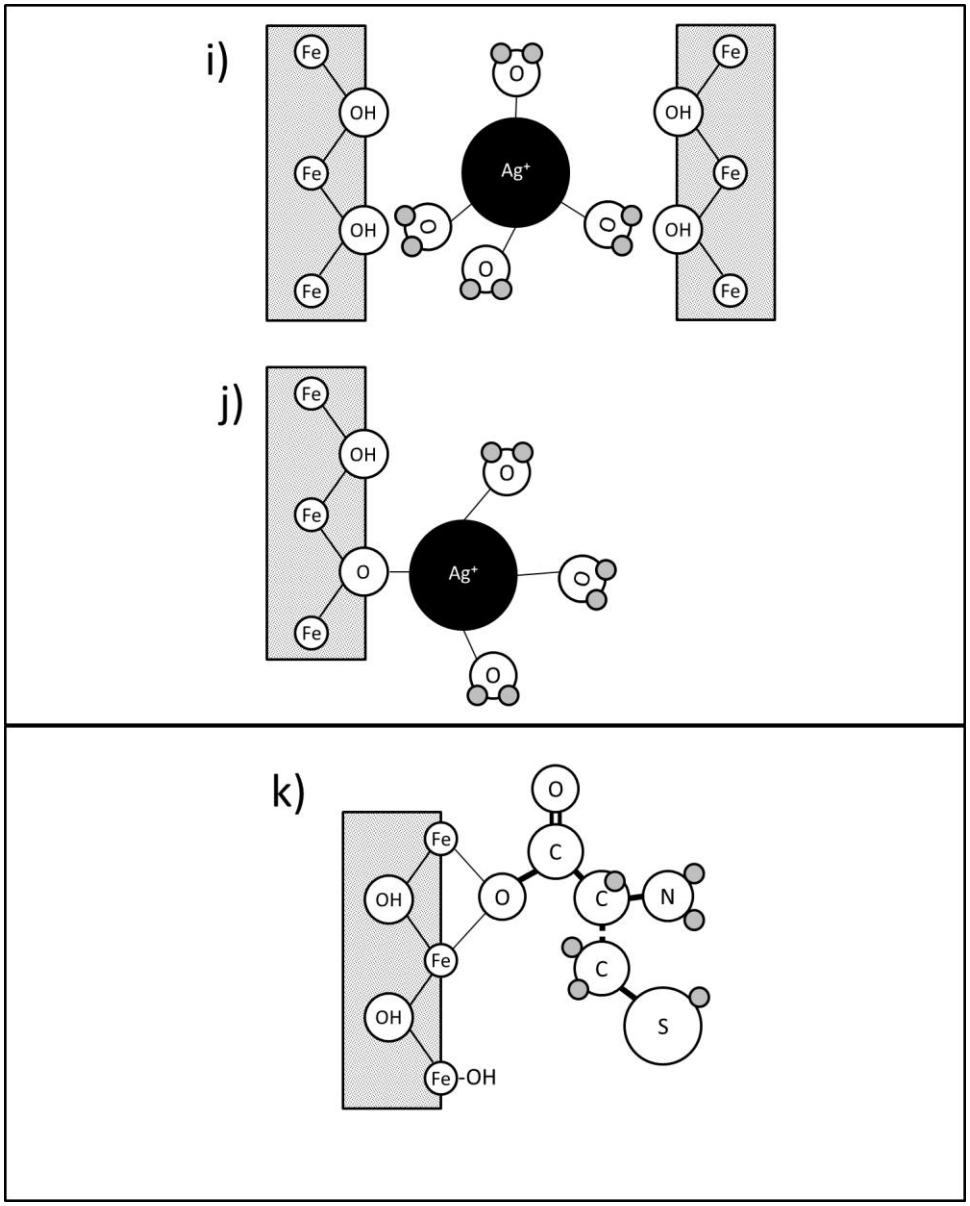

Figure 6.2. (continued) i) outer-sphere surface complex of Ag(I) on goethite surfaces; j) inner-sphere surface complex of Ag(I) on goethite surfaces; and k) inner-sphere surface complex of cysteine on goethite surfaces.

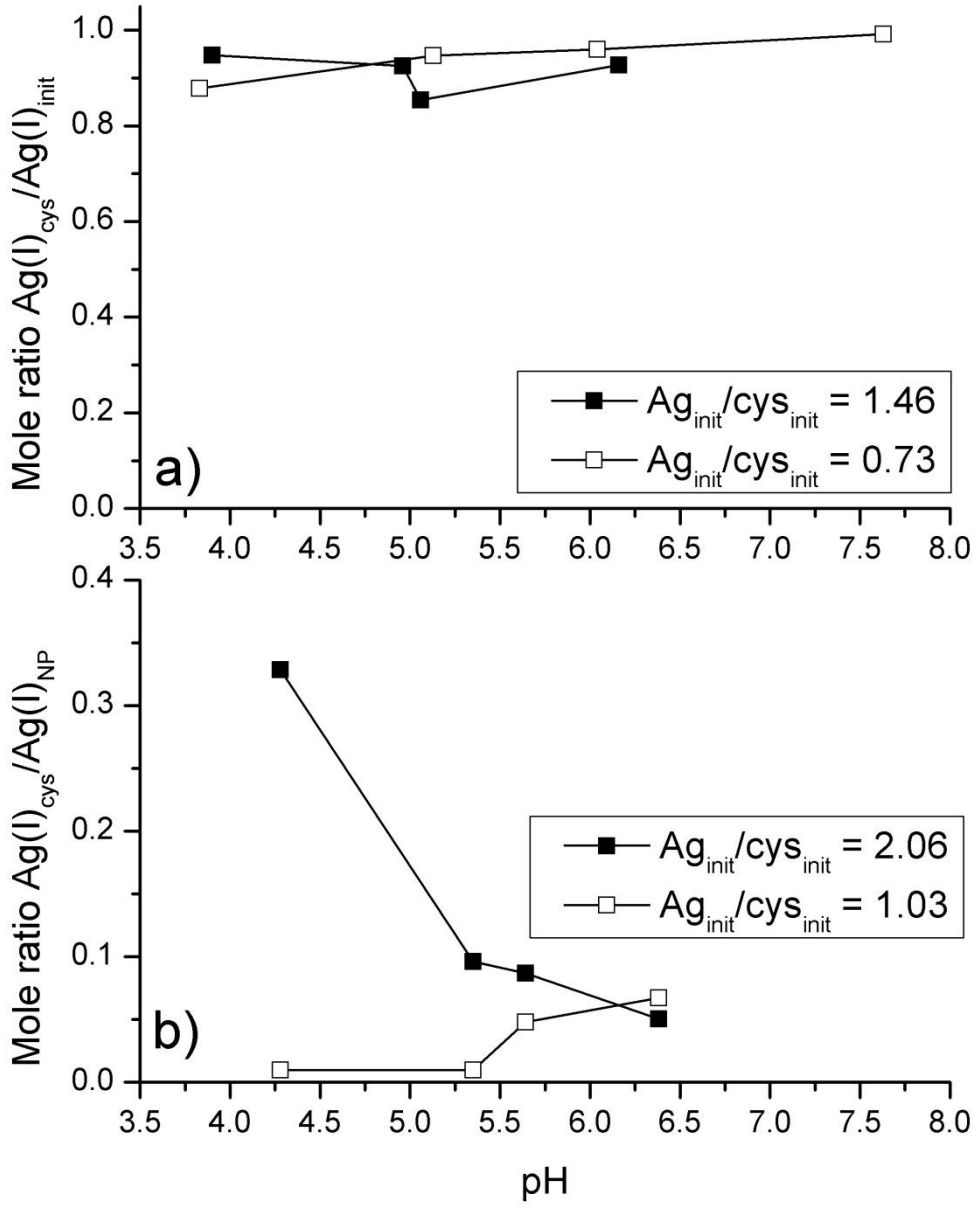

Figure 6.3. Molar ratio of silver(I)-cysteine complexes ($Ag(I)_{cys}$) to available Ag(I) across pH in a) Ag(I)-cysteine complexation experiment, and b) AgNP-cysteine complexation experiment. Available Ag(I) refers to a) initial Ag(I) added as Ag_2SO_4 and b) Ag(I) surface impurity of AgNPs.

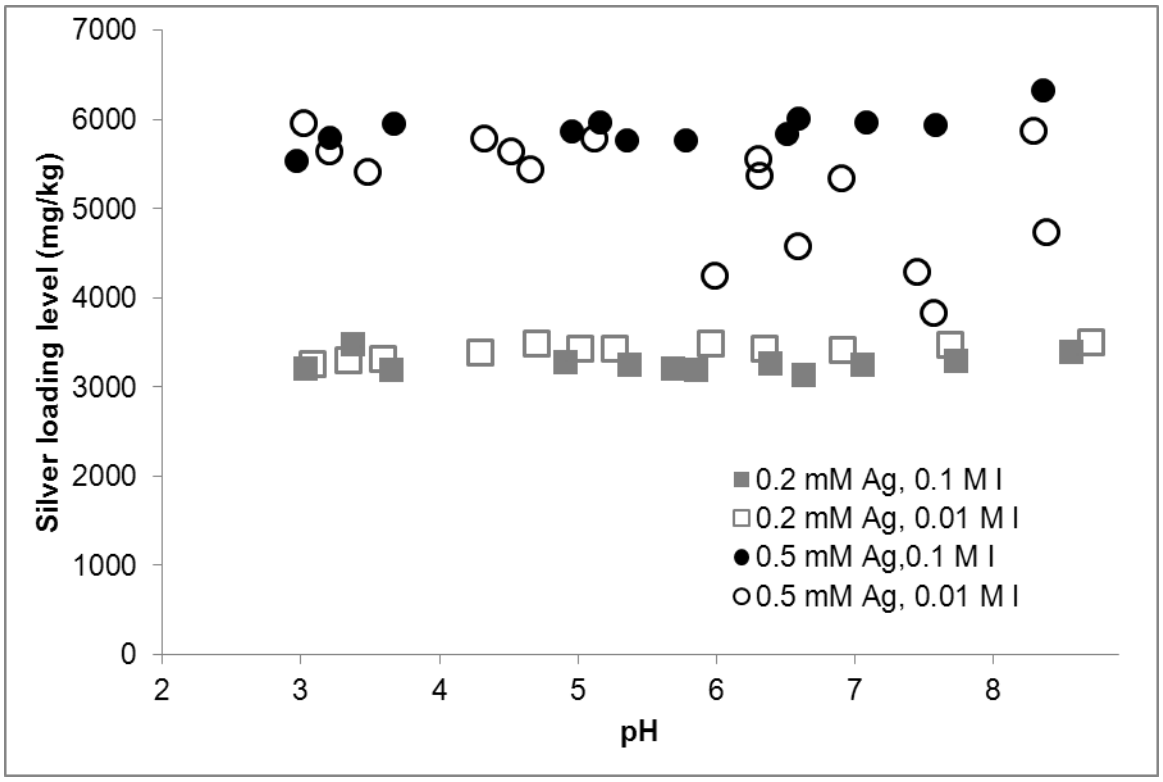

Figure 6.4. Ionic strength (0.1 M $NaNO_3$ or 0.01 M $NaNO_3$) effect on silver(I) sorption onto goethite surfaces at Ag(I) = 0.2 mM or 0.5 mM.

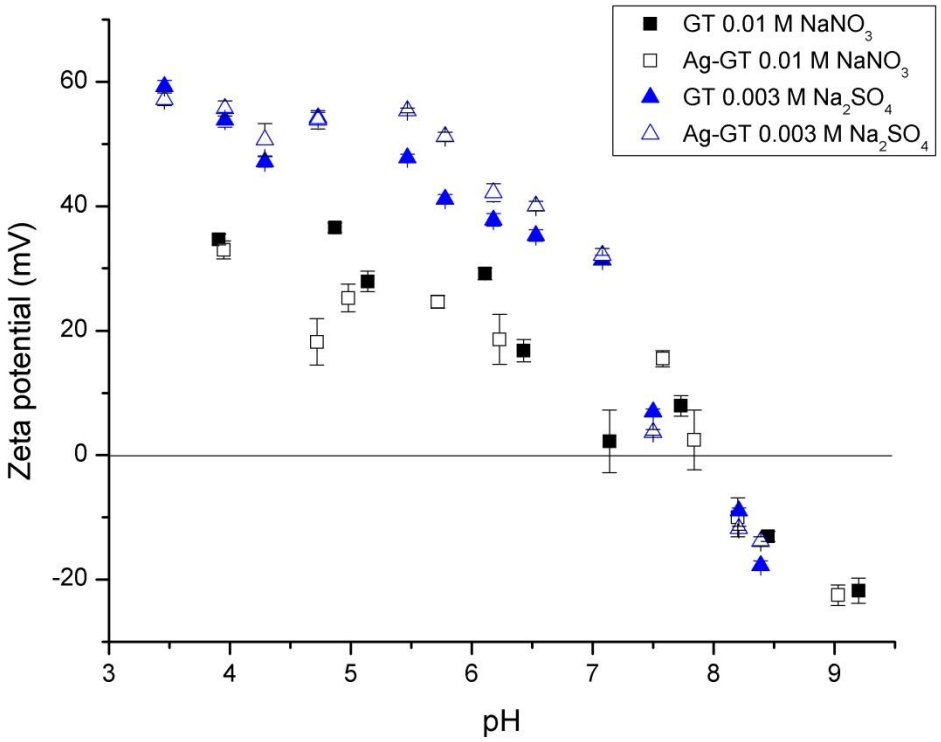

Figure 6.5. Zeta potential measurements of goethite suspensions (0.1 g/L in 0.003 M Na_2SO_4 or 0.1 M $NaNO_3$) in 0 mM or 0.1 mM Ag(I), across pH.

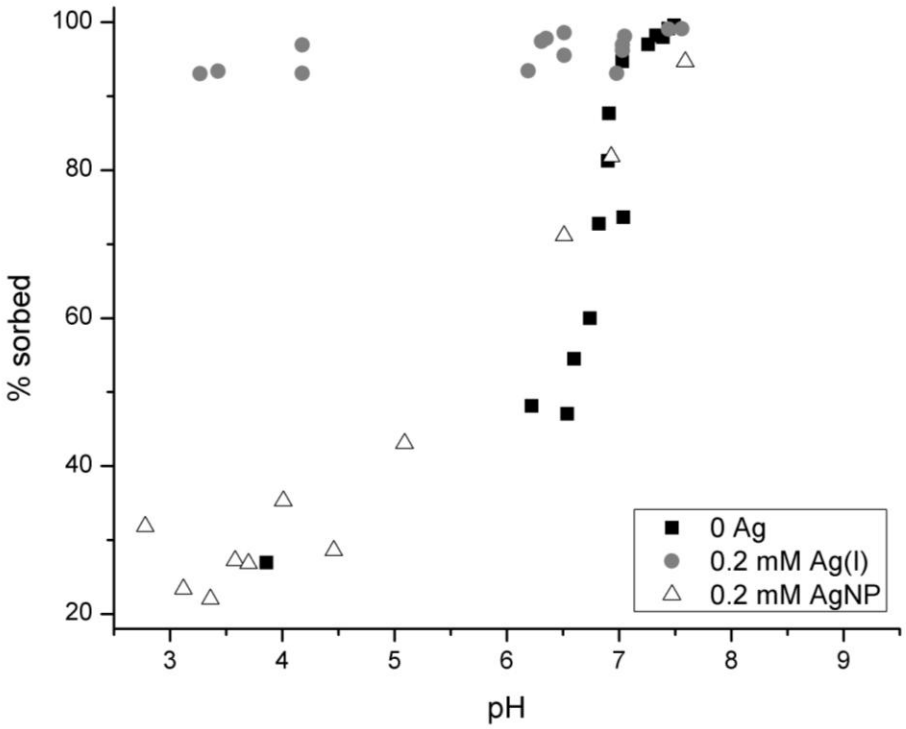

Figure 6.6. pH dependent sorption of cysteine on goethite surface as a function of silver species (0.2 mM Ag (I) and 0.2 mM AgNPs). All experiments were conducted in 0.003 M Na_2SO_4 solution.

CHAPTER SEVEN

CONCLUSIONS AND SIGNIFICANT FINDINGS

Nanoparticles (NPs), either natural or manufactured, have not been extensively studied in soil environments. Natural NPs exist in all soil environments, and are the smallest fraction of clay. Many studies use operationally defined size fractions for both "colloidal" and "nanoparticulate" fractions. Typically, colloids are between 0.1 and 1 μm (= 100 to 1,000 nm), while NPs are <100 nm in diameter.

Soil NPs have been shown in some studies (Heathwaite et al., 2005; Turner et al., 2004) to be a major route of phosphate transport from agricultural fields into ground and surface waters. Since phosphate sorbs strongly onto soil particles, phosphate typically does not leave agricultural soils as a dissolved species unless concentrations are excessive. Our first study of soil NPs (d = 10 to 200 nm) showed that in the sandy, acidic (pH 4.5 to 5.2), low-organic matter (<0.5%) soils of the southeastern United States, NP-facilitated phosphate transport may not be as important as hypothesized. A combination of oxalate and dithionite-citrate-bicarbonate extractions revealed that phosphate in the three soils studies was predominantly associated with amorphous Al and Fe oxyhydroxides in the soil. X-ray absorption spectroscopy (XAS) analysis indicated the predominance of amorphous forms of Si-substituted Fe oxyhydroxides in soil NPs that were dissimilar from reference Fe (oxyhydr)oxides.

The lack of NP-facilitated phosphate transport was observed in both batch and replenishment desorption studies. Scanning electron microscopy (SEM) outfitted with

electron dispersive spectroscopy (EDS) of recovered pellets from ultra-high-speed centrifugation showed a very small degree of P association with soil NPs, which further supported our previous finding of minimal NP-associated phosphate transport in the soils studied.

Overall, from Chapter 2 of this text, we can conclude that soil NPs between 10 and 200 nm at acidic soil pH conditions do not provide a major transport route for phosphate in the soils studied and at low ionic strength. These results may change, however, if the ionic strength, pH, and phosphate levels in soils drastically change after the application of fertilizer and/or lime.

The results of Chapter 2 led to a better understanding of the discrepancy between our findings (lack of colloid/NP facilitated transport of P) and widely-reported colloid facilitated transport processes in agricultural soils. Accordingly, the effects of ionic strength, pH, and added phosphate concentration on the soil NP facilitated transport of P were investigated in greater depth in Chapter 3. The mineralogy of soil NPs was investigated via high-resolution transmission electron microscopy (TEM) with EDS capabilities, and X-ray diffraction. Soil NPs were primarily composed of hematite and kaolinite, combined with amorphous aluminosilicate phases. A small amount of Ca-P rich particles was observed, indicating a minor presence of the P mineral apatite. However, the majority of P was associated with amorphous Fe-rich aluminosilicate phases or hematite.

After reviewing relevant colloidal P literature, it was observed that ionic strength often presented a change in the presence of colloids and/or NPs in soil solution, due to

the coagulating effect of increased ionic strength via a reduction in the diffuse double layer. For our second P study in Chapter 3, we used an operational definition of colloids as particles between 0.2 and 0.41 µm in diameter. The results of our desorption experiment with 0.1 mM added phosphate showed that colloidal P, Fe, and Al increased at 0.1 M ionic strength from their values at 0.01 M ionic strength, especially with increasing pH. An increase in ionic strength from 0.01 M $NaNO_3$ to 0.1 M $NaNO_3$ also caused an increase in the particle size of soil components hematite and kaolinite, along with goethite.

Varying P concentration resulted in interesting findings. With no added phosphate, a moderate amount of colloidal Fe and Al were released. At 1 mM phosphate, the colloidal component of Fe and Al increased, especially above pH 6. This could be due, in part, to precipitation of aluminum and calcium phosphates at the more alkaline pH levels (Lindsay, 1979). However, at 0.1 mM phosphate, there was nearly negligible quantity of colloidal Fe or Al. Due to our rather narrow definition of "colloid (0.2 to 0.41 µm)" in these experiments, it is possible that the nanoparticulate/colloidal soil particles are either smaller than 0.2 µm or larger than 0.41 µm, and are, therefore, not detected through our methods. The addition of phosphate has been known to increase particle size of goethite suspensions (Anderson et al., 1985). When particle size of various mineral suspensions (goethite, kaolinite, and hematite) was measured, the addition of P did generally increase particle size, though results varied for each component. Furthermore, zeta potential measurements of mineral suspensions with increasing phosphate concentration showed that the addition of 0.1 mM phosphate caused a dramatically more

negative zeta-potential than the 0 mM phosphate measurement. The addition of phosphate is clearly interacting strongly with soil NPs, and affecting their particle size, potentially causing them to be outside of our defined "colloids."

Chapter 3 of this text allowed us to conclude that soil NPs can be coagulated or dispersed via the specific adsorption of phosphate, or through changes in ionic strength and pH. A survey of the colloid-facilitated P transport literature revealed that colloidal P can be highly variable and is quite dependent on soil type, native P levels in soils associated with amendment history, soil organic matter content, sampling practices, size definitions, and experimental setup. Further studies conducted over a range of NP/colloid size definitions would be beneficial to better assess the risk of colloid facilitated P transport processes in soils.

Manufactured NPs, as well, are strongly affected by soil environments. Silver nanoparticles (AgNPs), in particular, are a very commonly used NP technology (PEN, 2010), and are quite reactive in soil/water environments. Since this technology is still rather new, studies on AgNP behavior in soil/water environments are still somewhat lacking. Three manufactured AgNPs (15 to 50 nm) with and without the capping agent polyvinylpyrrolidone (PVP), a commonly used polymer-based anti-coagulant, were used. A dissolution study was conducted under both oxidizing and reducing conditions to determine the amount of Ag(I) released from the Ag(0) AgNPs, which revealed that pAg15 (a 15 nm AgNP, coated in 90% PVP by wt.) had nearly 10 times the Ag(I) release of the other two particles, pAg50 (a 50 nm AgNP, coated in 0.3% PVP by wt.) and uAg50 (an uncoated 50 nm AgNP), under both redox conditions. When the chemical

speciation of AgNPs after the dissolution experiments was analyzed using X-ray absorption near edge structure spectroscopy, the analysis revealed that pAg15 was the most changed over 30 days, retaining only 82% and 89% of its original chemical form in reducing and oxidizing environments, respectively. The remaining portion was similar to various Ag(I) reference compounds. The most unchanged particle was uAg50, which remained essentially unchanged after 30 days in both redox environments.

The reactivity of the AgNPs in soils was also investigated through adsorption isotherm experiments for all three AgNPs and Ag(I) in a South Carolina agricultural soil, Toccoa entisol (coarse-loamy, thermic typic Udifluvents). All forms of silver showed a high affinity for the soil, however, the affinity was the weakest for Ag(I). Among the AgNPs, pAg15 showed the highest sorption capacity by far. Soil samples reacted with AgNPs, which aged for up to 30 days in a reducing environment, were also examined for changes in Ag chemical speciation via XAS analysis. The pAg15 sample, again, showed by far the greatest amount of change from its original form, retaining only 22% of its original chemical species after 30 days, and showed the most similarity to the Ag(I)-sorbed-humic-acid spectrum. A principal component analysis further confirmed that the pAg15 30 day spectrum was the most complex over time.

The study in Chapter 4 showed that AgNPs are as reactive as Ag(I) in soil environments. Furthermore, it appears that both physical properties (e.g., particle size) and chemical properties (e.g., surface coating) of AgNPs dictate the fate. The particle that was consistently the most reactive in soil environments was the smallest (15nm) and most highly coated (99%) with PVP. This provides evidence that regulation of AgNPs will

prove difficult, as many physicochemical factors affect their reactivity and fate in heterogeneous environments.

To further explore the physical properties of AgNPs, specifically their spatial distribution in soils, the soil-aged AgNPs were further examined in Chapter 5 of this text. In addition, the effects of physicochemical properties of AgNPs on toxicity to denitrifying bacteria were addressed. AgNPs are strong anti-microbial agents, which is their main selling-point as a commercial product. For this reason, it is reasonable to be concerned when they enter soil ecosystems containing the bacteria responsible for nutrient cycling, such as the denitrifiers, that we depend on for our global nutrient cycles. Each of the three AgNPs described above were incubated in anaerobic batch reactors containing fresh agricultural soil still retaining its native bacterial population. The rate and end-point of denitrification process for each condition was assessed. In our systems, Ag(I) was much more toxic to the bacteria community than any of the AgNPs. This may be due to inhibited Ag(I) release by AgNPs in the soil environment, as Ag(I) release is thought to be the primary mode of AgNP toxicity to bacteria (Xiu et al., 2012). Of the AgNPs, pAg15 was by far the most toxic, followed by uAg50. One additional AgNP was added to this study, uAg35 (an uncoated, 35 nm AgNP), which showed no toxicity, nor did pAg50.

Aged AgNP-reacted soils from the denitrification experiments were analyzed for the spatial distribution of AgNPs using microfocused(μ)-X-ray microprobe techniques. While uAg50 was present in distinct “hot-spots” within the soil matrix, pAg15 was much more evenly dispersed, with pAg50 in between. Analysis by SEM with EDS allowed for

confirmation of these data over a larger area. From the Ag localized areas in each X-ray fluorescence map, μ-XAS analysis was conducted to elucidate the micron-scale Ag chemical speciation. The analysis revealed that the "hot-spots" on uAg50 were very similar to the original AgNPs (i.e., metallic Ag(0)), as were spots from the other two maps. The fluorescence intensity at each hot spot was extrapolated to assess the aggregation state of AgNPs. The results showed a wide distribution of aggregated AgNPs in soils.

The study in Chapter 5 also revealed that AgNP toxicity in soil environments may be less than the same AgNP concentration in pure-culture environments. This is likely due to AgNP- and resulting Ag(I)-binding onto soil surfaces and/or aggregation of AgNPs. In addition, the toxicity of the AgNPs may be less so due to their initial size and/or surface coating, but more so due to their reactivity within the soil environment. In general, it appears that AgNPs that strongly aggregate within soil environments exhibit less toxicity than those that are more evenly dispersed. While it has been shown that AgNPs may be bioavailable in soil environments to earthworms (Shoults-Wilson et al., 2011), this is the first study showing AgNP bioavailability to soil bacteria in a soil environment.

To further investigate the reactions occurring at the mineral-water interface, Ag(I) and AgNP sorption in goethite was investigated in Chapter 6. As revealed in Chapter 4, Ag(I) shows a strong affinity for thiol functional group of humic substances due to its soft acid properties. Cysteine was chosen as a model thiol containing ligand for these experiments to represent soil humic substances. In this chapter, the effect of cysteine on

the partitioning process of Ag(I) and AgNPs onto goethite was specifically examined using macroscopic approaches.

The sorption of Ag(I) onto goethite surfaces was dramatically increased with the addition of cysteine. This was not true, however, for AgNPs. Ionic silver, AgNPs, and cysteine all independently show strong affinity for goethite. Cysteine did not largely affect the AgNP sorption because of the lack of Ag(I) availability on the AgNP surfaces. In this case, the strong hydrophobic interactions of AgNPs with goethite surfaces seemed to prevail. Likewise, cysteine sorption patterns are similarly unchanged with the addition of AgNPs.

The drastic increase in both cysteine sorption in goethite in the presence of Ag(I), as well as Ag(I) in the presence of cysteine, indicates a stronger sorption capacity by Ag(I)-cysteine complexes than by either Ag(I) or cysteine alone. The increased sorption of Ag(I) occurs at both equal molar ratios of Ag(I) and cysteine and at 2:1 Ag(I):cysteine ratios. Evidence from both ionic strength sorption experiments and zeta potential measurements indicate inner-sphere sorption of Ag(I) at the goethite-water interface. Based on the strong ligand exchange reaction, inner-sphere sorption of cysteine was also suggested between the surface hydroxyl of goethite and its carboxyl group of cysteine.

The findings in Chapter 6 provided strong evidence for the formation of Ag(I)-cysteine ternary surface complexes that are strongly sorbed onto variable charge mineral surfaces, such as goethite. However, it also showed that cysteine may not greatly affect the AgNP sorption in goethite although AgNPs are known to have a strong affinity for

humic substances. It appears that mineral surfaces might play an important role in the fate of AgNPs in aquatic-terrestrial environments.

The data presented in this dissertation provide a fresh outlook on the behavior of natural and manufactured NPs in natural environments. While these NPs may not directly participate in the contaminant transport process in all soil environments, it is clear that small changes in environmental conditions may have a large effect on the mobility of NPs and formation of colloids. Therefore, the fate and transport of contaminants (as ligands or NP components) can be retarded or facilitated by altering environmental conditions. Physicochemical properties of soil solutions such as ionic strength, ligand concentration, and pH, are variables that are in constant flux in natural environments, and are manipulated by anthropogenic and indigenous inputs. Small changes in these conditions could alter the NP characteristics/reactivity (e.g., particle size as aggregates, surface coating, the rate of dissolution, and affinity on soil minerals), and they may have a large impact on their toxicity to beneficial soil bacteria. Through this study, we learned that NP reactivity/behavior in heterogeneous environments is particle-specific and dependent on environmental conditions. For this reason, in terms of governmental regulation, it would be difficult to institute a blanket policy for regulation of all NP release to soil systems, without regard to particle-specific characteristics.

References

Anderson, M.A., M.I. Tejedor-Tejedor, and R.R. Stanforth. 1985. Influence of aggregation on the uptake kinetics of phosphate by goethite. Environ. Sci. Technol. 19:632-637.

Heathwaite, L., P. Haygarth, R. Matthews, N. Preedy, and P. Butler. 2005. Evaluating colloidal phosphorus delivery to surface waters from diffuse agricultural sources. J. Environ. Qual. 34:287-298.

Lindsay, W.L. 1979. Chemical Equilibria in Soils. John Wiley & Sons, New York.

PEN. 2010. The Project on Emerging Nanotechnologies: Nanotechnology consumer products inventory [Online]. Available by Woodrow Wilson International Center for Scholars http://www.nanotechproject.org/inventories/consumer/ (verified 10 July 2012).

Shoults-Wilson, W.A., B.C. Reinsch, O.V. Tsyusko, P.M. Bertsch, G.V. Lowry, and J.M. Unrine. 2011. Role of particle size and soil type in toxicity of silver nanoparticles to earthworms. Soil Sci. Soc. Am. J. 75:365-377.

Turner, B.L., M.A. Kay, and D.T. Westermann. 2004. Colloidal phosphorus in surface runoff and water extracts from semiarid soils of the western United States. J. Environ. Qual. 33:1464-1472.

Xiu, Z.-M., Q.-B. Zhang, H.L. Puppala, V.L. Colvin, and P.J.J. Alvarez. 2012. Negligible particle-specific antibacterial activity of silver nanoparticles. Nano Lett. 12:4271-4275.